Technische Universität München
TUM School of Life Sciences

Functional characterization of the interaction of the immune receptor LORE and 3-hydroxy fatty acid elicitors in Brassicaceae

Lin-Jie Shu

Vollständiger Abdruck der von der TUM School of Life Sciences der Technischen Universität München zur Erlangung des akademischen Grades eines

Doktors der Naturwissenschaften (Dr. rer. nat.)

genehmigten Dissertation.

Vorsitz: Prof. Dr. Corinna Dawid

Prüfer*innen der Dissertation:

1. Prof. Dr. Stefanie Ranf
2. Prof. Dr. Kay H. Schneitz

Die Dissertation wurde am 15.02.2023 bei der Technischen Universität München eingereicht und durch die TUM School of Life Sciences am 16.07.2023 angenommen.

Abstract

Various beneficial and detrimental microorganisms surround plants in nature. Plants can recognize these microorganisms by sensing microbe-associated molecular patterns (MAMPs) via cell surface-localized pattern recognition receptors (PRRs) to activate pattern-triggered immunity (PTI). Medium-chain 3-hydroxy fatty acids (mc-3-OH-FAs), derived from Gram-negative bacteria, are perceived as MAMPs by the S-domain (SD) receptor kinase LIPOOLIGOSACCHARIDE SPECIFIC REDUCED ELICITATION (LORE, alias SD1-29) in *Arabidopsis thaliana*. How mc-3-OH-FAs are sensed by LORE at the molecular level and whether other Brassicaceae species have functional LORE orthologs have yet to be determined in detail.

To study the interaction of LORE and 3-OH-FA, several reliable methods, from receptor expression and purification to ligand binding assays, were developed and used to successfully demonstrate 3-OH-FA binding by LORE *in vitro*. Investigation of the natural diversity of 3-OH-FA-triggered responses in a wide range of Brassicaceae species revealed that 3-OH-FA-responsiveness was variable compared to responsiveness to the bacterial flagellin elicitor. Subsequently, LORE orthologs and close homologs from 20 Brassicaceae species were functionally examined for 3-OH-FA binding and LORE-dependent responses upon heterologous expression in *Nicotiana benthamiana*. In contrast to the observed variability of 3-OH-FA-responsiveness in Brassicaceae, 3-OH-FA binding was conserved among all LORE orthologs, and only a few of these orthologs did not trigger LORE-dependent responses. Furthermore, not all LORE orthologs restored the function of sensing 3-OH-FA in the *A. thaliana lore* mutant, indicating that multiple factors in addition to ligand binding determine LORE-dependent immune signaling. By comparing the structures of 3-OH-FA-binding LORE ortholog with non-3-OH-FA binding homologs and utilizing a domain-swapping approach, the domain for binding 3-OH-FA was identified.

Overall, these findings shed light on the mechanism of LORE-mediated 3-OH-FA sensing as well as the natural diversity of this immune receptor ligand-pair in Brassicaceae.

Zusammenfassung

In der Natur sind Pflanzen von verschiedenen nützlichen und schädlichen Mikroorganismen umgeben. Pflanzen können diese Mikroorganismen erkennen, indem sie mikrobenassoziierte molekulare Muster (microbe-associated molecular patterns, MAMPs) über an der Zelloberfläche lokalisierte Mustererkennungsrezeptoren (pattern recognition receptors, PRRs) wahrnehmen, um die musterausgelöste Immunität (pattern-triggered immunity, PTI) zu aktivieren. Mittelkettige 3-Hydroxyfettsäuren (mk-3-OH-FS), die von gramnegativen Bakterien stammen, werden von der S-Domänen (SD)-Rezeptorkinase LIPOOLIGOSACCHARIDE SPECIFIC REDUCED ELICITATION (LORE, alias SD1-29) in Arabidopsis thaliana als MAMPs wahrgenommen. Wie mk-3-OH-FS von LORE auf molekularer Ebene wahrgenommen werden und ob andere Brassicaceae-Arten über funktionelle LORE-Orthologe verfügen, ist noch nicht im Detail geklärt.

Um die Interaktion zwischen LORE und 3-OH-FS zu untersuchen, wurden mehrere zuverlässige Methoden, von der Rezeptorexpression und -reinigung bis hin zu Ligandenbindungsassays, entwickelt und eingesetzt, um die Bindung von 3-OH-FS durch LORE in vitro erfolgreich nachzuweisen. Die Untersuchung der natürlichen Vielfalt der durch 3-OH-FS ausgelösten Reaktionen in einer Vielzahl von Brassicaceae-Arten ergab, dass die 3-OH-FS-Reaktion im Vergleich zur Reaktion auf den bakteriellen Flagellin-Elizitor variabel war. Anschließend wurden LORE-Orthologe und enge Homologe aus 20 Brassicaceae-Arten funktionell auf 3-OH-FS-Bindung und LORE-abhängige Reaktionen nach heterologer Expression in Nicotiana benthamiana untersucht. Im Gegensatz zur beobachteten Variabilität der 3-OH-FS-Reaktion in Brassicaceae war die 3-OH-FS-Bindung bei allen LORE-Orthologen konserviert, und nur wenige dieser Orthologe lösten keine LORE-abhängigen Reaktionen aus. Darüber hinaus stellten nicht alle LORE-Orthologe die Funktion der 3-OH-FS-Erkennung in der lore-Mutante von A. thaliana wieder her, was darauf hindeutet, dass neben der Ligandenbindung noch andere Faktoren die LORE-abhängige Immunsignaltransduktion bestimmen. Durch den Vergleich der Strukturen von 3-OH-FS-bindenden LORE-Orthologen mit nicht 3-OH-FS-bindenden Homologen und die Anwendung eines Domänenaustausch-Ansatzes wurde die Domäne, die 3-OH-FS bindet, identifiziert.

Insgesamt geben diese Ergebnisse Aufschluss über den Mechanismus der LORE-vermittelten 3-OH-FS-Erkennung sowie über die natürliche Vielfalt dieses Immunrezeptor-Ligandenpaares in Brassicaceae.

Acknowledgment

First of all, I would like to give my deepest gratitude to my doctoral supervisor, Prof. Stefanie Ranf. Although I did not expect the topic I was assigned, I gained the knowledge in the plant science field and found my strengths in academia by her skillful guidance and motivating discussions. I also appreciate her efforts to run the lab in a style that can give me the freedom and the finance to explore the joys of science.

I want to thank the members of my thesis committee, Prof. Corinna Dawid and Prof. Kay Schneitz for organizing my oral defense and examining my thesis thoroughly.

I would like to thank my doctoral project committee members: Prof. Ralph Hückelhoven, Dr. Martin Stegmann, and Dr. Antonella Di Pizio. Ralph is the father of all doctoral students in the chair, and I learned a lot from him not only about plant pathology, but also about the attitude of being a scientist and a leader. Martin gave our group some constructive suggestions on studying receptors. My mentor Antonella is one of our supportive cooperators who help us approach the goals from very different ways which really broaden my knowledge.

Thank all of you guys in AG LORE, Lars, Alex, Tim, Sabine, Lukas, and Parvindar, you are my family in Germany, and we all together went through the difficult time of pandemics. I also appreciate all the members in Chair of Phytopathology who keep the environment very international even I have half-Germanized by beer already. This thesis would not have been completed without the help of my colleagues and friends, and this is my pleasure to work together. I would also like to give my thank go to the kind reviewers of this thesis at such short notice.

My family in Taiwan, I love you, you are always my warm harbor.

The path to get doctoral degree is truly like a marathon, but it is not the end of the way to my dream. Reality never has mercy on anyone, but it will not restrain you from chasing the shining star in your heart.

Von Herzen, möge es wieder zu Herzen gehen.

Contents

Abbreviations

3-OH-C10:0	3-hydroxydecanoic acid
ADP	adenosine diphosphate
ARC1	Armadillo Repeat Containing 1
Avr	avirulence gene
AWF	apoplastic washing fluid
B-type	bulb-type
BAK1	BRASSINOSTEROID-INSENSITIVE 1-ASSOCIATED KINASE 1
BRI1	BRASSINOSTEROID-INSENSITIVE 1
C	competition binding
CARD1	CANNOT RESPOND TO DMBQ 1
CBB	Coomassie Brilliant Blue
CEBiP	CHITIN-ELICITOR BINDING PROTEIN
CERK1	CHITIN ELICITOR RECEPTOR 1
cpm	count per minute
CrRLK1L	*Catharanthus roseus* Receptor-Like Kinase 1-like
CV	column bed volume
DAMP	damage-associated molecular pattern
DMBQ	2,6-dimethoxy-1,4-benzoquinone
DORN1	DOES NOT RESPOND TO NUCLEOTIDES1
DUF	Domain of unknown function
eAtLORE	AtLORE ectodomain
eATP	extracellular adenosine triphosphate
ECD	extracellular domain or ectodomain
EF-Tu	ELONGATION FACTOR-TU
EFR	ELONGATION FACTOR-TU RECEPTOR
EGF	epidermal growth factor-like domain
eH_2O_2	extracellular hydrogen peroxide
EndoPG	endopolygalacturonase
ET	ethylene
ETI	effector-triggered immunity
ETS	effector-triggered susceptibility
flg22	flagellin 22
FLS2	FLAGELLIN SENSING 2
FPLC	fast protein liquid chromatography
G-type	GNA-type
GFP	Green fluorescent protein
GNA	*Galanthus nivalis* bulb
GPCR	G-protein-coupled receptor
GTP	guanosine triphosphate

HAA	3-hydroxyalkanoate
HPCA1	HYDROGEN-PEROXIDE-INDUCED Ca^{2+} INCREASES
HR	hypersensitive response
IF1	Proteobacterial translation-initiation factor 1
IPTG	isopropyl-β-D-thiogalactoside
IR	infrared
ITC	isothermal titration calorimetry
JA	jasmonic acid
Kd	dissociation constant
Km	kinase-mutated
L	lectin-like domain
LecRK	legume-like lectin receptor kinase
LORE	LIPOOLIGOSACCHARIDE SPECIFIC REDUCED ELICITATION
LORE-OE	Arabidopsis plant overexpressing *AtLORE* in the *lore*-1 mutant background
LPS	lipopolysaccharide
LRR	leucine-rich repeat
LRX	LEUCINE-RICH REPEAT EXTENSIN
LYK4/5	LYSIN MOTIF RECEPTOR KINASE 4/5
LYM1/3	LYSIN-MOTIF PROTEIN 1/3
LysM	Lysin motif
MAMP	microbe-associated molecular pattern
MAPK	mitogen-activated protein kinase
MBP	maltose-binding protein
mc-3-OH-FA	medium-chain 3-hydroxy fatty acid
MES	2-(N-morpholino)-ethanesulfonic acid
MIK2	MALE DISCOVERER 1-INTERACTING RECEPTOR-LIKE KINASE 2
MSP	melittin signal peptide
MST	microscale thermophoresis
MWCO	molecular weight cutoff
NAD^+	nicotinamide adenine dinucleotide
$NADP^+$	nicotinamide adenine dinucleotide phosphate
NC	no competition binding
NEP1	NECROSIS AND ETHYLENE-INDUCING PEPTIDE 1
NLP	NECROSIS AND ETHYLENE-INDUCING PEPTIDE 1-LIKE PROTEIN
NLR	nucleotide-binding domain leucine-rich repeat proteins
NS	nonspecific binding
PAMP	pathogen-associated molecular pattern
PAN	plasminogen-apple-nematode
PBL	PBS1-like 1
PBS1	AVRPPHB SUSCEPTIBLE 1
PCD	programmed cell death

PEP1	PLANT ELICITOR PEPTIDE 1
PCR	polymerase chain reaction
PEPR	PLANT ELICITOR PEPTIDE RECEPTOR
PG	peptidoglycan
PLO	protein lipid overlay assay
POI	protein-of-interest
PRR	pattern recognition receptor
PTI	pattern-triggered immunity
PUB	PLANT U-BOX
R	resistance gene
RALF	RAPID ALKALINIZATION FACTOR
RDA2	RESISTANT TO DFPM-INHIBITION OF ABSCISIC ACID SIGNALING 2
RIPK	RPM1-INDUCED PROTEIN KINASE
RLCK	receptor-like cytoplasmic kinases
RLK	receptor-like kinase
RLP	receptor-like protein
RLP23/32/42	RECEPTOR LIKE PROTEIN 23/32/42
RLU	relative light unit
ROQ1	RECOGNITION OF XOPQ 1
ROS	reactive oxygen species
RPM1	RESISTANCE TO P. SYRINGAE PV MACULICOLA 1
SA	Salicylic acid
SAR	systemic acquired resistance
SCOOP	SERINE-RICH ENDOGENOUS PEPTIDE
SCR	S-LOCUS CYSTEINE-RICH PEPTIDE
SD	S-domain
SDS	sodium dodecyl sulfate
SI	self-incompatibility
SIRK1	SUCROSE-INDUCED RECEPTOR KINASE 1
SLG	S-LOCUS GLYCOPROTEIN
SOBIR1	SUPPRESSOR OF BRI1-ASSOCIATED KINASE-INTERACTING RECEPTOR KINASE 1
SPA	scintillation proximity assay
SPR	surface plasmon resonance
SRK	S-LOCUS RECEPTOR KINASE
T	total binding
TBS	Tris-buffered saline buffer
TEV	*Tobacco Etch Virus*
THE1	THESEUS1
tHSP	heat shock protein terminator
TM	transmembrane domain

XopQ	XANTHOMONAS OUTER PROTEIN Q
YFP	Yellow fluorescent protein

1 Introduction

Food security is a significant issue humankind is still facing today. The problems like unstable water supply and extreme temperatures brought by climate change make food production more difficult. Due to biotic and abiotic stresses, such as disease, pests, and drought, 35% of the annual crop yield was lost in 2018 at the preharvest stage (Mesterházy *et al.*, 2020). To safeguard our food supply, improving crops to adapt to today's fast-changing environment is an important topic. To control crop diseases, the technology to enhance the resistance of plants against pathogens relies on advancing breeding methods. Identifying genes contributing to plant disease resistance is also crucial to reduce excessive agrochemical usage. Although plants lack the dedicated immune systems known from animals, they have evolved a repertoire of defense mechanisms to protect themselves from diseases (Spoel and Dong, 2012). To improve immune mechanisms in crops, it is essential to study the genes involved in disease resistance. Plant immune receptors are at the frontline of this process and are ideal targets for disease resistance engineering.

1.1 Plant immunity

Plants are constantly exposed to microbes some of which can be hostile to them in nature. To resist the threat and stay healthy, plants have evolved different mechanisms to recognize structures from pathogens or the damage caused by pathogens, and activate appropriate immune responses (Jones and Dangl, 2006). Plants detect pathogens by sensing the presence of conserved microbial structures, named pathogen-associated molecular patterns or microbe-associated molecular patterns (PAMPs or MAMPs), as danger signals (Couto and Zipfel, 2016). MAMPs are usually conserved structures which are indispensable for the microbes, such as chitin from fungal cell wall, and flagellin from bacterial flagellum, plants detect these patterns (Zipfel, 2014). MAMPs are recognized by cell surface-localized pattern recognition receptors (PRRs) and induce pattern-triggered immunity (PTI), which effectively wards off most microbes and non-adapted pathogens (Macho and Zipfel, 2014). In addition, plant-derived molecules known as damage-associated molecular patterns (DAMPs), released upon cell damage, can also be sensed as danger signals and induce PTI (Boller and Felix, 2009, Gust *et al.*, 2017). The activation of PTI leads to defense responses including the production of reactive oxygen species (ROS), cytoplasmic calcium ion influx, stomatal closure, accumulation of phytoalexins and antimicrobial proteins and enzymes, and transcriptional reprogramming that modulates the expression of defense-related genes and plant defense hormones (Bigeard *et al.*, 2015, Li *et al.*, 2016).

In order to successfully infect plant hosts, pathogens evolved effectors as virulence factors to interfere with plant immunity and to manipulate host physiology (Varden *et al.*, 2017). Pathogens secret effector proteins into the plant cytoplasm or apoplast and suppress PTI responses, resulting in effector-triggered susceptibility (ETS). To counteract ETS, plants evolved another layer of immunity to recognize virulence effectors. The apoplastic effectors are inhibited by the host-secreted proteins or recognized by the cell surface receptors (Asai and Shirasu, 2015). The intracellular nucleotide-binding domain leucine-rich repeat proteins (NLRs) are the receptors that can sense the cytoplasmic effectors or their actions (Cui *et al.*, 2015). Successful perception of effectors, also known as avirulence (Avr) proteins, by disease resistance (R) proteins activates effector-triggered immunity (ETI), which leads to stronger immune responses than PTI (Tsuda and Katagiri, 2010), often including the programmed cell death (PCD), called hypersensitive response (HR), which effectively restricts pathogens from further colonization at the infected site (Mur *et al.*, 2008, Coll *et al.*, 2011).

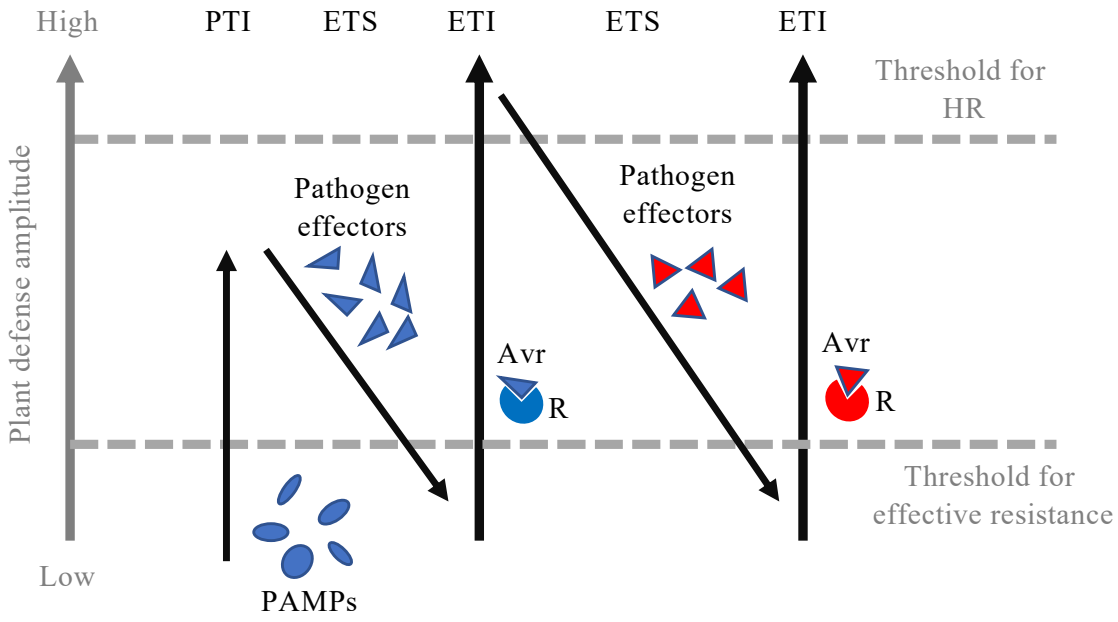

Figure 1. The zig-zag model of plant immunity. After the recognition of PAMPs from pathogens by receptors, a PTI response is activated. To suppress PTI (Pattern-triggered immunity) and successfully infect the host plant, pathogen effectors are secreted into the host plants and lead to ETS (Effector-triggered susceptibility). The host has receptors, called resistant proteins (R), to recognize specific effectors, called avirulence proteins (Avr). This induces

a more robust immune response that is often associated with a hypersensitive response (HR), leading to ETI (Effector-triggered immunity) and inhibition of pathogen spread. The zig-zag model illustrates the evolutionary arms race between pathogen and host. The arms race continues as new effectors and new R proteins evolve. (Adapted from Jones and Dangle, 2006).

While, pathogens evolve different effectors to suppress ETI, and plant hosts also develop more R proteins and PRRs to defend against them. In the zig-zag model of plant immunity, the arms race between host and pathogen during evolution pushes pathogens to hide or reshape their patterns and effectors or gain new effectors which can suppress ETI. Plant hosts acquire new receptors for sensing the new patterns and effectors (Figure 1) (Jones and Dangl, 2006). Although PTI and ETI are induced at different time scales and quantitative levels, they still share many signaling components (Li *et al.*, 2020). PTI and ETI potentiate each other synergistically. PTI strongly promotes the defense response of ETI, such as HR. Conversely, ETI enhances the full immune response of PTI (Ngou *et al.*, 2021, Yuan *et al.*, 2021). All in all, plant PTI and ETI together form an effective immune barrier to halt pathogen infection.

PTI and ETI initiate a series of signaling events. The canonical defense plant hormones, salicylic acid (SA), jasmonic acid (JA), and ethylene (ET) regulate immune signaling when plant hosts are exposed to pathogens having different lifestyles: necrotrophic pathogens, biotrophic pathogens and hemi-biotrophic pathogens (Pieterse *et al.*, 2009). Necrotrophic pathogens first impair host cells and then feed on the nutrient contents. Biotrophic pathogens absorb nutrients from living host cells, and hemi-biotrophic pathogens reveal necrotrophic and biotrophic lifestyles depending on their life cycle stages (Glazebrook, 2005). Plant hosts generally resist biotrophic pathogens through SA-dependent immune mechanisms. Upon infection by necrotrophic pathogens, plant hosts boost JA-regulated resistance in concert with ET-regulated signaling pathways (Pieterse *et al.*, 2012). Plant immune responses are activated at the infected site. Subsequently, systemic defense responses are often induced in distal plant tissues or organs to protect these uninfected parts against subsequent invasion by pathogens. This long-lasting and broad-spectrum disease resistance is called systemic acquired resistance (SAR), which is a SA-dependent defense mechanism (Vlot *et al.*, 2021). Overall, plant immunity relies on fine-tuning a large signaling network by coordinating numerous regulators.

1.2 Diverse plant PRRs and molecular patterns

Plant PRRs include several groups of plasma membrane-localized receptor-like kinases (RLKs) and receptor-like proteins (RLPs) with different kinds of extracellular domains (ectodomain, ECD) (Zipfel, 2014). A typical RLK contains a ligand-binding ECD, a transmembrane domain, and an intracellular kinase domain. An RLP shares equal parts with an RLK except for the intracellular kinase domain (Shiu and Bleecker, 2003). Plant PRRs can be further classified based on their ligand-binding ECDs (Figure 2).

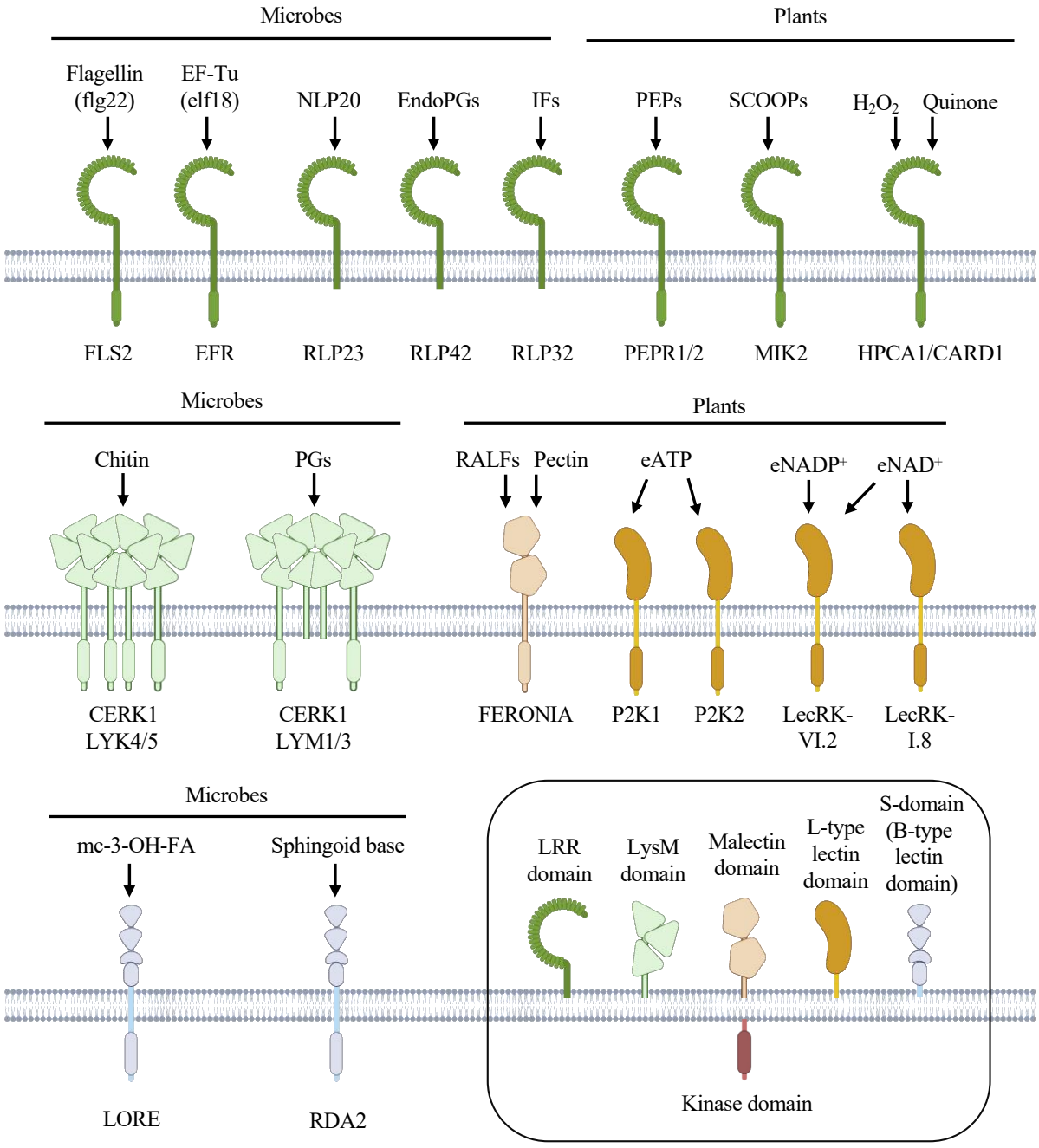

Figure 2. PRRs involved in plant immunity—some iconic receptor-ligand pairs in *Arabidopsis thaliana* as examples. Ligands shown at the top of each panel derived from microbes or plants were listed. Ligand abbreviations: EF-Tu, Elongation factor thermal unstable; NLP20, NECROSIS AND ETHYLENE-INDUCING PEPTIDE 1 (NEP1)-LIKE PROTEIN; EndoPG, Endopolygalacturonase; IF, proteobacterial translation initiation factor 1; PEP, Plant Elicitor Peptide; SCOOP, SERINE-RICH ENDOGENOUS PEPTIDE; PG, peptidoglycan; RALF, RAPID ALKALINIZATION FACTOR; eATP, extracellular adenosine triphosphate; $eNAD^+$, extracellular nicotinamide adenine dinucleotide; $eNADP^+$, extracellular nicotinamide adenine dinucleotide phosphate; mc-3-OH-FA, medium-chain 3-hydroxy fatty acid. Receptor abbreviations: FLS2, FLAGELLIN SENSING 2; EFR, EF-TU RECEPTOR; RLP23/42/32, RECEPTOR LIKE PROTEIN 23/42/32; PEPR1/2, PEP1 RECEPTOR 1/2; MIK2, MALE DISCOVERER 1-INTERACTING RECEPTOR-LIKE KINASE 2; CARD1, CANNOT RESPOND TO DMBQ 1; HPCA1, HYDROGEN-PEROXIDE-INDUCED Ca^{2+} INCREASES; CERK1, CHITIN ELICITOR RECEPTOR 1; LYK4/5, LYSIN MOTIF RECEPTOR KINASE 4/5; LYM1/3, LYSIN-MOTIF PROTEIN 1/3; LecRK, legume-like lectin receptor kinase; LORE, LIPOOLIGOSACCHARIDE SPECIFIC REDUCED ELICITATION; RDA2, RESISTANT TO DFPM-INHIBITION OF ABSCISIC ACID SIGNALING 2. Domain abbreviations: LRR, leucine-rich repeat; LysM, Lysin motif; L-type lectin, legume-like lectin; B-type, bulb-type lectin. The figure was created with BioRender.com.

Leucine-rich repeat (LRR)-RLK and LRR-RLP are the largest cell surface receptor family in Arabidopsis and rice (Shiu and Bleecker, 2003, Shiu *et al.*, 2004). Based on previous studies, LRR-RLKs and LRR-RLPs mainly perceive proteinaceous MAMPs or DAMPs (Dievart *et al.*, 2020). The best-characterized PRR in Arabidopsis is LRR-RLK FLAGELLIN SENSING 2 (FLS2), which perceives a conserved 22-amino acid peptide in the N-terminus of bacterial flagellin (Gómez-Gómez and Boller, 2000). FLS2 forms a complex with another LRR-RLK, BRASSINOSTEROID-INSENSITIVE 1-ASSOCIATED KINASE 1 (BAK1) to trigger complete immune responses upon flg22 treatment (Chinchilla *et al.*, 2007, Sun *et al.*, 2013b). Beyond Arabidopsis, FLS2 orthologs have been identified in many species, including tomato, grapevine, tobacco, soybean, and rice. These studies suggested that FLS2 is conserved in most plant species (Robatzek *et al.*, 2007, Takai *et al.*, 2008, Chakravarthy *et al.*, 2010, Trdá *et al.*, 2014, Wei *et al.*, 2020).

ELONGATION FACTOR-TU (EF-Tu) RECEPTOR (EFR) is another well-known LRR-RLK PRR that senses the N-terminal 18-amino-acid peptide of EF-Tu, elf18. This MAMP is a conserved and universal protein in most bacteria (Kunze *et al.*, 2004, Zipfel *et al.*, 2006). Similarly to FLS2, BAK1 acts as a co-receptor of EFR for elf18 perception (Chinchilla *et al.*, 2007). In contrast to FLS2, the perception of EF-Tu by EFR is restricted to Brassicales. Tobacco

and tomato can gain the function of sensing EF-Tu by ectopically expressing Arabidopsis EFR. Crops like rice, wheat, potato, and apple can also acquire resistance against a broad range of bacterial pathogens by expressing EFR (Lacombe *et al.*, 2010, Schoonbeek *et al.*, 2015, Schwessinger *et al.*, 2015, Boschi *et al.*, 2017).

In Arabidopsis, several LRR-RLPs were identified as receptors of MAMPs. RECEPTOR LIKE PROTEIN (RLP) 23 is a receptor for the conserved 20-amino acid peptide from NECROSIS AND ETHYLENE-INDUCING PEPTIDE 1 (NEP1)-LIKE PROTEINs (NLPs) called nlp20, a microbial pattern derived from bacteria, fungi, or oomycetes (Albert *et al.*, 2015). BAK1 and SUPPRESSOR OF BRI1-ASSOCIATED KINASE-INTERACTING RECEPTOR KINASE 1 (SOBIR1) form complexes with RLP23 to bind to nlp20 (Albert *et al.*, 2015). Endopolygalacturonases enzymes (EndoPGs) secreted by fungal pathogens are virulent enzymes for plant host cell wall decomposition. EndoPGs are recognized as PAMPs by RLP42 (Zhang *et al.*, 2014, Zhang *et al.*, 2021). 9-amino acid epitopes from EndoPGs are sufficient for triggering RLP42-dependent PTI in *A. thaliana*, while other Brassicaceae species, like *Brassica rapa*, only sense more extended epitopes as PAMPs (36 amino acids) (Zhang *et al.*, 2021). Proteobacterial translation-initiation factor 1 (IF1) is a conserved protein released from bacteria. RLP32, as RLP23, forms complexes with BAK1 and SOBIR1 to sense IF1 and induce immune responses. Interestingly, the tertiary structure of IF1 is essential for eliciting activity (Fan *et al.*, 2022).

LRR receptors can also sense a wide range of phytocytokines, which are plant peptide hormones that control plant immunity and development (Hou *et al.*, 2021a, Rzemieniewski and Stegmann, 2022). The first phytocytokine identified in Arabidopsis is Plant Elicitor Peptide (PEP) 1, a 23-amino acid peptide of the PEP family with eight members in *A. thaliana*, that can induce PTI and enhance resistance against pathogens (Huffaker *et al.*, 2006, Yamaguchi *et al.*, 2006, Yamaguchi *et al.*, 2010). The receptors of PEPs are LRR-RLK PEP1 RECEPTOR1 (PEPR1) and PEPR2 in Arabidopsis. PEPR1 and PEPR2-mediated signaling relies on BAK1 for full functions (Yamaguchi *et al.*, 2006, Krol *et al.*, 2010, Yamaguchi *et al.*, 2010). SERINE-RICH ENDOGENOUS PEPTIDEs (SCOOPs) were first identified as secreted peptides in Brassicaceae plants. Like phytocytokines, they are involved in defense responses and root development, respectively (Gully *et al.*, 2019). The LRR-RLK MALE DISCOVERER 1-INTERACTING RECEPTOR-LIKE KINASE 2 (MIK2) directly perceives most members of the SCOOP peptide

family and also forms complexes with BAK1 for signaling (Hou *et al.*, 2021b, Rhodes *et al.*, 2021). SCOOPs have two conserved serine residues, which determine their activities (Hou *et al.*, 2021b). The SCOOP-like sequences are also present in some fungal and bacterial pathogens, and these microbial SCOOP-like peptides can trigger MIK2-dependent defense responses (Hou *et al.*, 2021b, Rhodes *et al.*, 2021).

In addition to proteinaceous patterns, quinone and extracellular hydrogen peroxide (eH_2O_2) are sensed by a LRR-RLK named CANNOT RESPOND TO DMBQ 1 (CARD1) or HYDROGEN-PEROXIDE-INDUCED Ca^{2+} INCREASES (HPCA1). 2,6-dimethoxy-1,4-benzoquinone (DMBQ) was found to be released by host plants and detected by parasitic plants as a signal to form haustoria to invade the host plants. Arabidopsis senses DMBQ as a DAMP to activate immune responses (Laohavisit *et al.*, 2020). eH_2O_2 is a common ROS produced in most organisms. During plant immunity, eH_2O_2 is synthesized as a signaling molecule for, e.g. inducing stomatal closure, strengthening plant cell wall, regulating callose deposition, and being a toxic agent against pathogens (Kadota *et al.*, 2015). eH_2O_2 can activate HPCA1-mediated signaling by oxidizing cysteine residues in the LRR domain, leading to stomatal closure and other stress-induced responses (Wu *et al.*, 2020).

Lysin motif (LysM) RLKs and LysM RLPs are small group of receptors (Ngou *et al.*, 2022). Their sensing targets, glycans, are structurally different from proteinaceous ligands. Glycans are the essential components of the cell wall in plants, fungi, and bacteria, so glycans are ideal MAMPs or DAMPs sensed by plant immune receptors. Chitin, released from fungal and insect cell walls, is perceived by LysM receptors in plants but with different receptor complexes in diverse species. Chitin is sensed in the forms of oligomers by Arabidopsis. Heptamers (chitoheptaose) and octamers (chitooctaose) trigger the most robust responses (Liu *et al.*, 2012). CHITIN ELICITOR RECEPTOR 1 (CERK1) in Arabidopsis can perceive chitin and induce signaling by forming tetrameric complexes with LYSIN MOTIF RECEPTOR KINASE 4 (LYK4) or LYK5 (Kaku *et al.*, 2006, Miya *et al.*, 2007, Liu *et al.*, 2012, Wan *et al.*, 2012, Cao *et al.*, 2014, Xue *et al.*, 2019). As LYK4 and LYK5 lack kinase activity, kinase-induced downstream signaling depends on CERK1 (Wan *et al.*, 2012, Cao *et al.*, 2014). Both Gram-positive and Gram-negative bacteria utilize peptidoglycan (PG) to construct their cell walls. PG is also recognized as a MAMP by LysM receptor complexes, including CERK1 and two RLPs, LYSIN-MOTIF PROTEIN 1

(LYM1) and LYM3 (Willmann *et al.*, 2011). LYM1 and LYM3, which lack kinase domains, are responsible for ligand binding, whereas CERK1 activates downstream signaling transduction (Petutschnig *et al.*, 2010, Willmann *et al.*, 2011). Other glycans like chitosan, β-1,3-glucan/β-1,4-glucan can also act as MAMPs in Arabidopsis, rice, and other crops (Willmann *et al.*, 2011, Yang *et al.*, 2021).

Adenosine triphosphate (ATP) is an indispensable energy source in all organisms, and it is also a signal in stress responses in the extracellular compartment (Tanaka *et al.*, 2010). When cytosolic ATP is accidentally released from cells, this extracellular ATP (eATP) becomes a danger signal and triggers immune responses (Song *et al.*, 2006, Reichler *et al.*, 2009). The legume-like (L-type) lectin receptor kinase (LecRK), LecRK-I.9, also known as DORN1 (DOES NOT RESPOND TO NUCLEOTIDES1) and P2K1, was identified as an eATP receptor in the Arabidopsis plasma membrane (Choi *et al.*, 2014). A second receptor for sensing eATP, P2K2, was also identified (Pham *et al.*, 2020). P2K1-dependent elicitation is induced not only by ATP but also by other nucleotide derivatives like adenosine diphosphate (ADP) and guanosine triphosphate (GTP), and all of them can directly interact with the receptor ECDs (Choi *et al.*, 2014, Pham *et al.*, 2020). Nicotinamide adenine dinucleotide (NAD^+) and nicotinamide adenine dinucleotide phosphate ($NADP^+$) are universal redox carriers in all organisms, and they can induce immune responses when cytosolic NAD^+ and $NADP^+$ are accidentally leaked out of cells and become DAMPs (Berger *et al.*, 2004, Zhang and Mou, 2009). Similarly, LecRK-I.8 perceives extracellular NAD^+, and LecRK-VI.2 senses both extracellular NAD^+ and $NADP^+$ (Wang *et al.*, 2017, Wang *et al.*, 2019).

The malectin receptor kinase *Catharanthus roseus* receptor-like kinase 1-like (CrRLK1L), also called FERONIA, is involved in plant development and immunity. RAPID ALKALINIZATION FACTOR (RALF) peptides are perceived by FERONIA as phytocytokines and regulate plant cell expansion and PTI (Haruta *et al.*, 2014, Stegmann *et al.*, 2017). In a recent study, polygalacturonic acid from pectin was shown to directly bind to FERONIA in one of the malectin domains, suggesting that the two malectin domains in the ECD play distinct roles in plants (Lin *et al.*, 2022).

Other RLK ECDs, such as the wall-associated kinase domain, LRR-malectin domain, and proline-rich/extension domain have been genetically identified, but they are mechanistically not well explored (Dievart *et al.*, 2020).

1.3 S-domain receptor-like kinase

The family of S-domain (SD) receptor-like kinases, named after their ECDs, is the second-largest family of cell surface-localized receptors (Shiu and Bleecker, 2001, Shiu and Bleecker, 2003). An SD-RLK in maize was the first cloned and characterized RLK in 1990 (Walker and Zhang, 1990), even before the first LRR-RK (Dievart *et al.*, 2020). The “S-domain” was initially designated as the ECD of the S-locus receptor kinase (SRK) which contains an S-locus glycoprotein domain (SLG). *SRK* is localized close together with S-locus cysteine-rich peptide gene (*SCR/SP11*) in the *Brassica oleracea* locus, and this locus is called "S-locus" and is used to regulate the self-incompatibility (SI) response (Nasrallah *et al.*, 1987, Stein *et al.*, 1991). After self-pollen attachment to the stigma, SRKs can recognize specific SCRs from self-pollen. SRK interacts with SCR and induces a downstream signaling pathway that inhibits pollen germination during pollen-stigma interaction to avoid inbreeding (Kachroo *et al.*, 2001).

Homodimer, heterodimer, and oligomer are common forms in cell surface-localized receptors like PRRs introduced previously (Figure 2). The complex formation is an essential process for ligand binding and signaling (Couto and Zipfel, 2016). Firstly, SRK was found to form homodimers spontaneously without pollination and ligand induction, suggesting that the homodimerization of SRKs is SCR-independent (Giranton *et al.*, 2000, Shimosato *et al.*, 2007). In the *in vivo* studies, SRKs pre-form into dimers and shape binding pockets, which have higher binding affinity to SCR ligand compared with monomers. A yeast-based assays also proposed that an interface of SRK homodimer is involved in ligand-independent homodimerization (Naithani *et al.*, 2007, Shimosato *et al.*, 2007). However, *in vitro* studies elucidating the crystal structures of SRK9 and SRK8 from *Brassica* showed that SRK ECDs require SCR binding to enhance homodimerization and form hetero-tetramers (Ma *et al.*, 2016, Murase *et al.*, 2020). They suggested that other domains, like transmembrane domain (TM), are also involved in enhancing dimerization *in vivo*. After SCR ligand perception, SRKs activate downstream signaling via different cytoplasmic components. E3 ubiquitin ligase Armadillo Repeat Containing 1 (ARC1) is a direct interaction partner of the SRK intracellular domain (Gu *et al.*,

1998). When SRK phosphorylates ARC1, ARC1 can be translocated from the plasma membrane into the cytosol and activate the protein degradation process of unknown cytosolic proteins, leading to SI (Stone *et al.*, 2003). Disabling ARC1 can lead to losing SI (Abhinandan *et al.*, 2022).

The family of SD-RLKs has about 40 members in Arabidopsis. They primarily consist of two lectin-like domains (L), an epidermal growth factor-like domain (EGF), a plasminogen-apple-nematode domain (PAN) in their ECDs and a TM, a kinase domain, and a Domain of Unknown Function 3404 (DUF) in their intracellular domains (Figure 3a) (Shiu and Bleecker, 2003, Vaid *et al.*, 2012, Xing *et al.*, 2013, Teixeira *et al.*, 2018). In some studies and databases, the two lectin-like domains are annotated as a lectin-like domain and an SLG (Figure 3b) (Bellande *et al.*, 2017, Teixeira *et al.*, 2018). Due to the similarity of their lectin-like domains to the isolated agglutinin from *Galanthus nivalis* bulb (GNA), SD-RLKs are often termed bulb-type (B-type) or GNA-type (G-type) lectin RLKs (Teixeira *et al.*, 2018).

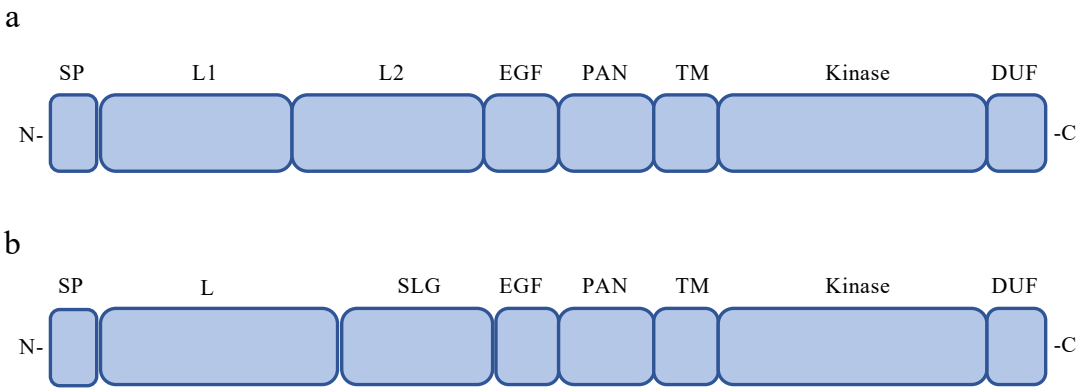

Figure 3. Schematic representation of domains in S-domain receptor-like kinases. The domains of SD-RLKs were annotated according to **a.** Naithani et al. and Ma et al. (Naithani *et al.*, 2007, Ma *et al.*, 2016) or **b.** Uniprot (ID: O64782, available on 2022 Oct. 28th). SP: signal peptide; L1: Lectin-like domain 1; L2: Lectin-like domain 2; L: Lectin-like domain; SLG: S-locus glycoprotein domain EGF: Epidermal growth factor-like domain; PAN: plasminogen-apple-nematode domain; TM: Transmembrane domain; Kinase: Kinase domain; DUF: Domain of unknown function 3404.

More than 40% of flowering plant species from over 100 families have SI systems. SRKs in S-loci were well-characterized for their roles in SI in Brassicaceae (Takayama and Isogai, 2005, Igic *et al.*, 2008). Yet, many other plants, such as rice, do not have SI systems but have SD-RLKs (Shiu *et al.*, 2004). The SI responses share many similarities with plant immunity. In SI, self-pollen is denied to block inbreeding, and PRRs recognize microbial patterns to prevent infection.

Both mechanisms are responsible for distinguishing between self- and non-self-objects, and they also share a similar way of signaling, but activate different pathways (Sanabria *et al.*, 2008). More functions of SD-RLKs, besides their role in reproduction have been identified. These SD-RLKs from, e.g., Arabidopsis, rice, tomato, wild soybean, and wheat are involved in abiotic stress responses, tissue development, cell growth, pathogen-host interactions, and symbiosis (Charpenteau *et al.*, 2004, Chen *et al.*, 2006, Bonaventure, 2011, Chen *et al.*, 2013, Cheng *et al.*, 2013, Sun *et al.*, 2013a, Zhao *et al.*, 2013, Catanzariti *et al.*, 2015, Ranf *et al.*, 2015, Zou *et al.*, 2015, Fan *et al.*, 2018, Pan *et al.*, 2020, Kato *et al.*, 2022, Pi *et al.*, 2022, Rosa *et al.*, 2022). *Glycine soja* S-LOCUS LecRK positively enhances plant stress tolerance under salt stress and regulates osmotic homeostasis (Sun *et al.*, 2013a, Sun *et al.*, 2018). SD-RLK OsSIK2 in rice confers abiotic stress resistance and regulates leaf senescence in rice (Chen *et al.*, 2013), Another rice SD-RLK was found to be involved in immune responses as well as seed germination (Cheng *et al.*, 2013). Rice SD-RLK OsESG1 regulates root development and drought resistance (Pan *et al.*, 2020). The tomato SD-RLK I-3 enhances the resistance against *Fusarium* wilt disease (Catanzariti *et al.*, 2015). The *Nicotiana benthamiana* SD-RLK expansin-regulating kinase 1 positively mediates plant resistance to *Phytophthora capsici* (Pi *et al.*, 2022). The SD-RLK RESISTANT TO DFPM-INHIBITION OF ABSCISIC ACID SIGNALING 2 (RDA2), also known as SD1-12 in Arabidopsis, was identified as a PRR for sensing derivatives of sphingolipids like 9-methyl sphingoid base. These immunogenic patterns are actively cleaved off from sphingolipids by Arabidopsis apoplastic ceramidase NEUTRAL CERAMIDASE 2 (Kato *et al.*, 2022). Although SD-RLKs were identified to be essential in stress response, development, and others, the mechanistic understanding of SD-RLK in regulating these functions remains mostly unknown, largely because their ligands are unknown.

1.4 LORE-dependent immunity — from LPS to 3-OH-FA

The SD-RLK LIPOOLIGOSACCHARIDE SPECIFIC REDUCED ELICITATION (LORE), also known as SD1-29 from *A. thaliana,* was initially identified as a PRR for sensing lipopolysaccharide (LPS) as a MAMP, which is released from Gram-negative bacteria (Ranf *et al.*, 2015). LPS from *Pseudomonas* and *Xanthomonas* trigger LORE-dependent PTI and induce systemic resistance against bacterial pathogens in Arabidopsis. The closest paralog of LORE, SD1-23 is not involved in LPS sensing, indicating that LORE is an indispensable receptor for LPS (Ranf *et al.*, 2015). LORE-mediated sensing of LPS was only discovered in Brassicaceae.

Species from Solanaceae, like *N. benthamiana* and *N. tabacum,* can gain the functions of perceiving LPS by transiently expressing LORE, implying that SD-RLK-induced downstream signaling may be commonly shared by many families (Ranf *et al.*, 2015). LPS was perceived specifically through its lipid A moiety, the part anchored in the bacterial plasma membrane, while its polysaccharide did not trigger LORE-dependent immune responses in Arabidopsis (Ranf *et al.*, 2015).

However, in 2019, it was shown that medium chain-3-hydroxy fatty acid (mc-3-OH-FA) was sufficient to induce LORE-dependent PTI. The elicitor-active LPS comprises a 3-hydroxyl medium acyl chain in its lipid A moiety. Highly purified LPS without mc-3-OH-FA contamination did not activate immune responses in Arabidopsis, meaning that the previous LPS used in the experiments was not a mc-3-OH-FA-free elicitor (Kutschera *et al.*, 2019). mc-3-OH-FAs with aliphatic tails of 8 to 12 carbons, particularly 3-hydroxydecanoic acid (3-OH-C10:0), trigger LORE-dependent immune responses, including ROS burst, cytoplasmic [Ca^{2+}] influx, activation of the mitogen-activated protein kinases (MAPKs), and other defense-related responses (Figure 4). However, 3-OH-FAs with longer aliphatic tails like 13, 14, and 16 carbons cannot trigger immune responses, indicating that LORE senses 3-OH-FAs in a chain length-specific manner (Kutschera *et al.*, 2019). As in the previous study, *N. benthamiana* can gain the function of sensing mc-3-OH-FAs in a chain length-specific manner by transiently expressing LORE (Kutschera *et al.*, 2019). In a detailed structure-activity study, 3-OH-FAs in their free forms revealed the strongest elicitor activity in Arabidopsis. The position of the hydroxyl group, modification of the carboxyl group, the saturation of acyl chain, as well as absolute configuration affect their immunogenic activities (Kutschera *et al.*, 2019). 3-hydroxyalkanoate (HAA), the precursor of bacterial rhamnolipid, consists of two 3-OH-C10:0 moieties and also elicits LORE-dependent immune response (Schellenberger *et al.*, 2021). The phosphorylation of the LORE kinase domain is also activated upon 3-OH-C10:0 elicitation, and subsequentially LORE kinase phosphorylates the downstream immune-related signaling components, including receptor-like cytoplasmic kinases (RLCK) AVRPPHB SUSCEPTIBLE 1 (PBS1)-like 1 (PBL) proteins (Luo *et al.*, 2020). Arabidopsis cytoplasmic Plant U-box proteins (PUBs) can directly interact with the LORE kinase domain (Samuel *et al.*, 2008). Recently, the RLCK RPM1-INDUCED PROTEIN KINASE (RIPK) was shown to be a regulator of the mc-3-OH-FA-induced signaling pathway (Li *et al.*, 2021, Wu *et al.*, 2022).

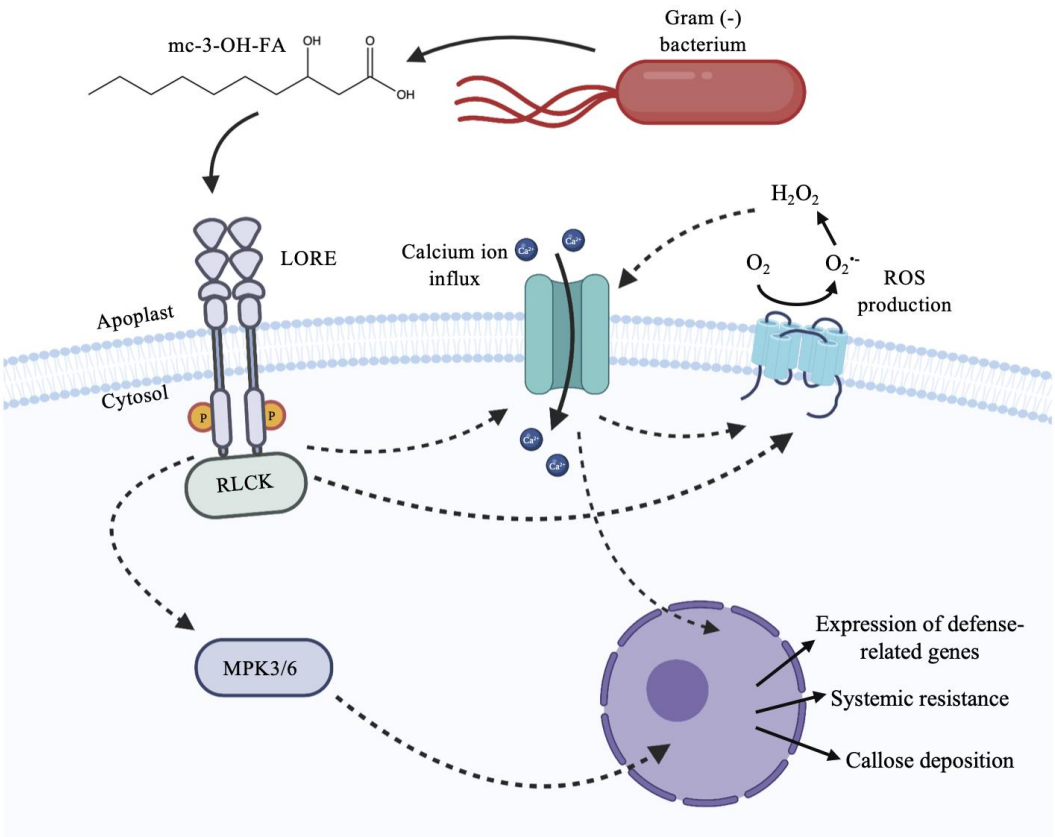

Figure 4. Overview of LORE-dependent immune signaling. Medium-chain 3-hydroxy fatty acid (mc-3-OH-FA) is released from gram-negative bacteria and perceived by LORE. After elicitation, the LORE dimer autophosphorylates and trans-phosphorylates receptor-like cytoplasmic kinases (RLCK) for further triggering cytosolic calcium ion influx and reactive oxygen species (ROS) production in the apoplast. These two mechanisms positively regulate each other. LORE also activates the mitogen-activated protein kinases (MAPKs) MPK3/6 and further induces plant defense-related responses. The figure was created with BioRender.com.

LORE expression could be activated upon damage in the early differentiated cells in the root. In addition, LORE-dependent responses were powerfully elicited by 3-OH-C10:0 directly in the root elongation zone, indicating that LORE expression is co-regulated by different stresses and reveals different expression patterns in the plant (Zhou *et al.*, 2020).

SRKs form homodimers for perceiving two SCRs according to crystallographic analyses (Ma *et al.*, 2016, Murase *et al.*, 2020). LORE also can homodimerize without ligand treatment (Figure 4) (Eschrig *et al.*, 2021). With experiments *in planta* and *in vitro*, LORE was shown to form homomers mainly through its ECD and TM (Eschrig *et al.*, 2021). *Arabidopsis lyrata* and *Arabidopsis halleri*, which have LORE orthologs, but do not respond to mc-3-OH-FA. These

LORE orthologs do not form dimers and activate immune signaling, implying that dimerization is essential for LORE-dependent signaling (Eschrig *et al.*, 2021). Co-expressing LORE and kinase domain-truncated LORE revealed that the LORE-dependent responses were suppressed by an excess of kinase-truncated LORE. These results suggest that homomerization and a functional kinase domain are indispensable for LORE-dependent signaling (Eschrig *et al.*, 2021).

1.5 Biomolecular interaction techniques

Ligand-receptor interactions are crucial for many physiological processes in plants, including cell development, tissue growth, and immunity. When receptors sense and bind ligands, downstream signaling pathways are induced or inhibited by them (Hohmann *et al.*, 2017). Exploring these essential receptor-ligand complexes can broaden the understanding of molecular mechanisms that govern physiological processes. Ligand-receptor interactions need to be carefully confirmed by different techniques. In the previous sections, many receptor-ligand pairs have been introduced, and the biochemical mechanisms in these cases were verified through various strategies and methods. Techniques *in vitro* can provide an independent environment to resolve the authentic interactions between molecules. Many quantitative methods for describing biomolecular interactions allow to access binding affinity, kinetics, and specificity. These characteristic findings can further explain the association between molecules (Sandoval and Santiago, 2020). However, there are considerable differences between different technologies, which may limit the types of receptor-ligand pairs that can be studied. Applying appropriate techniques according to the molecular properties of the research objects is an essential issue before starting the task. Performing binding assays with labeled ligands or labeled receptors are two major approaches. Chemical modification to receptor and ligand may enhance the detectability of some biomolecular interactions. Label-free ligand binding assay can determine receptor-ligand interactions without the potential interference from labels Next, several standard methods are discussed for their contribution to the research of plant receptor-ligand interaction.

Microscale thermophoresis (MST) is a powerful tool for measuring biomolecular interactions. MST is performed in solution and does not require immobilization of protein but labeling with a fluorophore. MST monitors the directed movement of molecules with fluorophore through temperature gradients in microliter volumes, allowing for the accurate analysis of binding manners. Because MST is able to measure mild changes in fluorescent intensity, precise

quantification of biomolecular interaction becomes achievable (Jerabek-Willemsen *et al.*, 2014). MST assays requires fluorophore labeling of the target protein for detection with the corresponding laser. The infrared (IR) laser generates a temperature gradient in the sample capillary. During the process of inducing the temperature gradient, the fluorescent signal is monitored by the objective, and the diffusion of fluorophores in the temperature gradient is measured (Figure 5). The property of receptor protein alone differs from the receptor-ligand complex, such as molecular weight, charge, hydration shell, or conformation, which affects the rate of diffusion in the temperature gradient (Figure 5). The changes in diffusion patterns at different concentrations of the target ligand are observed by performing dilution series of the ligand in capillaries. The changes of diffusion can be further plotted to acquire dissociation constant and compare binding affinity between different receptor-ligand combinations (Figure 5) (Jerabek-Willemsen *et al.*, 2014). In addition to the standard MST machine, performing label-free MST experiments is also achievable. The machine type equipped with an UV-light diode for excitation and a photomultiplier tube to monitor emission can detect tryptophan fluorescence in protein (Jerabek-Willemsen *et al.*, 2014). Although the MST assay requires specialized equipment and consumables, such as capillaries and protein-labeling dyes, the low volume requirement (less than 10 µL for each capillary) and the tolerance of crude samples make MST accessible to study the low-yield and low-purity proteins.

MST has been applied in plant science for over a decade and used to characterize a few cell surface-localized receptor-ligand pairs. Three RALF-receptor interactions, RALF4/19 with LEUCINE-RICH REPEAT EXTENSIN (LRX) 8, RALF1 with THESEUS1 (THE1), and RALF23 with FERONIA were verified by MST (Mecchia *et al.*, 2017, Stegmann *et al.*, 2017, Gonneau *et al.*, 2018). The binding of LRR-RLK SUCROSE-INDUCED RECEPTOR KINASE 1 (SIRK1) to PEP7 was also shown by MST (Wang *et al.*, 2022). Although performing MST with proteinaceous ligands seems to be a reliable approach that can measure the dissociation constant (Kd), the level of binding affinity, down to the pico-molar level, studying receptor-fatty acid interaction by MST proved to be difficult (Kutschera *et al.*, 2019).

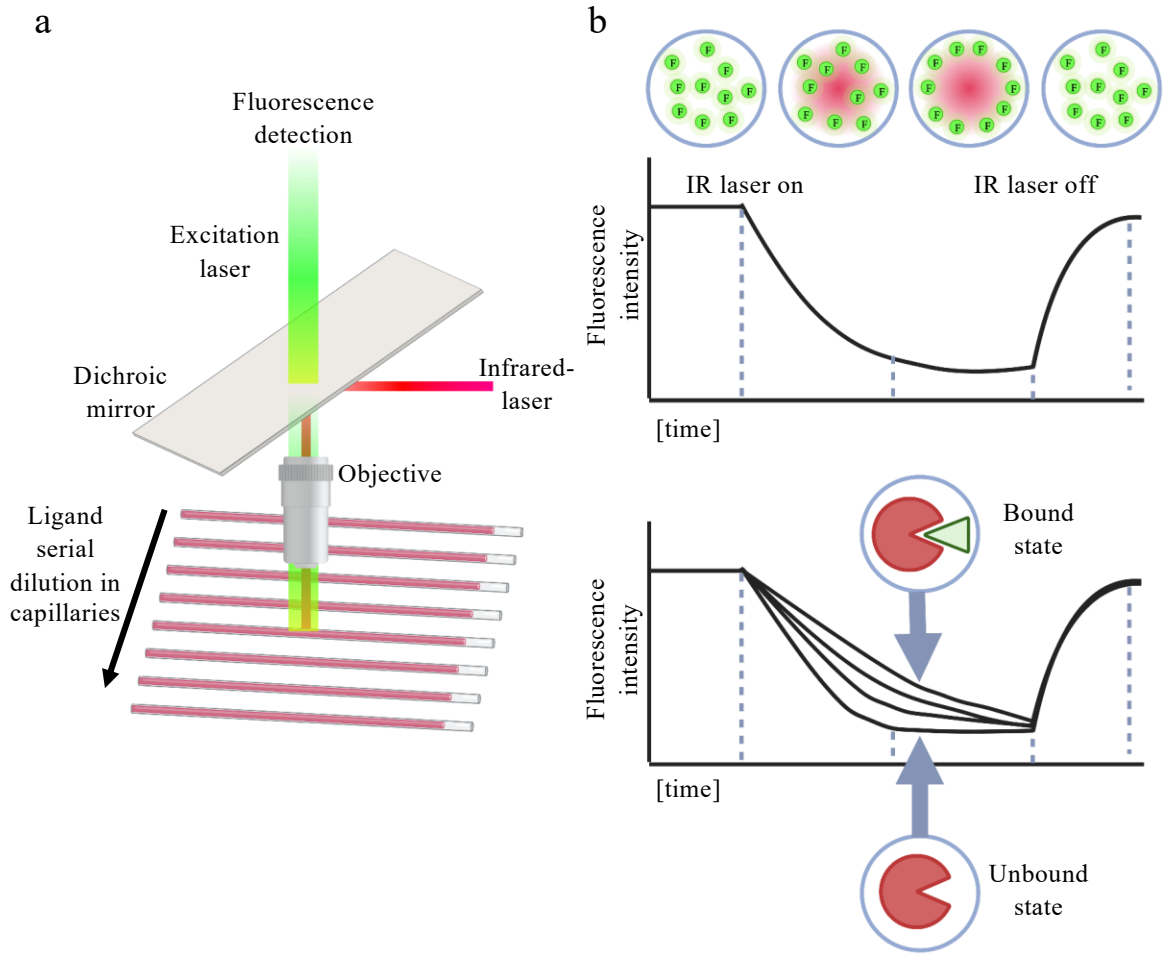

Figure 5. Binding assay by microscale thermophoresis (MST). a. Representation of MST setup. MST is measured in capillaries containing low-volume (less than 10 µL) mixtures. The ligand is two-fold serially diluted in different capillaries, and the target protein is kept constant in all mixtures. The target protein labeled with fluorophores in the capillary is excited by a designated laser and measured by the detector through the objective. The infrared (IR)-laser heats the sample in the capillaries, and fluorescence at the heated spot is detected. **b.** Representation of MST assay. Upper: The molecules with fluorophores are initially homogeneously distributed in the capillary and the initial fluorescent signal is measured. After exited by IR-laser, the molecules diffuse away from the center of the temperature gradient spot, and fluorescent intensity from the center gradually decreases. Based on the molecule's property, the molecule diffusion rate varies. After turning IR-laser off, the molecules diffuse back to the center space homogeneously. Lower: When the receptor binds to the ligand, the physical property of the receptor slightly changes and the diffusion rate of receptor-ligand complex is slower than unbound receptor. The higher thermostability of the complex at the temperature gradient spot leads to slower diffusion, and the proportion of bound ("Bound state") and unbound receptors ("Unbound state") determines the different rates of diffusion and the change of fluorescence intensity during IR-laser heating. The figure was created with BioRender.com.

The radiolabeled-ligand binding assay (hereafter, radiobinding assay) is a relatively simple, flexible, and powerful tool for studying biomolecular interaction. The target ligands are labeled by the radioisotopes which can emit alpha particles, beta particles, or gamma rays. Depending on the type of isotope, the radiation energy is usually high enough for the detection in a scintillation counter. Radiobinding assay can measure the affinity down to the picomolar level. Radiobinding assays to study cell surface-localized receptors can be performed with purified proteins, microsomal fractions containing the protein-of-interest, and even intact cells (Cosio *et al.*, 1988, Biswas *et al.*, 1995, Choi *et al.*, 2014, Vauquelin *et al.*, 2015, Wang *et al.*, 2019). There are two assay formats for measuring radioligands. Traditionally, filtration ligand binding assay requires filters for retaining complexes during washing steps to remove unbound radioligands. By contrast, scintillation proximity assay (SPA) does not need washing steps but utilizes special mircobeads to capture complexes and emit signals that can be measured (Xia *et al.*, 2016). Three types of assays for radioligand binding assays: saturation binding assay, competition binding assay (Figure 6), and kinetic binding assay are used to quantify the strength of the intermolecular interactions (Maguire *et al.*, 2012). Saturation binding assay can measure binding equilibrium by performing a titration of radioligand and keeping the concentration of protein-of-interest constant. With this, the maximal binding capacity and Kd of the protein-ligand complex can be determined (Figure 6). Competition binding assay can measure radioligand binding at a constant concentration with different concentrations of a "cold" competitor without radiolabeling. In this way, it can compare the binding affinity of various competitors without labeling each ligand candidate (Figure 6). Kinetic assays are utilized to evaluate the rates of the receptor-ligand association constant and Kd by measuring the binding levels at various times. Despite these advantages, a major disadvantage is the handling of hazardous radioactive compounds, which requires specialized facilities and sophisticated handling skills.

The radiobinding assay has been applied to verify the interactions of cell surface-localized receptor-ligand pairs. Brassinosteroid-insensitive 1 (BRI1), a LRR-RLK, was found to be the receptor for the phytohormone brassinosteroid, which is involved in plant development, by using tritium-labeled brassinosteroid and plant-expressed BRI1 (Wang *et al.*, 2001). The direct binding of FLS2 and flg22 was first characterized by the radiobinding assays with [^{125}I]-Tyr-flg22 and receptors extracted from plant cells (Chinchilla *et al.*, 2006). Two eATP binding receptors, P2K1 and P2K2, were also verified by using [^{32}P]-ATP and recombinant proteins from *E. coli* (Choi *et*

al., 2014, Pham *et al.*, 2020), and two LecRKs for sensing $NADP^+$ and NAD^+ were also characterized with a similar approach (Wang *et al.*, 2017, Wang *et al.*, 2019).

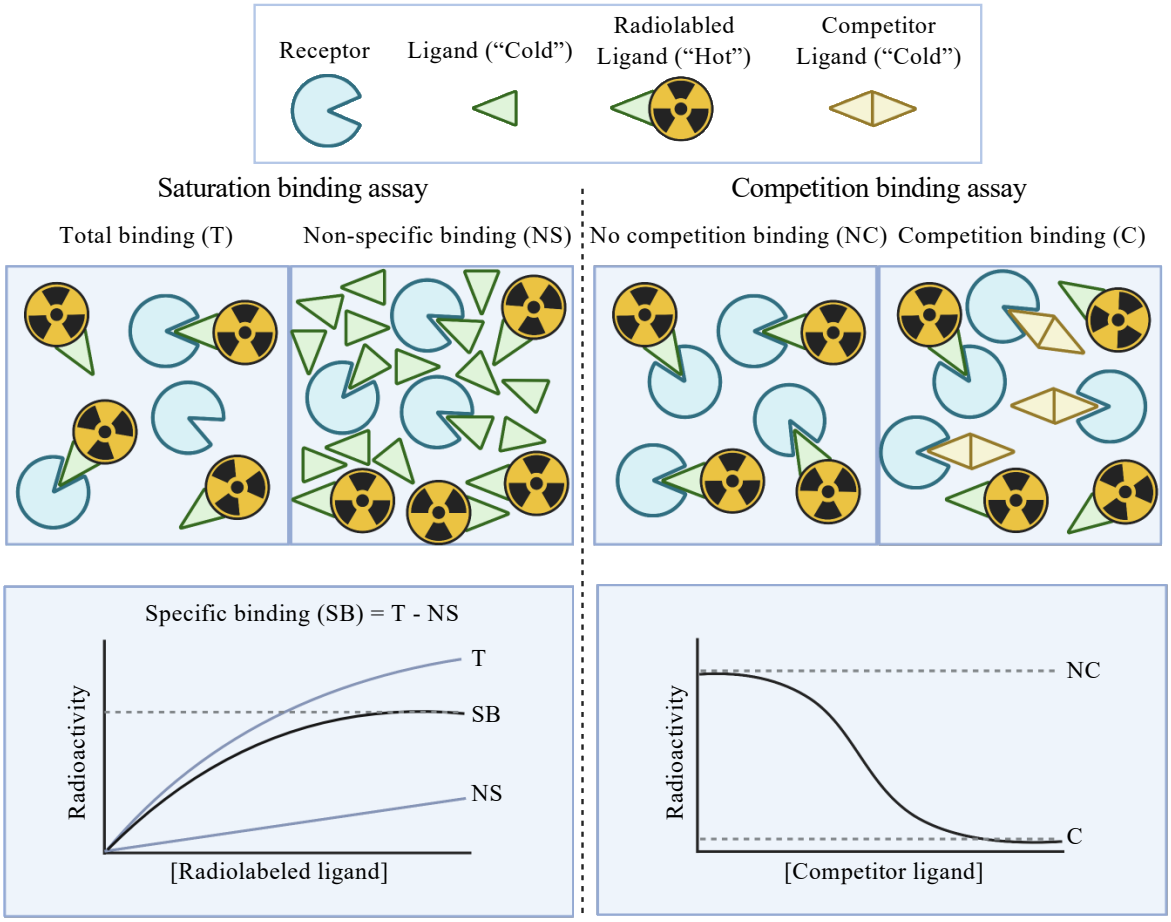

Figure 6. Radioligand binding assay. Ligand binding to a receptor can be evaluated using two kinds of radioligand binding assays: saturation binding assay (left) and competition binding assay (right). Saturation radioligand binding assay can determine the maximal binding capacity (B_{max}) and the ligand's dissociation constant (Kd) to the receptor. Total binding (T) and nonspecific binding (NS) need to be measured for the saturation binding assay. To measure T and NS bindings, the concentration of receptors is constant, and the concentration of labeled "hot" ligands is variable. The reaction of NS binding contains excess unlabeled "cold" ligands. T minus NS is equivalent to specific binding (SB). Kd can be calculated using nonlinear regression, and the concentration of the saturated state can determine B_{max}. Competition assays can compare the binding affinity between homologous ligands (unlabeled competitor ligands against identical radiolabeled ligands) or heterologous ligands (unlabeled analogs against radiolabeled ligands). In the competition assay, the concentrations of receptor and hot ligand are constant, and the concentration of unlabeled "cold" competitor varies. No competition binding (NC) indicates that the cold competitor with a specific concentration is insufficient to outcompete the hot ligand. At the same time, it reaches complete competition binding

(C) when the cold competitor with a higher concentration entirely outcompetes the hot ligand. This figure was adapted from Hellmuth and Calderón Villalobos's protocol and created with BioRender.com (Hellmuth and Calderón Villalobos, 2016).

Due to the required radioactive-labelled ligand, the radiobinding assay is not always suitable and available for every case. The chemiluminescent labeled-ligand binding assay is conceptually similar to the radiobinding assay but is based on luminescent labels, like acridinium-esters, labeled on the ligands, and this binding assay has verified some receptor-ligand pairs. In plant receptor-ligand research, FLS2-flg22 (Butenko *et al.*, 2014) and In-Vu-inceptin receptor (INR) (Steinbrenner *et al.*, 2020), both peptide-LRR receptor pairs, were characterized by this system. When a ligand can be biotinylated without affecting its bioactivity, the biotinylated ligand-receptor interaction can be detected by co-precipitating ligand-receptor complex with streptavidin. For instance, biotin-labeled chitin was used to prove chitin binding to CEBiP in rice (Hayafune *et al.*, 2014).

The label-free binding assay is another major approach for studying biomolecular interaction. Isothermal titration calorimetry (ITC) is a technique for measuring binding and enzymatic reactions by determining the thermodynamic changes of molecular interactions in solution (Freire *et al.*, 1990). The significant advantage of using ITC for the binding assay is that it does not require modification of the receptors or ligands, which may interfere with binding. It is also a robust technique for detecting mild interactions (Falconer, 2016). However, ITC measurement requires much large amounts of samples than the methods above and also needs specialized equipment. ITC was used to verify some plant receptor-ligand interactions in the past two decades, such as CERK1-chitin, MIK2-SCOOPs, and FERONIA-RALF23 (Liu *et al.*, 2012, Xiao *et al.*, 2019, Hou *et al.*, 2021b, Rhodes *et al.*, 2021). Another labeled-free binding assay requiring specialized devices and consumables is surface plasmon resonance (SPR), an optical technique that can monitor biomolecular interactions in real time, like association and dissociation (Jain *et al.*, 2016). Although the proteins for SPR assay require immobilization to a chip, it allows to determine the kinetics of the interactions (Olaru *et al.*, 2015). Recently, RDA2 was demonstrated to be able to bind to sphingolipids by SPR (Kato *et al.*, 2022). Other label-free ligand binding assays like grating-coupled interferometry, biolayer interferometry, and differential scanning

fluorimetry provide more options for application in studying diverse biomolecular interactions (Sandoval and Santiago, 2020).

1.6 Brassicaceae — a model family for plant science

Brassicaceae, previously called Cruciferae based on their cross-like flower, is a diverse plant family containing 372 genera and 4,060 species spread worldwide (Borsch *et al.*, 2020). Brassicaceae include many important crops like cabbage and broccoli (*Brassica oleracea*), turnip (*Brassica rapa*), arugula (*Eruca vesicaria*), and mustard (*Sinapis alba*). The most well-known model plant, *A. thaliana,* also belongs to Brassicaceae, and its genome databases, annotation, research tool, and a large number of mutants and ecotypes for genetic screening strongly contributed to the development of plant research (Somerville and Koornneef, 2002, Koornneef and Meinke, 2010, Koenig and Weigel, 2015). In the past ten years, many close or far relatives of *A. thaliana* within Brassicaceae and its sister family Cleomaceae have been whole-genome sequenced in the scope of several mega-sequencing programs, and their genetic information was analyzed based on the model plant. For example, Brassicales Map Alignment Project (BMAP) has generated and analyzed genome and transcriptome data from 20 species (DOE-JGI). The availability of Brassicaceae genomic resources brings substantial benefits to genomic, transcriptomic, proteomic, metabolomic and evolutionary studies. Therefore, Brassicaceae offers an excellent system for comparative studies and an open platform for mechanistic research, including PTI and various PRRs (Winkelmüller *et al.*, 2021).

1.7 Objectives

The previous studies revealed that LORE is an indispensable receptor for sensing mc-3-OH-FA, but not LPS, in a chain length-specific manner (Ranf *et al.*, 2015, Kutschera *et al.*, 2019). How LORE senses mc-3-OH-FAs at the molecular level and whether other Brassicaceae species closely related to *A. thaliana* have functional LORE orthologs have yet to be determined. To unveil the mechanism of LORE-mediated 3-OH-FA sensing in Brassicaceae in detail, the following subprojects were conducted in the scope of this thesis:

1. Method establishment for validating LORE-3-OH-FA interaction

The first goal of this study is to establish a reliable system *in vitro* that can assess the interaction btweeen LORE and mc-3-OH-FA.

2. Investigation of 3-OH-FA sensing diversity in Brassicaceae

This part of the study will investigate a wide range of Brassicaceae species and *A. thaliana* ecotypes for 3-OH-FA sensing.

3. Functional analysis of LORE orthologs in Brassicaceae

This research subject will systematically investigate the functions of LORE orthologs and related SD-RLKs from diverse Brassicaceae plants.

4. Identification of 3-OH-FA binding structure in LORE

This research subject will identify the potential 3-OH-FA-binding structure on LORE by *in silico* and *in vitro* approaches based on the previous results.

2 Results

2.1 Method establishment for validating LORE-3-OH-FA interaction

To uncover the mechanisms of LORE and mc-3-OH-FA interaction, the establishment of both biological and chemical approaches is required. The previous study showed by different genetic and biochemical approaches that *A. thaliana* LORE (hereafter AtLORE) is the receptor for mc-3-OH-FA; unfortunately, the biochemical approach used in this study is quite costly and not easily applicable to screening a large number of candidates (Kutschera *et al.*, 2019). To study the receptor-3-OH-FA interaction in molecular detail, I aimed for reliable, widely applicable, and also less costly protein expression procedures and biomolecular interaction techniques. This section introduces three alternative approaches to the expression of the AtLORE ECD protein and shows two commonly used and one newly-established ligand-binding assays for assessing LORE-3-OH-FA interaction.

2.1.1 Establishment of AtLORE ECD protein expression methods

E. coli recombinant protein expression of AtLORE ECD

Expressing recombinant proteins in *E. coli* is a widely used method, often for rapidly and economically producing large quantities of protein. In previous studies, no plant SD-RLK ECD was expressed in *E. coli*, and it is unknown whether this was related to the inability of bacteria to express SD-RLK ECDs and fold them correctly. To answer this question and develop an efficient protein expression system, the AtLORE ECD (eAtLORE) was attempted to be expressed in *E. coli*. eAtLORE fused with maltose-binding protein (MBP) was expressed under the control of the isopropyl-β-D-thiogalactoside (IPTG)-inducible T7 lac promoter in several commercial protein expression strains. However, the expressed eAtLORE-MBP proteins were not soluble and aggregated mainly in inclusion bodies in insoluble fractions (Supplementary Figure 1a, 1b). Different conditions for expression, such as concentration of IPTG, temperature, and incubation time, were also tested. While these optimized the yield of expressed eAtLORE, they did not improve protein solubility (Supplementary Figure 1c). The results suggested that expressing eAtLORE in bacteria does not yield soluble protein, which is the required form for most functional studies, including binding assay. To test the possibility of reducing the size of the protein to increase its solubility, two adjacent N-terminal subdomains of AtLORE, lectin-like domain 1 and lectin-like domain 2, were expressed as MBP fusions in *E. coli*. The recombinant

protein remained insoluble and accumulated in inclusion bodies (Supplementary Figure 1d). Taken together, recombinant eAtLORE proteins could not be expressed in a soluble form in *E. coli*.

Cell-free protein expression system for AtLORE ECD

Expressing recombinant proteins in *in vitro* systems is an alternative approach. The cell-free protein expression method was developed for target proteins that are difficult to express, such as toxic and insoluble proteins. Target proteins are translated in cell lysate which can be derived from various cells containing the necessary expression apparatus with the addition of energy sources, amino acids, and salts (Silverman *et al.*, 2020). The most widely commercial cell-free protein expression systems are from *E. coli*, wheat germ cell, rabbit cell, and insect cell (Khambhati *et al.*, 2019). To utilize the suitable cell type for expressing eAtLORE, tobacco cell-based cell-free protein expression system ALiCE (LenioBio, Germany) was chosen as tobacco can ectopically express functional AtLORE for 3-OH-FA-triggered signaling (Kutschera *et al.*, 2019). For cell-free expression, AtLORE was fused with a Strep-tag for purification and a yellow fluorescent protein (YFP) as a marker for microscopy and immunoblot. Alternatively, melittin signal peptide (MSP) was also fused to one of the AtLORE-expressing constructs to potentially guide eAtLORE through the post-translational modification and enter microsomes. The soluble eAtLORE-YFP-Strep proteins were expressed by the ALiCE system. eAtLORE-YFP-Strep with MSP was slightly bigger than eAtLORE-YFP-Strep without MSP, suggesting that it was indeed post-translationally modified (Supplementary Figure 2a). However, the expression of AtLORE-YFP-Strep was less efficient than the control YFP-Strep (Supplementary Figure 2a). Subsequently, eAtLORE-YFP-Strep was subjected to Strep-Tag purification, but it failed to be entirely retained by Strep-Tactin and could not be properly eluted (Supplementary Figure 2b). The cell-free protein expression coupled with Strep-tag purification is not an applicable process for producing pure eAtLORE in sufficient amounts; possibly, fusing other epitopes at different positions might be a way to improve expression efficiency.

AtLORE ECD expressed in *N. benthamiana* leaves can be collected in apoplastic washing fluids

The third method tested in this study was the transient expression of eAtLORE in *Nicotiana benthamiana*. The previous study showed that *N. benthamiana* does not respond to 3-OH-C10:0 elicitation, indicating it does not have a receptor for mc-3-OH-FA (Kutschera *et al.*, 2019), so

eAtLORE expression in *N. benthamiana* may circumvent the potential problem of interference from functionally similar proteins. Moreover, *N. benthamiana* gained the function of responding to mc-3-OH-FAs by transiently expressing full-length AtLORE, but not a kinase-inactive control, indicating eAtLORE was able to perceive mc-3-OH-FA upon ectopic expression (Kutschera *et al.*, 2019). eAtLORE fused to mCherry, a red fluorescent protein to supply a visual tag for the localization of the protein and an epitope for detection, was expressed. In addition, as a control, mCherry was fused to the signal peptide of AtLORE (amino acids 1st-21st) and secreted to the apoplast (apo-mCherry) (Figure 7a) (Shu *et al.*, 2021). To test whether it could be applied to other ECDs of SD-RLKs, eCrubLORE, the AtLORE ortholog from *Capsella rubella* (sharing 93% amino acid identity), and eAtSD1-23, the closest SD-RLK homolog of AtLORE (sharing 77% amino acid identity) in Arabidopsis, were transiently expressed in *N. benthamiana.* Expression levels of eCrubLORE-mCherry and eAtSD1-23-mCherry were comparable to eAtLORE-mCherry in tobacco apoplasts (Figure 7a) (Shu *et al.*, 2021). The apoplastic mCherry fusion proteins in the tobacco leaves were extracted by collecting apoplastic washing fluids (AWFs) without cell lysis. The mCherry fusion proteins were visible in AWFs (Figure 7a). The concentrated target proteins were largely degraded in AWFs (Figure 7b). The degradation is likely due to proteases present in the apoplast and degradation of the protein-of-interest before harvesting, which is not prevented by adding protease inhibitors during AWF collection (Robert *et al.*, 2013).

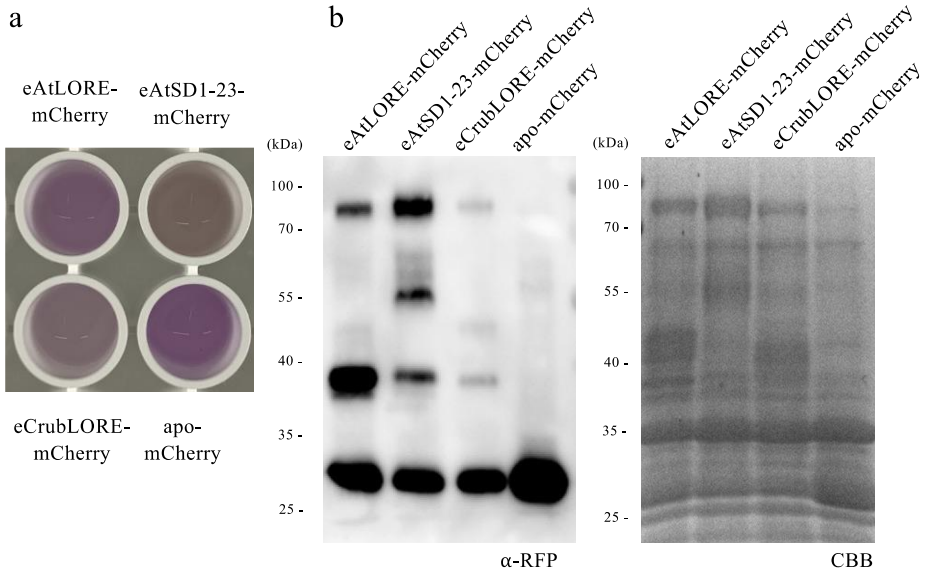

Figure 7. Transient expression of SD-RLK extracellular domains (ECDs) in the apoplast of *Nicotiana benthamiana* leaves. **a** Photograph of apoplastic washing fluid (AWF) of *N. benthamiana* leaves expressing

different SD-RLK ECD-mCherry fusion proteins and apoplastic mCherry. **b** Anti-RFP immunoblot of desalted and concentrated AWFs from *N. benthamiana* leaves expressing different SD-RLK ECD-mCherry fusion proteins or apo-mCherry. AWFs corresponding to 7.5 μg total proteins were loaded. The calculated molecular weights of SD-RLK ECD-mCherry fusions and mCherry are 70-75 kDa and 26.7 kDa, respectively. Equal loading of the samples was confirmed by Coomassie Brilliant Blue (CBB) staining of the SDS-polyacrylamide gel before blotting. One representative immunoblot of three experiments is shown.

2.1.2 Ligand-depletion binding assay

mc-3-OH-FA depletion assay

To verify the AtLORE-mc-3-OH-FA interaction, I utilized the molecular weight difference between proteins of interest (POI, 65-75 kDa for SD-RLK ECD-mCherry fusions and 25-30 kDa for apo-mCherry) (Figure 8) and 3-OH-FA ligands (<1 kDa). After incubation of a defined amount of 3-OH-C10:0 ligand with concentrated AWF containing an excess of POI, the unbound ligand was separated from ECD-ligand complexes by filtration through a membrane with a molecular weight cutoff (MWCO) of 30 kDa, which is between the molecular weight of the free ligand and the MW of the ECD-ligand complex (Figure 8). In case 3-OH-C10:0 binds to the POI, it is retained in the retentate (>30 kDa), whereas free 3-OH-C10:0 ligand passes through the filter and is found in the filtrate (<30 kDa).

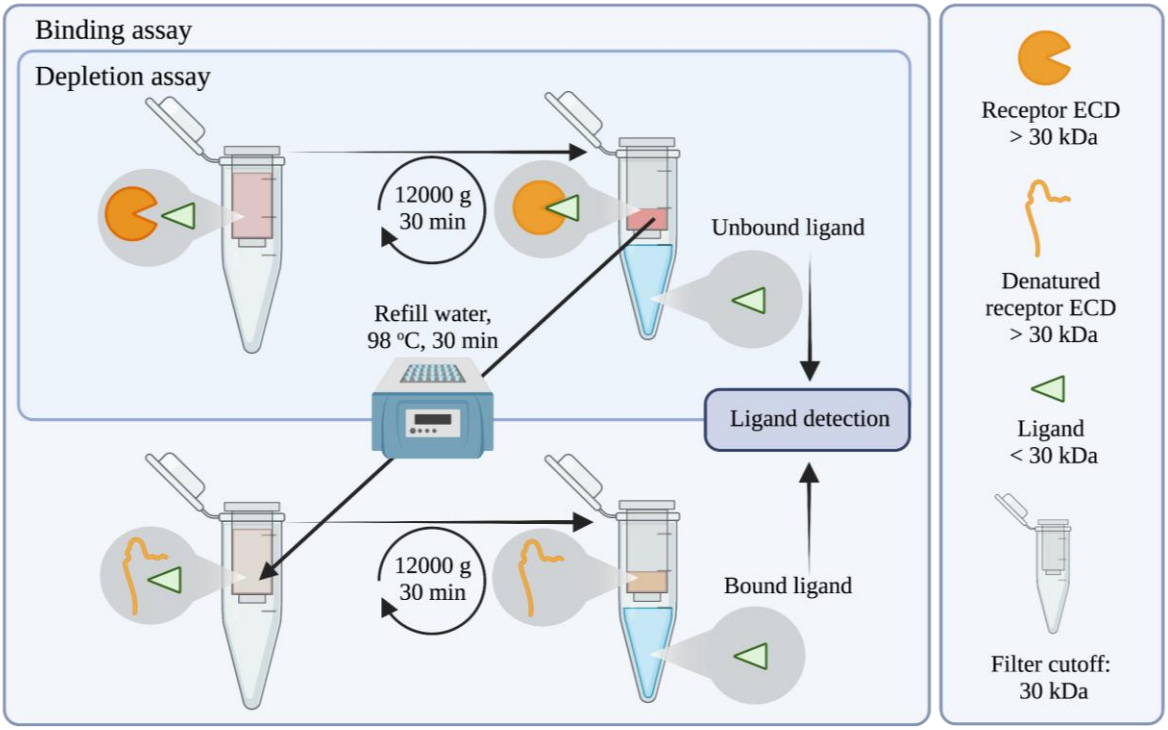

Figure 8. Schematic overview of the depletion-binding assay. The ligand (<30 kDa) is incubated with concentrated apoplastic washing fluids collected from *Nicotiana benthamiana* leaves transiently expressing the ECD of the receptor fused to mCherry (>30 kDa). Depletion assay: The mixture is loaded into a centrifugal filter with a 30 kDa molecular weight cut-off. After centrifugation, the unbound ligand is found in the filtrate and ECD-ligand complexes in the retentate. The unbound ligand is detected by a designated method. Depletion of the ligand from the filtrate indicates binding to the ECD. Binding assay: The concentrated retentate is refilled with water up to the original volume, and proteins in the retentate are heat-denatured at 98°C for 30 minutes. The released ligand is separated from the protein by another filtration step. The ligand released from the ECD-ligand complex is found in the filtrate and detected by a designated method. The schematic was created with BioRender.com.

Unbound 3-OH-C10:0 in the filtrate was measured in a sensitive bioassay by using the luminescent calcium reporter aequorin to measure 3-OH-C10:0-triggered cytosolic calcium signaling in Col-0^{AEQ} Arabidopsis seedlings (Knight et al., 1991). Col-0^{AEQ} can respond to 3-OH-C10:0 at concentrations of about 50 nM and above, covering the concentration of 3-OH-C10:0 used in the depletion assay (Figure 9) (Kutschera *et al.*, 2019, Shu *et al.*, 2021).

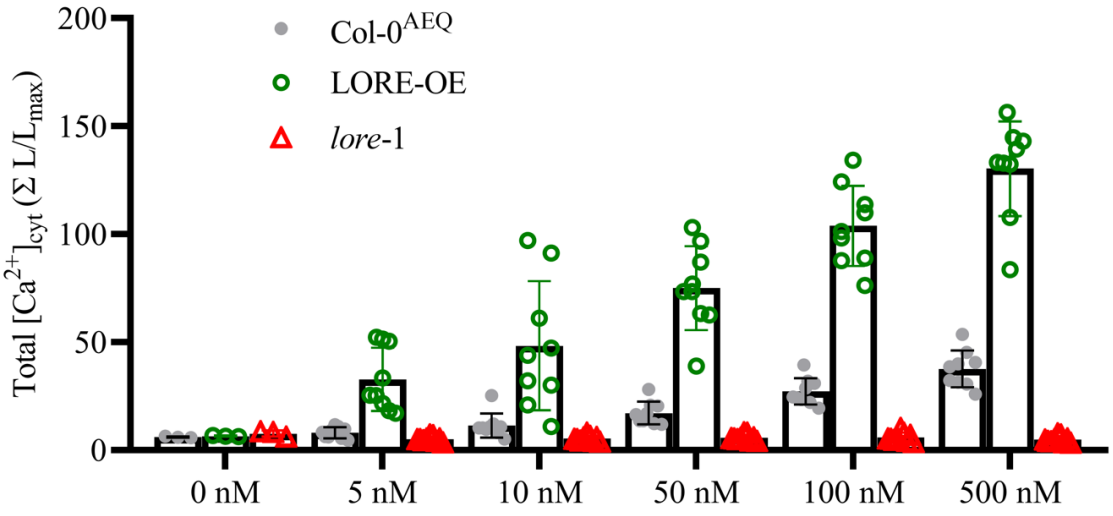

Figure 9. LORE-dependent increase of $[Ca^{2+}]_{cyt}$ induced by 3-OH-C10:0 in a dose-dependent manner. Total $[Ca^{2+}]_{cyt}$ level measurements of Col-0^{AEQ}, *lore*-1 mutant overexpressing AtLORE (LORE-OE), or *lore*-1 seedlings elicited with different concentrations of 3-OH-C10:0 in the range of 0-500 nM (mean ± SD, n = 9 seedlings, data from three independent experiments were pooled).

AWF containing apo-mCherry did not decrease 3-OH-C10:0 levels in the filtrate compared to a control containing water instead of AWF, suggesting that neither apo-mCherry nor apoplastic

proteins of *N. benthamiana* bound significant amounts of 3-OH-C10:0 (Figure 10). In addition, the treatment of AWFs containing apo-mCherry with methanol as a negative control merely triggered an increase in $[Ca^{2+}]_{cyt}$ above the background level, indicating that the AWF filtrate does not contain significant amounts of other elicitors, which may mask LORE-dependent responses. In contrast, 3-OH-C10:0 levels were largely depleted in filtrates of AWF containing eAtLORE-mCherry. Therefore, the depletion assay is sufficient to prove that eAtLORE expressed in the *N. benthamiana* apoplast can bind 3-OH-C10:0.

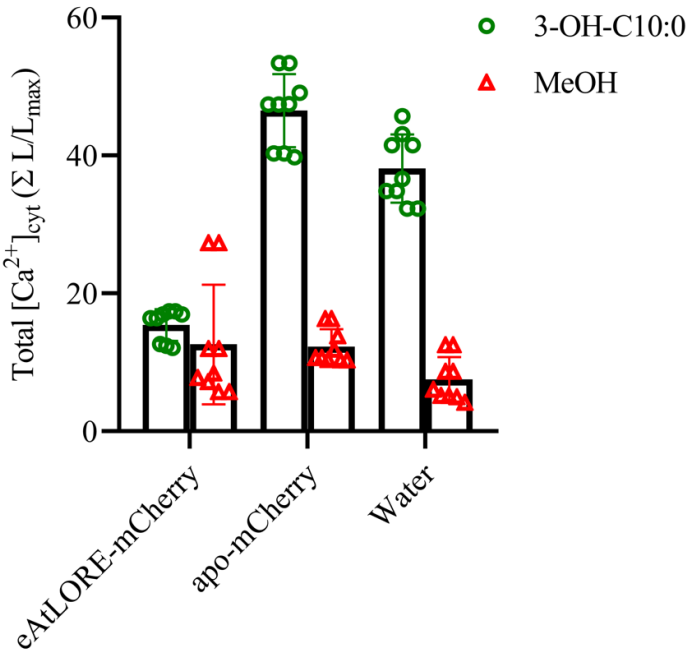

Figure 10. 3-OH-C10:0 is depleted by eAtLORE. Total $[Ca^{2+}]_{cyt}$ levels in Col-0^{AEQ} seedlings after treatment with filtrate of depletion assay performed with apoplastic washing fluids containing eAtLORE-mCherry, apoplastic mCherry (apo-mCherry) or water control incubated with 5 µM 3-OH-C10:0 or the same volume of MeOH as control. The total protein concentration of each apoplastic washing fluid was 5.1 mg/mL. Data from three independent experiments were pooled (mean ± SD, n = 9 seedlings).

Improving 3-OH-FA ligand depletion assay by a sensitive biosensor

In order to completely deplete ligands, receptor protein amounts that exceed the ligand concentration are required. To reach that, highly concentrated AWF (Protein concentration: 5.1 mg/mL) was utilized in the depletion assay. To reduce the concentration of proteins in AWF used in the depletion assay, a more sensitive plant biosensor that allows the detection of 3-OH-C10:0

at lower concentrations was constructed. A stable transgenic Arabidopsis plant overexpressing *AtLORE* in the *lore*-1 mutant background, which is an aequorin calcium reporter line, was generated (LORE-OE) (Ranf *et al.*, 2015, Schäffer, 2019). LORE-OE seedlings detected 3-OH-C10:0 concentrations in the range of 5-500 nM and responded with stronger $[Ca^{2+}]_{cyt}$ bursts than wild-type Col-0^{AEQ} when elicited with the same concentrations of 3-OH-C10:0 (Figure 9). The depletion assay could be accomplished with a 10-fold lower 3-OH-C10:0 concentration (500 nM) with this more sensitive plant biosensor. Based on the same level of $[Ca^{2+}]_{cyt}$ signal triggered by filtrates of AWF with 3-OH-C10:0, 30% of originally concentrated AWF containing eAtLORE-mCherry (total protein concentration of 1.5 mg/mL) was sufficient to entirely deplete 3-OH-C10:0 with the same procedure (Figure 11). Additionally, the less concentrated AWF did not trigger any non-specific $[Ca^{2+}]_{cyt}$ response in the calcium measurement in *lore*-1 seedlings, indicating that the less concentrated AWFs do not contain amounts of compounds that interfere with the response of Arabidopsis to 3-OH-C10:0 (Figure 10, 11).

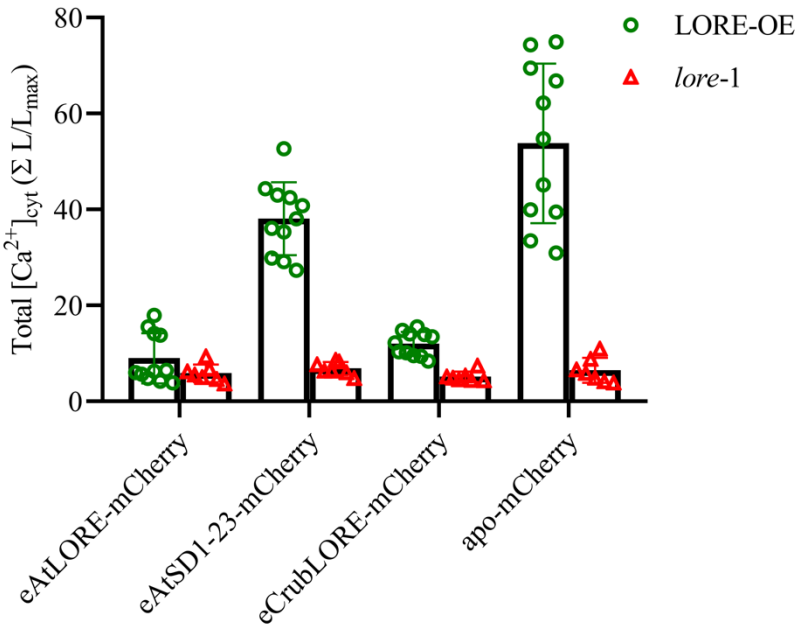

Figure 11. 3-OH-C10:0 is depleted by AtLORE and CrubLORE extracellular domains. Depletion assay (Fig. 2) was performed using 500 nM 3-OH-C10:0 and concentrated apoplastic washing fluid from *Nicotiana benthamiana* containing the indicated SD-RLK ECD-mCherry fusion proteins or apoplastic mCherry (apo-mCherry) as control. Increases in $[Ca^{2+}]_{cyt}$ were measured in Arabidopsis LORE-OE and *lore*-1 seedlings treated with the respective filtrates from the depletion assay (mean ± SD, LORE-OE: n = 11 seedlings, *lore*-1: n = 7 seedlings, pooled

data from three independent experiments). The total protein concentration of apoplastic washing fluids was 1.5 mg/mL.

The LORE ortholog from *Capsella rubella* is a mc-3-OH-FA receptor

To further expand the application and confirm the depletion assay's reliability, I checked the 3-OH-C10:0-binding of eCrubLORE-mCherry and eAtSD1-23-mCherry. AWF containing eCrubLORE-mCherry depleted 3-OH-C10:0, but AWF containing eAtSD1-23-mCherry did not (Figure 11). The binding of 3-OH-C10:0 to the eCrubLORE revealed its role as a bona fide mc-3-OH-FA receptor, which previously lacked evidence of direct interaction with ligand. eAtSD1-23 did not bind 3-OH-C10:0, which matches the results displayed in the *sd1-23* mutant in the previous study (Ranf *et al.*, 2015). Hence, eAtSD1-23 can be used as a negative control for the mc-3-OH-FA depletion assays with different SD-RLKs.

mc-3-OH-FA binding assay

The depletion assay offers indirect evidence of AtLORE-mc-3-OH-FA interaction by measuring the unbound fraction of mc-3-OH-FA (Figure 8). To directly detect the fraction containing the 3-OH-C10:0 bound by a receptor, the ligand needs to be released from the ligand-receptor complex to be free and available for detection by the LORE-OE biosensor. Based on the concept of the depletion assay, the receptor proteins present in the retentate from the depletion step were denatured by heat treatment and lost the affinities for ligands. The released 3-OH-C10:0 ligand was isolated by filtration through a 30 kDa MWCO filter and measured by the same LORE-OE biosensor assay as in the previous step (Figure 12a). The results showed that significant amounts of 3-OH-C10:0 were released from eAtLORE-mCherry and eCrubLORE-mCherry. Seemingly, eAtSD1-23-mCherry and apo-mCherry retained some 3-OH-C10:0 but significantly less than eAtLORE-mCherry and eCrubLORE-mCherry (Figure 12a). Alternatively, some 3-OH-C10:0 may be stuck in the concentrators or 3-OH-C10:0 may be non-specifically bound by proteins in the AWF and be released by the heat treatment. Additionally, 3-OH-C10:0 is stable and retains its eliciting activity after long high-temperature treatment, indicating that the effect of heat treatment on 3-OH-C10:0 in the binding assay is not a concern (Figure 12b). Without any complex isolation technique, the proportion of 3-OH-C10:0 ligand bound by receptors can be confirmed directly with this second binding step.

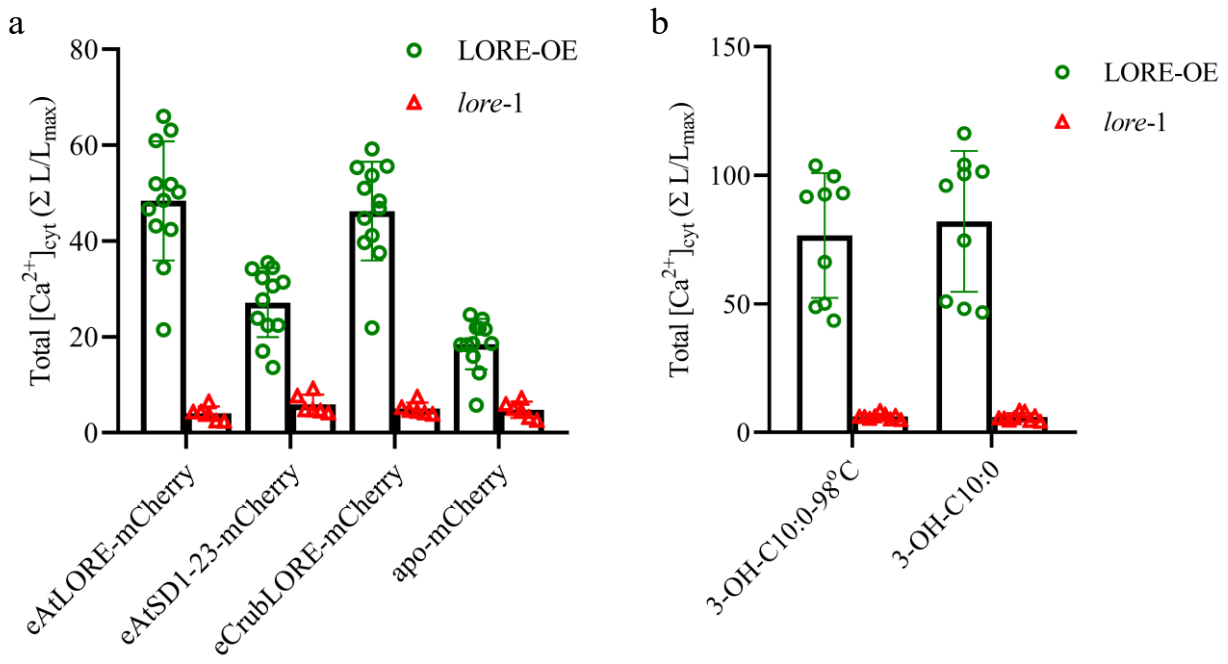

Figure 12. 3-OH-C10:0 binds to the AtLORE and CrubLORE extracellular domains. a. Binding assay was performed using 500 nM 3-OH-C10:0 and apoplastic washing fluid from *Nicotiana benthamiana* containing extracellular domains of the indicated SD-RLK ectodomain (eAtLORE, eAtSD1-23, and eCrubLORE) -mCherry fusion proteins or apoplastic mCherry (apo-mCherry) as control. Increases in $[Ca^{2+}]_{cyt}$ of Arabidopsis LORE-OE or *lore*-1 seedlings treated with the respective filtrates of heat-denatured retentates obtained in the binding assay. (mean ± SD, LORE-OE: n = 12 seedlings, *lore*-1: n = 6 seedlings). Data from three independent experiments were pooled. The total protein concentration of apoplastic washing fluids was 1.5 mg/mL. **b.** Elicitor activity of 3-OH-C10:0 after heat treatment. $[Ca^{2+}]_{cyt}$ was measured in *Arabidopsis* seedlings of the LORE-overexpressing line (LORE-OE) and *lore*-1 treated with 100 nM 3-OH-C10:0 heat-treated at 98°C for 30 minutes (3-OH-C10:0-98°C) or without heat treatment (3-OH-C10:0). Data from three independent experiments were pooled (mean ± SD, n = 9 seedlings each).

AtLORE is a 3-hydroxyalkanoate receptor

The depletion assay demonstrated its capability of proving the 3-OH-C10:0-binding activities of receptors. Following the same procedure, HAA, an elicitor of LORE-dependent immune response, was tested. Due to its lower activity of triggering LORE-dependent response (Schellenberger *et al.*, 2021), a higher concentration of HAA (5000 nM) was applied in the depletion assay, followed by adding more proteins (2 mg/mL) to acheive complete depletion. HAA is a small molecular weight fatty acid (<1 kDa), so the process of isolating free ligands could follow the procedure established for 3-OH-C10:0. HAA, as 3-OH-C10:0, was depleted by eAtLORE-mCherry but not apo-mCherry (Figure 13). The results demonstrated that the depletion assay for studying

AtLORE-3-OH-C10:0 interaction could be potentially adapted and applied in other SD-RLK ECD-low MW fatty acid interactions.

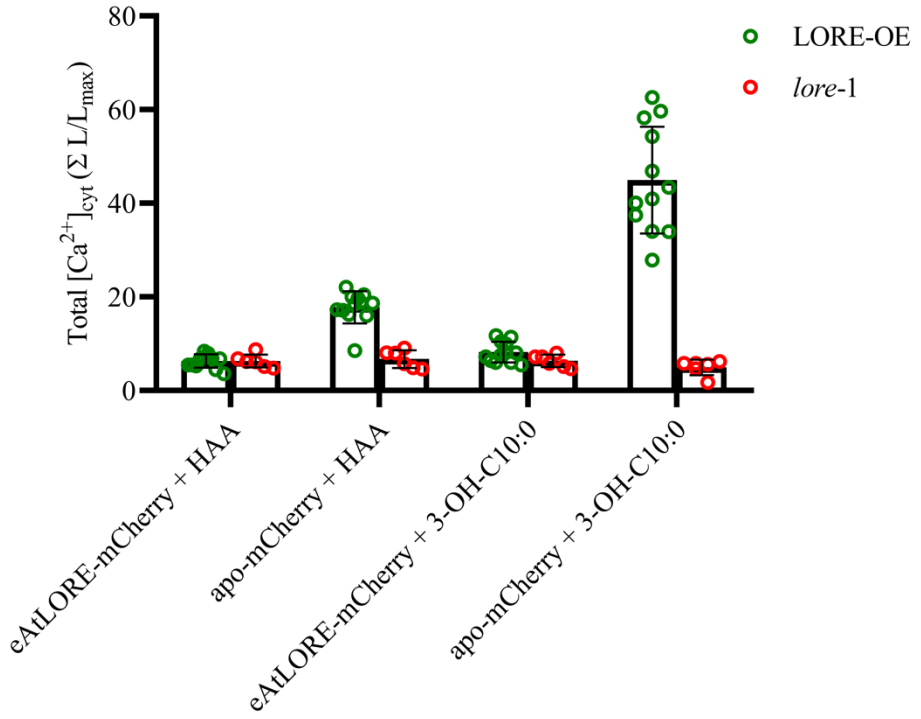

Figure 13. (R)-3-hydroxyalkanoate is depleted by AtLORE extracellular domain. Depletion assay was performed using 5000 nM (R)-3-hydroxyalkanoate (HAA) and 500 nM 3-OH-C10:0 and concentrated apoplastic washing fluid from *Nicotiana benthamiana* containing the indicated eAtLORE-mCherry fusion proteins or apoplastic mCherry (apo-mCherry) as control. Increases in $[Ca^{2+}]_{cyt}$ were measured in Arabidopsis LORE-OE and *lore*-1 seedlings treated with the respective filtrates from the depletion assay (mean ± SD, LORE-OE: n = 12 seedlings, *lore*-1: n = 6 seedlings, pooled data from three independent experiments). The total protein concentration of apoplastic washing fluids was 2 mg/mL.

2.1.3 Protein purification of tobacco-expressing AtLORE ECD

The depletion binding assay for AtLORE-3-OH-FA interaction indicated that the protein expressed by *N. benthamiana* is functional, and the protein yields were sufficient for the experiments. However, using unpurified proteins for ligand binding experiments leads to some uncertainties and limitations, such as non-specific binding to impurities or the difficulty in accurately quantifying the binding affinity. These issues can make the results difficult to compare directly with other approaches using purified proteins, so establishing an eAtLORE purification system will allow to overcome such limitations. Several affinity tags commonly used for protein detection and purification were attached to eAtLORE at different positions and the fusion

proteins tested for expression in *N. benthamiana* and successful 3-OH-FA binding in the ligand-depletion assay. Ultimately two tags could be effectively detected by the antibodies at specific termini on eAtLORE and pulled down by affinity matrices. eAtLORE human influenza hemagglutinin (HA)-fusion protein could be pulled down by anti-HA magnetic matrix (Schäffer, 2019). To purify proteins with a gentle method, the anti-HA agarose matrix was used to capture eAtLORE, and HA peptide was utilized to elute eAtLORE from the antibody without denaturation (Supplementary Figure 3). Although it is possible to purify eAtLORE with the HA tag, the costly anti-HA agarose matrix and HA peptide used for purification make the process of purifying large amounts of eAtLORE uneconomical, especially when the elution efficiency is not optimal. The purification methods without immunogenic affinity tags are usually preferable for large-scale purification, and purifying proteins with Strep-tag is an ideally commercialized approach. eAtLORE fused with the N-terminal Twin-Strep-tag and C-terminal HA tag was well purified by Strep-Tactin resin and the whole procedure could be done by integrating Strep-Tactin into fast protein liquid chromatography (FPLC) system (Figure 14, Supplementary Figure 4a, b). Full-length eAtLORE, together with a lower-MW fragment, could be purified. By immunoblot detecting N-terminal and C-terminal tags of eAtLORE, the fragment was shown to be the eAtLORE lacking the C-terminal part and HA tag (Figure 14, Supplementary Figure 4a, b). The purified eAtLORE protein was subjected to the depletion binding assay to confirm that its function was maintained during purification and it still displays its binding ability to 3-OH-FA (Supplementary Figure 4c). The results demonstrated that the ECDs expressed by *N. benthamiana*, in combination with the Strep-tag purification method, can be utilized for the production of functional 3-OH-FA binding proteins, such as eAtLORE.

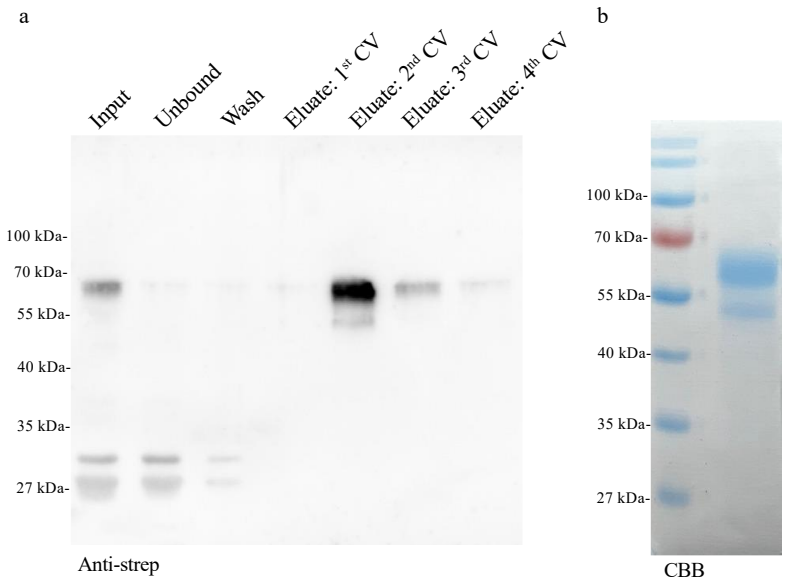

Figure 14. Purification of AtLORE ECD with Strep-tag. The AtLORE ECD (eAtLORE) fused at its N terminus with Twin-Strep-tag and at its C terminus with HA tag was expressed in *Nicotiana benthamiana* in the apoplast of leaves by *Agrobacterium*-mediated transient expression. The eAtLORE was purified using Strep-tag column Strep-Tactin®XT 4Flow cartridge with 5 mL column bed volume (CV) coupled with ÄKTA system. **a**. Anti-strep immunoblot analysis of the protein purification. The calculated molecular weight of the protein is 55-60 kDa. Lane Input: apoplast washing fluid (10 µl; 30 mL in total) before subjecting into the cartridge. Lane Unbound: column flow-through (10 µl; 30 mL in total). Lane Wash: the cartridge was washed with wash buffer (10 µl; 50 mL in total). Lane Eluate 1st CV to 4th CV: elution fractions having the purified eAtLORE (10 µl each lane; 5 ml each fraction in total). **b.** Purified eAtLORE in SDS-polyacrylamide gel stained with Coomassie brilliant blue. The purified protein pooling from all fractions of the eluates was concentrated to 0.15 μg/μL by concentrator (30 kDa cut-off), and 10 μL of concentrate was loaded.

2.1.4 Binding assay by microscale thermophoresis

MST is commonly used to investigate protein-ligand interactions and protein-protein interactions, and it does not require stringent protein purity and a complicated labeling process. MST is also a reliable method that can quantify the binding affinity, which ligand depletion binding assay cannot measure. Due to these advantages, MST was used to study the interaction of AtLORE with 3-OH-FA. Because of the requirement for fluorophores for detection of target proteins, the concentrated eAtLORE-mCherry in AWF in the ligand depletion binding was assayed in the MST experiment. However, the results of the MST experiment showed that the eAtLORE-mCherry had almost no ability to bind to 3-OH-C10:0, similar as apo-mCherry, although the concentrations of 3-OH-C10:0 used in MST assays were far higher than in the depletion binding

assays (Supplementary Figure 5). In the previous study, the purified eAtLORE protein expressed by an insect cell system was labeled by dyes either on their histidine tag or amine group before being subjected to MST assays. However, the observed binding affinity was relatively low under those conditions (Kutschera *et al.*, 2019). Following the previous study, eAtLORE histidine-tag with HA-tag fusion protein expressed by *N. benthamiana* was labeled by the histidine-tag-directed dye, together with two negative controls, eAtLORE-HA, which was not able to be labeled, and the polyhistidine peptide. With the high concentrations of 3-OH-C10:0, which was used in the previous study, the eAtLORE-His-HA fusion protein-3-OH-C10:0 interaction was observed; however, both negative controls also showed binding to 3-OH-C10:0 (Figure 15, Supplementary Figure 6). The MST results indicated that 3-OH-FA was non-specifically bound to fluorophores and proteins and induced the change of fluorescence when the concentration was higher than 0.1 to 1 mM. These data also imply that the results in previous research might have encountered these issues in MST assays (Kutschera *et al.*, 2019).

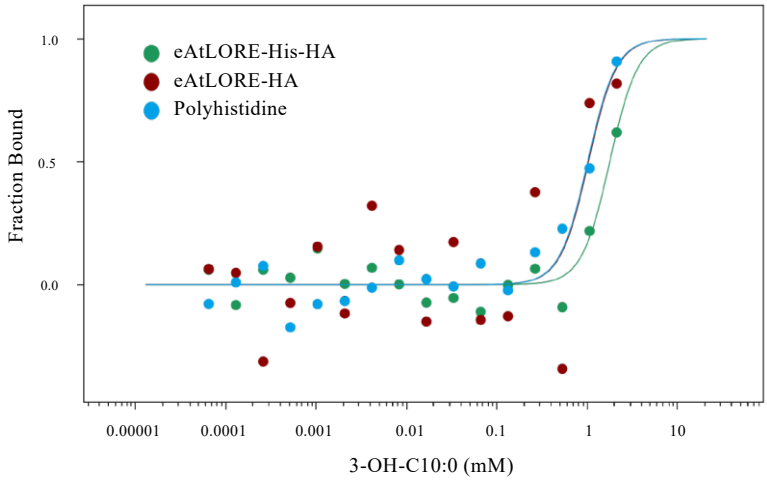

Figure 15. 3-OH-C10:0 non-specifically binds proteins and dyes at high concentrations. Measurement of binding between 3-OH-C10:0 and the eAtLORE fused with His- and HA-tag, HA-tag, and polyhistidine peptide by microscale thermophoresis (MST). Data points indicate the fraction of His-tag labeled proteins bound to different concentrations of 3-OH-C10:0 (fraction bound). Proteins were fluorescently labeled using the His-Tag labeling kit. eAtLORE-HA was used as a negative control of labeling, and polyhistidine was a positive control of labeling and a negative control of binding. Measurements were performed at 40% LED power and medium MST power at room temperature. Two independent experiments were done with similar results.

In order to exclude that some factors, like protein purity and different protein expression systems, interfered with the MST assay, eAtLORE purified by Twin-Strep-tag was tested. The purified eAtLORE was still unable to strongly bind up to 50 μM 3-OH-C10:0 in the MST assay, although the ligand depletion binding assays demonstrated that it bound 3-OH-C10:0 (Supplementary Figure 7). Taken together, MST failed to verify the interaction between AtLORE and 3-OH-FA, and non-specific binding due to high fatty acid concentration is a concern when developing binding assays.

2.1.5 Investigation of AtLORE 3-OH-FA binding specificity by radiobinding assay

Because of the stringent structural requirements of 3-OH-FA-dependent elicitation, there are only a few ways to label 3-OH-FA with detectable tags (Kutschera *et al.*, 2019). For radiochemical labeling, the options for replacement on 3-OH-FA are carbon and hydrogen. I utilized tritium-labeled 3-hydroxydecanoic acid ([^{3}H]-3-OH-C10:0), which still preserves its activity to perform radiobinding assay. The strategy of detecting bound [^{3}H]-3-OH-C10:0 is similar to the previous ligand binding assay (Figure 8), but the denaturation of protein and detection by biosensor were skipped and replaced by the scintillation counter, respectively (Figure 6). In the saturation binding assay, the Twin-Strep-purified eAtLORE showed a specific binding ability to [^{3}H]-3-OH-C10:0 between 3-1000 nM (Figure 16a). Although eAtLORE was not entirely saturated by [^{3}H]-3-OH-C10:0 in the study due to the limited availability of [^{3}H]-3-OH-C10:0, the potential Kd of the ligand binding is approximately in the range of 700 nM to 4 μM. Moreover, the competition binding assay was performed to compare the binding affinities of eAtLORE to different mc-3-OH-FAs, 3-OH-C10:0, 3-OH-C12:0, and 3-OH-C14:0, which have different activities of elicitation (Kutschera *et al.*, 2019). 1000 nM of cold 3-OH-C10:0, which was 33-fold higher than [^{3}H]-3-OH-C10:0 in the same system, was able to outcompete hot ligand, but it needed more than 1000 nM of cold 3-OH-C12:0 to compete comparable amount of [^{3}H]-3-OH-C10:0. 30000 nM cold 3-OH-C14:0 was unable to replace [^{3}H]-3-OH-C10:0 on eAtLORE even though it was 1000-fold more than the hot ligand (Figure 16b). The results from the competition assay were comparable with 3-OH-FA-induced immune responses *in planta*, which showed no significant difference between the treatment of 3-OH-C10:0 alone and the co-treatment of 3-OH-C10:0 with the excess amount of 3-OH-C14:0 (Supplementary Figure 8). Taken together, 3-OH-C10:0 had a stronger binding affinity to eAtLORE than 3-OH-C12:0 and 3-OH-C14:0, and these

also indicated that the binding affinity was positively correlated to the activity of AtLORE-dependent elicitation in Arabidopsis.

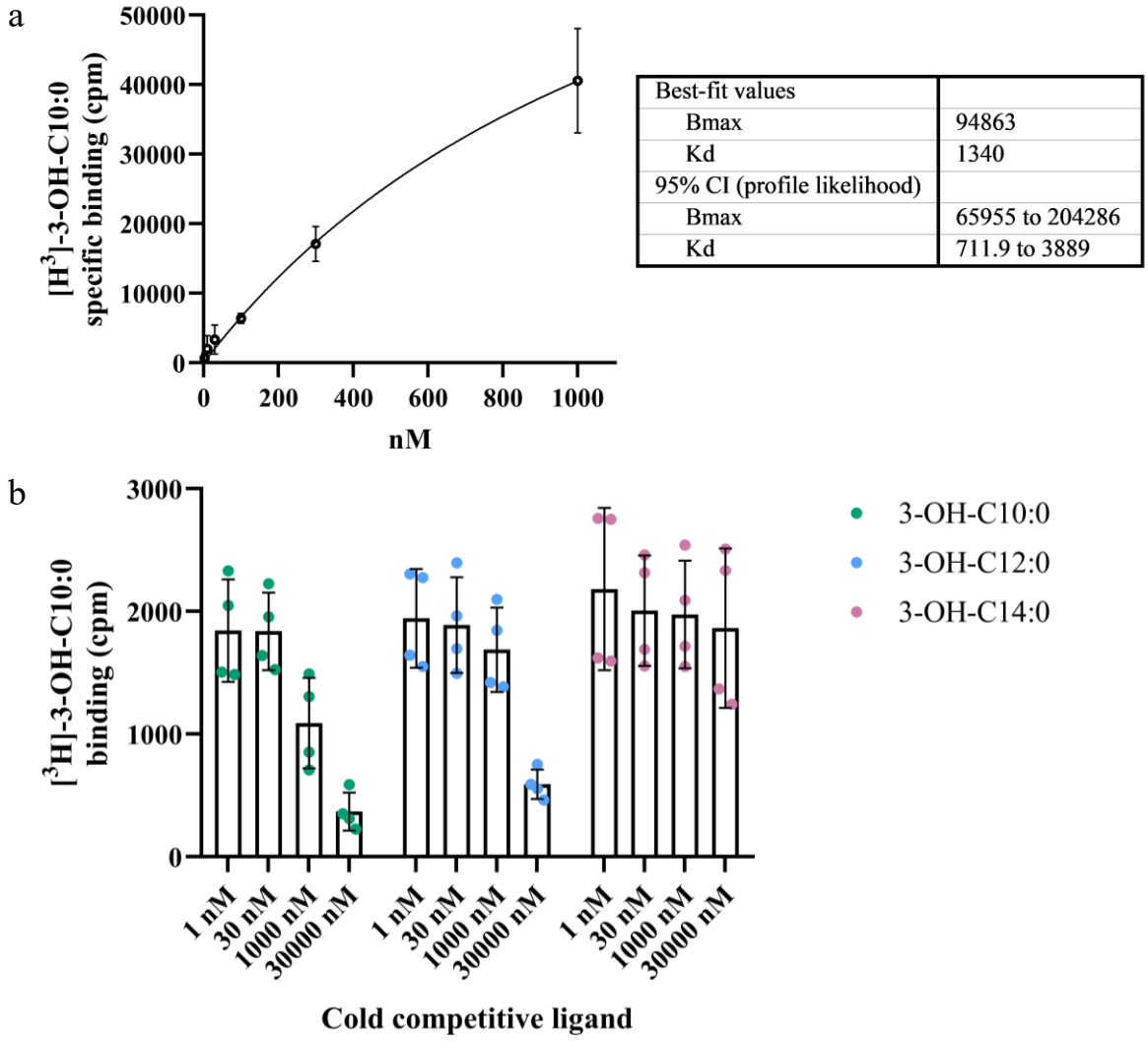

Figure 16. Radiobinding assays of mc-3-OH-FA with eAtLORE. a. Saturation binding assay of [^{3}H]-3-hydroxydecanoic acid ([^{3}H]-3-OH-C10:0) and eAtLORE. Purified eAtLORE proteins were incubated with the indicated concentrations of [^{3}H]-3-OH-C10:0 for measuring total binding and incubated with an excess amount of cold 3-OH-C10:0 for detecting non-specific binding. The specific binding results from subtracting non-specific binding from total binding. The dissociation constant (Kd), maximal binding (B_{max}), and their 95% confidence intervals (CI) were estimated by GraphPad Prism 8 with one-site specific binding saturation model (nM). **b.** Competition binding assay of [^{3}H]-3-OH-C10:0 and cold medium-chain 3-OH-FAs. The mixtures contained 30 nM [^{3}H]-3-OH-C10:0 and purified eAtLORE, and they were incubated with the indicated concentrations of cold competitors, 3-OH-C10:0, 3-OH-C12:0, and 3-OH-C14:0. cpm: count per unit. The pooled results in **a.** and **b.** were from two independent assays, and the error bars indicate standard deviation.

2.2 Investigation of 3-OH-FA sensing diversity in Brassicaceae

Sensing of mc-3-OH-FA is not universal in Kingdom Plantae, and mc-3-OH-FA-sensitive species were only found in Brassicaceae in previous studies (Ranf *et al.*, 2015, Schäffer, 2019). The Brassicaceae plants might evolve similar mechanisms for perceiving mc-3-OH-FA as LORE in *A. thaliana*. To further understand the responsiveness of mc-3-OH-FA, *A. thaliana* ecotype accessions and diverse species in Brassicaceae were systematically investigated.

2.2.1 Investigation of 3-OH-FA sensing diversity in *A. thaliana* accessions

As a model species, *A. thaliana* has a wide range of ecotypes available that show diverse phenotypic variations. This population has the potential to uncover the intraspecies diversity of immunogenic pattern-triggered responses. In addition, the whole genome database, 1001 Genomes, provides the sequence information about the underlying genetic variations (1001_Genomes_Consortium, 2016). 68 Arabidopsis accessions that have non-synonymous SNPs in their *AtLORE* sequences were selected and tested with 3-OH-C10:0, 3-OH-C12:0, and well-studied flg22 for comparison in ROS assays. Only one accession (T740) did not respond to 3-OH-C10:0 at all (Figure 17), while six flg22-insensitive accessions were found. 3-OH-FA-sensing was conserved but relatively weaker than flg22-triggered ROS responses under the same conditions (Figure 17). The intensity of ROS burst triggered by 3-OH-FAs did not correlate to the intensity of the flg22-triggered response, indicating that the differences in 3-OH-FA-sensing among the accessions are not due to the different activity of the ROS-producing molecular machinery (Figure 17). LORE senses mc-3-OH-FAs in a chain length-specific manner in Col-0 (Kutschera *et al.*, 2019). ROS response in Col-0 elicited by 3-OH-C10:0 was stronger than by 3-OH-C12:0. This tendency is also conserved in all sensitive accessions (Figure 17). The only insensitive accession, T740 has one non-synonymous SNP L29F in the ECD of AtLORE compared with Col-0; how this SNP affects 3-OH-FA-sensing or LORE signaling needs to be further validated.

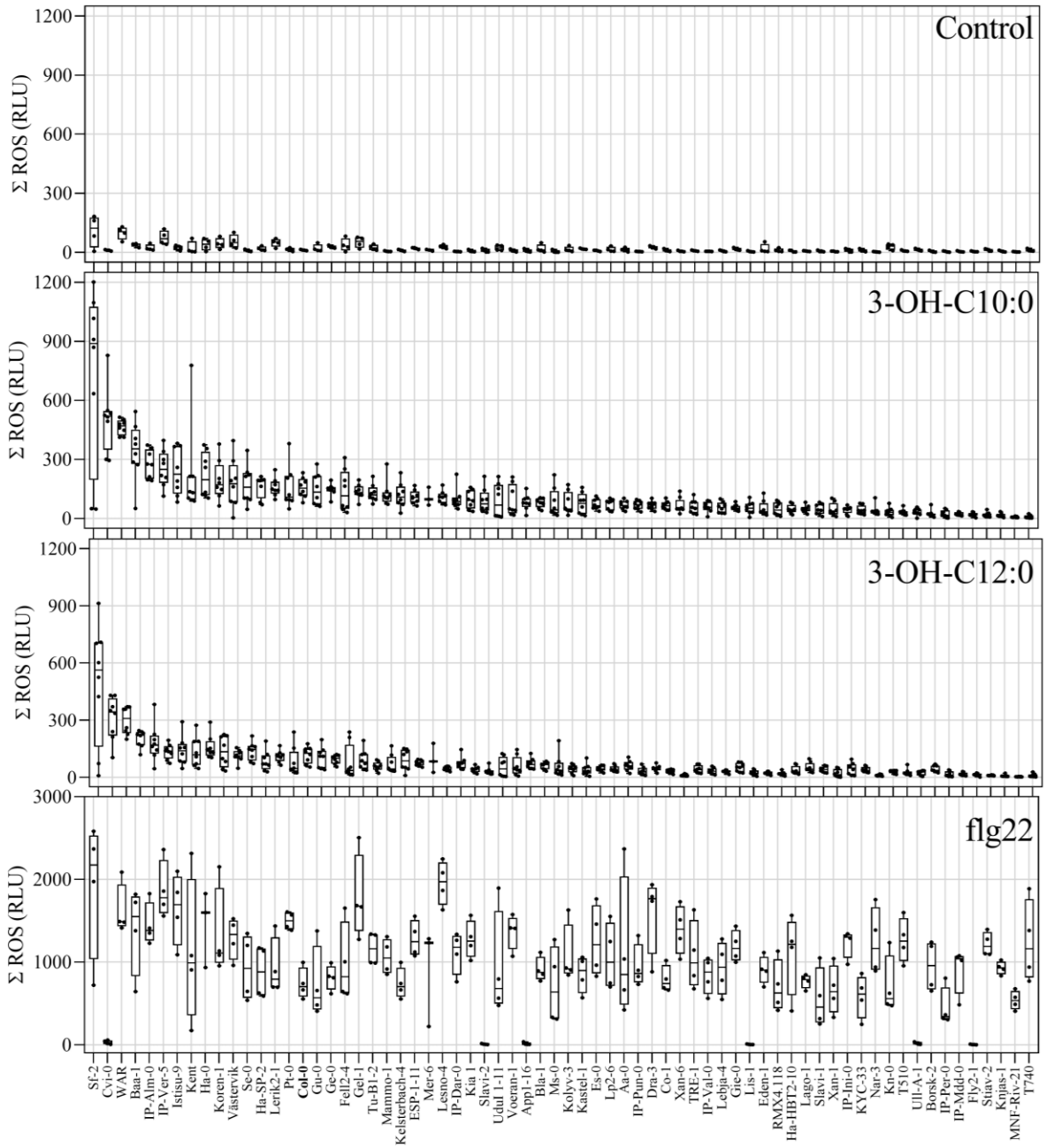

Figure 17. Sensitivity to 3-OH-C10:0, 3-OH-C12:0, and flg22 in Arabidopsis accessions. 68 accessions were tested by ROS measurement. Leaf discs of 9-week-old accessions were treated with 1 μM 3-OH-C10:0, 1 μM 3-OH-C12:0, 0.1 μM flg22, or MeOH (solvent control of 3-OH-C10:0) as control (mean ± SD, 3-OH-C10:0 n = 8; 3-OH-C12:0 n = 8; flg22 n = 4; control n = 4). No statistically significant difference in ROS accumulation was shown between 3-OH-C10:0 or 3-OH-C12:0 and control treatment in accession T740 (two-sided Student's t-test). Luminescence (relative light units, RLU) was measured at one-minute intervals over 45 minutes after treatment. RLU in each treated sample was summed up and plotted as box and whiskers plots (Center lines are medians; Boxes extend from 1st quartile to 3rd quartile; whiskers plot up to maximal values and down to minimal values).

To investigate the potential genes correlated to 3-OH-FA-sensing in Arabidopsis, a genome-wide association study (GWAS) was carried out by utilizing phenotypic results and whole genome sequences of the 68 Arabidopsis accessions tested (Figure 17) (Seren, 2018). However, none of the SNP was significantly associated with the ROS responsiveness after the Benjamini-Hochberg correction (Figure 18). The loci having SNPs above the background may contain target genes, so mining the potential candidates from this GWAS analysis may still be a practical approach.

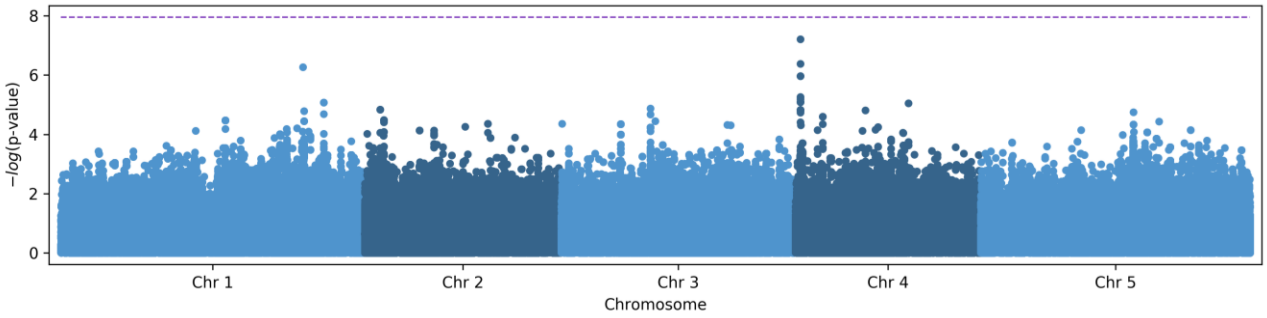

Figure 18. Genome-wide association of 3-OH-C10:0-responsiveness in 68 Arabidopsis accessions. The Manhattan plot for the GWAS on total luminescence of ROS measurement with genome-wide SNP associations was analyzed by GWA-Portal. The Arabidopsis chromosomes are revealed. The x-axis indicates the positions of SNPs within chromosomes. The y-axis indicates -$\log_{10}$(p-value) significant values of SNPs. The purple horizontal dashed line indicates the Benjamini-Hochberg significance threshold, meaning a false discovery rate of 5% of the associations (Benjamini and Hochberg, 1995).

2.2.2 Investigation of 3-OH-FA sensing diversity in Brassicaceae

A. thaliana shows low intraspecies diversity upon the 3-OH-FA-triggered immune response even though the tested accessions were pre-selected for having SNPs in the LORE coding sequences. But the low diversity is insufficient to pinpoint the key factors why AtLORE from 3-OH-FA-sensitive or -insensitive ecotypes can or cannot respond to 3-OH-FA. To broaden the understanding of the diversity of 3-OH-FA-dependent immune response, the species in the same family of *A. thaliana* were screened. 41 species in Brassicaceae and 1 in Cleomaceae, the closest related family to Brassicaceae, were included, and the collections covered the four major lineages, basal lineage, and lineage I, II (including extended lineage II), and III (Huang *et al*., 2016, Kiefer *et al*., 2019; Nikolov *et al*., 2019).

In contrast to the conserved phenotypes within *A. thaliana* accessions, 3-OH-FA-sensing in Brassicaceae species was relatively diverse. The proportion of 3-OH-FA-insensitive species was 30%; on the contrary, only two flg22-insensitive species were found (*Arabis alpina* and *Eutrema salsugineum*). The conserved flg22-triggered ROS response in the collections indicated that ROS production was functional in most species, implying that absence of 3-OH-FA-triggered ROS response was not due to inability to produce ROS (Figure 19). In lineage I, II, and III, each containing at least two species in the screening, both 3-OH-FA-sensitive and insensitive species were found (Figure 19). This pattern suggests that lineage I, II, and III may share the same ancestral receptor for perceiving 3-OH-FA. Basal lineage had one tested species, *Aethionema arabicum,* which is insensitive to 3-OH-FA, so it remained unclear whether the 3-OH-FA-triggered immune response is universal in Brassicaceae (Figure 19). In addition, *Cleome violacea* in the sister family Cleomaceae was insensitive to 3-OH-FA (Figure 19).

Brassicaceae genera were also classified into different tribes (Al-Shehbaz, 2012), but the classification of tribes did also not correlate with the sensitivity to 3-OH-FA. The tribes Camelineae (genera *Arabidopsis* and *Capsella*), Cardamineae (genera *Cardamine*, *Nasturtium*, and *Rorippa*), and Brassiceae (genera *Brassica*, *Crambe*, *Eruca*, *Raphanus,* and *Sinapis*) had both 3-OH-FA-sensitive and insensitive species. All Isatideae (genera *Isatis* and *Myagrum*) plants showed responsiveness to 3-OH-FA (Figure 19). Furthermore, not all species from the same genera in this study responded to 3-OH-FA. *Lepidium* and *Conringia*, having at least two species, revealed the consistencies upon 3-OH-FA treatment; however, *Arabidopsis*, *Brassica*, and *Sisymbrium* had distinct phenotypes in response to 3-OH-FA (Figure 19). All in all, the gain and loss of 3-OH-FA-sensing in Brassicaceae during evolution were variable, and the phenotype was not strictly determined at any classification level.

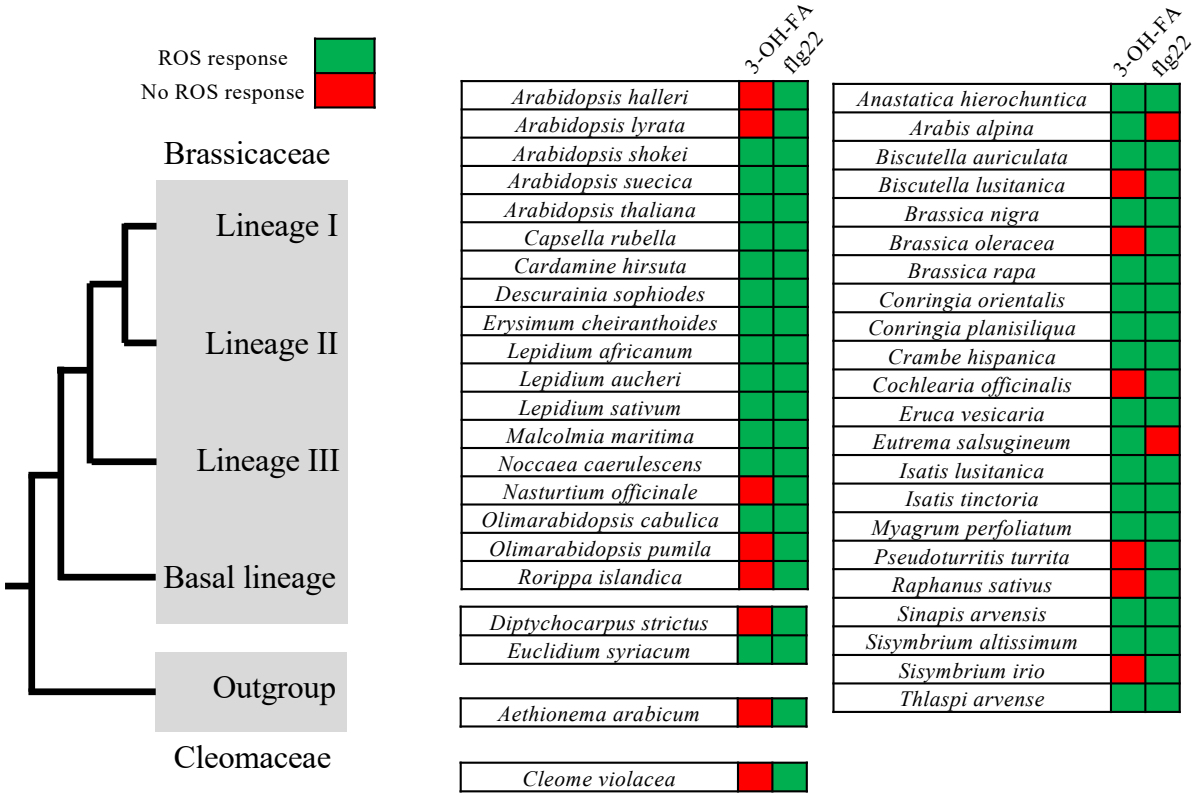

Figure 19. Diversity of mc-3-OH-FA and flg22-sensing in Brassicaceae. The summary tables of 3-OH-FA and flg22-induced ROS accumulation in 42 species. The nuclear genome phylogeny of Brassicaceae and Cleomaceae was adapted from the previous studies. The lineages of all tested species were assigned according to the classification of Brassicaceae species in previous studies (Huang et al., 2016, Kiefer et al., 2019; Nikolov et al., 2019). The results of summary tables were from ROS measurements with 3-OH-FA (5 μM), flg22 (0.5 μM), and methanol control (solvent of 3-OH-FA) treatments, and the data of 3-OH-C10:0 treatment represent 3-OH-FA. The complete experiments of ROS measurement were plotted in Figure 20 and Supplementary Figure 9. ROS measurements of *Arabidopsis lyrata* and *Arabidopsis halleri* were accomplished by Dr. Schäffer (Schäffer, 2019).

Arabidopsis LORE senses mc-3-OH-FAs in a chain length-specific manner, and the ROS response elicited by 3-OH-C10:0 was more robust than by other mc-3-OH-FAs. The long-chain 3-OH-FAs, such as 3-OH-C13:0 and 3-OH-C14:0, do not trigger AtLORE-dependent immune responses (Kutschera *et al.*, 2019). To understand whether the chain length-specificity is conserved within Brassicaceae as well, 3-OH-C10:0-sensitive species were further tested with other mc-3-OH-FAs (Figure 20, Supplementary Figure 9). None of the candidates responded to 3-OH-C14:0; however, 3-OH-C13:0 induced significant ROS accumulations in some species in lineage I and II, suggesting that the longest mc-3-OH-FA that plants can perceive is 3-OH-C13:0,

rather than 3-OH-C12:0 (Figure 20, Supplementary Figure 9). All 3-OH-C10:0-sensitive species also perceived other mc-3-OH-FA, showing that 3-OH-C10:0 could be a type elicitor of active mc-3-OH-FAs in different experiments (Figure 20, Supplementary Figure 9). 3-OH-C10:0 was still the strongest elicitor among the tested 3-OH-FAs in the tested species. Only one species, *Malcolmia maritima*, is more sensitive to 3-OH-C12:0 than 3-OH-C10:0 (Figure 20). In the previous study, *A. thaliana* did not respond evenly to each 3-OH-FA longer or shorter than 3-OH-C10:0 according to ROS and calcium measurements (Kutschera *et al.*, 2019) (Figure 20). Unlike *A. thaliana*, *Descurainia sophiodes* and *Lepidium sativum*, as examples, were equally sensitive to 3-OH-C10:0, 3-OH-C11:0, and 3-OH-C12:0, and less sensitive to 3-OH-C9:0 and 3-OH-C8:0. Similarly, species like *C. rubella* and *Brassica nigra* nearly equally perceived 3-OH-C8:0, 3-OH-C9:0, 3-OH-C11:0 and 3-OH-C12:0 (Figure 20). Although the chain length-specific eliciting activity was comprehensively investigated by ROS assays, whether other factors, such as tissue type and age, can influence the sensing specificity needs to be further investigated. In summary, the results suggested that the chain length-specificity in Brassicaceae is substantially conserved, but not all species share the same specificity and sensitivity patterns with *A. thaliana*.

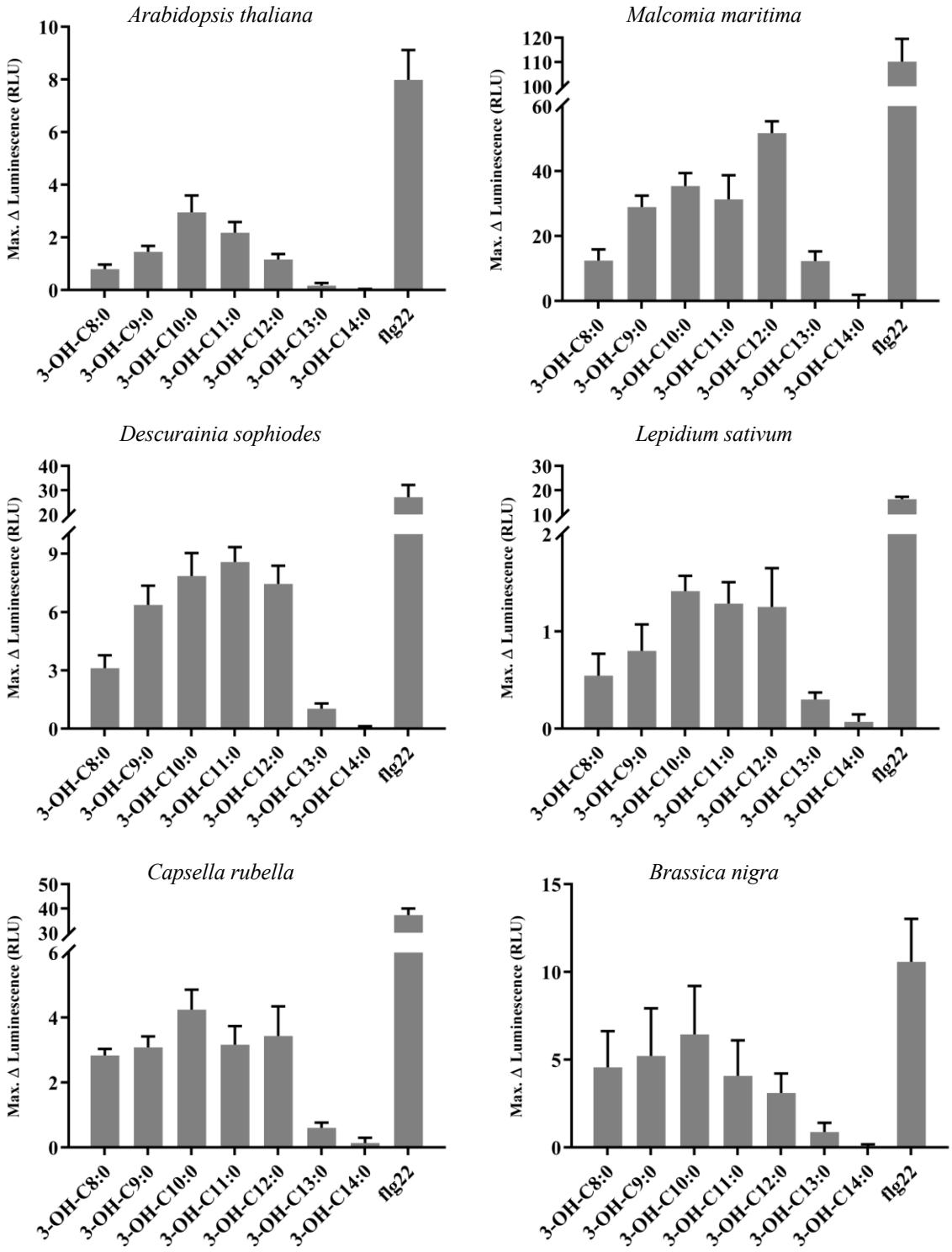

Figure 20. 3-OH-FAs trigger ROS accumulations in acyl chain length-specific manners in sensitive Brassicaceae species. Maximum ROS accumulation in leaf discs of Brassicaceae species, *Arabidopsis thaliana*, *Malcolmia maritima*, *Descurainia sophiodes*, *Lepidium sativum*, *Capsella rubella*, and *Brassica nigra* elicited by 5 μM 3-OH-FAs and 0.5 μM flg22 (mean ± SD, n = 8). Maximal luminescence was normalized to the average

luminescence of 5 minutes before treatment, and subtracted by mock controls. Two or three independent experiments were done with similar results.

2.3 Functional analysis of LORE orthologs in Brassicaceae

Brassicaceae species show a great diversity of 3-OH-FA-sensitivity. AtLORE in *A. thaliana* is associated with 3-OH-FA perception, while other genetically similar SD-RLKs, such as AtSD1-23, cannot detect 3-OH-FAs. These findings suggest that LORE-like receptors may be the main factor in facilitating the detection of 3-OH-FAs in most species in Brassicaceae. Moreover, many Brassicaceae species still fail to sense 3-OH-FAs, which might also be related to the presence or function of their SD-RLKs. To explain these patterns, a systematic investigation of LORE-like receptors in Brassicaceae plants was undertaken to clarify this hypothesis by genetic analysis with functional validation.

2.3.1 Phylogeny of LORE/SD1-23 orthologs

To understand the gains and losses of Brassicaceae plants' perception of mc-3-OH-FAs, the *AtLORE* cognate genes in available reference genomes were analyzed. 23 whole-genome sequenced Brassicaceae species containing 3-OH-FA sensitive and insensitive plants are distributed across the four lineages. Taking the well-studied AtLORE as a reference, the BLASTp search identified SD-RLKs that share 60% or higher protein sequence identities with AtLORE. All candidate species had at least one hit in the investigation. The phylogenetic analysis with the Neighbor-Joining method further classified candidate SD-RLKs into different clades. The investigation was supplemented with 5 *A. thaliana* SD-RLKs, AtSD1-23, AtSD1-27, AtSD1-28, AtSD1-30, and AtSD1-12 (also known as AtRDA2) as references of different outgroups in the phylogeny. The previously verified LORE ortholog, CrubLORE, was clustered with AtLORE and other LORE-like proteins, which are also from lineage I species, in the same clade (Figure 21). In addition, AtSD1-23 was classified into an independent clade and was distant from AtLORE (Figure 21). Most LORE orthologs from lineage II were clustered in the same clade, which could be further separated into multiple sub-clades (Figure 21). Several LORE orthologs in these clades originated from the same lineage II species, meaning that the duplication events in the LORE evolution might have had happened in lineage II more times than in lineage I (Figure 21). LORE-like receptors in lineage III and basal lineage were divided into several clades that did not belong to the clades of lineage I and II LORE orthologs (Figure 21). LORE-like and SD1-

23-like receptors were not identified in the outgroup species *C. violacea*, suggesting that *LORE* was restricted to Brassicaceae in evolution (Figure 21). Interestingly, all Brassicaceae species in this study were found to contain LORE-like protein sequences, so it is evident that possession of *LORE* genes does not correlate with 3-OH-FA sensing of the species (Figure 21). The analyses displayed that LORE-like receptors were spread in all Brassicaceae species and clustered into different groups based on their origins. It also implied that LORE receptors in the 3-OH-FA insensitive species might not be functional.

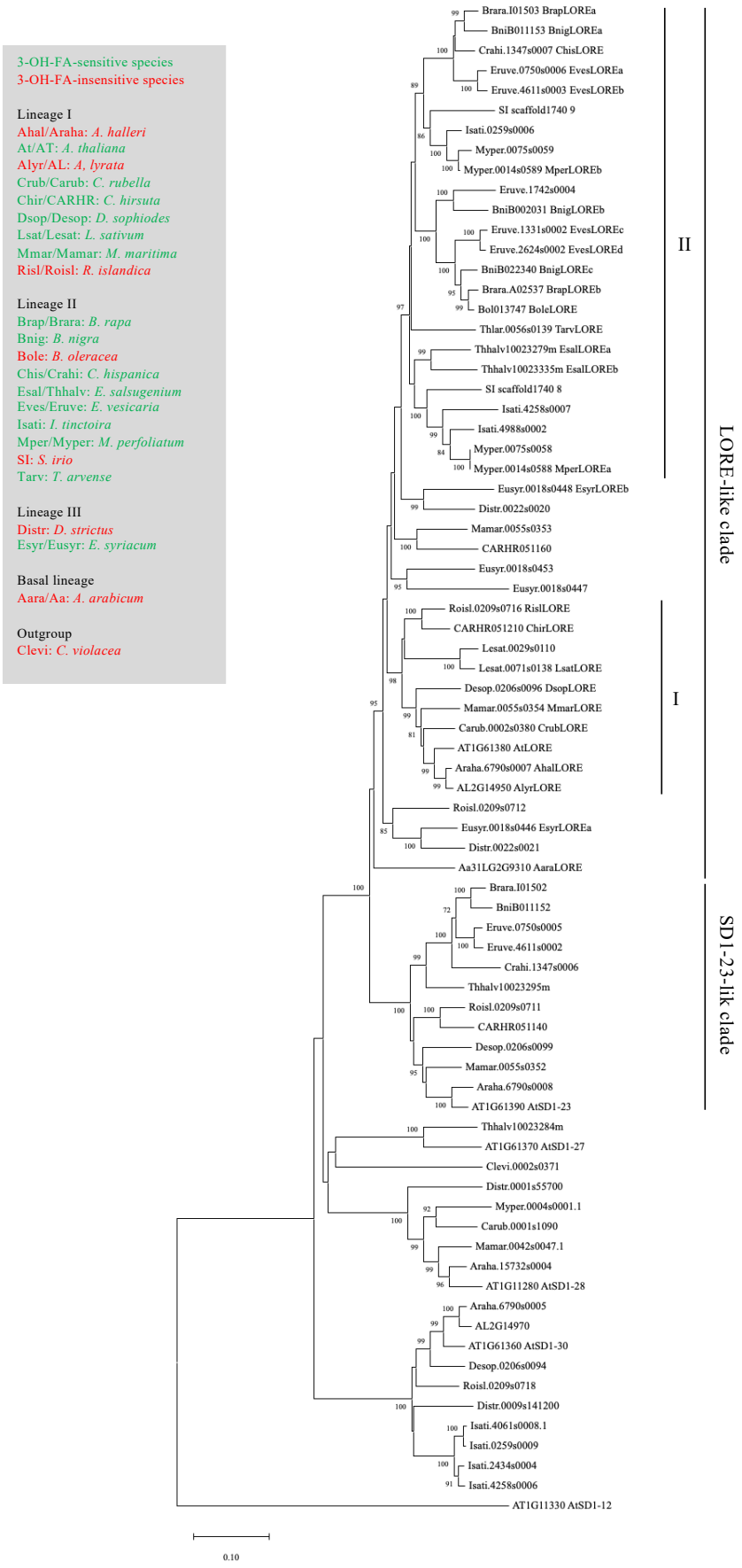
3-OH-FA-sensitive species
3-OH-FA-insensitive species
Lineage I
Ahal/Araha: A. halleri
At/AT: A. thaliana
Alyr/AL: A, lyrata
Crub/Carub: C. rubella
Chir/CARHR: C. hirsuta
Dsop/Desop: D. sophiodes
Lsat/Lesat: L. sativum
Mmar/Mamar: M. maritima
Risl/Roisl: R. islandica
Lineage II
Brap/Brara: B. rapa
Bnig: B. nigra
Bole: B. oleracea
Chis/Crahi: C. hispanica
Esal/Thhalv: E. salsugenium
Eves/Eruve: E. vesicaria
Isati: I. tinctoira
Mper/Myper: M. perfoliatum
SI: S. irio
Tarv: T. arvense
Lineage III
Distr: D. strictus
Esyr/Eusyr: E. syriacum
Basal lineage
Aara/Aa: A. arabicum
Outgroup
Clevi: C. violacea
Brara.I01503 BrapLOREa
BniB011153 BnigLOREa
Crahi.1347s0007 ChisLORE
Eruve.0750s0006 EvesLOREa
Eruve.4611s0003 EvesLOREb
SI scaffold1740 9
Isati.0259s0006
Myper.0075s0059
Myper.0014s0589 MperLOREb
Eruve.1742s0004
BniB002031 BnigLOREb
Eruve.1331s0002 EvesLOREc
Eruve.2624s0002 EvesLOREd
BniB022340 BnigLOREc
Brara.A02537 BrapLOREb
Bol013747 BoleLORE
Thlar.0056s0139 TarvLORE
Thhalv10023279m EsalLOREa
Thhalv10023335m EsalLOREb
SI scaffold1740 8
Isati.4258s0007
Isati.4988s0002
Myper.0075s0058
Myper.0014s0588 MperLOREa
Eusyr.0018s0448 EsyrLOREb
Distr.0022s0020
Mamar.0055s0353
CARHR051160
Eusyr.0018s0453
Eusyr.0018s0447
Roisl.0209s0716 RislLORE
CARHR051210 ChirLORE
Lesat.0029s0110
Lesat.0071s0138 LsatLORE
Desop.0206s0096 DsopLORE
Mamar.0055s0354 MmarLORE
Carub.0002s0380 CrubLORE
AT1G61380 AtLORE
Araha.6790s0007 AhalLORE
AL2G14950 AlyrLORE
Roisl.0209s0712
Eusyr.0018s0446 EsyrLOREa
Distr.0022s0021
Aa31LG2G9310 AaraLORE
Brara.I01502
BniB011152
Eruve.0750s0005
Eruve.4611s0002
Crahi.1347s0006
Thhalv10023295m
Roisl.0209s0711
CARHR051140
Desop.0206s0099
Mamar.0055s0352
Araha.6790s0008
AT1G61390 AtSD1-23
Thhalv10023284m
AT1G61370 AtSD1-27
Clevi.0002s0371
Distr.0001s55700
Myper.0004s0001.1
Carub.0001s1090
Mamar.0042s0047.1
Araha.15732s0004
AT1G11280 AtSD1-28
Araha.6790s0005
AL2G14970
AT1G61360 AtSD1-30
Desop.0206s0094
Roisl.0209s0718
Distr.0009s141200
Isati.4061s0008.1
Isati.0259s0009
Isati.2434s0004
Isati.4258s0006
AT1G11330 AtSD1-12
0.10
II
I
LORE-like clade
SD1-23-lik clade

Figure 21. The phylogenetic analysis of LORE-like receptors and other SD-RLKs. I and II, covered by the LORE-like clade, indicated the main lineages of the original species of the LORE-like receptors. MAFFT constructed the alignment of 76 protein sequences. The phylogeny was analyzed by MEGA XI software using the Neighbor-Joining method in the bootstrap test (1000 replicates). The bootstrap values next to the branches over 70 were shown, and the scale bar indicated the evolutionary distance computed using the Poisson correction method. The 3-OH-FA sensitivities of the original species of the candidate receptors were demonstrated in the legend based on Figure 19.

2.3.2 LORE-dependent 3-OH-FA binding in Brassicaceae is conserved

LORE-like genes were found in 3-OH-FA sensitive and insensitive Brassicaceae species with at least one candidate. This raised the question why 3-OH-FA-insensitive species could not respond to 3-OH-FA. One hypothesis was that the ECD of LORE orthologs from insensitive species may not perceive 3-OH-FA. To determine whether only LORE orthologs from sensitive species have 3-OH-FA-binding ECDs, a wide range of *LORE*-like genes were cloned and subsequently investigated by the ligand depletion assay (Figure 8). SD1-23-like receptors from the adjacent clade were included as negative controls (Figure 11). AtSD1-12, which is a receptor for derivatives of sphingolipids, was also included as a negative control (Kato *et al.*, 2022). Candidates from 20 species were selected from all Brassicaceae lineages and Cleomaceae. To focus on the structure known to bind 3-OH-FA, the ECD, a phylogenetic analysis of the candidate receptor ECD protein sequences was performed. Similar to the phylogeny based on full-length LORE sequences, this phylogeny also displayed that the LORE-like candidates were classified into different clades based on their origins in Brassicaceae lineages (Figure 22a). Intriguingly, compared with AtSD1-23 and other SD-RLKs, all LORE-like receptor ECDs were able to deplete 3-OH-C10:0 (Figure 22). No specific classification, such as lineage, tribe to genus, was correlated with ligand binding, apart from *C. violacea* in the outgroup, which does not have LORE-like protein (Figure 22). In the tribe Camelineae, lineage I, all four LORE orthologs, AtLORE and CrubLORE from sensitive species, as well as AhalLORE and AlyrLORE from insensitive species, could bind 3-OH-C10:0 (Figure 22) (Eschrig *et al.*, 2021). The RislLORE ECD from insensitive species *Rorripa islandica*, as other LORE-like receptors in lineage I, also bound 3-OH-C10:0. Some species in linage II have multiple 3-OH-C10:0-binding LORE ortholog ECDs, including *Brassica rapa* (BrapLOREa, BrapLOREb), *B. nigra* (BnigLOREa, BnigLOREb, BnigLOREc), *Eutrema salsugineum* (EsalLOREa, EsalLOREb), *M. maritima* (MmarLOREa, MmarLOREb), and *Eruca vesicaria* (EvesLOREa, EvesLOREb, EvesLOREc, EvesLORED) (Figure 22). The

ECDs of EsyrLOREa and EsyrLOREb from lineage III species *Euclidium syriacum* genetically evolved into two distinct clades, and both ECDs did not lose their binding activities to 3-OH-C10:0 (Figure 22). The only LORE-like receptor in 3-OH-FA-insensitive *A. arabicum* from basal lineage species, AaraLORE also bound 3-OH-C10:0 (Figure 22). Overall, the LORE-dependent 3-OH-FA binding in Brassicaceae was found to be highly conserved, and apparently, none of the selected LORE ortholog ECDs lost their receptor function during evolution. The results demonstrated that the lack of 3-OH-FA responsiveness in some Brassicaceae species is not caused by the loss of 3-OH-FA-binding activity of the respective LORE orthologs. Hence, there are multiple factors controlling 3-OH-FA responsiveness in addition to the LORE-3-OH-FA interaction.

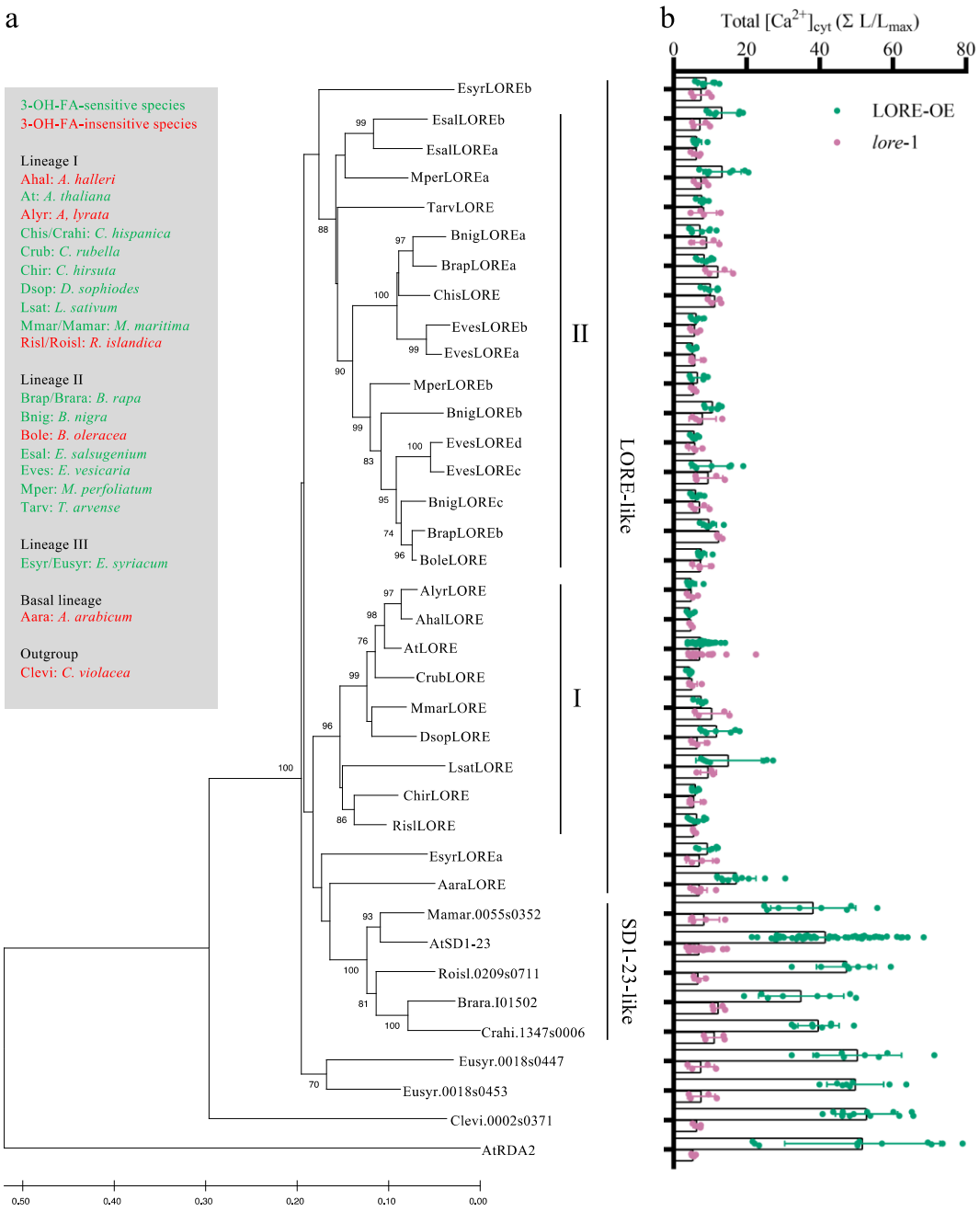

Figure 22. Function analysis of the interaction of LORE-like and other SD-RLK ECDs with 3-OH-FA. **a.** The phylogenetic analysis of selected ECDs of LORE-like receptors and other SD-RLKs. I and II indicated the major lineages of the original species of the LORE-like receptors. The alignment of 37 protein sequences was constructed by MUSCLE. The phylogeny was analyzed by MEGA XI software using the Neighbor-Joining method in the bootstrap test (1000 replicates). The bootstrap values next to the branches over 70 were shown, and the scale bar indicated the evolutionary distance, computed using the Poisson correction method. Based on Figure 19, the 3-OH-FA sensitivities of the original species of the candidate receptors are shown in the legend with color codes. **b.** The

depletion assays of LORE-like receptors and other SD-RLKs. Depletion assays were performed using 500 nM 3-OH-C10:0 and concentrated apoplastic washing fluids from *Nicotiana benthamiana* containing the indicated ECD-mCherry fusion proteins. Increases in $[Ca^{2+}]_{cyt}$ were measured in Arabidopsis LORE-OE and *lore*-1 seedlings treated with the respective filtrates from the depletion assay (mean ± SD, pooled data from at least two independent experiments for each ECD. eAtLORE-mCherry and eAtSD1-23-mCherry: LORE-OE: n = 67 seedlings, *lore*-1: n = 34 seedlings, eAtSD1-12, eAaraLORE-mCherry, eCrubLORE-mCherry, and eClevi.0002s0371-mCherry: LORE-OE: n = 12 seedlings, *lore*-1: n = 6 seedlings; Other ECDs: LORE-OE: n = 8 seedlings, *lore*-1: n = 4 seedlings.). The total protein concentration of apoplastic washing fluids was 1.5 mg/mL. The Anti-RFP immunoblots of desalted and concentrated AWFs from *N. benthamiana* leaves expressing different SD-RLK ECD-mCherry fusion proteins are shown in Supplementary Figure 10.

2.3.3 LORE-dependent response in Brassicaceae is conserved

As a cell surface receptor kinase, the LORE kinase domain is indispensable for conveying signals from the apoplast to the cytosol (Ranf *et al.*, 2015). In previous studies, the LORE kinase domain was shown to be phosphorylated *in planta* upon 3-OH-FA activation (Luo *et al.*, 2020). In another recent study, the activation of LORE-dependent responses was shown to be correlated with receptor homomerization and kinase functionality. In addition, overexpressing AtLORE and CrubLORE in *N. benthamiana* caused cell death symptoms without 3-OH-FA elicitation, but overexpressing kinase-mutated AtLORE (AtLORE-Km, K516A), AlyrLORE and AhalLORE did not (Eschrig *et al.*, 2021). It has been revealed above that the LORE orthologs from insensitive species did not lose their 3-OH-FA-binding activities, meaning that the unresponsiveness was due to other factors, possibly homomerization and/or kinase activity. The cell death phenotype by transiently overexpressing candidate receptors in *N. benthamiana* provides an indicator of SD-RLK functionality, like homomerization and kinase activity (Eschrig *et al.*, 2021). By measuring chlorophyll fluorescence as a cell death indicator upon overexpression of LORE orthologs in *N. benthamiana*, a conserved pattern was displayed within the LORE-like clade. Only two receptors, BnigLOREa and BnigLOREb, from 3-OH-FA-sensitive *B. nigra* did not trigger cell death, indicating that BnigLOREc may be the only functional RLK sensing 3-OH-FA in *B. nigra* (Figure 23). All selected LORE orthologs from lineage I, III, and basal significantly induced cell death upon overexpression in *N. benthamiana*, while a few non-LORE-like receptors could not activate it (Figure 23). The 3-OH-FA insensitive species, *A. lyrata* and *A. halleri*, have malfunctioned LORE orthologs, which match the responsiveness of the plants (Eschrig *et al.*, 2021). However, LORE orthologs from 3-OH-FA insensitive *A. arabicum*, *B. oleracea*, and *R. islandica* still activated cell death upon overexpression (Figure 23). The results and the previous

finding demonstrated that overexpression of most LORE orthologs could induce cell death in *N. benthamiana*. Furthermore, these implied that there are still other factors mediating 3-OH-FA responsiveness apart from homomerization, kinase activity, and ligand binding.

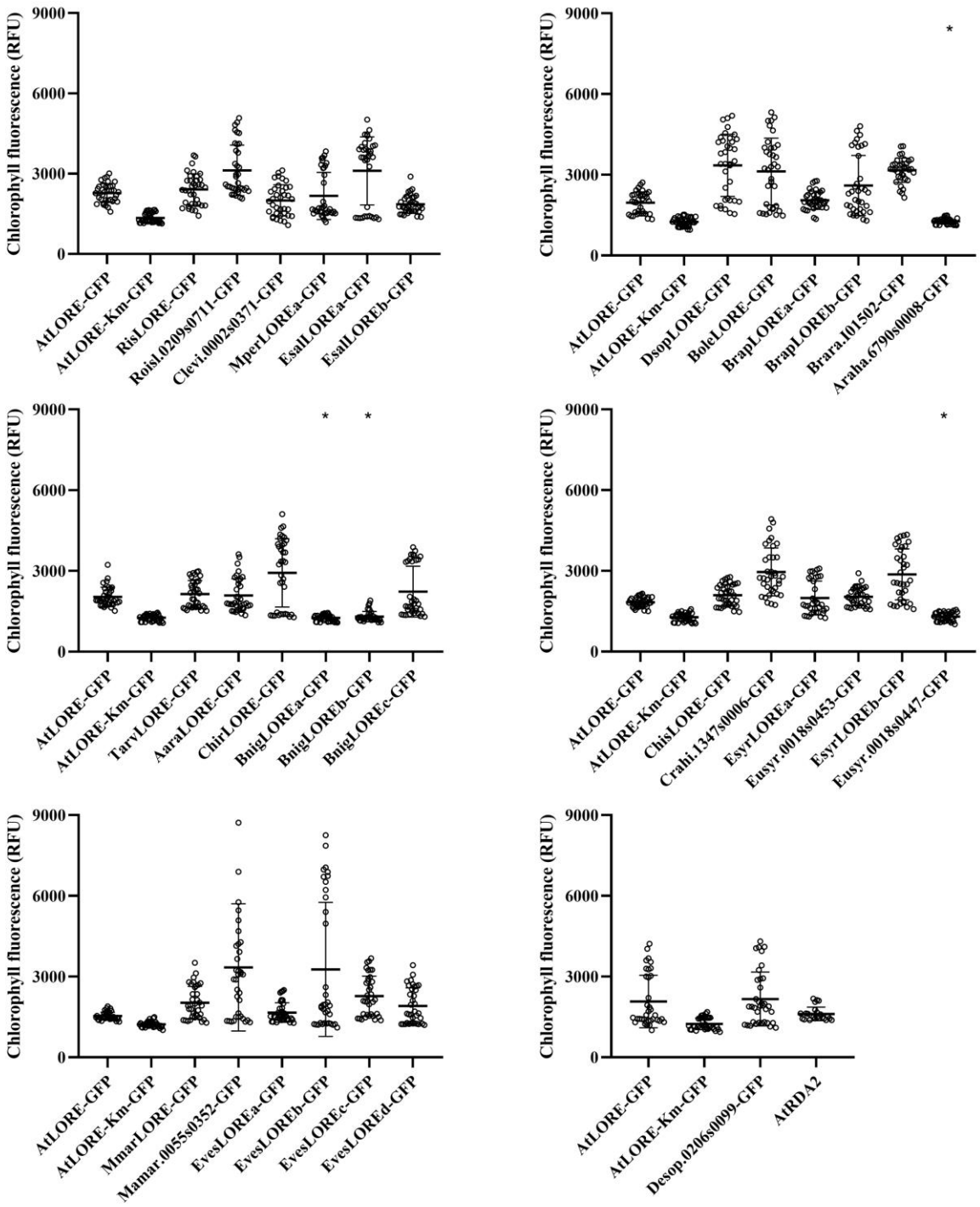

Figure 23. Function analysis of LORE-like and other SD-RLK-induced signaling. Chlorophyll fluorescence

measurement (RFU, relative fluorescence unit) of *Nicotiana benthamiana* leaves transiently overexpressing different SD-RLK GFP fusion proteins 40-42 hours after infiltration with *Agrobacterium*. AtLORE-GFP and AtLORE-Km-GFP in all assays were technically positive and negative control, respectively. Based on Figure 19, the 3-OH-FA sensitivities of the original species of the candidate receptors are shown in the legend. Pooled data were from three independent experiments (mean ± SD, n=36 leaf discs), but pooled data of AtRDA2 were from two independent experiments (mean ± SD, n=24 leaf discs). The asterisks indicate that the results were not statistically significantly different from AtLORE-Km-GFP in the same assays. Statistics were analyzed by one-way ANOVA with Dunnett's multiple comparisons test, α=0.05.

2.3.4 Functional investigation of LORE orthologs in Arabidopsis

By ligand depletion assay and cell death assay, two main functions of LORE were systemically investigated. In order to understand the integral functions of the LORE orthologs in plants, 16 candidate LORE orthologs were introduced into the Arabidopsis *lore*-1 mutant. Arabidopsis complementation lines ectopically expressing LORE orthologs from four lineages regulated by *AtLORE* promoter were generated. From basal lineage, lineage I to III, most LORE orthologs complemented the *lore*-1 mutant and perceive 3-OH-FAs. This suggests 3-OH-FA receptors have been preserved in evolution since the ancestral existence of the Brassicaceae species (Figure 24). Although not all LORE orthologs restored the 3-OH-FA responses in *lore*-1, all 3-OH-FA-sensitive species had at least one LORE ortholog which reinstated the $[Ca^{2+}]_{cyt}$ responses to 3-OH-C10:0 (Figure 24). BnigLOREa and BnigLOREc from 3-OH-FA-sensitive *B. nigra* could sense 3-OH-C10:0 with medium and strong responses, respectively, whereas BnigLOREb did not restore the $[Ca^{2+}]_{cyt}$ response upon 3-OH-C10:0 treatment in *lore*-1. BnigLOREa and BnigLOREb did not caused cell death symptom in *N. benthamiana* (Figure 23), but only BnigLOREb was defective in the Arabidopsis *lore*-1 mutant. Interestingly, RislLORE from insensitive species triggered cell death in *N. benthamiana*, but did not restore the mutant phenotype of *lore*-1. These results suggests that LORE orthologs expressed in Arabidopsis or tobacco may interact with their intrinsic components differently and reveal distinct phenotypes (Figure 24). Two EsalLORE receptors of *E. salsugineum* had different intensities of $[Ca^{2+}]_{cyt}$ responses to 3-OH-FA, although evolutionarily they were clustered together (Figure 24). Two EsyrLORE receptors, clustered in two distinct clades, could independently restore *lore*-1 with similar responsiveness, showing that they may be functionally redundant in *E. syriacum* (Figure 24). AaraLORE and BoleLORE from 3-OH-FA-insensitive species in basal lineage and lineage II complemented the $[Ca^{2+}]_{cyt}$ burst upon 3-OH-C10:0 treatment, which meant that the receptors

were possibly not expressed in the leaf tissues of *A. arabicum* and *B. oleracea* for the ROS experiments (Figure 24). In summary, all Brassicaceae plants in this study have LORE orthologs which can bind 3-OH-FA, yet a few LORE orthologs cannot complement the Arabidopsis *lore*-1 mutant phenotype. These results suggested that the mechanism of LORE-dependent 3-OH-FA-triggered response is not limited to ligand binding.

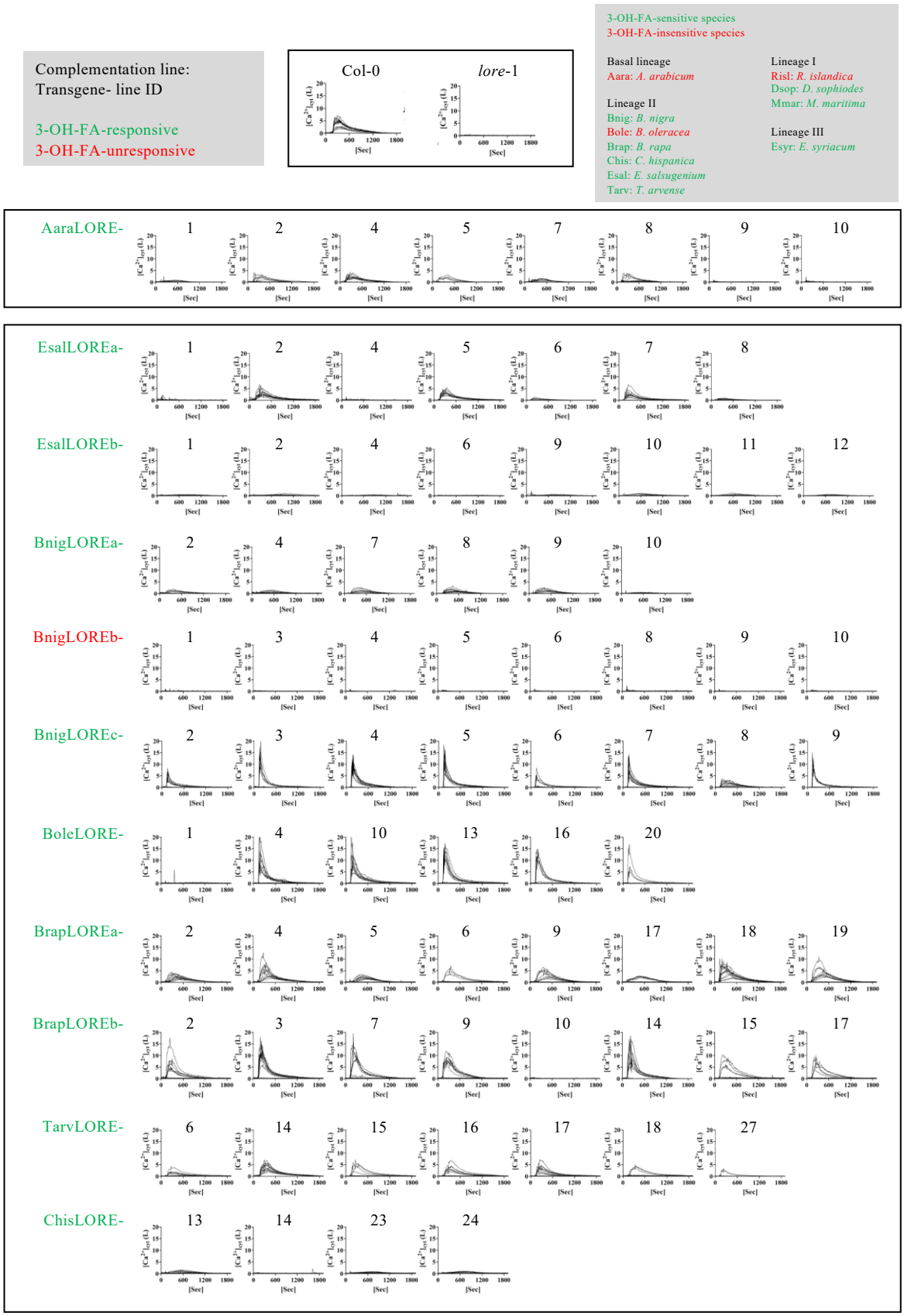

Figure 24. (Continued)

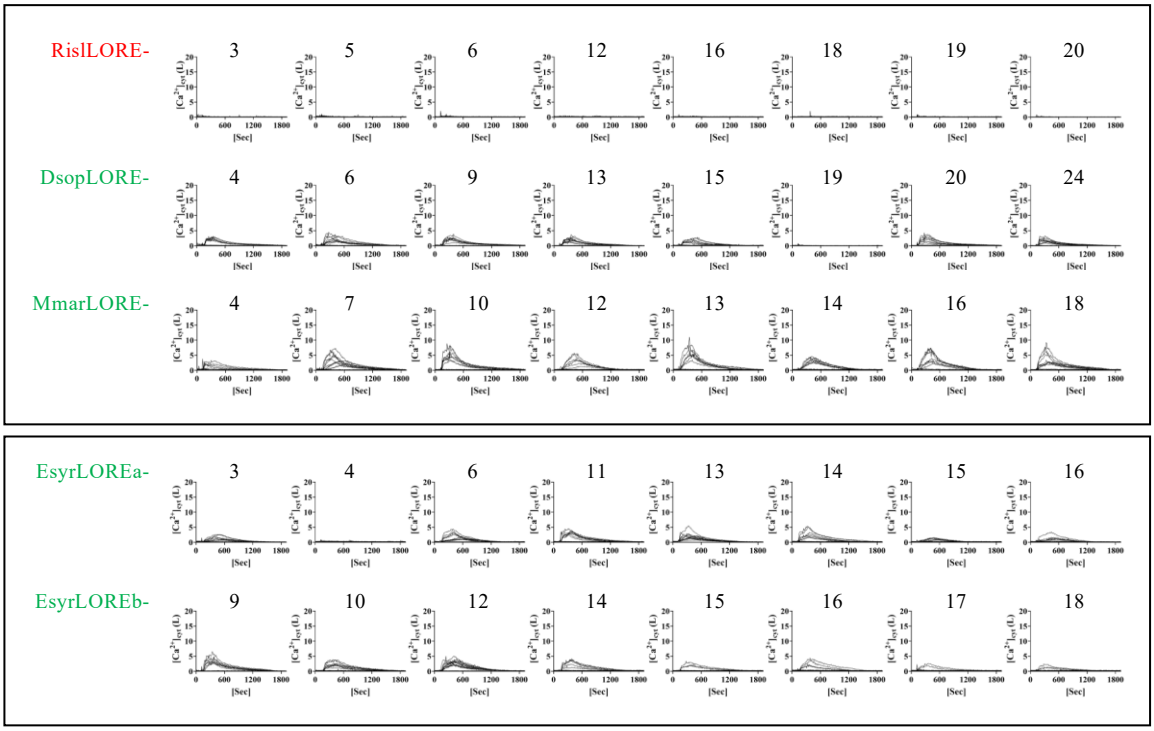

Figure 24. 3-OH-FA-triggered immune responses in various LORE ortholog-expressing *Arabidopsis thaliana lore*-1 lines. $[Ca^{2+}]_{cyt}$ kinetics was measured in LORE ortholog-complemented Arabidopsis *lore*-1 lines after elicitation by 1 μM 3-OH-C10:0. The names of LORE orthologs indicate the expressed transgenes, and the line IDs above each kinetics graph represent independent transgenic lines. LORE orthologs were highlighted in green when they restored $[Ca^{2+}]_{cyt}$ response upon 3-OH-C10:0 treatment in complementation lines, and the orthologs which did not rescue the responsiveness to 3-OH-C10:0 were highlighted in red. The responsiveness to 3-OH-FA in the original species of the candidate receptors based on Figure 19 are shown in the legend. Col-0^{AEQ} and *lore*-1 plants were included as positive and negative controls of $[Ca^{2+}]_{cyt}$ assays, respectively. T2 populations of all independent lines were used. T2 plants from the same populations for experiments were randomly selected without checking the selection marker. The kinetics of 12 individual plants from a single T2 population were shown in the same graph, and one of two independent experiments with the same patterns was plotted. The data of all measurements were not normalized. Transgene expression of all complemention lines measured by RT-PCR is provided in Supplementary Figure 11.

2.4 Identification of 3-OH-FA binding structure in LORE

As a receptor comprising several heterogeneous domains, the only well-described domain in LORE is the kinase domain, which is essential for inducing immune signaling with its phosphorylation activity (Ranf *et al.*, 2015, Kutschera *et al.*, 2019, Luo *et al.*, 2020). Although the whole ECD of LORE is known to be a 3-OH-FA binding domain and to form homomers

(Eschrig *et al.*, 2021), the ligand-binding structure has not been functionally investigated. Four subdomains, including two lectin-like domains, EGF domain and PAN domain (Figure 3), in LORE orthologs and non-3-OH-FA-binding SD-RLKs, were further analyzed *in silico*. Subsequently, the potential ligand binding domain was pinpointed using chimeric receptors and ligand-depletion binding assay.

2.4.1 Analysis of LORE ortholog ECDs for potential 3-OH-FA binding pocket

By performing the ligand depletion assay, 28 LORE ortholog ECDs were found to be 3-OH-FA binding proteins, and five close AtSD1-23-like receptors were not (Figure 22). This finding provided significant phenotypic results to clarify the decisive differences in sequences and structures between receptors with and without the binding function. LORE orthologs from lineage I species compared with SD1-23-like receptors share 70% to 82% identity, and LORE orthologs from lineage II share protein identity from 69% to 79% with SD1-23-like receptors. The sequence identity between LORE orthologs from lineage I and lineage II is around 73% to 83%, slightly higher than the identity between SD1-23-like receptors (Supplementary Figure 12). To identify the site of the LORE ortholog ECDs involved in ligand binding, a protein alignment was made between receptors and non-receptors to identify distinct residues. Among four subdomains, EGF and PAN domains do not reveal any residue exclusively present in SD1-23-like receptors but not in LORE-orthologs, and lectin-like domain 1 only possesses one such residue in its 136 residues. Strikingly, among the 149 amino acids in the lectin-like domain 2 protein sequences, up to 9 amino acids are unique between LORE ortholog ECDs and SD1-23-like ECDs, suggesting that lectin-like domain 2 may determine the difference between ligand-binding and -nonbinding ECDs (Supplementary Figure 13). In order to strengthen this assumption, eAtLORE homology modeling was performed by SWISS-MODEL based on the SRK9 structure. A neural network-based predictor, DEEPSITE, was used to explore potential pockets for ligand binding in lectin-like domain 2 (Supplementary Figure 14) (Ma *et al.*, 2016, Jiménez *et al.*, 2017, Waterhouse *et al.*, 2018). Because lectin-like domain 2 was proposed to be a suitable site for ligand binding, eAtLORE-3-OH-C10:0 docking was conducted by an open docking tool (Murail *et al.*, 2021). Based on the prediction results, one potential 3-OH-C10:0 binding site was identified in lectin-like domain 2, and the acyl chain of 3-OH-C10:0 was shown to dock into the core of lectin-like domain 2 (Figure 25). Taken together, the results suggested that LORE lectin-like domain contains a potential 3-OH-FA binding pocket, and the analyses of

LORE orthologous sequences and homology modeling-coupled ligand docking strongly support the hypothesis. Whether lectin-like domain 2 is indeed a binding pocket of 3-OH-FA still needs to be further verified by experiments.

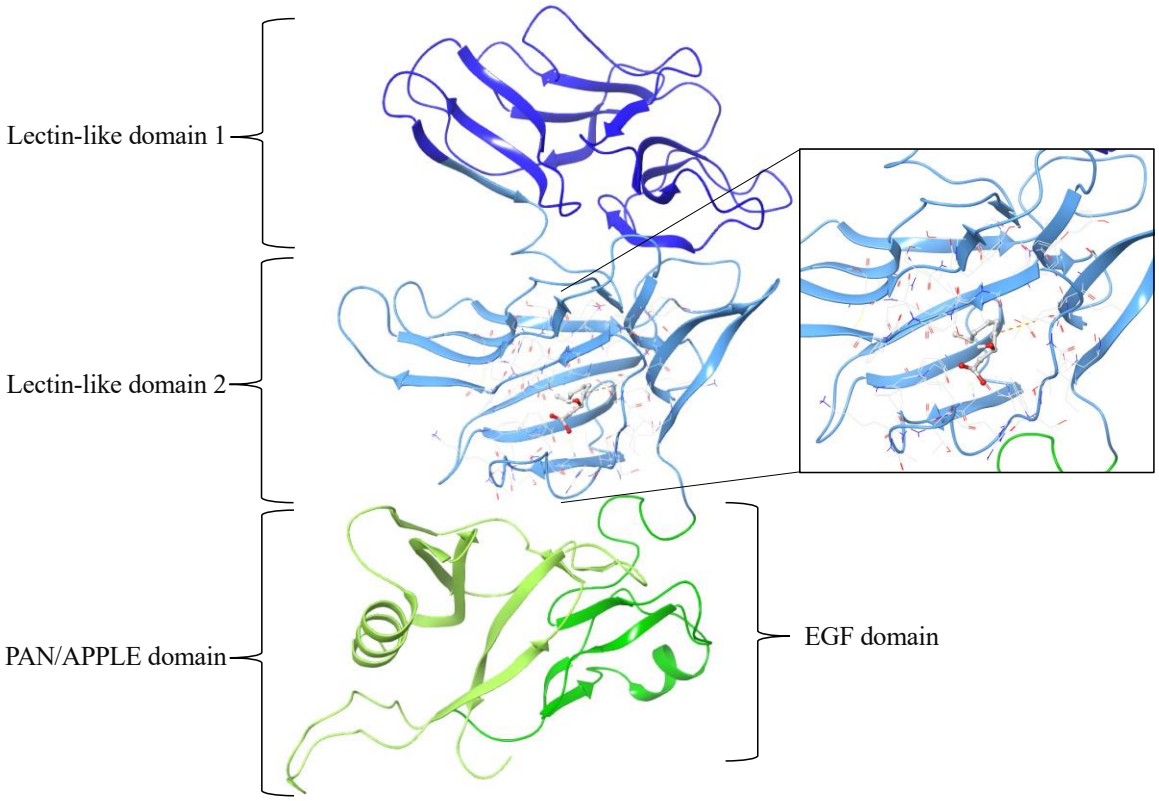

Figure 25. Prediction of AtLORE ECD structure and its 3-OH-C10:0 binding pocket. The protein model of AtLORE ECD (residue 23-420) was predicted by SWISS-DOCK, and the ligand binding was predicted by the software Autodock in SeamDock and visualized by Maestro. The 3-OH-C10:0 in green in lectin-like domain 2 is the putative ligand binding site. The side chains of amino acids around 3-OH-C10:0, which interact with the ligand, are shown. The dashed line in orange indicates the potential hydrogen bond. The domains in ribbon style were labeled in different colors based on the annotation in Supplementary Figure 13.

2.4.2 Investigation of LORE 3-OH-FA binding domain

To functionally identify the responsible structure for 3-OH-FA-binding in eAtLORE, the chimeric ECDs of AtLORE and AtSD1-23 were assembled according to their four subdomains. AtSD1-23 ECD swapped with different AtLORE subdomains might gain the function of 3-OH-FA-binding, and the swapped subdomains could be the essential binding structure. Although not all domain-swapped receptors were successfully cloned or expressed, all four major domains, lectin-like domain 1, lectin-like domain 2, EGF-like domain, and PAN domain from AtLORE

were swapped with AtSD1-23 at least once in this study. Two chimeric ECD (eDS123-L1P and eDS123-L1) revealed 3-OH-C10:0-binding activities, and these two ECD shared AtLORE lectin-like domain 2 and EGF domain. EGF domain might not have a 3-OH-C10:0-binding site because AtLORE EGF domain did not restore the binding abilities in two chimeras containing AtLORE EGF domains (eDS123-L1L2P and eDS123-L1L2). To narrow down the potential 3-OH-C10:0-binding structure, AtLORE lectin-like domain 2 was further divided into two parts (Residue 137-202 and 202-302) and swapped with AtSD1-23. However, none of these four chimeras bound to 3-OH-C10:0. These results indicated that 3-OH-FA binding site is located in AtLORE lectin-like domain 2, and the complete AtLORE lectin-like domain 2 seems to form the binding pocket.

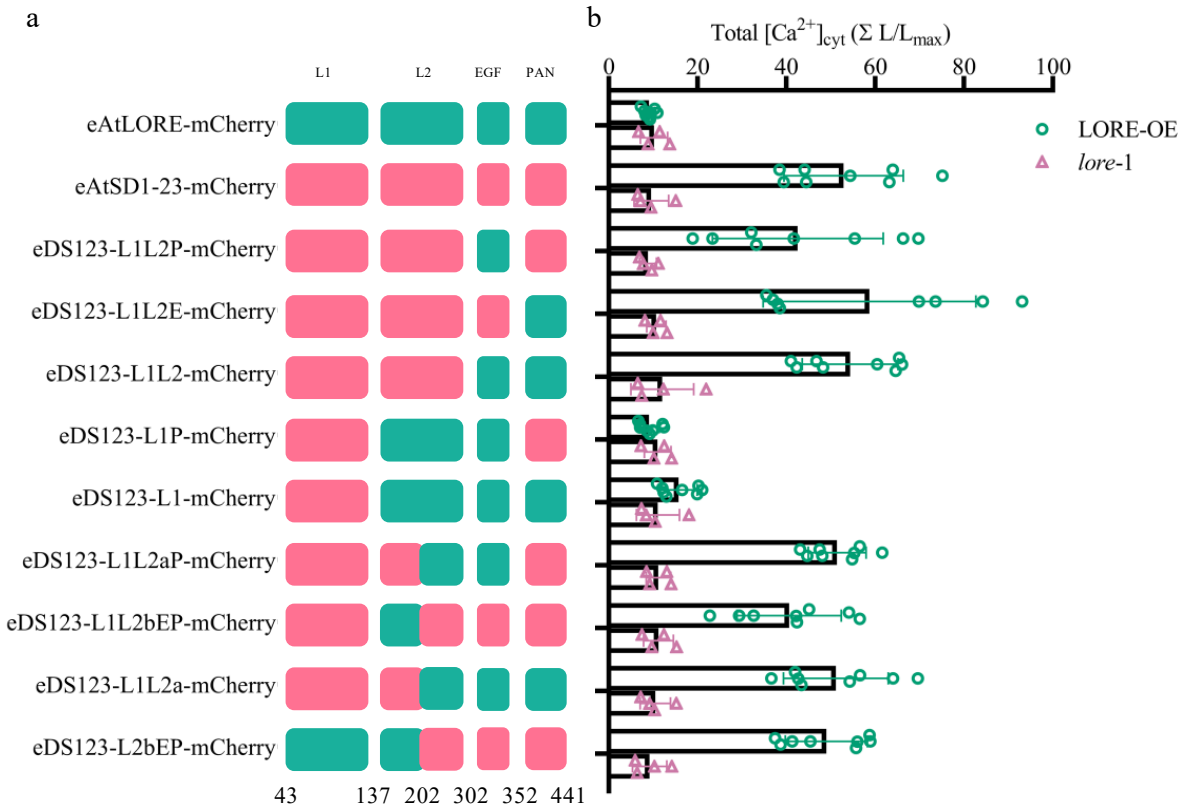

Figure 26. Domain-swapped receptors indicate that lectin-like domain 2 is essential for 3-OH-FA binding. a. Schematic represents AtLORE, AtSD1-23, and nine domain-swapped ectodomains of receptors used for domain-ligand binding analysis. The domains were defined according to the SRK9 structure (Ma, *et al*., 2016). L1, lectin-like domain 1. L2, lectin-like domain 2. EGF, EGF-like domain. PAN, plasminogen-apple-nematode domain. The boxes in green indicate the domains from AtLORE, and the boxes in red indicate the domains from AtSD1-23. Below the scheme, the numbers indicate the positions of amino acids between the domains. The signal peptide from AtSD1-23 (Residue: 1-42) was used in all 11 ectodomains. **b.** Depletion assay was performed using 500 nM 3-OH-C10:0

and concentrated apoplastic washing fluid from *Nicotiana benthamiana* containing the indicated mCherry fusion proteins of domain-swapped ECD of receptors. Increases in $[Ca^{2+}]_{cyt}$ were measured in Arabidopsis LORE-OE and *lore*-1 seedlings treated with the respective filtrates from the depletion assay (mean ± SD, LORE-OE: n = 8 seedlings, *lore*-1: n = 4 seedlings; pooled data were from two independent assays). The total protein concentration of apoplastic washing fluids was 1.5 mg/mL. The Anti-RFP immunoblots of desalted and concentrated AWFs from *N. benthamiana* leaves expressing different domain-swapped AtLORE-AtSD1-23 ECD-mCherry fusion proteins are shown in Supplementary Figure 15.

3 Discussion

3.1 The hardship of SD-RLK ECD recombinant protein expression

An efficient protein expression protocol is the first step in determining the protein-fatty acid interactions. Making the system applicable to other receptors and less costly is also preferred. Recombinant protein expression in the bacterium *E. coli* is the most popular system of producing protein-of-interest for all organisms because *E. coli* is a well-established host, which provides many advantages. *E. coli* can be grown and expresses recombinant proteins in a very short incubation time, and it grows rapidly in simple but in-house made broth media and reagents with low cost, which makes it easy to scale up to large volumes (Sørensen and Mortensen, 2005). In addition, *E. coli* has a long history of being a tool for expressing a wide range of different types of proteins, giving this approach a wide variety of methods for genetic construction and manipulation. However, eAtLORE was only expressed and accumulated in inclusion bodies (Supplementary Figure 1), meaning that the eAtLORE protein was insoluble under the conditions tested in this study. The limitation of using a bacterial expression system is that eukaryotic proteins are not always folded properly by the prokaryotic protein machinery (Sørensen and Mortensen, 2005). Due to insufficient posttranslational modification, some recombinant proteins are not shaped as they are expressed in their origin host. Glycosylation is one of the steps for posttranslational modification, which is essential for ligand binding, protein accumulation, and localization of PRRs in plant cells (Häweker *et al.*, 2010, Trempel *et al.*, 2016). Although the strains used in the study are equipped with the genes for improving disulfide bridge formation, which is also known to be essential for stabilizing SRKs (Ma *et al.*, 2016, Murase *et al.*, 2020), they still could not avoid the aggregation of eAtLORE in bacterial cells. Only a few PRR ECDs were expressed by *E. coli* and were still functional. Four LecRK ECDs, P2K1 and P2K2, for binding eATP, and LecRK-I.8, LecRK-VI.2 for sensing $eNAD^+$ were successfully expressed by bacteria and used in radiobinding assays (Choi *et al.*, 2014, Wang *et al.*, 2017, Wang *et al.*, 2019, Pham *et al.*, 2020). FERONIA ECD generated by *E. coli* was able to pull down RALF23 in the co-immunoprecipitation assay (Stegmann *et al.*, 2017). SD-RLK ERK1 in *N. benthamina* was expressed in *E. coli* and purified; nevertheless, it did not reveal its association with BAK1 as it showed *in planta* (Pi *et al.*, 2022). Functional LRR-RK ECDs expressed by *E. coli* have not been described, and LRR-containing cytosolic proteins were mostly accumulated in inclusion bodies when they were overexpressed in bacteria (Guo *et al.*, 2017).

Insect cell protein expression system has been established for more than 30 years (Van Oers *et al.*, 2015). In the past decades, baculovirus-based insect cell protein expression became a mainstream of PRR ECD expression for experiments which have the demand for high-quality, like the crystallographic analysis. This eukaryotic expression system is a reasonably quick expression method from plasmid construction to protein harvesting and can be scaled up (Berger and Poterszman, 2015). Compared with the prokaryotic system, insect cell produces secreted eukaryotic proteins and membrane proteins relatively well, which are post-translationally modified by the eukaryotic machinery offering a suitable condition for protein folding (Shi and Jarvis, 2007). By contrast, the cost of growing insect cells is far more than the bacterial expression system and needs relatively sophisticated handling skills. Insect cell systems mainly expressed LRR-RK and LRR-RP ECDs for crystallography and binding assays in recent years, like MIK2 (Hou *et al.*, 2021b, Rhodes *et al.*, 2021), INR-Vu (Steinbrenner *et al.*, 2020), FLS2-BAK1 complex (Sun *et al.*, 2013b), Phytosulfokine receptor (PSKR) 1 (Wang *et al.*, 2015), BRI1-SERK3 (SOMATIC EMBRYOGENESIS RECEPTOR KINASE 3) complex, and many others (Tang *et al.*, 2015, Smakowska-Luzan *et al.*, 2018). Functional FERONIA malectin ECD was also expressed by the insect cell system (Xiao *et al.*, 2019), and LysM ECDs also displayed some successful cases (Liu *et al.*, 2012, Bozsoki *et al.*, 2020). In the SD-RLK family, the insect cell system largely expressed both SRK9 and SRK8 ECDs, which were able to be crystalized (Ma *et al.*, 2016, Murase *et al.*, 2020). Similarly, the RDA2 ECD was directly harvested from the intact silkworm larvae, which is also an insect-based system (Kato *et al.*, 2022). In the previous study, eAtLORE was expressed by the insect cell system with baculovirus. It was indeed able to produce eAtLORE, which was sufficient for the following purification steps (Kutschera *et al.*, 2019); however, the protein yield was quite low and the protein tended to aggregate in solution (unpublished results, personal communication with Dr. Stefanie Ranf, TU München). In this thesis, the insect cell system is not considered due to these issues, but the cultural conditions, purification methods, and types of insect cells could be further tested to improve this approach.

Cell-free protein expression is another popular alternative to *in vitro* protein expression systems (Silverman *et al.*, 2020). The protein is expressed in a cell-free environment using a combination of cell extracts from specific organisms, DNA-carrying target genes and expression cassettes, amino acids, and other necessary supplements in this system. Currently, the commonly used cell

lysates for cell-free protein expression are from *E. coli*, rabbit reticulocytes, wheat germ cells, insect cells, and tobacco cells (Khambhati *et al.*, 2019). With many sources of cell lysates, cell-free protein expression can be used to express proteins from a wide range of organisms. The system can be easily adapted to high-throughput protocols and coupled with purification steps in an automated manner, so it can be utilized to screen many candidates more efficiently than other expression systems. Moreover, this approach can also produce proteins that are toxic to organisms, and it even can synthesize the proteins with toxic labeling. However, the major drawback of the cell-free expression system is its costly cell lysates; therefore, it is unsuitable for mass production (Khambhati *et al.*, 2019). To date, only minor studies in plant sciences utilized the cell-free system for protein expression, and the FERONIA ECD was the only successful one in plant PRR studies (Minkoff *et al.*, 2017). *Nicotiana tabacum* can gain the function of sensing 3-OH-FA by overexpressing AtLORE (Kutschera *et al.*, 2019), demonstrating that *N. tabacum* can synthesize a functional AtLORE ECD. The tobacco-based cell-free expression system can generate plant transcription factors (Huck *et al.*, 2017). The small-scale protein expression is sufficient for many biochemical assays. In this study, the tobacco cell lysate indeed expressed eAtLORE (Supplementary Figure 2). Although this plant-based expression system expressed the eAtLORE ECD with a N-terminal signal peptide, which enables the formation of disulfide bonds in the process (Buntru *et al.*, 2015), the eAtLORE protein could not be affinity-purified, unfortunately (Supplementary Figure 2).

Protein expression by tobacco is applied in analytical to preparative-scale protein expression systems, and the platforms for protein expression are transgenic plant, transient expression, and cell and callus suspension cultures (Gomes *et al.*, 2019). The reason for using the platform of Agrobacterium-mediated transient expression in tobacco is its advantages, such as the flexible and easy operation, shorter processing time, fewer steps, and lower cost. This approach is suitable for testing many candidates in parallel compared to tediously generating multiple transgenic plants or culturing different tobacco cells in expensive bioreactors (Komarova *et al.*, 2010). In recent decades, plant-based protein expression has been massively applied in the commercial protein production of pharmaceutical drugs and vaccines, suggesting that plant-generated recombinant proteins are competitive compared with other eukaryotic systems (Schillberg *et al.*, 2019, Bolaños-Martínez and Strasser, 2022). Gain-of-function studies in *N. benthamiana* demonstrated that it expressed the AtLORE receptor, capable of sensing mc-3-OH-FAs

(Kutschera *et al.*, 2019). Additionally, *N. benthamiana*, lacking a 3-OH-FA sensing system, is a suitable host to express functional AtLORE ECD that can be used for the binding assays from the mc-3-OH-FA receptor-free background (Shu *et al.*, 2021). Compared with tobacco cell-based cell-free protein expression, this approach can express target ECD via a complete transcriptional-translational process. The ECD with a signal peptide for secretory pathway could be folded and post-translationally modified *in planta*. The ECDs were expressed and localized in apoplast by tobacco, which can be easily harvested from *N. benthamiana* plants in AWF (Shu *et al.*, 2021). Because the ECDs have to pass the protein quality control system *in vivo*, presumably, the proteins in AWF are post-translationally modified and correctly folded. This plant expression method supplies receptor ECDs in soluble form without the extraction of cell lysates and solubilization of membranes, which could impair the subsequent functional studies. Though the yield of ECD in *N. benthamiana* was not exceedingly abundant even after concentration, and the degradation of ECD was observed in immunoblot analysis (Figure 7a, b), the concentration of ECD collected in AWF was adequate for the following ligand depletion-binding assay (Figure 10, 11, 12). Moreover, tobacco-expressed eAtLORE fused with Twin-Strep-tag can be purified. This demonstrates the potential for purifying large-scale eAtLORE (Figure 14). The R protein ROQ1 (recognition of XopQ 1) in *N. benthamiana* recognizes the effector protein XopQ (Xanthomonas outer protein Q) from pathogenic *Xanthomonas*, and ROQ1-XopQ complexes form tetramers, also known as resistosome, for immune response (Ma *et al.*, 2020, Martin *et al.*, 2020). The ROQ1 and XopQ proteins for cryo-electron microscopy in these groundbreaking findings were expressed and purified from *N. benthamiana* plants and insect cells done by two independent groups, showing the potential of protein expression by tobacco is as comparable as other popular eukaryotic systems (Ma *et al.*, 2020, Martin *et al.*, 2020). LRR-RLK CARD1 is also an example of PRRs displaying that *N. benthamiana* has the capability to produce high amounts of target proteins and secret them into AWF (Laohavisit *et al.*, 2020). One of the major protein expression issues in plants is proteolysis. This study shows that eAtLORE and ortholog mCherry fusion proteins have many fragments in the immunoblots (Figure 7) (Shu *et al.*, 2021), as well as two fragments in purified eAtLORE sample (Figure 14). Although adding protease inhibitors can prevent proteolysis during the AWF harvesting process, most recombinant proteins are gradually broken down during the incubation process, which cannot be avoided (Robert *et al.*, 2013, Mandal *et al.*, 2016). Expressing proteinaceous protease inhibitors and supplementing

protein stabilizing agents are potential strategies to reduce the loss of intact recombinant proteins in plant systems (Häkkinen *et al.*, 2014, Grosse-Holz *et al.*, 2018).

3.2 Diverse methods for characterizing LORE-3-OH-FA interaction

Deciphering protein-ligand interactions is a core topic of dissecting the molecular mechanisms of PTI. Developing an ideal technique for measuring bimolecular interactions is challenging, especially in developing new strategies to precisely describe and quantify the protein-ligand affinity (Sandoval and Santiago, 2020). Compared with protein-protein interactions and protein-peptide interactions in plant immunity, the methods for protein-fatty acid interactions have not been extensively developed, and the bottleneck of PRR protein expression elevates the difficulty of verification. AtLORE is a PRR for mc-3-OH-FAs, and its ECD binds 3-OH-C10:0 *in vitro*; nevertheless, the affinities measured in this study were relatively low (Kutschera *et al.*, 2019). To investigate the AtLORE-mc-3-OH-FA interaction in more detail, I aimed to establish reliable and versatile assays that can validate not only AtLORE-3-OH-C10:0 interaction but also screen multiple receptor variants and mc-3-OH-FAs. One commonly used assay for protein-lipid interaction is the protein lipid overlay assay (PLO). It is even commercially available for some lipid species essential for the constitution of the plasma membrane and lipid metabolism (Dowler *et al.*, 2002). With tagged protein targets, PLO assay can screen many lipids in a high-throughput manner and even measure the binding affinity. Arabidopsis RDA2-sphingoid base interaction *in vitro* was described by PLO assay, and their binding affinity was also estimated (Kato *et al.*, 2022). However, the lipid species mostly applied in PLO assays are long-chain lipids and fatty acids, which are highly hydrophobic. mc-3-OH-FAs are not compatible with this convenient method. mc-3-OH-FAs are well water-soluble, especially 3-OH-C10:0, and they may not be retained in the PLO membranes with their short acyl chains (Han *et al.*, 2020).

Since covalent modification of the mc-3-OH-FA ligand disturbs its immunogenic activity (Kutschera *et al.*, 2019), presumably by affecting receptor binding, fluorescence labeling of mc-3-OH-FAs and other similar strategies are not possible. The depletion-binding assay was therefore developed to research the binding of the AtLORE ECD with unlabeled 3-OH-C10:0 in solution (Figure 8). I utilized a wild-type *A. thaliana* and a highly mc-3-OH-FA-sensitive LORE-OE line as biosensors to detect 3-OH-C10:0 below micromolar concentrations (Figure 9). These biosensors are more sensitive to 3-OH-C10:0 than mass spectrometry-based methods (Kutschera

et al., 2019). Notwithstanding, the LORE-OE line cannot be used to measure the depletion of non-immunogenic 3-OH-FAs with longer acyl chains, such as 3-OH-C14:0, and it also cannot differentiate different mc-3-OH-FAs based on the eliciting activities (Kutschera *et al.*, 2019). Alternatively, ligands could be detected by other analytical approaches, like mass spectrometry, which requires improvements in the 3-OH-FA quantification limit. The results of the depletion-binding assay measured in this study with eAtLORE are comparable with previous results and further reveal direct AtLORE-3-OH-C10:0/HAA interactions (Figure 10, 11, 12, and 13) (Kutschera *et al.*, 2019, Schellenberger *et al.*, 2021). To challenge the reliability of the depletion-binding assay, I also checked the ECDs of two SD-RLKs, eAtSD1-23, and eCrubLORE, for binding of mc-3-OH-FA, which are genetically similar to AtLORE, sharing 81% and 92% amino acid identity, respectively. eAtSD1-23 neither significantly depleted nor tightly bound detectable amounts of 3-OH-C10:0 (Figure 11, 12). *C. rubella*, a close relative of *A. thaliana*, is sensitive to mc-3-OH-FAs (Figure 20). Its putative LORE ortholog, CrubLORE, was identified as an mc-3-OH-FA-binding receptor (Figure 11, 12). From tobacco-based protein expression to the ligand depletion-binding assay, the pipeline developed here for studying interactions between plant SD-RLK ECDs and mc-3-OH-FAs requires simple equipment and techniques available in most plant research labs. The straightforward workflow makes this assay applicable for screening SD-RLK-ligand interactions in medium throughput. The assay workflow is also very flexible regarding protein source and ligand detection method and can be adjusted to study other receptor-ligand pairs.

MST was used to measure eAtLORE-3-OH-FA interaction with the purified insect cell-expressed eAtLORE; however, the results did not conclude that there was a strong binding affinity between them (Kutschera *et al.*, 2019). In this study, I utilized the proteins expressed by tobacco to substitute the insect cell system. These proteins, either in AWF or purified, were still unable to reveal significant binding signals in all combinations tested (Supplementary Figure 5, 6, 7). In addition, the weak binding between eAtLORE and 3-OH-FA acquired in the previous study might possibly be due to the nonspecific signals, and may be caused by the formation of micelles or vesicles at high concentrations of 3-OH-FA (Supplementary Figure 6) (Kutschera *et al.*, 2019). In previous ligand depletion-binding assays with the same protein sources as used for MST analysis, eAtLORE was determined to bind 3-OH-FA, but the MST assays did not confirm these results. 3-OH-FA is likely bound to eAtLORE in the MST assay; however, 3-OH-FA did not

significantly alter the properties of eAtLORE and thus did not change the diffusion rate. These results suggest that the validation of biomolecular interactions cannot be concluded by only one verification method.

Radiobinding assay provides a straightforward way to test the interaction of eAtLORE and 3-OH-FA, although the radiochemicals and consumables are very costly compared to methods like ligand depletion assay. The specific binding of 3-OH-C10:0 to eAtLORE was measured, and their dissociation constant is approximately 700 nM to 4 μM, which is far lower than the results measured by the MST assays (Figure 16a) (Kutschera *et al.*, 2019). The radiobinding assay not only measured the interaction of 3-OH-C10:0 and eAtLORE but also compared the binding abilities of 3-OH-C10:0 with 3-OH-C12:0 and 3-OH-C14:0. 3-OH-C10:0 has a higher binding affinity to eAtLORE than 3-OH-C12:0 and 3-OH-C14:0, indicating that the binding affinity positively correlates with the activity of AtLORE-dependent elicitation in Arabidopsis (Figure 16b). Radiobinding assays also assessed the DORN1-eATP interaction, showing that radiolabeled ATP was strongly competed by unlabeled ATP and ADP. Similarly, it revealed far less competition by ITP, GTP, and UTP, which are weak or not DORN1-dependent elicitors, indicating that the ligand-binding affinity determines the strength of immune responses in Arabidopsis (Choi *et al.*, 2014). On the contrary, RDA2 can strongly bind to the most active elicitor 9-Methyl–branched sphingoid base (the dissociation constant is less than 1 μM) but also bind the other less active sphingosine-related compounds with similar binding affinities, which do not positively correlate with their activities of elicitation (Kato *et al.*, 2022). These results suggest that the verification of biomolecular interactions cannot be concluded only by either biological assay or biochemical experiment but require a comprehensive examination based on different methods assessing different properties of the protein-ligand pairs.

3.3 Natural diversity of 3-OH-FA sensing in Brassicaceae—intraspecies and interspecies

Species in Kingdom Plantae evolved an immune system to resist pathogens and PRRs localized at the cell plasma membrane were dedicated to monitoring pathogenic microbes and inducing immune responses. Many conserved microbial patterns are known to trigger immunity in plants; however, only a few of them have been found to induce PTI in a wide range of plant families, such as flagellin-sensing and nlp20-sensing in Arabidopsis, tomato, soybean, grape, rice, lettuce. (Chinchilla *et al.*, 2006, Robatzek *et al.*, 2007, Takai *et al.*, 2008, Böhm *et al.*, 2014, Trdá *et al.*,

2014, Wei *et al.*, 2020). Currently, the plant species which can respond to mc-3-OH-FA and EndoPG have only been identified in Brassicaceae (Ranf *et al.*, 2015, Schäffer, 2019, Zhang *et al.*, 2021). Based on the narrow specificities of elicitors above, it is likely that mc-3-OH-FA-sensitive plants evolved similar systems for detecting mc-3-OH-FA as LORE in *A. thaliana*.

Arabidopsis has a wide range of accessions that have diverse phenotypes and come from different geographical regions, and this collection provides a model for studying intraspecies diversity of different phenotypes like PTI. Based on the phenotypic variations and the comprehensive Arabidopsis ecotype genome database, it is a straightforward strategy for positioning potential genes involved in PTI. The PRRs like Arabidopsis RLP32 for sensing IF1 were identified by utilizing these beneficial resources (Fan *et al*., 2022). 68 *A. thaliana* accessions were systematically screened with 3-OH-C10:0 and 3-OH-C12:0, and flg22 elicitation was used as a standard of conserved PTI. The 3-OH-FA responsiveness was conserved in Arabidopsis accessions, and only one accession did not respond to mc-3-OH-FA, compared with flg22, which did not trigger ROS burst in six accessions (Figure 17). Flg22-triggered immune responses were known to be conserved among Arabidopsis ecotypes, and over 90% of them were sensitive to flg22 in previous screening studies, which is similar to this study (Figure 17) (Winkelmüller *et al.*, 2021, Zhang *et al.*, 2021). In other Arabidopsis ecotype PTI screenings, like with nlp20, eMAX, IF1, and SCLEROTINIA CULTURE FILTRATE ELICITOR1 (SCFE1), but not EndoPG, displayed conserved activities to over 90% of Arabidopsis accessions (Jehle *et al.*, 2013, Zhang *et al.*, 2013, Albert *et al.*, 2015, Zhang *et al.*, 2021, Fan *et al.*, 2022). mc-3-OH-FA-triggered immune responses in *A. thaliana* were not strongly diversified in evolution. Still, the intensities of ROS responses to mc-3-OH-FA are variable within *A. thaliana*, implying that other factors involved in mc-3-OH-FA-triggered responses determine the intensity of elicitation (Figure 17). LORE senses mc-3-OH-FAs in a chain length-specific manner in Arabidopsis, and ROS response in Col-0 triggered by 3-OH-C10:0 was stronger than by 3-OH-C12:0 (Kutschera *et al.*, 2019). The pattern is also conserved in all sensitive accessions, suggesting that the SNPs in LORE ECD of the ecotypes do not disturb the chain length-specificity (Figure 17). Although the genotypic and phenotypic results were acquired, GWAS for mining the components of LORE-dependent signaling did not reveal significant SNPs, including synonymous and non-synonymous SNPs (Figure 18). Insufficient ecotypes of Arabidopsis for GWAS usually lead to no significant SNP, so significant SNPs may likely be revealed after supplying more than 100

accessions into GWAS (Korte and Farlow, 2013). The insensitive accession T740 has one non-synonymous SNP in the ECD of LORE; however, the SNP is a conserved residue among the Brassicaceae LORE orthologs (Supplementary Figure 13), implying that the ECD of T740 may not be functional for 3-OH-FA-sensing likely due to protein misfolding. Whether this SNP in T740 is correlated with ligand-binding or other mechanisms must be further verified.

The variations within Arabidopsis are likely insufficient for deciphering the differences of LORE between sensitive and insensitive versions, so comparing interspecies differences in mc-3-OH-FA-sensing is the way to uncover the critical factors for LORE-dependent signaling. Brassicaceae, as a model family, provides a wide range of species for systematic studies, and its well-established genomic resources are publicly available. The diversities of sensing different patterns in Brassicaceae have yet to be well-described. Previous studies usually tested less than ten candidates with elicitors, which are numerically insufficient to fully illustrate the evolutionary footprint of gaining and losing the functions of PTI. The 43 Brassicaceae species tested here cover all the major lineages of the family, and allow to study the evolutionary patterns in Brassicaceae. Flg22-sensing in Brassicaceae was still shown to be highly conserved in these candidates, and the conservation is supported by previous studies (Figure 19) (Dunning *et al.*, 2007, Winkelmüller *et al.*, 2021). Nevertheless, mc-3-OH-FA-triggered responses are not as conserved as flg22-triggered responses in Brassicaceae. Several species were identified to be insensitive to mc-3-OH-FA, while they still responded to flg22 (Figure 19). The taxonomic ranks of these Brassicaceae species cannot classify the responsiveness of species to mc-3-OH-FA, and the phylogeny of Brassicaceae species cannot adequately describe the gain and loss of mc-3-OH-FA sensing (Figure 19). In the proposed evolutionary scenarios of Brassicaceae, the species of lineage I, II, and III, except basal lineage, evolved after the first diverging event within Brassicaceae, meaning they share the same ancestor (Walden *et al.*, 2020b). All Brassicaceae lineages contain both 3-OH-FA sensitive and insensitive species, suggesting that the function of sensing 3-OH-FA acquired from their ancestor may be mutated or restricted in 3-OH-FA-insensitive species. EndoPG and IF1 can trigger immune responses in some Brassicaceae species, including *A. thaliana*. Likewise, not all species in the same genera respond to EndoPG and IF1, suggesting that the loss of the functions of recognizing these microbial patterns is common in the family (Zhang *et al.*, 2021, Fan *et al.*, 2022). The unique chain length-specific manners are conserved in the mc-3-OH-FA sensitive species. The responsiveness to 3-OH-C13:0 among the

tested species does not correlate with the phylogeny (Figure 20). 3-OH-C10:0 is still the strongest elicitor among the other mc-3-OH-FAs in most of the species. The species which is more sensitive to 3-OH-C12:0 than to 3-OH-C10:0 was also observed (Figure 20, Supplementary Figure 9). Brassicaceae species did not evolve the receptors for detecting 3-OH-C14:0, indicating that sensing longer 3-OH-FAs may not benefit plant immunity (Figure 20, Supplementary Figure 9). Taken together, the chain length-specific manners were well-preserved in the evolution.

3.4 Conserved LORE orthologs in Brassicaceae

Evolutionary investigation of diverse plant immune responses to a single MAMP or DAMP is seldom demonstrated beyond a single model plant, although this is a promising approach to uncover the emergence of specific PRR functions (Snoeck *et al.*, 2022b). 3-OH-FA-induced immune responses were only found in Brassicaceae, and the LORE-like receptors were explicitly identified in Brassicaceae as well, implying that Brassicaceae evolved this unique sensing system for the 3-OH-FA elicitor (Ranf *et al.*, 2015, Kutschera *et al.*, 2019). Because LORE is phylogenetically restricted to Brassicaceae, it simplifies the search for an ancestor who evolved LORE. After comprehensive ROS assays, I learned that at least three major Brassicaceae lineages must have the receptors for 3-OH-FA recognition (Figure 19). The sequences of cognate LORE receptors and close SD-RLKs were retrieved from candidate species. All of the selected Brassicaceae species were found to have LORE-like protein sequences, meaning the possession of *LORE* genes is not correlated with 3-OH-FA sensing (Figure 21). The outgroup species in the sister family *C. violacea* does not have LORE-like receptors, proving that LORE-dependent response was evolutionarily restricted to Brassicaceae (Figure 21). Moreover, the ancestor of Brassicaceae evolved the first 3-OH-FA receptor after the divergent event of Brassicaceae and Cleomaceae, and before the tribe Aethionemeae in the basal lineage diverged from the other Brassicaceae lineages around 35 to 40 million years ago (Schranz and Mitchell-Olds, 2006, Hohmann *et al.*, 2015). The evolutionary diversification of the main Brassicaceae lineages I, II, and III, from around 23 million years ago, did not increase the chance of loss of LORE receptors in all species (Walden *et al.*, 2020a). The gain and loss of PRR within the same family also occurred in In11 recognition, which is restricted to specific legume species in the clade of Phaseoloid, and the species which preserved the In11 receptor INRs from their common ancestor are sensitive to In11 (Snoeck *et al.*, 2022a).

The LORE phylogenetic analysis reveals that LORE receptors are present in every Brassicaceae species and classified into different clades based on their taxonomic lineages, suggesting that LORE receptors in the 3-OH-FA insensitive species are not functional, such as no 3-OH-FA binding. The medium-throughput ligand depletion assay screened 37 SD-RLK ECDs from 20 species, and the ECDs which can bind 3-OH-FA are explicitly grouped into the clade of LORE (Figure 22). All LORE orthologs from all lineages can bind 3-OH-C10:0, and this consistency illustrates that the 3-OH-FA binding structure was highly conserved in evolution. In contrast, SD1-23 and all other close SD-RLK ECDs cannot bind 3-OH-FA, suggesting that Brassicaceae evolved LORE specifically for sensing mc-3-OH-FAs, which other SD-RLKs cannot substitute. LORE orthologs from both 3-OH-FA sensitive and insensitive species can bind 3-OH-C10:0, indicating that 3-OH-FA binding is one of many factors determining the functionality of LORE orthologs. FLS2 and PEPR directly bind their ligands, while they still rely on their co-receptors like BAK1 to fully activate immune responses (Yamaguchi *et al.*, 2006, Chinchilla *et al.*, 2007). LYM1 and LYM2 directly bind PG, but the downstream signaling could only be elicited by forming complexes with CERK1 (Willmann *et al.*, 2011).

The intracellular domain of SD-RLK transmits signaling from the extracellular domain to the downstream component, and the kinase domain of LORE can activate RLCKs by phosphorylation (Luo *et al.*, 2020). In a previous study, the induction of LORE-dependent immune responses was found to be correlated with receptor homomerization. Overexpressing AtLORE and CrubLORE in *N. benthamiana* caused cell death symptoms without 3-OH-FA treatment, but AlyrLORE and AhalLORE, which originated in 3-OH-FA insensitive species, did not induce cell death symptom (Eschrig *et al.*, 2021). AlyrLORE and AhalLORE can still bind 3-OH-FA, but they cannot form homomers, meaning that LORE kinase activity is unable to be activated without forming complexes in the plasma membrane (Eschrig *et al.*, 2021). The conserved phenotypes were shown again in LORE-like receptors by testing LORE orthologs and other SD-RLKs with cell death assays (Figure 23). The candidate species from all Brassicaceae lineages contain at least one LORE ortholog which can trigger cell death. 3-OH-FA insensitive *A. arabicum*, *B. oleracea,* and *R. islandica* also have cell death-inducing LORE orthologs, suggesting that regulatory mechanisms other than homomerization, kinase activity, and ligand binding are involved in LORE-dependent signaling (Figure 23). AlyrLORE and AhalLORE among Brassicaceae LORE orthologs might be two rare cases that lost the functions of

homomerization. They might also be incompatible with the *N. benthamiana* working background, which lacks specific components like co-receptors for inducing cell death with them (Eschrig *et al.*, 2021).

The previous two assays are established on *N. benthamiana*, which is taxonomically far from Brassicaceae compared with Arabidopsis, and it may not be sufficient to reflect the scenarios in the original species. 16 candidate LORE orthologs were stably expressed in *lore*-1, and most them rescued the mutant phenotype (Figure 24). Although *B. oleracea* did not respond to mc-3-OH-FAs, BoleLORE complemented the *lore*-1 phenotype, suggesting that *B. oleracea* did not express BoleLORE in the tested tissues or it might lack specific cytoplasmic components for inducing ROS accumulation (Figure 19, 24). AaraLORE can fully restore *lore*-1, indicating that functional mc-3-OH-FA sensing mechanisms are present in all major clades, including basal lineage, and they were not lost after the divergence of Brassicaceae and Cleomaceae (Figure 24) (Hohmann *et al.*, 2015). *B. rapa*, *B. nigra*, *E. salsugineum*, and *E. syriacum* have two or three mc-3-OH-FA receptors. Possessing multiple functionally similar PRRs may help the hosts recognize a wide range of pathogens. Wild grape *Vitis riparia* evolved two FLS2 orthologs for perceiving flg22, and one of them has extended specificity to *Agrobacterium tumefaciens* flagellin (Fürst *et al.*, 2020). Similarly, soybean contains two FLS2 orthologs, and one of them can strongly responds to *Ralstonia solanacearum* flagellin without BAK1 (Wei *et al.*, 2020). Whether these LORE orthologs differ in 3-OH-FA binding affinity, chain-length specificity, kinase activity, or expression level requires more quantitative analyses. Although there was no induced cell death phenotype, BnigLOREa still slightly complemented *lore*-1 (Figure 23, 24). *R. islandica* RislLORE is the only 3-OH-FA binder and cell death inducer that fails to rescue the 3-OH-FA sensing function in the Arabidopsis background (Figure 22, 23, 24). These two contradictory cases remind us that different ectopic expression systems may have different compatible conditions and strongly suggest that other factors are involved in LORE-dependent mc-3-OH-FA-induced signaling transduction. SRK9 dimerization in some systems does not require SCR9 as an inducing agent, such as yeast-two-hybrid system, but SRK9 exhibits the opposite manner *in vitro* with the insect cell expression system (Naithani *et al.*, 2007, Shimosato *et al.*, 2007, Ma *et al.*, 2016). Taken together, all LORE orthologs are able to bind mc-3-OH-FA and most of them can induce LORE-dependent signaling, but a few defective LORE orthologs lack certain functions, like homomerization, which is independent of 3-OH-FA binding.

3.5 LORE lectin-like domain as a potential 3-OH-FA binding pocket

The ECD of LORE is known to be a 3-OH-FA binding domain and forms a homodimer. Having three kinds of subdomains, including two lectin-like domains, an EGF domain, and a PAN domain (Figure 3), LORE ECD potentially has multiple functions for different regulatory mechanisms. The dimerization and protein-ligand binding interfaces of SRK8 and SRK9 are mainly formed by their EGF domains, PAN domains, and partially lectin-like domains, and the intramolecular interactions are meditated by several polar residues and hydrogen bonds in these domains (Ma *et al.*, 2016, Murase *et al.*, 2020). AtLORE homomerization is mediated by the ECD and the transmembrane domain; however, it is unknown which subdomains are involved in the formation of the dimerization interface (Eschrig *et al.*, 2021). The *in-silico* analyses, including sequence alignment of LORE orthologs and homology modeling-coupled ligand docking, showed that LORE lectin-like domain 2 is an independent 3-OH-FA binding domain (Figure 25, Supplementary Figure 13, 14). Chimeric receptors formed by mc-3-OH-FA binder, AtLORE, and non-binder, AtSD1-23, revealed that ligand binding requires the AtLORE lectin-like domain 2 (Figure 26). The EGF domain plays a role in calcium binding in the animal system, and the PAN domain can interact with proteins and polysaccharides (Tordai *et al.*, 1999, Zhou *et al.*, 1999, Wouters *et al.*, 2005). Lectins are known to be a carbohydrate-binding structure, and the glycans on glycoproteins or glycolipids are also recognized by it (Bellande *et al.*, 2017, Siukstaite *et al.*, 2021). L-type lectin domains in four plant LecRKs can recognize nucleotide derivatives like ATP and $NADP^+$, and an L-type lectin domain constitutes the entire ECD of LecRK (Choi *et al.*, 2014, Wang *et al.*, 2017, Wang *et al.*, 2019, Pham *et al.*, 2020). So far, SD-RLKs have been identified to sense proteins and fatty acids, but their lectin-like domains have not been mechanistically described (Ranf, 2017, Sun *et al.*, 2020). LORE contains tandem lectin-like domains, but only one functions as a ligand-binding pocket. Among the mechanistically studied PRRs, receptors with repetitive domains, including LysM RLKs and FERONIA, exploit only one of these structures to bind patterns. Owning three LysM domains, CERK1 was found to bind chitin by LysM domain 2, but a recent study showed LysM RLKs bind ligands, including lipochitooligosaccharides by LysM domain 1 (Liu *et al.*, 2012, Bozsoki *et al.*, 2020). FERONIA directly binds polygalacturonic acid released from pectin by its first malectin domain, and its second malectin domain is involved in binding peptides (Stegmann *et al.*, 2017, Xiao *et al.*, 2019, Lin *et al.*, 2022). Most of the studied LRR-RKs, such as FLS2 and PEPRs, bind ligands with their

LRR domains (around 21 to 29 LRRs), and some LRR co-receptors also involve in ligand-binding by the LRR domains (Hohmann *et al.*, 2017). HPCA1/CARD1 senses quinones and H_2O_2 by the same part of ECD, implying that it recognizes the elicitors by the same mechanism (Laohavisit *et al.*, 2020, Wu *et al.*, 2020). It is a valid hypothesis that the two lectin-like domains in LORE have two different functions. One of the well-studied fatty acid-sensing plasma membrane proteins in the animal system is the G-protein-coupled receptor (GPCR), which mediates lipid metabolism and various cellular responses (Rosenbaum *et al.*, 2009). GPCRs can bind a wide range of fatty acids and lipids with their structures constituted by multiple transmembrane helices, and the hydrophobic fatty acyl chains extend into the hydrophobic binding pocket in the receptors (Liu *et al.*, 2022, Xu *et al.*, 2022). The ligand docking prediction in this study also reveals that the acyl chain of 3-OH-C10:0 adapts to the cleft on LORE (Figure 25). The exact 3-OH-FA binding site on LORE still needs to be identified, and how LORE binds mc-3-OH-FAs in a chain length-specific manner also needs further investigation. The biochemical and biophysical approaches like nuclear magnetic resonance (NMR) can facilitate the exploration of binding sites. Mutagenesis of the putative binding site can also verify the binding pocket of the ligand.

3.6 Summary and outlook

This thesis used diverse techniques to demonstrate the interaction of LORE and mc-3-OH-FA, then extended the application of these techniques to the studies of the natural diversity of 3-OH-FA sensing as well as LORE orthologs in Brassicaceae. The comprehensive research illustrates the evolution of LORE receptors in Brassicaceae. Beyond that, the mechanism of LORE-mc-3-OH-FA binding is better understood at the molecular level by this thesis and two previous studies together (Kutschera *et al.*, 2019, Eschrig *et al.*, 2021).

Indeed, this thesis resolves some mechanistic and evolutionary questions about LORE, but it also raises further questions that need to be addressed. Although the homology modeling provides a brief insight into the LORE protein model, the authentic LORE structure resolved by crystallographic analysis, cryogenic electron microscopy, or NMR can provide a better picture to decipher more complicated mechanisms of biological activities. The expression of LORE requires a considerable range of assays to obtain better quality and quantity, and the expression system is worth trying in other non-Plantae organisms. Following the LORE protein structure,

the binding site of mc-3-OH-FA can be precisely validated by these biochemical supports. This will allow us to further understand the mechanisms of ligand-binding specificity, homodimerization, and signal transmission. Finally, the LORE orthologs, which strengthen the immune responses in plants, can be applied to promote translational research in the agricultural industry and improve crop resistance to pathogens.

4 Materials and methods

4.1 Plant materials

Arabidopsis thaliana Col-0 was mainly used in this study if not specified. *A. thaliana* Col-0^{Aeq} and *lore*-1 are cytosolic apoaequorin-expressing lines used in the measurement of cytosolic calcium ion influx (Ranf *et al.*, 2015). Tobacco in this study is *Nicotiana benthamiana*. The ecotypes of *A. thaliana* and other Brassicaceae species for ROS measurement are listed in Table 1 and Table 2. Arabidopsis and Brassicaceae plants grown on potting soil (ED73, Einheitserde, Germany) with vermiculite (9:1) were cultured in the chambers under short day (8-hour daylight) conditions at 22ºC/20ºC (Day/Night) (Hu *et al.*, 2011, Briskine *et al.*, 2017, Kiefer *et al.*, 2019, Fernandez-Pozo *et al.*, 2021). *N. benthamiana* and Arabidopsis for seed propagation were grown under long day (16-hour daylight) conditions at 23ºC/21ºC (Day/Night).

Table 1. *Arabidopsis thaliana* ecotype accessions used for ROS measurement in this study. All accessions were obtained from The Nottingham Arabidopsis Stock Centre (NASC).

Name	1001 Genome Accession ID	NASC Stock ID
Voeran-1	9979	N76365
Mammo-1	9964	N76367
Lago-1	9963	N76387
Xan-1	10014	N76395
Kastel-1	10006	N76414
Mer-6	9946	N76419
Slavi-1	9985	N76421
Borsk-2	9957	N76428
Aa-0	7000	N76442
Baa-1	7002	N76451
Bla-1	8264	N76468
Co-1	7077	N76484
Es-0	7126	N76492
Gel-1	7143	N76493
Gie-0	7147	N76498
Gu-0	6922	N76500
Ha-0	7163	N76525

Kelsterbach-4	8420	N76555
Ms-0	6938	N76597
Se-0	6961	N76660
IP-Alm-0	9518	N76669
App1-16	5832	N76789
Cvi-0	6911	N76792
IP-Dar-0	9840	N76826
Eden-1	6009	N76847
ESP-1-11	9908	N76856
Fell2-4	9780	N76863
Fly2-1	6023	N76875
Ge-0	8297	N76899
Ha-HBT2-10	9797	N76904
Ha-SP-2	9801	N76945
IP-Ini-0	9852	N76953
Istisu-9	9099	N76967
Kent	8238	N76968
Kia-1	9409	N76969
Kn-0	7186	N76971
Knjas-1	9749	N76978
Kolyv-3	9626	N76983
Koren-1	9719	N76992
KYC-33	801	N77017
Lebja-4	9633	N77025
Lerik2-1	9079	N77034
Lesno-4	9610	N77042
Lis-1	8326	N77052
Lp2-6	7521	N77076
IP-Mdd-0	9866	N77101
MNF-Riv-21	1890	N77109
Nar-3	9089	N77119
IP-Per-0	9879	N77169
IP-Pun-0	9887	N77196
Sf-2	7328	N77247
Slavi-2	9723	N77252

Stiav-2	9729	N77280
T510	6109	N77301
T740	6128	N77313
TRE-1	9926	N77385
Tu-B1-2	9794	N77391
Dra-3	5860	N77913
UduI 1-11	6296	N78774
Ull-A-1	9471	N78820
IP-Val-0	9903	N78829
Västervik	9058	N78834
IP-Ver-5	9596	N78841
WAR	7477	N78853
Xan-6	9070	N78862
Pt-0	7305	N78915

Table 2. Brassicaceae species used in ROS measurement in this study.

Species Name	NASC Stock ID / Accession Name / Reference
Anastatica hierochuntica	Kiefer *et al.*, 2019
Aethionema arabicum	TUR / Fernandez-Pozo et al., 2021
Arabidopsis lyrata	MN47 / Hu *et al.*, 2011
Arabidopsis shokei	N1676
Arabidopsis suecica	N22505
Arabidopsis thaliana	Col-0 / Ranf *et al.*, 2015
Arabis alpina	PAJ
Biscutella auriculata	Kiefer *et al.*, 2019
Biscutella frustenscens	Kiefer *et al.*, 2019
Biscutella lusitanica	Kiefer *et al.*, 2019
Brassica nigra	CR 2744
Brassica oleracea	N29002
Brassica rapa	BRA 1322
Capsella rubella	N22697
Cardamine hirsuta	N28981
Chochlearia officinalis	Kiefer *et al.*, 2019

*Cleome violacea**	N29053
Conringia orientalis	CON 13
Conringia planisiliqua	Kiefer *et al.*, 2019
Crambe hispanica	N29063
Descurainia sophioides	N29058
Diptychocarpus strictus	N29054
Eruca vesicaria	ERU119
Euclidium syriacum	N29055
Eutrema salsugineum	N22504
Erysimum cheiranthoides	N68097
Isatis lusitanica	Kiefer *et al.*, 2019
Isatis tinctoria	Kiefer *et al.*, 2019
Lepidium africanum	Kiefer *et al.*, 2019
Lepidium aucheri	Kiefer *et al.*, 2019
Lepidium sativum	LEP 4
Malcolmia maritima	N29059
Myagrum perfoliatum	N29062
Nasturtium officinale	Kiefer *et al.*, 2019
Noccaea caerulescens	N9685
Olimarabidopsis cabulica	N4653
Olimarabidopsis pumila	N22562
Pseudoturritis turrita	Kiefer *et al.*, 2019
Raphanus sativus	RA22
Rorippa islandica	N29057
Sinapis arvensis	CR515
Sisymbrium altissimum	Kiefer *et al.*, 2019
Sisymbrium irio	N22563
Thlaspi arvense	N9661

*Family Cleomaceae

4.2 Bacterial materials

Escherichia coli

The strain for cloning and plasmid amplification is DH5a. The recombinant protein expression strains used were as follows: Rosetta 2, Rosetta-gami 2, Rosetta-gami B, Rosetta Blue, and Origami 2 were from Merck (Germany), SHuffle T7 Express and SHuffle T7 Express LysY were from New England Biolabs (USA).

Agrobacterium tumefaciens

The strain for Arabidopsis transformation and tobacco transient expression was GV3101, rifampicin and gentamycin resistant.

4.3 Elicitors for triggering plant immune responses

The medium-chain 3-OH-FAs, 3-hydroxydecanoic acid (3-OH-C10:0), 3-hydroxyoctanoic acid (3-OH-C8:0), 3-hydroxynonanoic acid (3-OH-C9:0), 3-hydroxyundecanoic acid (3-OH-C11:0), 3-hydroxydodecanoic acid (3-OH-C12:0), 3-hydroxytridecanoic acid (3-OH-C13:0), 3-hydroxytetradecanoic acid, (3-OH-C14:0) were commercially available (Matreta LLC, USA), and 3-hydroxyalkanoate precursors (HAA) was synthesized in the previous study (Schellenberger *et al.*, 2021). The proteinaceous elicitor flg22 (QRLSTGSRINSAKDDAAGLQIA) was synthesized accordingly (Pepmic, China).

4.4 Measurement of plant reactive oxygen species

Leaf discs (4 mm) punched from 8- to 12-week-old *A. thaliana* and Brassicaceae species were incubated and floated on 200 µL water in 96-well white plate in the dark overnight. No more than 30 minutes before the measurements, water in the well was replaced by 100 µL water with 5 µM L-012 (FUJIFILM Wako chemicals, Japan) and 2 µg/mL horseradish peroxidase (Roche, Switzerland). Microplate luminometer Luminoskan Ascent 2.1 (Thermo, USA) was used to first measure ROS level in 10 minutes as background measurement with 1-minute intervals. After the leaf disc was treated with 25 µL of elicitors, the ROS burst was monitored for 45 min. Water with comparable methanol or ethanol was the negative control. Total luminescence signals were calculated by summing up the relative light unit (RLU) from the 1st to the 45th minute. Data of maximal luminescence were plotted after normalization by the average luminescence of 5 minutes before elicitation and subtraction by the MeOH controls, which were measured from different plants on the same plate.

4.5 Measurement of Arabidopsis cytosolic calcium ion influx

Arabidopsis cytosolic apoaequorin-expressing lines were cultured in half-strength MS liquid medium (2.2 g/L MS salt (Duchefa Biochemie, Netherland), 2.5 g/L sucrose, 0.195 g/L 2-(N-morpholino)-ethanesulfonic acid (MES), pH 5.7) under long day (16-hour daylight) conditions at 23ºC/21ºC (day/night) for 8-9 days. They were transferred into 96-well white plate and incubated in 100 µL water with 5 µM coelenterazine-h (p.j.k. GmbH, Germany) in the dark overnight. The luminescence signal was measured in a microplate luminometer Luminoskan Ascent 2.1. The seedlings were first measured ten times as background signals with 10-second intervals. Each seedling was treated with 25 µL of elicitor, and its luminescence was measured every 10 seconds until 30 minutes after treatment. Water with comparable methanol or ethanol was the negative control. For calculating the total aequorin in each seedling, the seedling was treated with 150 µl discharging solution (2 M $CaCl_2$, 20% ethanol). Luminescence signals were normalized to L/Lmax (luminescence counts per second/total luminescence counts). Total $[Ca^{2+}]_{cyt}$ signals were calculated by summing up L/L_{max} from the 2^{nd} to the 30^{th} minute.

4.6 Genome-wide association study of Arabidopsis accessions

GWAS was performed in the GWA-Portal (Seren, 2018). Total luminescence of ROS measurement from all Arabidopsis accessions was used as phenotype for GWA analysis. The phenotypic data were transformed by BOX-COX transformation before analysis. The GWA analysis was done by the accelerated mixed model with 1001 full sequence dataset, TAIR9 (1001_Genomes_Consortium, 2016). The false discovery rate was calculated using the Benjamini-Hochberg correction, and the 5% false discovery rate threshold was plotted as a dashed horizontal line (Benjamini and Hochberg, 1995).

4.7 Phylogenetic analysis of LORE orthologs and other SD-RLK

The sequences of LORE orthologs and other SD-RLKs were entirely retrieved from public databases, and the sources of proteins, identities of proteins, and versions of genome data used in the phylogenetic analysis were listed below (Table 3). The protein sequences were checked by SignalP-5.0 and TMHMM-2.0 to confirm that the candidates have signal peptides and transmembrane domains, respectively (Krogh *et al.*, 2001, Almagro Armenteros *et al.*, 2019). The protein sequences of candidates which lack signal peptides were further examined based on the references of RNA-seq. The candidates having contigs that cover the missing N-terminal

DNA sequences were corrected manually. The ECDs defined in this study are from signal peptides to the positions around amino acid 410th to 440th that contain serine-glutamate motifs, which are conserved in all LORE orthologs. The transmembrane and juxtamembrane domains defined in this study are from serine-glutamate motifs to the positions around amino acid 490th to 530th containing lysine-leucine motifs. The intracellular domains defined in this study are from lysine-leucine motifs to the glycine-arginine motifs beside stop codons. The online tools MAFFT and MUSCLE aligned the protein sequences from EMBL-EBI website. Phylogenetic trees were drawn using MEGA XI software with the Neighbor-Joining method and the bootstrap test (1000 replicates), and scale bars were calculated using the Poisson correction method (Tamura *et al.*, 2021).

Table 3. Analyzed LORE-like and other S-domain receptor kinase-like protein sequences.
*The N-terminal sequence was corrected.

Species	Database, genome version	Candidate ID	Database reference
Aethionema arabicum	Ae. arabicum DB, v3.1	Aa31LG2G9310_AaraLORE*	Fernandez-Pozo *et al*., 2021
Arabidopsis halleri	Phytozome 13, v1.1	Araha.6790s0007_AhalLORE Araha.6790s0005 Araha.15732s0004 Araha.6790s0008	Briskine *et al*., 2016
Arabidopsis lyrata	Phytozome 13, v2.1	AL2G14950_AlyrLORE AL2G14970	Hu *et al*., 2011
Arabidopsis thaliana	TAIR 10	AT1G11330_AtSD1-12 AT1G61390_AtSD1-23 AT1G61370_AtSD1-27 AT1G11280_AtSD1-28 AT1G61380_AtLORE AT1G61360_AtSD1-30	Lamesch *et al*., 2011
Brassica rapa	Phytozome 13, v1.3	Brara.I01503_BrapLOREa Brara.A02537_BrapLOREb Brara.I01502	Phytozome 13, DOE-JGI, http://phytozome-next.jgi.doe.gov
Brassica oleracea	Phytozome 13, v1.0	Bol013747_BoleLORE	Liu *et al*., 2014
Brassica nigra	Brassicaceae Database, v1.1	BniB011153_BnigLOREa BniB002031_BnigLOREb BniB022340_BnigLOREc BniB011152	Paritosh *et al*., 2020
Capsella rubella	Phytozome 13, v1.1	Carub.0002s0380_CrubLORE	Slotte *et al*., 2013

		Carub.0001s1090	
Cleome violacea	Phytozome 13, v2.1	Clevi.0002s0371	Brassicales Map Alignment Project, DOE-JGI, http://bmap.jgi.doe.gov/
Crambe hispanica	Phytozome 13, v1.1	Crahi.1347s0007_ChisLORE Crahi.1347s0006	Brassicales Map Alignment Project, DOE-JGI, http://bmap.jgi.doe.gov/
Cardamine hirsuta	*Cardamine hirsuta* Genetic and genomic	CARHR051210_ChirLORE CARHR051160 CARHR051140	Gan *et al*., 2016
Descurainia sophioides	Phytozome 13, v1.1	Desop.0206s0096_DsopLORE* Desop.0206s0094 Desop.0206s0099*	Brassicales Map Alignment Project, DOE-JGI, http://bmap.jgi.doe.gov/
Diptychocarpus strictus	Phytozome 13, v1.1	Distr.0009s141200 Distr.0022s0020 Distr.0022s0021* Distr.0001s55700	Brassicales Map Alignment Project, DOE-JGI, http://bmap.jgi.doe.gov/
Euclidium syriacum	Phytozome 13, v1.1	Eusyr.0018s0446_EsyrLOREa* Eusyr.0018s0448_EsyrLOREb Eusyr.0018s0447* Eusyr.0018s0453	Brassicales Map Alignment Project, DOE-JGI, http://bmap.jgi.doe.gov/
Eruca vesicaria	Phytozome 13, v1.1	Eruve.0750s0006_EvesLOREa Eruve.4611s0003_EvesLOREb Eruve.1331s0002_EvesLOREc Eruve.2624s0002 EvesLORED Eruve.0750s0005 Eruve.4611s0002 Eruve.1742s0004	Brassicales Map Alignment Project, DOE-JGI, http://bmap.jgi.doe.gov/
Eutrema salsugineum	Phytozome 13, v1.0	Thhalv10023284m Thhalv10023279m_EsalLOREa Thhalv10023335m_EsalLOREb* Thhalv10023295m	Yang *et al*., 2013
Isatis tinctoria	Phytozome 13, v1.1	Isati.4061s0008 Isati.2434s0004 Isati.4988s0002 Isati.0259s0009 Isati.0259s0006 Isati.4258s0006 Isati.4258s0007	Brassicales Map Alignment Project, DOE-JGI, http://bmap.jgi.doe.gov/
Lepidium sativum	Phytozome 13, v1.1	Lesat.0071s0138_LsatLORE* Lesat.0029s0110	Brassicales Map Alignment Project, DOE-JGI, http://bmap.jgi.doe.gov/
Malcolmia maritima	Phytozome 13, v1.1	Mamar.0055s0354_MmarLORE* Mamar.0055s0353*	Brassicales Map Alignment Project, DOE-JGI, http://bmap.jgi.doe.gov/

		Mamar.0055s0352* Mamar.0042s0047	
Myagrum perfoliatum	Phytozome 13, v2.1	Myper.0014s0588_MperLOREa Myper.0014s0589_MperLOREb* Myper.0004s0001 Myper.0075s0059 Myper.0075s0058	Brassicales Map Alignment Project, DOE-JGI, http://bmap.jgi.doe.gov/
Rorippa islandica	Phytozome 13, v1.1	Roisl.0209s0716_RislLORE Roisl.0209s0718 Roisl.0209s0712* Roisl.0209s0711	Brassicales Map Alignment Project, DOE-JGI, http://bmap.jgi.doe.gov/
Sisymbrium irio	Brassicaceae Database, v1.0	SI_scaffold1740_8 SI_scaffold1740_9	Haudry *et al*., 2013
Thlaspi arvense	Phytozome 13, v1.1	Thlar.0056s0139_TarvLORE*	Brassicales Map Alignment Project, DOE-JGI, http://bmap.jgi.doe.gov/

4.8 Molecular cloning

4.8.1 Plasmid purification

Plasmids from *E. coli* cultured in LB medium (10 g/L pepton, 5 g/L yeast extract, 10 g/L NaCl) with proper antibiotics overnight were extracted using the NucleoSpin Plasmid Mini kit (Macherey-Nagel, Germany) according to the manual. DNA concentrations were measured by NanoDrop 2000 spectrophotometer (Thermo Fisher Scientific, USA).

4.8.2 Polymerase chain reaction for molecular cloning

Polymerase chain reaction (PCR) for constructing vectors and cloning was done with Phusion High-Fidelity DNA-polymerase (Thermo, USA) following the manufacturer's manual. 50 µL PCR mixture containing 1x Phusion HF buffer, 200 µM dNTPs, 0.5 µM forward and reserve primers, 1 U Phusion High-Fidelity DNA-polymerase, and approximately 10 ng template was mixed. The reaction was incubated under the following touchdown PCR conditions: 95ºC for 1 minute. Then the first 15 cycles of 95ºC for 10 seconds, 72ºC to 58ºC (reduced 1°C each cycle) for 30 seconds, and 72ºC for 30 seconds (DNA fragment less than 1 kb) or 90 seconds (DNA fragment more than 1 kb). The last 20 cycles of 95ºC for 10 seconds, 58ºC for 30 seconds, and 72ºC for 30 seconds (DNA fragment less than 1 kb) or 90 seconds (DNA fragment more than 1 kb). Last step of 72ºC for 10 minutes.

4.8.3 PCR clean-up and DNA gel elution

DNA fragments amplified in PCR mixtures or agarose gels separated by electrophoresis were purified using NucleoSpin Gel and PCR Clean-up Mini kit (Macherey-Nagel, Germany) according to the manual. DNA concentrations were measured by NanoDrop 2000 spectrophotometer (Thermo Fisher Scientific, USA).

4.8.4 Restriction enzyme digestion

Restriction enzyme digestion was used to check plasmids, apart from Type IIS restriction enzymes for golden gate cloning. Restriction enzymes were ordered from Thermo Fisher Scientific (USA) and New England Biolabs (USA). Restriction digestions were performed according to the guidelines, and the digested DNA products were separated and visualized by electrophoresis.

4.8.5 Transformation of *E. coli* and *A. tumefaciens*

E. coli transformation by heat shock

200 µL of chemically competent cells in 0.1 M calcium chloride solution were thawed on ice. 2-10 µL of plasmids were mixed with the cells and incubated for 5 minutes on ice. After the cells were incubated in a dry bath at 42ºC for 90 seconds, the cells were cooled on ice for no longer than 5 minutes. The cells were added with 900 µl LB medium and incubated for one to two hours at 37ºC, 200 rpm. The cells were plated onto LB agar (10 g/L pepton, 5 g/L yeast extract, 10 g/L NaCl, 20 g/L agar) containing proper antibiotics and incubated at 37°C overnight.

E. coli transformation by electroporation

E. coli strains for electroporation in this study were Rosetta 2, Rosetta-gami 2, Rosetta-gami B, Rosetta Blue, and Origami 2. 100 µl of competent cells in 10% glycerol solution were thawed on ice, 5 µl of plasmids were mixed with the cells and incubated on ice for 5 minutes. The cells were transferred to a cold 2 mm electroporation cuvette (Bio-Rad, USA) and shocked) by MicroPulser Electroporation Apparatus (Bio-Rad, USA) with program “EC2” (voltage 2.5 kV, one pulse). 1000 µL LB medium was added to the cuvettes, transferred to new microtubes with the shocked

cells, and incubated for one hour at 37°C, 200 rpm, followed by plated on selective LB agars containing proper antibiotics and incubated at 37°C overnight.

A. tumefaciens transformation by heat shock

100 µL of chemically competent cells in 20 mM $CaCl_2$ solution were thawed on ice for 10 minutes, and 100 ng of plasmids in 5 µL water were mixed with the cells and incubated for 10 minutes on ice. The cells were frozen in liquid nitrogen for 1 minute and incubated in a dry bath at 37°C for 5 minutes. After heat shock, the cells were immediately cooled on ice for no longer than 5 minutes. The cells were added with 900 µl of LB medium and incubated for two to three hours at 27ºC, 200 rpm. The cells were plated onto LB agar containing proper antibiotics and incubated at 28°C for 48 hours.

4.8.6 Golden Gate cloning

Type IIS restriction enzymes BpiI, BveI, LguI, Esp3I, and T4 DNA ligase for golden gate cloning were ordered from Thermo Fisher Scientific (USA). The Golden Gate cloning of different enzymes performed in this study followed the protocol below. All enzymes' reaction conditions were as follows: 50 cycles of 37ºC for 5 minutes and 16ºC for 5 minutes, followed by 16ºC for three hours and 80ºC for 10 minutes.

BpiI Golden Gate cloning:

2 µL 1x Buffer G, 1 µL BpiI, 2 µL 10 mM ATP, and 0.5 µL T4 DNA ligase in a volume of 20 µL with 50 ng of each DNA fragment and plasmid.

BveI Golden Gate cloning:

1 µL 1x Buffer O, 0.25 µL BveI, 1 µL 10 mM ATP, and 0.25 µL T4 DNA ligase in a volume of 10 µL with 50 ng of each DNA fragment and plasmid.

LguI Golden Gate cloning:

1 µL 1x Tango buffer, 0.25 µL LguI, 1 µL 10 mM ATP, and 0.25 µL T4 DNA ligase in a volume of 10 µL with 50 ng of each DNA fragment and plasmid.

Esp3I Golden Gate cloning:

1 µL 1x Tango buffer, 0.25 µL Esp3I, 1 µL 10 mM ATP, 1 µL 10 mM DTT, and 0.25 µL T4 DNA ligase in a volume of 10 µL with 50 ng of each DNA fragment and plasmid.

4.8.7 Construction of expression vectors

pGGPXhc:

pGGPXhc vector was designed based on *A. tumefaciens* binary vector pICSL4723 carrying a kanamycin resistance gene from Addgene, and it was entirely synthesized by Twist Bioscience (USA) with slight modifications. Apart from the T-DNA regions, pGGPXhc and pICSL4723 shared identical sequences, but all BveI and NotI sites in pGGPXhc were removed without non-synonymous mutation. The T-DNA region contains two BveI sites for Fast-Red marker gene cassette assembly and two LguI sites for gene expression cassette assembly. pGGPXhc were assembled by BpiI Golden Gate cloning from 6 synthesized DNA fragments.

pGGPXhcFR:

To construct the vector containing a selection marker for transgenic Arabidopsis, pGGPXhcFR was assembled. The Fast-Red marker cassette was synthesized based on the sequence in the previous studies (Shimada *et al.*, 2010, Ursache *et al.*, 2021), and two fragments of the cassette were inserted into the T-DNA region in pGGPXhc by BveI Golden Gate cloning.

pGGPXhc-35S-LacZ-mCherry-tHSP:

For constructing the vector of mCherry fusion protein overexpression, the synthetic DNA fragments, including 35S promoter, LacZ-fragment with its promoter (LacZ), and Esp3I sites (cleavage site sequences: 5'-AATG-3', 5'-TCAG-3') on both termini, GS linker (GGSGGSG) with mCherry, and heat shock protein terminator (tHSP) were assembled in the T-DNA of pGGPXhc by LguI Golden Gate cloning (Nagaya *et al.*, 2010, de Felippes *et al.*, 2020).

pGGPXhc-35S promoter-LacZ-GFP-tHSP:

For constructing the vector of GFP fusion protein overexpression, the synthetic DNA fragments, including 35S promoter, LacZ, and Esp3I sites (cleavage site sequences: 5'-AATG-3', 5'-ACGC-3') on both termini, GS linker with GFP, and tHSP were assembled in the T-DNA of pGGPXhc by LguI Golden Gate cloning.

pGGPXhcFR-LORE promoter-LacZ-tHSP:

For constructing the vector expressing target genes by AtLORE promoter, the synthetic DNA fragments, including AtLORE promoter, LacZ, and Esp3I sites (cleavage site sequences: 5'-AATG-3', 5'-ACGC-3') on both termini, and tHSP were assembled in the T-DNA of pGGPXhc by LguI Golden Gate cloning.

pGGPXhc-35S-LacZ-HA-tHSP:

For constructing the vector of HA-tag fusion protein overexpression, the synthetic DNA fragments, including 35S promoter, LacZ, and Esp3I sites (cleavage site sequences: 5'-AATG-

3', 5'-TCAG-3') on both termini, GS linker with HA peptide sequence, and tHSP were assembled in the T-DNA of pGGPXhc by LguI Golden Gate cloning.

4.8.8 Cloning of LORE orthologs and AtSD1-23 and apo-mCherry in plant expression vectors

AtLORE, AtLORE-GFP, AtLORE-GFP-Km, eAtLORE-mCherry, eAtSD1-23-mCherry, eCrubLORE-mCherry, eAlyrLORE-mCherry, eAhalLORE-mCherry, and apo-mCherry were cloned into pGGPXB vectors in previous studies, which are the *A. tumefaciens* binary vectors with 35S promotors and 35S terminators (Eschrig *et al.*, 2021, Shu *et al.*, 2021).

4.8.9 Cloning of eAtLORE and eAtLORE lectin-like domains in vectors for recombinant protein expression in *E. coli*.

eAtLORE and AtLORE tandem lectin-like domains with no signal peptide sequence were amplified by PCR using the plasmid having *AtLORE* as a template (section 4.8.8) and primers pairs having Esp3I sites listed below (Table 4). The PCR products were cloned into a Gold Gate cloning-compatible Gateway cloning entry vector used in previous research by Esp3I Golden Gate cloning (Eschrig *et al.*, 2021). The clones were further transferred via Gateway cloning with LR-clonase (Thermo Fisher Scientific, USA, according to manufacturer's instruction) into destination vector pDEST-N112-MBP to express N-terminal MBP fusion protein in *E. coli* (Dyson *et al*., 2004).

Table 4. Primers for cloning eAtLORE and its lectin-like domains into the recombinant protein expression vector.

Name	Sequence (5'-3')	Note
eSD1-29-noSP_Esp3I-F	TTCGTCTCTAATGGCTATAAACACATCAAGTCCTTTG	AtLORE without signal peptide
eSD1-29-noSP_Esp3I-R	TTCGTCTCTACTAGCTTCCAGCCAATTCTG	AtLORE without signal peptide
eSD1-29-noSP-LL_Esp3I-F	TTCGTCTCTAATGGAAAACCTGTATTTTCAGGGCTACCCATACGATGTTCCTGA	AtLORE lectin-like domains without signal peptide
eSD1-29-noSP-LL2_Esp3I-R	GACGTCTCTACTAATCCCAGAGGATCTTCATTTTCCC	AtLORE lectin-like domains without signal peptide

4.8.10 Cloning of eAtLORE in vectors for cell-free protein expression system

pALiCE vectors were ordered together with ALiCE cell-free protein expression system (LenioBio, Germany). pALiCE01 and pALiCE02 have intrinsic Strep-tag epitopes and YFP genes without or with an N-terminal melittin signal peptide beside the NcoI cleavage sites, respectively. To insert eAtLORE into pALiCE vectors, NcoI restriction enzyme sites on the N-termini of Strep-tag and YFP gene were used. The eAtLORE fragment without signal peptide sequence was amplified by PCR using the plasmid having *AtLORE* as a template (section 7.8.8) and primers pairs having NcoI cleavage sites (eSD1-29_CDS-NcoI-F: 5'-CCAACCATGGCTATAAACACATCAAGTCC-3'; eSD1-29_CDS-NocI-R: 5'-AACCCCATGGTTGCGCTTCCAGCCAATTCTGAAC-3'). The NcoI-treated plasmids and PCR products were assembled by T4 DNA ligase at 16ºC for one hour.

4.8.11 Cloning of LORE orthologs, other SD-RLKs, and domain-swapped receptors vectors for plant expression

To be compatible with two pGGPXhc and a pGGPXhcFR vectors, the synthesized DNA fragments of LORE orthologs and other SD-RLKs have no Esp3I site in the coding sequences but on two termini. The DNA fragments of ECDs, transmembrane and juxtamembrane domains, and intracellular domains were synthesized independently, and the sequence-conserved borders of the domains were defined in section 4.7. The AtLORE signal peptide replaced original signal peptide sequences in all ECDs to fit into Arabidopsis and *N. benthamiana*. The signal peptides in the SD-RLKs were annotated by SignalP-5.0 in section 4.7. The ECD of AtLORE-AtSD1-23 domain-swapped receptors were amplified by PCR using primers listed below, and six fragments from eAtLORE or eAtSD1-23, with Esp3I sites on both termini, were generated (Table 5).

To clone SD-RLK ECD-mCherry fusion proteins, DNA fragments of ECDs were cloned into pGGPXhc-35S-LacZ-mCherry-tHSP by Esp3I Golden Gate cloning with blue-white screening.

To clone SD-RLK-GFP fusion proteins, DNA fragments of ECDs, transmembrane and juxtamembrane domains, and intracellular domains were cloned into pGGPXhc-35S promoter-LacZ-GFP-tHSP by Esp3I Golden Gate cloning with blue-white screening.

To clone SD-RLK proteins for stable expression in Arabidopsis by *AtLORE* promoter, DNA fragments of ECDs, transmembrane and juxtamembrane domains, and intracellular domains were assembled in pGGPXhcFR-LORE promoter-LacZ-tHSP by Esp3I Golden Gate cloning with blue-white screening.

To clone eAtLORE-HA and eAtLORE-Twin-Strep-tag-HA fusion proteins, DNA fragments of ECDs were cloned into pGGPXhc-35S-LacZ-HA-tHSP by Esp3I Golden Gate cloning with blue-white screening. eAtLORE with Twin-Strep-tag and Tobacco Etch Virus (TEV) site was synthesized together, and Twin-Strep-tag and TEV sites were inserted between the signal peptide and the remaining eAtLORE.

To clone ECDs of AtLORE-AtSD1-23 domain-swapped receptor mCherry fusion proteins, six DNA fragments of ECDs were cloned into pGGPXhc-35S-LacZ-mCherry-tHSP by Esp3I Golden Gate cloning with blue-white screening.

Table 5. Primers for construction of ectodomain of domain-swapped receptors. The Gold Gate cleavage sites are underlined.

Name	Sequence (5'-3')	Note
SD1-23-SP-Esp3_F	ATATCGTCTCAAATGTACAAACTTCCACAAAG	AtSD1-23 signal peptide
SD1-23-SP-Esp3_ R23	TGACCGTCTCATATCTGCATAGCCAAAAGTTGG	AtSD1-23 signal peptide with linkage site for AtSD1-23
SD1-23-SP-Esp3_ R29	GACCGTCTCAATAGCTG CATAGCCAAAAGTTGG	AtSD1-23 signal peptide with linkage site for AtLORE
SD1-23-L1-Esp3_ F	AGGACCGTCTCAGATATAAACACATCAAGTCC	AtSD1-23 lectin-like domain 1
SD1-23-L1-Esp3_ R	GACCCGTCTCAATAAAGTTTTTCCGGAAACATC	AtSD1-23 lectin-like domain 1
SD1-23-L2a-Esp3 _F	AAGCCGTCTCATTATGGAAAAGCTTCGAGAATC	AtSD1-23 lectin-like domain 2, a.a. 137-202
SD1-23-L2a-Esp3 _R	ATGACCGTCTCATCCAGTAGGGCGATGAGCCTC	AtSD1-23 lectin-like domain 2, a.a. 137-202
SD1-23-L2b-Esp3 _F	CTAGCGTCTCATGGAGAAGTGGTCCATGGGC	AtSD1-23 lectin-like domain 2, a.a. 202-302
SD1-23-L2b-Esp3 _R	ATGCCGTCTCACACATGAGCTTGTTGGAGCCTC	AtSD1-23 lectin-like domain 2, a.a. 202-302
SD1-23-EGF-Esp 3_F	ATGACGTCTCATGTGATCTATATCGTGCTTGTG	AtSD1-23 EGF domain
SD1-23-EGF-Esp 3_R	ATGACGTCTCAAAGATAATTGTGTACGTCTGAC	AtSD1-23 EGF domain
SD1-23-PAN-Esp 3_F	ATGACGTCTCATCTTGCCATACGAATTCTTC	AtSD1-23 PAN domain

SD1-23-PAN-Esp 3_R	ATGACGTCTCACTGAACTTGCAAGCCGAAGGG	AtSD1-23 PAN domain
SD1-29-L1-Esp3_F	ATGACGTCTCGCTATAAACACATCAAGTCC	AtLORE lectin-like domain 1
SD1-29-L1-Esp3_R	GACTCGTCTCAATAATTT ATTCCCTGAAACATC	AtLORE lectin-like domain 1
SD1-29-L2a-Esp3 _F	AGCACGTCTCATTATGGCAAAGCTTCGAGCATC	AtLORE lectin-like domain 2, a.a. 137-202
SD1-29-L2a-Esp3 _R	ACTACGTCTCATCCAGT AAGGTACTGAGCCTC	AtLORE lectin-like domain 2, a.a. 137-202
SD1-29-L2b-Esp3 _F	ACTACGTCTCATGGAGA TGTGGTCCTTGGGC	AtLORE lectin-like domain 2, a.a. 202-281
SD1-29-L2b-Esp3 _R	ACTACGTCTCACACATG GGTTCTCTGGGAGAG	AtLORE lectin-like domain 2, a.a. 202-281
SD1-29-EGF-Esp 3_F	ACATCGTCTCATGTGAT CTATATGGTAGATGCG	AtLORE EGF domain
SD1-29-EGF-Esp 3_R	ACTACGTCTCAAAGATAA TTTTGTACGTCTAAC	AtLORE EGF domain
SD1-29-PAN-Esp 3_F	AGCACGTCTCATCTTGC CAAGCAAAATCTTC	AtLORE PAN domain
SD1-29-PAN-Esp 3_R	TAAACGTCTCTCTGAACTTGCAAGACGAATG	AtLORE PAN domain

4.8 Agrobacterium-mediated transient protein expression in tobacco

Proteins of interest were expressed in leaves of 6-week-old *N. benthamiana* plants via *Agrobacterium*-mediated transformation. *A. tumefaciens* GV3101 carrying expression constructs were grown on YEB agar (1 g/L yeast extract, 5 g/L beef extract, 5 g/L peptone, 5 g/L sucrose, 0.5 g/L $MgSO_4$-$7H_2O$. 10 g/L agar) with 30 µg/mL gentamycin, 10 µg/mL rifampicin, and 50 µg/mL kanamycin for 48 hours, and then inoculated and cultured in AB medium (4.1 g/L MES pH 5.5, 10.6 g/L glucose, 60 g/L K_2HPO_4, 20 g/L NaH_2PO_4, 20 g/L NH_4Cl, 6 g/L $MgSO_4$, 3 g/L KCl, 0.2 g/L $CaCl_2$, 50 mg/L $FeSO_4$-$7H_2O$) supplemented with 50 µg/mL kanamycin and 100 µM acetosyringone (3 mL AB medium per construct for syringe-infiltration) or in LB broth with 30 µg/mL gentamycin, 10 µg/mL rifampicin, 50 µg/mL kanamycin and 100 µM acetosyringone (200 mL LB medium per construct for vacuum-infiltration) at 28°C, 200 rpm overnight. *Agrobacterium* was harvested (1900 g, 10 min), washed three times with the infiltration buffer (10 mM MgSO4, 10 mM MES pH 5.5, 150 µM acetosyringone), and incubated at 28°C for two

to three hours. The OD_{600} of *Agrobacterium* was measured and adjusted to 0.5 with the infiltration buffer. All Agrobacteria with constructs were mixed with an equal volume and OD_{600} of *Agrobacterium* carrying the silencing suppressor p19. For syringe infiltration, Agrobacterial suspension was infiltrated into fully expanded leaves of *N. benthamiana* using a needleless syringe. For vacuum infiltration, 1 L of Agrobacterial suspension in the beaker was first mixed with Silwet-77 (Kurt Obermeier, Germany) to the final concentration of 0.01%, and the whole tobacco plant was submerged in the beaker in the desiccator connected to a vacuum pump, followed by vacuum for 2 minutes. The proteins expressed and secreted to tobacco apoplast were harvested 3, 4, or 5 days after infiltration.

4.9 Harvesting of tobacco apoplastic washing fluid

N. benthamiana AWF was harvested from the inoculated leaves aforementioned (Rutter *et al.*, 2017). The detached leaves were submerged in the beaker containing Tris-buffered saline buffer (TBS, Tris-base 50 mM, NaCl 150 mM, pH 7.6), and vacuumed to ~26-inch Hg vacuum. After the leaves were entirely infiltrated with TBS buffer, they were taken out, and the excess buffer on their surfaces was gently removed with paper towels. One or two leaves were rolled into a column with a 1 mL pipette tip and put into a 30 mL syringe barrel. The barrel without plugger was placed in a 50 mL falcon tube without a lid, and the whole assembly was centrifuged at 800 g, 4ºC, for 20 minutes. The AWF in the bottom of the tube was further cleared by centrifugation (20 minutes, 8000 g, 4°C). For depletion binding assay, the AWF was desalted by PD-10 desalting columns (Cytiva, USA) and concentrated to the indicated total protein concentration by Vivaspin 20, 30 000 MWCO (Sartorius, Germany).

4.10 SDS-polyacrylamide gel electrophoresis and western blot

All of the protein samples for sodium dodecyl sulfate (SDS)-polyacrylamide gel electrophoresis were mixed with 5x Laemmli sample buffer (60 mM Tris-Cl pH 6.8, 10% glycerol, 2% SDS, 5% β-mercaptoethanol, 0.01% bromophenol blue), and incubated at 95ºC for 10 minutes. Acrylamide gels were used in the protein electrophoresis in this study with the following components: 5% stacking gel (680 µL/mL H_2O, 170 µL/mL 30% acrylamide/bis-solution (29:1) (Carl Roth, Germany), 130 µL/mL 1 M Tris pH 6.8, 10 µL/mL 10% SDS, 10 µL/mL 10% ammonium persulfate, 1 µL/mL TEMED (N, N, N′, N′ tetramethylethylenediamine)) and 10% resolving gel (380 µL/mL dH_2O, 340 µL/mL 30% acrylamide/bis-solution (29:1), 260 µL/mL 1.5 M Tris pH

8.8, 10 μL/mL 10% SDS, 10 μL/mL 10% ammonium persulfate, 0.4 μL/mL TEMED). The PageRuler Prestained Protein Ladder or PageRuler Plus Prestained Protein Ladder (Thermo Fisher Scientific, USA) was used as a marker. The electrophoresis was run at 120 V in 1x Laemmli running buffer (10 g/L Tris base, 14.4 g/L glycine, and 0.1 g/L SDS, pH 8.3) until the bromophenol blue in every sample reached the bottom of the resolving gel. For Coomassie blue gel staining, the resolving gel was first washed with water for 10 minutes, then stained for 1 hour by RAPIDstain (G-Biosciences, USA), and then destained with water for 1 hour. For immunoblot analysis, the proteins in the resolving gels were transferred onto a 0.2 μm Protran nitrocellulose membrane (Cytiva, USA) by Trans-Blot SD Semi-Dry Transfer Cell (Bio-Rad, USA) with 1x transfer buffer (3.03 g/L Tris base, 14.4 g/L glycine, 20% methanol, and 0.05% SDS) at 1 mA/cm^2 for 70 minutes. The nitrocellulose membrane was incubated in BlueBlock PF protein-free blocking buffer (SERVA, Germany) at room temperature for 1 hour. The primary antibody was subjected into the blocking buffer with the concentration shown in Table 6, and the membrane was incubated for 2 hours at room temperature or 4°C overnight. Subsequently, the membrane was washed three times with 1xTBS-T buffer (TBS buffer, pH7.6, 0.05% Tween20) for 10 minutes and incubated with the secondary antibody in TBS-T buffer for 1 hour at room temperature, if applicable. Finally, the membrane was washed three times with 1xTBS-T buffer and then covered by SuperSignal West Dura Extended Duration Substrate (Thermo, USA) for 5 minutes at room temperature in the dark. The chemiluminescent signal on the membrane was visualized by CCD camera system Fusion-SL4 (Vilber Lourmat, France).

Table 6. Antibodies in this study

Primary antibody	Secondary antibody
anti-GFP 3H9 (ChromoTek, Germany), 1: 2000	anti-rat-peroxidase-conjugated (HRP) A9542 (Sigma-Aldrich, USA), 1:20000
anti-RFP 5F8 (ChromoTek, Germany), 1: 2000	anti-rat-HRP A9542, 1:20000
anti-HA 7C9 (ChromoTek, Germany), 1:2000	anti-rat-HRP A9542, 1:20000
anti-Strep-tag StrepMAB-classic (IBA Lifesciences, Germany), 1:10000	anti-mouse-peroxidase-conjugated (HRP) A9044 (Sigma-Aldrich, USA), 1:20000
anti-Strep-tag StrepMAB-classic-HRP (IBA Lifesciences, Germany), 1:10000	

4.11 *E. coli* recombinant protein expression

The vectors for protein expression were transformed into *E. coli* T7 protein expression strains. The transformed *E. coli* strains were grown in liquid LB medium with 50 µg/mL kanamycin overnight at 37ºC. The E. coli strains were sub-cultured in the liquid LB medium with antibiotics for 3 hours or until OD_{600} reached approximately 0.5 at 37ºC, and subsequently, IPTG was added into the liquid LB medium with the indicated concentrations. The induced *E. coli* strains were incubated at 16ºC for 16 hours or 30ºC for 3 hours, and harvested by centrifugation at 4000 g, 4ºC for 15 minutes. The pellets were suspended with lysis buffer (20 mM Tris-HCl pH 7.5, 20 mM NaCl, 1 mM EDTA, 1% protease inhibitor (Sigma-Aldrich, USA), 1 mg/ml lysozyme) in a ratio of 0.01/20 (g/µL) with or without 1% Triton X-100 or 1% Tween 20, and incubated at room temperature for 1 hour. The suspensions were frozen in liquid nitrogen for 1 minute and thawed at room temperature, and then the suspensions were processed with the same steps twice. The samples were centrifuged at 13000 g, 4ºC for 20 minutes, and the supernatants (the soluble fractions) and the pellets (the insoluble fractions) were transferred to separate tubes and analyzed by SDS-PAGE and immunoblot.

4.12 Cell-free protein expression

The cell-free protein expression system used in the thesis is ALiCE (LenioBio, Germany). The vectors carrying proteins of interest are pALiCE01 and pALiCE02, without and with N-terminal

melittin signal peptide, respectively. The plasmids for ALiCE system were exclusively isolated by NucleoBond Xtra Midi (Macherey-Nagel, Germany) for less RNase contamination, according to the manual. 50 µL of ALiCE reaction mix was thawed and mixed with 2 µL of plasmid (~5 nM in the reaction mix), and the reaction mix was incubated in an orbital shaker at 700 rpm and 25ºC for 48 hours. The reaction mixtures with plasmids having melittin signal peptide were incubated with 0.5% n-dodecyl-β-maltoside in an orbital shaker at 700 rpm and 25ºC for 10 minutes, and the supernatant containing proteins of interest was transferred to a new tube after centrifugation at 16000 g for 10 minutes at room temperature.

4.13 Protein purification

4.13.1 Twin-Strep-tag purification

For Twin-Strep-tag purification, the AWF containing eAtLORE-nTWST-cHA was first centrifuged at 12000 g, 4ºC, for 10 minutes to remove the debris. The Twin-Strep-tag purification was performed with Strep-Tactin®XT 4Flow® cartridge (IBA Lifesciences, Germany), 5 mL per column bed volume (CV) coupled with ÄKTA system (Cytiva, USA) at 4ºC. The cartridge was pre-equilibrated by 5 CVs of Buffer W (100 mM Tris-HCl, pH 8.0, 150 mM NaCl, 1 mM EDTA), 2 mL/min flow rate. The cleared AWF (30-40 mL) was applied to the cartridge with a 1 mL/min flow rate, and the flow-through was collected for western blot analysis. The cartridge was washed by 10 CVs of Buffer W, 2 mL/min flow rate, and the flow-through was collected for western blot analysis. The eAtLORE-nTWST-cHA protein was eluted by 4 CVs of Buffer BXT (100 mM Tris-HCl, pH 8.0, 150 mM NaCl, 1 mM EDTA, 50 mM biotin), 1 mL/min flow rate. The cartridge was regenerated by 6 CVs of Buffer XT-R (3 M $MgCl_2$) and 8 CVs of Buffer W with a 2 mL/min flow rate for reuse.

Twin-Strep-tag purification of ALiCE expressing Twin-Strep-tag fusion proteins was done with Strep-Tactin®XT Spin Column (IBA Lifesciences, Germany). 100 µL of diluted cleared cell lysate was subjected to the pre-hydrated column and centrifuge for 30 seconds at 700 g, and the flow-through was collected for western blot analysis. The column was washed four times with 100 µl of Buffer W and centrifugation for 30 seconds at 15000 g, and the first flow-through was collected for western blot analysis. The spin column was placed into a new 1.5 ml tube, and the protein was eluted from the spin column by 100 µl of Buffer BXT with centrifugation for 30 seconds at 700 g, followed by centrifugation for 15 seconds at 15000 g.

4.13.2 Human influenza hemagglutinin (HA) purification

120μL (1 CV) of Pierce Anti-HA Agarose (Thermo, USA) resin was added to the microtube and washed with 1 CV of water. The resin was pelleted with a 5-10 second centrifugation at 12000 g. After discarding the supernatant, 400 μL of concentrated AWF containing eAtLORE-nHA (1.5 mg/mL) was mixed with resin and incubated on a rotator at 4ºC for one hour. The resin was then pelleted with a 5-10 second pulse at 12,000g, 4ºC, and the supernatant was collected for western blot analysis. The resin was washed with 4 CVs of water and pelleted twice, and the supernatant was discarded or collected for western blot analysis. The resin was suspended with 100 μL of water and 100 μL of 2 mg/mL HA peptides (Thermo, USA) and incubated at 4ºC on a rotator for 1 hour. The resin was centrifuged at 12,000g for a few seconds, and the supernatant was collected as an eluate. The elution step was repeated twice, and the eluates and 10 μL of the resin were analyzed by western blot. The remaining resin was further regenerated by 1 CV of 3M NaSCN to remove bound HA peptides, followed by washing the resin ten times with 1 CV of TBS buffer and preserving the resin in 50 μL of TBS at 4ºC.

4.14 Microscale thermophoresis

eAtLORE-mCherry, eAtLORE-His-HA, eAtLORE-HA, and apo-mCherry in AWFs were desalted by water and concentrated to 10-fold before MST assay. The purified eAtLORE-nTWST-cHA was concentrated to 0.1 mg/mL before the assay. Water in eAtLORE-mCherry and apo-mCherry concentrates were replaced by MST buffer (50 mM Tris-HCl, 250 mM NaCl, 10 mM $MgCl_2$, pH 7.8) with 0.05% Tween 20. The poly-histidine tag in eAtLORE-His-HA was labeled by His-Tag Labeling Kit RED-tris-NTA 2nd Generation (NanoTemper, Germany) based on the manufacturer's instruction, and the water in samples was replaced by PBS buffer (50 mM NaH_2PO_4/Na_2HPO_4 pH 7.5, 100 mM NaCl) with 0.05% Tween 20. eAtLORE-HA was a negative control of his-tag labeling, and the poly-histidine peptide was a positive control of labeling as well as a negative control for the MST assay. 2 μM of purified eAtLORE-nTWST-cHA was labeled by Protein Labeling Kit RED-NHS 2nd Generation (NanoTemper, Germany) based on the manufacturer’s guideline, and the labeled proteins were in TBS buffer with 0.05% Tween 20. 3-OH-C10:0 was adjusted to the indicated concentrations by two-fold serial dilution in designated buffers and mixed with an equal volume of protein solution. The mixture was loaded into Monolith NT.115 Capillaries (NanoTemper, Germany). Monolith NT.115 equipped with the RED fluorescent channel was utilized in the MST assay at room temperature (NanoTemper,

Germany). LED power and MST power were used based on the optimal fluorescent intensity automatically determined by MO.Control 2 in Monolith NT.115 (NanoTemper, Germany), and the final conditions were indicated in the results individually. Further data analyses were performed by both MO.Control 2 and MO.Affinity Analysis 3 (NanoTemper, Germany).

4.15 Ligand depletion binding assay

Both concentrated tobacco AWFs and purified and then desalted eAtLORE were used in this assay. The protein was adjusted to the indicated concentration by water. For the depletion assay, the protein sample was mixed in a 9:1 ratio (v:v) with the indicated concentration of elicitors prepared in water with less than 1% of methanol and incubated for one hour at 4°C on a rotator. Unbound ligands were isolated from the mixture by Vivaspin 500, 30000 MWCO (Sartorius, Germany). For the binding assay, the retentate was refilled with water up to the original volume of the mixture and then transferred to a new PCR tube and incubated at 98°C for 30 minutes. The bound elicitors released from denatured AWFs were isolated by Vivaspin 500 concentrators with a 30000 MWCO. The ligands in the filtrates from both depletion and binding assays were detected by $[Ca^{2+}]_{cyt}$ measurements using Col-0^{AEQ}, LORE-OE, and *lore*-1 seedlings.

4.16 Radiobinding assay

The Twin-Strep-purified eAtLORE was applied in the radiobinding assay. The tritium-labeled 3-hydroxydecanoic acid ([^{3}H]-3-OH-C10:0, 11.2 Ci/mmol) was synthesized by Moravek Inc. (USA) with radiochemical purity 97.9% (checked by HPLC and Tritium NMR). The assay in the thesis using [^{3}H]-3-OH-C10:0 was performed 40 months after synthesis (In February 2019). [^{3}H]-3-OH-C10:0 was adjusted to 100 µM by dissolved in 201µL pure methanol.

4.16.1 Saturation binding assay

In each 80 µL mixture for total binding, 600 nM of eAtLORE in TBS buffer was incubated with different concentrations of [^{3}H]-3-OH-C10:0 (1000, 300, 100, 30, 10, 3 nM) in the same volume of methanol. The mixtures for measuring nonspecific binding were additionally incubated with 1 mM cold 3-OH-C10:0 (Stock concentration: 50 mM in methanol). The mixtures without cold ligands were supplied with additional methanol (3% in every mix). The mixtures were incubated at 4°C for one hour and then subjected to Vivaspin 500 concentrators with a 30000 MWCO, followed by centrifugation at 12000 g at room temperature for 5 minutes. To remove unbound ligands, the retentates were washed with 80 µL of TBS buffer and centrifuged at 12000 g at room

temperature for 3 minutes twice, and the retentates were transferred to 20 mL scintillation vials by adding 80 µL of TBS buffer into the concentrators. After mixing thoroughly with 2 mL of scintillation cocktail (Carl Roth, Germany), the radioactivity of the mixture was measured by 5-minute liquid scintillation counting with scintillation counter Tri-Carb 4910TR (PerkinElmer, USA). The radioactivity was shown as count per minute (cpm).

4.16.2 Competition binding assay

In each 80 µL mixture, 600 nM of eAtLORE in TBS buffer was incubated with 30 nM of [^{3}H]-3-OH-C10:0, and the different concentrations of cold 3-OH-C10:0, 3-OH-C12:0 or 3-OH-C14:0 (1, 30, 1000, 30000 nM) in the same proportion of methanol (3% in every mixture). The following steps, from incubation to liquid scintillation counting, were identical to the saturation binding assay.

4.17 Measurement of chlorophyll fluorescence for cell death analysis on tobacco

Red chlorophyll fluorescence emitted from leaves was measured to quantify the cell death phenotype (Eschrig *et al.*, 2021, Landeo Villanueva *et al.*, 2021). The Agrobacteria carrying overexpression vectors of LORE ortholog-eGFP fusion proteins were cultured, harvested, and syringe-infiltrated into *N. benthamiana,* as above, and the leaf discs from infiltrated leaves were harvested 40-42 hours after infiltration. The leaf discs were incubated and floated on 200 µL water in 96-well black plate. Tecan Luminescence plate reader (Tecan Infinite F200 PRO, Switzerland) was used with an excitation wavelength 535 nm, an emission wavelength 590 nm, integration time of 20 µs, 16 reads per well, and gain value of 80, to measure the leaf discs.

4.18 Generation of transgenic Arabidopsis

Transgenic Arabidopsis plants were generated using the floral dip method (Zhang *et al*., 2006). *A. tumefaciens* GV3101 was transformed with binary vectors pGGPXhcFR containing different LORE orthologs induced by the promoter of *AtLORE* and FastRed selection marker or pGGPXB containing AtLORE induced by the 35S promoter and BASTA selection marker. *A. tumefaciens* was grown on LB agar for two days, then washed and suspended in the solution containing 5% sucrose. The OD_{600} of *A. tumefaciens* suspension was adjusted to 2.0, and the suspension was added Silwet-77 to the final concentration of 0.02%. 8 to 10-week-old *lore*-1, under long-day conditions having inflorescences, was dipped in the suspension for 30-60 seconds and maintained in a plastic bag with high humidity overnight. The transformed TagRFP-expressing seeds were

screened by a stereomicroscope equipped with Fluorescent Adaptor, Green set (Excitation: 510-540 nm, emission filter: 600 nm longpass) (Nightsea, USA). T1 and T2 lines were also examined by $[Ca^{2+}]_{cyt}$ measurements, ROS measurement, and RT-PCR for their *LORE*-ortholog expression. The transgenic AtLORE overexpression line was previously generated by Dr. Schäffer (Schäffer, 2019, Shu *et al.*, 2021).

Table 7. List of transgenic Arabidopsis lines expressing LORE or LORE orthologs in *lore*-1 background used/generated in this study.

Plant line	Transgene ID	Transformed construct (Promoter::Transgene::Terminator)	Vector backbone	Note
LORE-OE	At1g61380 (*LORE*)	p35S::LORE::t35S	pGGPXB	Dr. Schäffer, Milena
EsalLOREa	Thhalv10023279	pLORE:Thhalv10023279::tHSP	pGGPXhcFR	
EsalLOREb	Thhalv10023335	pLORE::Thhalv10023335::tHSP	pGGPXhcFR	
EsyrLOREa	Eusyr.0018s0446	pLORE::Eusyr.0018s0446::tHSP	pGGPXhcFR	
EsyrLOREb	Eusyr.0018s0448	pLORE::Eusyr.0018s0448::tHSP	pGGPXhcFR	
RislLORE	Roisl.0209s0716	pLORE::Roisl.0209s0716::tHSP	pGGPXhcFR	
DsopLORE	Desop.0206s0096	pLORE::Desop.0206s0096::tHSP	pGGPXhcFR	
BoleLORE	Bol013747	pLORE::Bol013747::tHSP	pGGPXhcFR	
BrapLOREa	Brara.I01503	pLORE::Brara.I01503::tHSP	pGGPXhcFR	
BrapLOREb	Brara.A02537	pLORE::Brara.A02537::tHSP	pGGPXhcFR	
ChisLORE	Crahi.1347s0007	pLORE::Crahi.1347s0007::tHSP	pGGPXhcFR	
TarvLORE	Thlar.0056s0139	pLORE::Thlar.0056s0139::tHSP	pGGPXhcFR	
MmarLORE	Mamar.0055s0354	pLORE::Mamar.0055s0354::tHSP	pGGPXhcFR	
BnigLOREa	BniB011153	pLORE::BniB011153::tHSP	pGGPXhcFR	
BnigLOREb	BniB002031	pLORE::BniB002031::tHSP	pGGPXhcFR	
BnigLOREc	BniB022340	pLORE::BniB022340::tHSP	pGGPXhcFR	
AaraLORE	Aa31LG2G9310	pLORE::Aa31LG2G9310:::tHSP	pGGPXhcFR	

4.19 Arabidopsis RNA isolation and RT-PCR

Arabidopsis RNA was extracted according to the procedure of Direct-zol RNA Mini Prep kit (Zymo Research) with TRIzol® Reagent (Thermo Fisher Scientific, USA). Approximately 10 to 15 9-day-old seedlings grown in half-strength MS liquid medium were collected in 2.0 mL microtubes with two 2 mm sterilized glass beads and frozen in liquid nitrogen immediately. The seedlings were ground using TissueLyserII (Qiagen, Germany) for 1 minute at 30 f/s. The

homogenized seedlings were mixed well with 0.7 mL TRIzol® Reagent and incubated at RT for 5 minutes. After centrifugation at 12000g for 10 minutes at 4ºC, the supernatant was transferred into a new tube and mixed with an equal volume of absolute ethanol. The 700 µL mixture was transferred into Zymo-Spin™ IICR Column and centrifuged at 12000g for 1 minute at 4ºC. The column was washed twice with 400 µL Direct-zol™ RNA PreWash, followed by 700 µL RNA Wash Buffer. The RNA was eluted from the column with 50 µL nuclease-free water. Nanodrop Spectrophotometer ND-100 measured the concentration of RNA.

cDNA was synthesized by RevertAid RT Reverse Transcription Kit (Thermo Fisher Scientific, USA), and the manufacturer's instruction was followed. 2 µg of each RNA sample was treated with DNaseI (In total 10 µL, 1 U DNaseI, DNaseI buffer 1X, 40 U Ribolock, Thermo Fisher Scientific, USA) at 37°C for 30 minutes, followed by 1 µL 50 mM EDTA at 70°C for 10 minutes. After the DNaseI-treated sample was mixed with 1 µL 10 µM Oligo(dT)18 (Eurofins, Germany) and incubated at 70°C for 5 minutes, 200 U RevertAid Reverse Transcriptase, 20U Ribolock, 2 µL 10 mM dNTPs, 5xRT buffer (Thermo Fisher Scientific, USA) were added. The 20 µL mixture was incubated at 37°C for 5 minutes, at 42°C for 60 min, then at 72°C for 15 minutes. Semi-quantitative PCR was performed with SupraTherm Taq Polymerase (Genecraft, Germany) with the primers listed below (Table 8). The PCR mixture was incubated under the following conditions: 95ºC for 1 minute, then 28 cycles (*EF1-alpha*) or 36 cycles (*LORE*-ortholog) of 95ºC for 10 seconds, 54ºC for 10 seconds, and 72ºC for 45 seconds, followed by 72ºC for 5 minutes. The amplified PCR products were analyzed by using 2% agarose gel electrophoresis.

Table 8. Primers for RT-PCR

Name	Sequence (5'-3')	Note
EF1-alpha-F	TCACATCAACATTGTGGTCATTGGC	Ranf *et al*., 2015
EF1-alpha-R	TTGATCTGGTCAAGAGCCTCAAG	Ranf *et al*., 2015
LORE-ortholog-F	GAGTTTATGGTGAACAAAAG	Identical sequence in all targets
LORE-ortholog-R	TCATCTTCATATGTTCTAGCGT	On tHSP and last 7 bps of transgenes

5 References

1001_Genomes_Consortium (2016) 1,135 genomes reveal the global pattern of polymorphism in *Arabidopsis thaliana*. *Cell*, **166**, 481-491.

Abhinandan, K., Hickerson, N.M.N., Lan, X. and Samuel, M.A. (2022) Disabling of ARC1 through CRISPR/CAS9 leads to a complete breakdown of self-incompatibility responses in *Brassica napus*. *bioRxiv*.

Al-Shehbaz, A.A. (2012) A generic and tribal synopsis of the Brassicaceae (Cruciferae). *Taxon*, **61**, 931-954.

Albert, I., Böhm, H., Albert, M., Feiler, C.E., Imkampe, J., Wallmeroth, N., Brancato, C., Raaymakers, T.M., Oome, S., Zhang, H., Krol, E., Grefen, C., Gust, A.A., Chai, J., Hedrich, R., Van den Ackerveken, G. and Nurnberger, T. (2015) An RLP23-SOBIR1-BAK1 complex mediates NLP-triggered immunity. *Nat Plants*, **1**, 15140.

Almagro Armenteros, J.J., Tsirigos, K.D., Sonderby, C.K., Petersen, T.N., Winther, O., Brunak, S., von Heijne, G. and Nielsen, H. (2019) SignalP 5.0 improves signal peptide predictions using deep neural networks. *Nat Biotechnol*, **37**, 420-423.

Asai, S. and Shirasu, K. (2015) Plant cells under siege: plant immune system versus pathogen effectors. *Curr Opin Plant Biol*, **28**, 1-8.

Bellande, K., Bono, J.J., Savelli, B., Jamet, E. and Canut, H. (2017) Plant Lectins and Lectin Receptor-Like Kinases: How Do They Sense the Outside? *Int J Mol Sci*, **18**, 1164.

Benjamini, Y. and Hochberg, Y. (1995) Controlling the false discovery rate: a practical and powerful approach to multiple testing. *J R Stat Soc Series B Stat Methodol*, **57**, 289-300.

Berger, F., Ramirez-Hernandez, M.H. and Ziegler, M. (2004) The new life of a centenarian: signalling functions of NAD(P). *Trends Biochem Sci*, **29**, 111-118.

Berger, I. and Poterszman, A. (2015) Baculovirus expression: old dog, new tricks. *Bioengineered*, **6**, 316-322.

Bigeard, J., Colcombet, J. and Hirt, H. (2015) Signaling mechanisms in pattern-triggered immunity (PTI). *Mol Plant*, **8**, 521-539.

Biswas, S., Dalal, B., Sen, M. and Biswas, B.B. (1995) Receptor for myo-inositol trisphosphate from the microsomal fraction of *Vigna radiata*. *Biochem J*, **306 (Pt 3)**, 631-636.

Böhm, H., Albert, I., Oome, S., Raaymakers, T.M., Van den Ackerveken, G. and Nurnberger, T. (2014) A conserved peptide pattern from a widespread microbial virulence factor triggers pattern-induced immunity in Arabidopsis. *PLoS Pathog*, **10**, e1004491.

Bolaños-Martínez, O.C. and Strasser, R. (2022) Plant-made poliovirus vaccines - Safe alternatives for global vaccination. *Front Plant Sci*, **13**, 1046346.

Boller, T. and Felix, G. (2009) A renaissance of elicitors: perception of microbe-associated molecular patterns and danger signals by pattern-recognition receptors. *Annu Rev Plant Biol*, **60**, 379-406.

Bonaventure, G. (2011) The *Nicotiana attenuata* LECTIN RECEPTOR KINASE 1 is involved in the perception of insect feeding. *Plant Signal Behav*, **6**, 2060-2063.

Borsch, T., Berendsohn, W., Dalcin, E., Delmas, M., Demissew, S., Elliott, A., Fritsch, P., Fuchs, A., Geltman, D., Güner, A., Haevermans, T., Knapp, S., le Roux, M.M., Loizeau, P.-A., Miller, C., Miller, J., Miller, J.T., Palese, R., Paton, A., Parnell, J., Pendry, C., Qin, H.-N., Sosa, V., Sosef, M., von Raab-Straube, E., Ranwashe, F., Raz, L., Salimov, R., Smets, E., Thiers, B., Thomas, W., Tulig, M., Ulate, W., Ung, V., Watson, M., Jackson, P.W. and Zamora, N. (2020) World Flora Online: Placing

taxonomists at the heart of a definitive and comprehensive global resource on the world's plants. *Taxon*, **69**, 1311-1341.

Boschi, F., Schvartzman, C., Murchio, S., Ferreira, V., Siri, M.I., Galván, G.A., Smoker, M., Stransfeld, L., Zipfel, C., Vilaró, F.L. and Dalla-Rizza, M. (2017) Enhanced bacterial wilt resistance in potato through expression of Arabidopsis EFR and introgression of quantitative resistance from *Solanum commersonii*. *Front Plant Sci*, **8**, 1642.

Bozsoki, Z., Gysel, K., Hansen, S.B., Lironi, D., Kronauer, C., Feng, F., de Jong, N., Vinther, M., Kamble, M., Thygesen, M.B., Engholm, E., Kofoed, C., Fort, S., Sullivan, J.T., Ronson, C.W., Jensen, K.J., Blaise, M., Oldroyd, G., Stougaard, J., Andersen, K.R. and Radutoiu, S. (2020) Ligand-recognizing motifs in plant LysM receptors are major determinants of specificity. *Science*, **369**, 663-670.

Briskine, R.V., Paape, T., Shimizu-Inatsugi, R., Nishiyama, T., Akama, S., Sese, J. and Shimizu, K.K. (2017) Genome assembly and annotation of *Arabidopsis halleri*, a model for heavy metal hyperaccumulation and evolutionary ecology. *Mol Ecol Resour*, **17**, 1025-1036.

Buntru, M., Vogel, S., Stoff, K., Spiegel, H. and Schillberg, S. (2015) A versatile coupled cell-free transcription-translation system based on tobacco BY-2 cell lysates. *Biotechnol Bioeng*, **112**, 867-878.

Butenko, M.A., Wildhagen, M., Albert, M., Jehle, A., Kalbacher, H., Aalen, R.B. and Felix, G. (2014) Tools and strategies to match peptide-ligand receptor pairs. *Plant Cell*, **26**, 1838-1847.

Cao, Y., Liang, Y., Tanaka, K., Nguyen, C.T., Jedrzejczak, R.P., Joachimiak, A. and Stacey, G. (2014) The kinase LYK5 is a major chitin receptor in Arabidopsis and forms a chitin-induced complex with related kinase CERK1. *Elife*, **3**.

Catanzariti, A.M., Lim, G.T.T. and Jones, D.A. (2015) The tomato I-3 gene: a novel gene for resistance to *Fusarium* wilt disease. *New Phytol*, **207**, 106-118.

Chakravarthy, S., Velasquez, A.C., Ekengren, S.K., Collmer, A. and Martin, G.B. (2010) Identification of *Nicotiana benthamiana* genes involved in pathogen-associated molecular pattern-triggered immunity. *Mol Plant Microbe Interact*, **23**, 715-726.

Charpenteau, M., Jaworski, K., Ramirez, B.C., Tretyn, A., Ranjeva, R. and Ranty, B. (2004) A receptor-like kinase from *Arabidopsis thaliana* is a calmodulin-binding protein. *Biochem J*, **379**, 841-848.

Chen, L.J., Wuriyanghan, H., Zhang, Y.Q., Duan, K.X., Chen, H.W., Li, Q.T., Lu, X., He, S.J., Ma, B., Zhang, W.K., Lin, Q., Chen, S.Y. and Zhang, J.S. (2013) An S-domain receptor-like kinase, OsSIK2, confers abiotic stress tolerance and delays dark-induced leaf senescence in rice. *Plant Physiol*, **163**, 1752-1765.

Chen, X., Shang, J., Chen, D., Lei, C., Zou, Y., Zhai, W., Liu, G., Xu, J., Ling, Z., Cao, G., Ma, B., Wang, Y., Zhao, X., Li, S. and Zhu, L. (2006) A B-lectin receptor kinase gene conferring rice blast resistance. *Plant J*, **46**, 794-804.

Cheng, X., Wu, Y., Guo, J., Du, B., Chen, R., Zhu, L. and He, G. (2013) A rice lectin receptor-like kinase that is involved in innate immune responses also contributes to seed germination. *Plant J*, **76**, 687-698.

Chinchilla, D., Bauer, Z., Regenass, M., Boller, T. and Felix, G. (2006) The Arabidopsis receptor kinase FLS2 binds flg22 and determines the specificity of flagellin perception. *Plant Cell*, **18**, 465-476.

Chinchilla, D., Zipfel, C., Robatzek, S., Kemmerling, B., Nurnberger, T., Jones, J.D., Felix, G. and Boller, T. (2007) A flagellin-induced complex of the receptor FLS2 and BAK1 initiates plant defence. *Nature*, **448**, 497-500.

Choi, J., Tanaka, K., Cao, Y., Qi, Y., Qiu, J., Liang, Y., Lee, S.Y. and Stacey, G. (2014) Identification of a plant receptor for extracellular ATP. *Science*, **343**, 290-294.

Coll, N.S., Epple, P. and Dangl, J.L. (2011) Programmed cell death in the plant immune system. *Cell Death Differ*, **18**, 1247-1256.

Cosio, E.G., Popperl, H., Schmidt, W.E. and Ebel, J. (1988) High-affinity binding of fungal beta-glucan fragments to soybean (*Glycine max* L.) microsomal fractions and protoplasts. *Eur J Biochem*, **175**, 309-315.

Couto, D. and Zipfel, C. (2016) Regulation of pattern recognition receptor signalling in plants. *Nat Rev Immunol*, **16**, 537-552.

Cui, H., Tsuda, K. and Parker, J.E. (2015) Effector-triggered immunity: from pathogen perception to robust defense. *Annu Rev Plant Biol*, **66**, 487-511.

Dievart, A., Gottin, C., Perin, C., Ranwez, V. and Chantret, N. (2020) Origin and diversity of plant receptor-like kinases. *Annu Rev Plant Biol*, **71**, 131-156.

DOE-JGI. Brassicales Map Alignment Project.

Dowler, S., Kular, G. and Alessi, D.R. (2002) Protein lipid overlay assay. *Sci STKE*, **2002**, pl6.

Dunning, F.M., Sun, W., Jansen, K.L., Helft, L. and Bent, A.F. (2007) Identification and mutational analysis of Arabidopsis FLS2 leucine-rich repeat domain residues that contribute to flagellin perception. *Plant Cell*, **19**, 3297-3313.

Dyson, M.R., Shadbolt, S.P., Vincent, K.J., Perera, R.L. and McCafferty, J. (2004) Production of soluble mammalian proteins in *Escherichia coli*: identification of protein features that correlate with successful expression. *BMC Biotechnol*, **4**, 32.

Eschrig, S., Schäffer, M., Illig, T., Eibel, S., Shu, L.-J., Fernandez, A. and Ranf, S. (2021) LORE homomerization is required for 3-OH-C10: 0 induced immune signaling. *bioRxiv*.

de Felippes, F., McHale, M., Doran, R.L., Roden, S., Eamens, A.L., Finnegan, E.J. and Waterhouse, P.M. (2020) The key role of terminators on the expression and post-transcriptional gene silencing of transgenes. *Plant J*, **104**, 96-112.

Falconer, R.J. (2016) Applications of isothermal titration calorimetry - the research and technical developments from 2011 to 2015. *J Mol Recognit*, **29**, 504-515.

Fan, J., Bai, P., Ning, Y., Wang, J., Shi, X., Xiong, Y., Zhang, K., He, F., Zhang, C., Wang, R., Meng, X., Zhou, J., Wang, M., Shirsekar, G., Park, C.H., Bellizzi, M., Liu, W., Jeon, J.S., Xia, Y., Shan, L. and Wang, G.L. (2018) The monocot-specific receptor-like kinase SDS2 controls cell death and immunity in rice. *Cell Host Microbe*, **23**, 498-510 e495.

Fan, L., Frohlich, K., Melzer, E., Pruitt, R.N., Albert, I., Zhang, L., Joe, A., Hua, C., Song, Y., Albert, M., Kim, S.T., Weigel, D., Zipfel, C., Chae, E., Gust, A.A. and Nurnberger, T. (2022) Genotyping-by-sequencing-based identification of Arabidopsis pattern recognition receptor RLP32 recognizing proteobacterial translation initiation factor IF1. *Nat Commun*, **13**, 1294.

Fernandez-Pozo, N., Metz, T., Chandler, J.O., Gramzow, L., Merai, Z., Maumus, F., Mittelsten Scheid, O., Theissen, G., Schranz, M.E., Leubner-Metzger, G. and Rensing, S.A. (2021) *Aethionema arabicum* genome annotation using PacBio full-length transcripts provides a valuable resource for seed dormancy and Brassicaceae evolution research. *Plant J*, **106**, 275-293.

Freire, E., Mayorga, O.L. and Straume, M. (1990) Isothermal titration calorimetry. *Anal Chem*, **62**, 950A-959A.

Fürst, U., Zeng, Y., Albert, M., Witte, A.K., Fliegmann, J. and Felix, G. (2020) Perception of *Agrobacterium tumefaciens* flagellin by FLS2(XL) confers resistance to crown gall disease. *Nat Plants*, **6**, 22-27.

Gan, X., Hay, A., Kwantes, M., Haberer, G., Hallab, A., Ioio, R.D., Hofhuis, H., Pieper, B., Cartolano, M., Neumann, U., Nikolov, L.A., Song, B., Hajheidari, M., Briskine, R., Kougioumoutzi, E., Vlad, D., Broholm, S., Hein, J., Meksem, K., Lightfoot, D., Shimizu, K.K., Shimizu-Inatsugi, R., Imprialou, M., Kudrna, D., Wing, R., Sato, S., Huijser, P., Filatov, D., Mayer, K.F., Mott, R. and Tsiantis, M. (2016) The *Cardamine hirsuta* genome offers insight into the evolution of morphological diversity. *Nat Plants*, **2**, 16167.

Giranton, J.L., Dumas, C., Cock, J.M. and Gaude, T. (2000) The integral membrane S-locus receptor kinase of *Brassica* has serine/threonine kinase activity in a membranous environment and spontaneously forms oligomers in planta. *Proc Natl Acad Sci U S A*, **97**, 3759-3764.

Glazebrook, J. (2005) Contrasting mechanisms of defense against biotrophic and necrotrophic pathogens. *Annu Rev Phytopathol*, **43**, 205-227.

Gomes, C., Oliveira, F., Vieira, S.I. and Duque, A.S. (2019) Prospects for the production of recombinant therapeutic proteins and peptides in plants: Special focus on Angiotensin I-Converting Enzyme Inhibitory (ACEI) peptides. In *Genetic Engineering-A Glimpse of Techniques and Applications*: IntechOpen.

Gómez-Gómez, L. and Boller, T. (2000) FLS2: an LRR receptor-like kinase involved in the perception of the bacterial elicitor flagellin in Arabidopsis. *Mol Cell*, **5**, 1003-1011.

Gonneau, M., Desprez, T., Martin, M., Doblas, V.G., Bacete, L., Miart, F., Sormani, R., Hématy, K., Renou, J., Landrein, B., Murphy, E., Van De Cotte, B., Vernhettes, S., De Smet, I. and Höfte, H. (2018) Receptor kinase THESEUS1 is a Rapid Alkalinization Factor 34 receptor in Arabidopsis. *Curr Biol*, **28**, 2452-2458.e2454.

Grosse-Holz, F., Madeira, L., Zahid, M.A., Songer, M., Kourelis, J., Fesenko, M., Ninck, S., Kaschani, F., Kaiser, M. and van der Hoorn, R.A.L. (2018) Three unrelated protease inhibitors enhance accumulation of pharmaceutical recombinant proteins in *Nicotiana benthamiana*. *Plant Biotechnol J*, **16**, 1797-1810.

Gu, T., Mazzurco, M., Sulaman, W., Matias, D.D. and Goring, D.R. (1998) Binding of an arm repeat protein to the kinase domain of the S-locus receptor kinase. *Proc Natl Acad Sci U S A*, **95**, 382-387.

Gully, K., Pelletier, S., Guillou, M.C., Ferrand, M., Aligon, S., Pokotylo, I., Perrin, A., Vergne, E., Fagard, M., Ruelland, E., Grappin, P., Bucher, E., Renou, J.P. and Aubourg, S. (2019) The SCOOP12 peptide regulates defense response and root elongation in *Arabidopsis thaliana*. *J Exp Bot*, **70**, 1349-1365.

Guo, Y., Bian, W., Zhang, Y. and Li, H. (2017) Expression in *Escherichia coli*, purification and characterization of LRSAM1, a LRR and RING domain E3 ubiquitin ligase. *Protein Expr Purif*, **129**, 158-161.

Gust, A.A., Pruitt, R. and Nurnberger, T. (2017) Sensing danger: key to activating plant immunity. *Trends Plant Sci*, **22**, 779-791.

Häkkinen, S.T., Raven, N., Henquet, M., Laukkanen, M.L., Anderlei, T., Pitkanen, J.P., Twyman, R.M., Bosch, D., Oksman-Caldentey, K.M., Schillberg, S. and Ritala, A. (2014) Molecular farming in tobacco hairy roots by triggering the secretion of a pharmaceutical antibody. *Biotechnol Bioeng*, **111**, 336-346.

Han, X., Yang, Y., Zhao, F., Zhang, T. and Yu, X. (2020) An improved protein lipid overlay assay for studying lipid-protein interactions. *Plant Methods*, **16**, 33.

Haruta, M., Sabat, G., Stecker, K., Minkoff, B.B. and Sussman, M.R. (2014) A peptide hormone and its receptor protein kinase regulate plant cell expansion. *Science*, **343**, 408-411.

Haudry, A., Platts, A.E., Vello, E., Hoen, D.R., Leclercq, M., Williamson, R.J., Forczek, E., Joly-Lopez, Z., Steffen, J.G., Hazzouri, K.M., Dewar, K., Stinchcombe, J.R., Schoen, D.J., Wang, X., Schmutz, J., Town, C.D., Edger, P.P., Pires, J.C., Schumaker, K.S., Jarvis, D.E., Mandáková, T., Lysak, M.A., van den Bergh, E., Schranz, M.E., Harrison, P.M., Moses, A.M., Bureau, T.E., Wright, S.I. and Blanchette, M. (2013) An atlas of over 90,000 conserved noncoding sequences provides insight into crucifer regulatory regions. *Nat Genet*, **45**, 891-898.

Häweker, H., Rips, S., Koiwa, H., Salomon, S., Saijo, Y., Chinchilla, D., Robatzek, S. and von Schaewen, A. (2010) Pattern recognition receptors require N-glycosylation to mediate plant immunity. *J Biol Chem*, **285**, 4629-4636.

Hayafune, M., Berisio, R., Marchetti, R., Silipo, A., Kayama, M., Desaki, Y., Arima, S., Squeglia, F., Ruggiero, A., Tokuyasu, K., Molinaro, A., Kaku, H. and Shibuya, N. (2014) Chitin-induced activation of immune signaling by the rice receptor CEBiP relies on a unique sandwich-type dimerization. *Proc Natl Acad Sci U S A*, **111**, E404-413.

Hellmuth, A. and Calderón Villalobos, L.I. (2016) Radioligand binding assays for determining dissociation constants of phytohormone receptors. *Methods Mol Biol*, **1450**, 23-34.

Hohmann, N., Wolf, E.M., Lysak, M.A. and Koch, M.A. (2015) A time-calibrated road map of Brassicaceae species radiation and evolutionary history. *Plant Cell*, **27**, 2770-2784.

Hohmann, U., Lau, K. and Hothorn, M. (2017) The structural basis of ligand perception and signal activation by receptor kinases. *Annu Rev Plant Biol*, **68**, 109-137.

Hou, S., Liu, D. and He, P. (2021a) Phytocytokines function as immunological modulators of plant immunity. *Stress Biol*, **1**, 8.

Hou, S., Liu, D., Huang, S., Luo, D., Liu, Z., Xiang, Q., Wang, P., Mu, R., Han, Z., Chen, S., Chai, J., Shan, L. and He, P. (2021b) The Arabidopsis MIK2 receptor elicits immunity by sensing a conserved signature from phytocytokines and microbes. *Nat Commun*, **12**, 5494.

Hu, T.T., Pattyn, P., Bakker, E.G., Cao, J., Cheng, J.F., Clark, R.M., Fahlgren, N., Fawcett, J.A., Grimwood, J., Gundlach, H., Haberer, G., Hollister, J.D., Ossowski, S., Ottilar, R.P., Salamov, A.A., Schneeberger, K., Spannagl, M., Wang, X., Yang, L., Nasrallah, M.E., Bergelson, J., Carrington, J.C., Gaut, B.S., Schmutz, J., Mayer, K.F., Van de Peer, Y., Grigoriev, I.V., Nordborg, M., Weigel, D. and Guo, Y.L. (2011) The *Arabidopsis lyrata* genome sequence and the basis of rapid genome size change. *Nat Genet*, **43**, 476-481.

Huang, C.H., Sun, R., Hu, Y., Zeng, L., Zhang, N., Cai, L., Zhang, Q., Koch, M.A., Al-Shehbaz, I., Edger, P.P., Pires, J.C., Tan, D.Y., Zhong, Y. and Ma, H. (2016) Resolution of Brassicaceae phylogeny using nuclear genes uncovers nested radiations and supports convergent morphological evolution. *Mol Biol Evol*, **33**, 394-412.

Huck, N.V., Leissing, F., Majovsky, P., Buntru, M., Aretz, C., Flecken, M., Müller, J.P.J., Vogel, S., Schillberg, S., Hoehenwarter, W., Conrath, U. and Beckers, G.J.M. (2017) Combined (15)N-labeling and TandemMOAC quantifies phosphorylation of MAP kinase substrates downstream of MKK7 in Arabidopsis. *Front Plant Sci*, **8**, 2050.

Huffaker, A., Pearce, G. and Ryan, C.A. (2006) An endogenous peptide signal in Arabidopsis activates components of the innate immune response. *Proc Natl Acad Sci U S A*, **103**, 10098-10103.

Igic, B., Lande, R. and Kohn, J.R. (2008) Loss of self-incompatibility and its evolutionary consequences. *Int J Plant Sci*, **169**, 93-104.

Jain, P., Arora, D. and Bhatla, S. (2016) Surface plasmon resonance based recent advances in understanding plant development and related processes. *Biochem Anal Biochem*, **5**, 2161-1009.1000300.

Jehle, A.K., Lipschis, M., Albert, M., Fallahzadeh-Mamaghani, V., Furst, U., Mueller, K. and Felix, G. (2013) The receptor-like protein ReMAX of Arabidopsis detects the microbe-associated molecular pattern eMax from *Xanthomonas*. *Plant Cell*, **25**, 2330-2340.

Jerabek-Willemsen, M., André, T., Wanner, R., Roth, H.M., Duhr, S., Baaske, P. and Breitsprecher, D. (2014) MicroScale Thermophoresis: Interaction analysis and beyond. *J Mol Struct*, **1077**, 101-113.

Jiménez, J., Doerr, S., Martinez-Rosell, G., Rose, A.S. and De Fabritiis, G. (2017) DeepSite: protein-binding site predictor using 3D-convolutional neural networks. *Bioinformatics*, **33**, 3036-3042.

Jones, J.D. and Dangl, J.L. (2006) The plant immune system. *Nature*, **444**, 323-329.

Kachroo, A., Schopfer, C.R., Nasrallah, M.E. and Nasrallah, J.B. (2001) Allele-specific receptor-ligand interactions in *Brassica* self-incompatibility. *Science*, **293**, 1824-1826.

Kadota, Y., Shirasu, K. and Zipfel, C. (2015) Regulation of the NADPH oxidase RBOHD during plant immunity. *Plant Cell Physiol*, **56**, 1472-1480.

Kaku, H., Nishizawa, Y., Ishii-Minami, N., Akimoto-Tomiyama, C., Dohmae, N., Takio, K., Minami, E. and Shibuya, N. (2006) Plant cells recognize chitin fragments for defense signaling through a plasma membrane receptor. *Proc Natl Acad Sci U S A*, **103**, 11086-11091.

Kato, H., Nemoto, K., Shimizu, M., Abe, A., Asai, S., Ishihama, N., Matsuoka, S., Daimon, T., Ojika, M., Kawakita, K., Onai, K., Shirasu, K., Yoshida, M., Ishiura, M., Takemoto, D., Takano, Y. and Terauchi, R. (2022) Recognition of pathogen-derived sphingolipids in Arabidopsis. *Science*, **376**, 857-860.

Khambhati, K., Bhattacharjee, G., Gohil, N., Braddick, D., Kulkarni, V. and Singh, V. (2019) Exploring the potential of cell-free protein synthesis for extending the abilities of biological systems. *Front Bioeng Biotechnol*, **7**, 248.

Kiefer, C., Willing, E.M., Jiao, W.B., Sun, H., Piednoel, M., Humann, U., Hartwig, B., Koch, M.A. and Schneeberger, K. (2019) Interspecies association mapping links reduced CG to TG substitution rates to the loss of gene-body methylation. *Nat Plants*, **5**, 846-855.

Knight, M.R., Campbell, A.K., Smith, S.M. and Trewavas, A.J. (1991) Transgenic plant aequorin reports the effects of touch and cold-shock and elicitors on cytoplasmic calcium. *Nature*, **352**, 524-526.

Koenig, D. and Weigel, D. (2015) Beyond the thale: comparative genomics and genetics of Arabidopsis relatives. *Nat Rev Genet*, **16**, 285-298.

Komarova, T.V., Baschieri, S., Donini, M., Marusic, C., Benvenuto, E. and Dorokhov, Y.L. (2010) Transient expression systems for plant-derived biopharmaceuticals. *Expert Rev Vaccines*, **9**, 859-876.

Koornneef, M. and Meinke, D. (2010) The development of Arabidopsis as a model plant. *Plant J*, **61**, 909-921.

Korte, A. and Farlow, A. (2013) The advantages and limitations of trait analysis with GWAS: a review. *Plant Methods*, **9**, 29.

Krogh, A., Larsson, B., von Heijne, G. and Sonnhammer, E.L. (2001) Predicting transmembrane protein topology with a hidden Markov model: application to complete genomes. *J Mol Biol*, **305**, 567-580.

Krol, E., Mentzel, T., Chinchilla, D., Boller, T., Felix, G., Kemmerling, B., Postel, S., Arents, M., Jeworutzki, E., Al-Rasheid, K.A., Becker, D. and Hedrich, R. (2010) Perception of the Arabidopsis danger signal peptide 1 involves the pattern recognition receptor AtPEPR1 and its close homologue AtPEPR2. *J Biol Chem*, **285**, 13471-13479.

Kunze, G., Zipfel, C., Robatzek, S., Niehaus, K., Boller, T. and Felix, G. (2004) The N terminus of bacterial elongation factor Tu elicits innate immunity in Arabidopsis plants. *Plant Cell*, **16**, 3496-3507.

Kutschera, A., Dawid, C., Gisch, N., Schmid, C., Raasch, L., Gerster, T., Schaffer, M., Smakowska-Luzan, E., Belkhadir, Y., Vlot, A.C., Chandler, C.E., Schellenberger, R., Schwudke, D., Ernst, R.K., Dorey, S., Huckelhoven, R., Hofmann, T. and Ranf, S. (2019) Bacterial medium-chain 3-hydroxy fatty acid metabolites trigger immunity in Arabidopsis plants. *Science*, **364**, 178-181.

Lacombe, S., Rougon-Cardoso, A., Sherwood, E., Peeters, N., Dahlbeck, D., van Esse, H.P., Smoker, M., Rallapalli, G., Thomma, B.P., Staskawicz, B., Jones, J.D. and Zipfel, C. (2010) Interfamily transfer of a plant pattern-recognition receptor confers broad-spectrum bacterial resistance. *Nat Biotechnol*, **28**, 365-369.

Lamesch, P., Berardini, T.Z., Li, D., Swarbreck, D., Wilks, C., Sasidharan, R., Muller, R., Dreher, K., Alexander, D.L., Garcia-Hernandez, M., Karthikeyan, A.S., Lee, C.H., Nelson, W.D., Ploetz, L., Singh, S., Wensel, A. and Huala, E. (2012) The Arabidopsis Information Resource (TAIR): improved gene annotation and new tools. *Nucleic Acids Res*, **40**, D1202-1210.

Landeo Villanueva, S., Malvestiti, M.C., van Ieperen, W., Joosten, M. and van Kan, J.A.L. (2021) Red light imaging for programmed cell death visualization and quantification in plant-pathogen interactions. *Mol Plant Pathol*, **22**, 361-372.

Laohavisit, A., Wakatake, T., Ishihama, N., Mulvey, H., Takizawa, K., Suzuki, T. and Shirasu, K. (2020) Quinone perception in plants via leucine-rich-repeat receptor-like kinases. *Nature*, **587**, 92-97.

Li, B., Meng, X., Shan, L. and He, P. (2016) Transcriptional regulation of pattern-triggered immunity in plants. *Cell Host Microbe*, **19**, 641-650.

Li, P., Lu, Y.J., Chen, H. and Day, B. (2020) The lifecycle of the plant immune system. *CRC Crit Rev Plant Sci*, **39**, 72-100.

Li, P., Zhao, L., Qi, F., Htwe, N., Li, Q., Zhang, D., Lin, F., Shang-Guan, K. and Liang, Y. (2021) The receptor-like cytoplasmic kinase RIPK regulates broad-spectrum ROS signaling in multiple layers of plant immune system. *Mol Plant*, **14**, 1652-1667.

Lin, W., Tang, W., Pan, X., Huang, A., Gao, X., Anderson, C.T. and Yang, Z. (2022) Arabidopsis pavement cell morphogenesis requires FERONIA binding to pectin for activation of ROP GTPase signaling. *Curr Biol*, **32**, 497-507 e494.

Liu, S., Liu, Y., Yang, X., Tong, C., Edwards, D., Parkin, I.A., Zhao, M., Ma, J., Yu, J., Huang, S., Wang, X., Wang, J., Lu, K., Fang, Z., Bancroft, I., Yang, T.J., Hu, Q., Wang, X., Yue, Z., Li, H., Yang, L., Wu, J., Zhou, Q., Wang, W., King, G.J., Pires, J.C., Lu, C., Wu, Z., Sampath, P., Wang, Z., Guo, H., Pan, S., Yang, L., Min, J., Zhang, D., Jin, D., Li, W., Belcram, H., Tu, J., Guan, M., Qi, C., Du, D., Li, J., Jiang, L., Batley, J., Sharpe, A.G., Park, B.S., Ruperao, P., Cheng, F., Waminal, N.E., Huang, Y., Dong, C., Wang, L., Li, J., Hu, Z., Zhuang, M., Huang, Y., Huang, J., Shi, J., Mei, D., Liu, J., Lee, T.H., Wang, J., Jin, H., Li, Z., Li, X., Zhang, J., Xiao, L.,

Zhou, Y., Liu, Z., Liu, X., Qin, R., Tang, X., Liu, W., Wang, Y., Zhang, Y., Lee, J., Kim, H.H., Denoeud, F., Xu, X., Liang, X., Hua, W., Wang, X., Wang, J., Chalhoub, B. and Paterson, A.H. (2014) The *Brassica oleracea* genome reveals the asymmetrical evolution of polyploid genomes. *Nat Commun*, **5**, 3930.

Liu, S., Paknejad, N., Zhu, L., Kihara, Y., Ray, M., Chun, J., Liu, W., Hite, R.K. and Huang, X.Y. (2022) Differential activation mechanisms of lipid GPCRs by lysophosphatidic acid and sphingosine 1-phosphate. *Nat Commun*, **13**, 731.

Liu, T., Liu, Z., Song, C., Hu, Y., Han, Z., She, J., Fan, F., Wang, J., Jin, C., Chang, J., Zhou, J.M. and Chai, J. (2012) Chitin-induced dimerization activates a plant immune receptor. *Science*, **336**, 1160-1164.

Luo, X., Wu, W., Liang, Y., Xu, N., Wang, Z., Zou, H. and Liu, J. (2020) Tyrosine phosphorylation of the lectin receptor-like kinase LORE regulates plant immunity. *EMBO J*, **39**, e102856.

Ma, R., Han, Z., Hu, Z., Lin, G., Gong, X., Zhang, H., Nasrallah, J.B. and Chai, J. (2016) Structural basis for specific self-incompatibility response in *Brassica*. *Cell Res*, **26**, 1320-1329.

Ma, S., Lapin, D., Liu, L., Sun, Y., Song, W., Zhang, X., Logemann, E., Yu, D., Wang, J., Jirschitzka, J., Han, Z., Schulze-Lefert, P., Parker, J.E. and Chai, J. (2020) Direct pathogen-induced assembly of an NLR immune receptor complex to form a holoenzyme. *Science*, **370**, eabe3069.

Macho, A.P. and Zipfel, C. (2014) Plant PRRs and the activation of innate immune signaling. *Mol Cell*, **54**, 263-272.

Maguire, J.J., Kuc, R.E. and Davenport, A.P. (2012) Radioligand binding assays and their analysis. *Methods Mol Biol*, **897**, 31-77.

Mandal, M.K., Ahvari, H., Schillberg, S. and Schiermeyer, A. (2016) Tackling unwanted proteolysis in plant production hosts used for molecular farming. *Front Plant Sci*, **7**, 267.

Martin, R., Qi, T., Zhang, H., Liu, F., King, M., Toth, C., Nogales, E. and Staskawicz, B.J. (2020) Structure of the activated ROQ1 resistosome directly recognizing the pathogen effector XopQ. *Science*, **370**, eabd9993.

Mecchia, M.A., Santos-Fernandez, G., Duss, N.N., Somoza, S.C., Boisson-Dernier, A., Gagliardini, V., Martinez-Bernardini, A., Fabrice, T.N., Ringli, C., Muschietti, J.P. and Grossniklaus, U. (2017) RALF4/19 peptides interact with LRX proteins to control pollen tube growth in Arabidopsis. *Science*, **358**, 1600-1603.

Mesterházy, Á., Oláh, J. and Popp, J. (2020) Losses in the grain supply chain: Causes and solutions. *Sustainability*, **12**, 2342.

Minkoff, B.B., Makino, S.I., Haruta, M., Beebe, E.T., Wrobel, R.L., Fox, B.G. and Sussman, M.R. (2017) A cell-free method for expressing and reconstituting membrane proteins enables functional characterization of the plant receptor-like protein kinase FERONIA. *J Biol Chem*, **292**, 5932-5942.

Miya, A., Albert, P., Shinya, T., Desaki, Y., Ichimura, K., Shirasu, K., Narusaka, Y., Kawakami, N., Kaku, H. and Shibuya, N. (2007) CERK1, a LysM receptor kinase, is essential for chitin elicitor signaling in Arabidopsis. *Proc Natl Acad Sci U S A*, **104**, 19613-19618.

Mur, L.A., Kenton, P., Lloyd, A.J., Ougham, H. and Prats, E. (2008) The hypersensitive response; the centenary is upon us but how much do we know? *J Exp Bot*, **59**, 501-520.

Murail, S., de Vries, S.J., Rey, J., Moroy, G. and Tuffery, P. (2021) SeamDock: an interactive and collaborative online docking resource to assist small compound molecular docking. *Front Mol Biosci*, **8**, 716466.

Murase, K., Moriwaki, Y., Mori, T., Liu, X., Masaka, C., Takada, Y., Maesaki, R., Mishima, M., Fujii, S., Hirano, Y., Kawabe, Z., Nagata, K., Terada, T., Suzuki, G., Watanabe, M., Shimizu, K., Hakoshima, T. and Takayama, S. (2020) Mechanism of self/nonself-discrimination in *Brassica* self-incompatibility. *Nat Commun*, **11**, 4916.

Nagaya, S., Kawamura, K., Shinmyo, A. and Kato, K. (2010) The HSP terminator of *Arabidopsis thaliana* increases gene expression in plant cells. *Plant Cell Physiol*, **51**, 328-332.

Naithani, S., Chookajorn, T., Ripoll, D.R. and Nasrallah, J.B. (2007) Structural modules for receptor dimerization in the S-locus receptor kinase extracellular domain. *Proc Natl Acad Sci U S A*, **104**, 12211-12216.

Nasrallah, J., Kao, T.-H., Chen, C.-H., Goldberg, M. and Nasrallah, M. (1987) Amino-acid sequence of glycoproteins encoded by three alleles of the S locus of *Brassica oleracea*. *Nature*, **326**, 617-619.

Ngou, B.P.M., Ahn, H.K., Ding, P. and Jones, J.D.G. (2021) Mutual potentiation of plant immunity by cell-surface and intracellular receptors. *Nature*, **592**, 110-115.

Ngou, B.P.M., Heal, R., Wyler, M., Schmid, M.W. and Jones, J.D.G. (2022) Concerted expansion and contraction of immune receptor gene repertoires in plant genomes. *Nat Plants*, **8**, 1146-1152.

Nikolov, L.A., Shushkov, P., Nevado, B., Gan, X., Al-Shehbaz, I.A., Filatov, D., Bailey, C.D. and Tsiantis, M. (2019) Resolving the backbone of the Brassicaceae phylogeny for investigating trait diversity. *New Phytol*, **222**, 1638-1651.

Olaru, A., Bala, C., Jaffrezic-Renault, N. and Aboul-Enein, H.Y. (2015) Surface plasmon resonance (SPR) biosensors in pharmaceutical analysis. *Crit Rev Anal Chem*, **45**, 97-105.

Pan, J., Li, Z., Wang, Q., Yang, L., Yao, F. and Liu, W. (2020) An S-domain receptor-like kinase, OsESG1, regulates early crown root development and drought resistance in rice. *Plant Sci*, **290**, 110318.

Paritosh, K., Pradhan, A.K. and Pental, D. (2020) A highly contiguous genome assembly of *Brassica nigra* (BB) and revised nomenclature for the pseudochromosomes. *BMC Genom*, **21**, 887.

Petutschnig, E.K., Jones, A.M., Serazetdinova, L., Lipka, U. and Lipka, V. (2010) The lysin motif receptor-like kinase (LysM-RLK) CERK1 is a major chitin-binding protein in Arabidopsis thaliana and subject to chitin-induced phosphorylation. *J Biol Chem*, **285**, 28902-28911.

Pham, A.Q., Cho, S.H., Nguyen, C.T. and Stacey, G. (2020) Arabidopsis lectin receptor kinase P2K2 Is a second plant receptor for extracellular ATP and contributes to innate immunity. *Plant Physiol*, **183**, 1364-1375.

Pi, L., Yin, Z., Duan, W., Wang, N., Zhang, Y., Wang, J. and Dou, D. (2022) A G-type lectin receptor-like kinase regulates the perception of oomycete apoplastic expansin-like proteins. *J Integr Plant Biol*, **64**, 183-201.

Pieterse, C.M., Leon-Reyes, A., Van der Ent, S. and Van Wees, S.C. (2009) Networking by small-molecule hormones in plant immunity. *Nat Chem Biol*, **5**, 308-316.

Pieterse, C.M., Van der Does, D., Zamioudis, C., Leon-Reyes, A. and Van Wees, S.C. (2012) Hormonal modulation of plant immunity. *Annu Rev Cell Dev Biol*, **28**, 489-521.

Ranf, S. (2017) Sensing of molecular patterns through cell surface immune receptors. *Curr Opin Plant Biol*, **38**, 68-77.

Ranf, S., Gisch, N., Schaffer, M., Illig, T., Westphal, L., Knirel, Y.A., Sanchez-Carballo, P.M., Zahringer, U., Huckelhoven, R., Lee, J. and Scheel, D. (2015) A lectin S-domain

receptor kinase mediates lipopolysaccharide sensing in *Arabidopsis thaliana*. *Nat Immunol*, **16**, 426-433.

Reichler, S.A., Torres, J., Rivera, A.L., Cintolesi, V.A., Clark, G. and Roux, S.J. (2009) Intersection of two signalling pathways: extracellular nucleotides regulate pollen germination and pollen tube growth via nitric oxide. *J Exp Bot*, **60**, 2129-2138.

Rhodes, J., Yang, H., Moussu, S., Boutrot, F., Santiago, J. and Zipfel, C. (2021) Perception of a divergent family of phytocytokines by the Arabidopsis receptor kinase MIK2. *Nat Commun*, **12**, 705.

Robatzek, S., Bittel, P., Chinchilla, D., Kochner, P., Felix, G., Shiu, S.H. and Boller, T. (2007) Molecular identification and characterization of the tomato flagellin receptor LeFLS2, an orthologue of Arabidopsis FLS2 exhibiting characteristically different perception specificities. *Plant Mol Biol*, **64**, 539-547.

Robert, S., Khalf, M., Goulet, M.C., D'Aoust, M.A., Sainsbury, F. and Michaud, D. (2013) Protection of recombinant mammalian antibodies from development-dependent proteolysis in leaves of *Nicotiana benthamiana*. *PLoS One*, **8**, e70203.

Rosa, M.P., Manuel, G.A., Ricardo, L., Carmen, C., Benito, P., Begoña, G.S., Juan de Dios, A., Ana, O.A., Sandra, B. and Juan, Y.L.F. (2009) (2022) The tomato POD2 encodes a G-type lectin receptor kinase required for viable pollen grain formation. *J Exp Bot*, **74**, 178-193.

Rosenbaum, D.M., Rasmussen, S.G. and Kobilka, B.K. (2009) The structure and function of G-protein-coupled receptors. *Nature*, **459**, 356-363.

Rutter, B.D., Rutter, K.L. and Innes, R.W. (2017) Isolation and quantification of plant extracellular vesicles. *Bio Protoc*, **7**, e2533.

Rzemieniewski, J. and Stegmann, M. (2022) Regulation of pattern-triggered immunity and growth by phytocytokines. *Curr Opin Plant Biol*, **68**, 102230.

Samuel, M.A., Mudgil, Y., Salt, J.N., Delmas, F., Ramachandran, S., Chilelli, A. and Goring, D.R. (2008) Interactions between the S-domain receptor kinases and AtPUB-ARM E3 ubiquitin ligases suggest a conserved signaling pathway in Arabidopsis. *Plant Physiol*, **147**, 2084-2095.

Sanabria, N., Goring, D., Nurnberger, T. and Dubery, I. (2008) Self/nonself perception and recognition mechanisms in plants: a comparison of self-incompatibility and innate immunity. *New Phytol*, **178**, 503-514.

Sandoval, P.J. and Santiago, J. (2020) *In vitro* analytical approaches to study plant ligand-receptor interactions. *Plant Physiol*, **182**, 1697-1712.

Schäffer, M. (2019) Regulation of the cell surface receptor kinase LORE in the *Pseudomonas syringae-Arabidopsis thaliana* interaction. *TUM Dissertation*.

Schellenberger, R., Crouzet, J., Nickzad, A., Shu, L.-J., Kutschera, A., Gerster, T., Borie, N., Dawid, C., Cloutier, M., Villaume, S., Dhondt-Cordelier, S., Hubert, J., Cordelier, S., Mazeyrat-Gourbeyre, F., Schmid, C., Ongena, M., Renault, J.H., Haudrechy, A., Hofmann, T., Baillieul, F., Clément, C., Zipfel, C., Gauthier, C., Déziel, E., Ranf, S. and Dorey, S. (2021) Bacterial rhamnolipids and their 3-hydroxyalkanoate precursors activate Arabidopsis innate immunity through two independent mechanisms. *Proc Natl Acad Sci U S A*, **118**.

Schillberg, S., Raven, N., Spiegel, H., Rasche, S. and Buntru, M. (2019) Critical analysis of the commercial potential of plants for the production of recombinant proteins. *Front Plant Sci*, **10**, 720.

Schoonbeek, H.J., Wang, H.H., Stefanato, F.L., Craze, M., Bowden, S., Wallington, E., Zipfel, C. and Ridout, C.J. (2015) Arabidopsis EF-Tu receptor enhances bacterial disease resistance in transgenic wheat. *New Phytol*, **206**, 606-613.

Schranz, M.E. and Mitchell-Olds, T. (2006) Independent ancient polyploidy events in the sister families Brassicaceae and Cleomaceae. *Plant Cell*, **18**, 1152-1165.

Schwessinger, B., Bahar, O., Thomas, N., Holton, N., Nekrasov, V., Ruan, D., Canlas, P.E., Daudi, A., Petzold, C.J., Singan, V.R., Kuo, R., Chovatia, M., Daum, C., Heazlewood, J.L., Zipfel, C. and Ronald, P.C. (2015) Transgenic expression of the dicotyledonous pattern recognition receptor EFR in rice leads to ligand-dependent activation of defense responses. *PLoS Pathog*, **11**, e1004809.

Seren, Ü. (2018) GWA-Portal: Genome-wide association studies made easy. *Methods Mol Biol*, **1761**, 303-319.

Shi, X. and Jarvis, D.L. (2007) Protein N-glycosylation in the baculovirus-insect cell system. *Curr Drug Targets*, **8**, 1116-1125.

Shimada, T.L., Shimada, T. and Hara-Nishimura, I. (2010) A rapid and non-destructive screenable marker, FAST, for identifying transformed seeds of *Arabidopsis thaliana*. *Plant J*, **61**, 519-528.

Shimosato, H., Yokota, N., Shiba, H., Iwano, M., Entani, T., Che, F.S., Watanabe, M., Isogai, A. and Takayama, S. (2007) Characterization of the SP11/SCR high-affinity binding site involved in self/nonself recognition in *Brassica* self-incompatibility. *Plant Cell*, **19**, 107-117.

Shiu, S.H. and Bleecker, A.B. (2001) Plant receptor-like kinase gene family: diversity, function, and signaling. *Sci STKE*, **2001**, re22.

Shiu, S.H. and Bleecker, A.B. (2003) Expansion of the receptor-like kinase/Pelle gene family and receptor-like proteins in Arabidopsis. *Plant Physiol*, **132**, 530-543.

Shiu, S.H., Karlowski, W.M., Pan, R., Tzeng, Y.H., Mayer, K.F. and Li, W.H. (2004) Comparative analysis of the receptor-like kinase family in Arabidopsis and rice. *Plant Cell*, **16**, 1220-1234.

Shu, L.-J., Schäffer, M., Eschrig, S. and Ranf, S. (2021) Low cost, medium throughput depletion-binding assay for screening S-domain-receptor ligand interactions using in planta protein expression. *bioRxiv*.

Silverman, A.D., Karim, A.S. and Jewett, M.C. (2020) Cell-free gene expression: an expanded repertoire of applications. *Nat Rev Genet*, **21**, 151-170.

Siukstaite, L., Imberty, A. and Romer, W. (2021) Structural diversities of lectins binding to the glycosphingolipid Gb3. *Front Mol Biosci*, **8**, 704685.

Slotte, T., Hazzouri, K.M., Ågren, J.A., Koenig, D., Maumus, F., Guo, Y.L., Steige, K., Platts, A.E., Escobar, J.S., Newman, L.K., Wang, W., Mandáková, T., Vello, E., Smith, L.M., Henz, S.R., Steffen, J., Takuno, S., Brandvain, Y., Coop, G., Andolfatto, P., Hu, T.T., Blanchette, M., Clark, R.M., Quesneville, H., Nordborg, M., Gaut, B.S., Lysak, M.A., Jenkins, J., Grimwood, J., Chapman, J., Prochnik, S., Shu, S., Rokhsar, D., Schmutz, J., Weigel, D. and Wright, S.I. (2013) The *Capsella rubella* genome and the genomic consequences of rapid mating system evolution. *Nat Genet*, **45**, 831-835.

Smakowska-Luzan, E., Mott, G.A., Parys, K., Stegmann, M., Howton, T.C., Layeghifard, M., Neuhold, J., Lehner, A., Kong, J., Grünwald, K., Weinberger, N., Satbhai, S.B., Mayer, D., Busch, W., Madalinski, M., Stolt-Bergner, P., Provart, N.J., Mukhtar, M.S., Zipfel, C., Desveaux, D., Guttman, D.S. and Belkhadir, Y. (2018) An extracellular network of Arabidopsis leucine-rich repeat receptor kinases. *Nature*, **553**, 342-346.

Snoeck, S., Abramson, B.W., Garcia, A.G.K., Egan, A.N., Michael, T.P. and Steinbrenner, A.D. (2022a) Evolutionary gain and loss of a plant pattern-recognition receptor for HAMP recognition. *Elife*, **11**, e81050.

Snoeck, S., Guayazan-Palacios, N. and Steinbrenner, A.D. (2022b) Molecular tug-of-war: Plant immune recognition of herbivory. *Plant Cell*, **34**, 1497-1513.

Somerville, C. and Koornneef, M. (2002) A fortunate choice: the history of Arabidopsis as a model plant. *Nat Rev Genet*, **3**, 883-889.

Song, C.J., Steinebrunner, I., Wang, X., Stout, S.C. and Roux, S.J. (2006) Extracellular ATP induces the accumulation of superoxide via NADPH oxidases in Arabidopsis. *Plant Physiol*, **140**, 1222-1232.

Sørensen, H.P. and Mortensen, K.K. (2005) Soluble expression of recombinant proteins in the cytoplasm of *Escherichia coli*. *Microb Cell Fact*, **4**, 1.

Spoel, S.H. and Dong, X. (2012) How do plants achieve immunity? Defence without specialized immune cells. *Nat Rev Immunol*, **12**, 89-100.

Stegmann, M., Monaghan, J., Smakowska-Luzan, E., Rovenich, H., Lehner, A., Holton, N., Belkhadir, Y. and Zipfel, C. (2017) The receptor kinase FER is a RALF-regulated scaffold controlling plant immune signaling. *Science*, **355**, 287-289.

Stein, J.C., Howlett, B., Boyes, D.C., Nasrallah, M.E. and Nasrallah, J.B. (1991) Molecular cloning of a putative receptor protein kinase gene encoded at the self-incompatibility locus of *Brassica oleracea*. *Proc Natl Acad Sci U S A*, **88**, 8816-8820.

Steinbrenner, A.D., Munoz-Amatriain, M., Chaparro, A.F., Aguilar-Venegas, J.M., Lo, S., Okuda, S., Glauser, G., Dongiovanni, J., Shi, D., Hall, M., Crubaugh, D., Holton, N., Zipfel, C., Abagyan, R., Turlings, T.C.J., Close, T.J., Huffaker, A. and Schmelz, E.A. (2020) A receptor-like protein mediates plant immune responses to herbivore-associated molecular patterns. *Proc Natl Acad Sci U S A*, **117**, 31510-31518.

Stone, S.L., Anderson, E.M., Mullen, R.T. and Goring, D.R. (2003) ARC1 is an E3 ubiquitin ligase and promotes the ubiquitination of proteins during the rejection of self-incompatible *Brassica* pollen. *Plant Cell*, **15**, 885-898.

Sun, M., Qian, X., Chen, C., Cheng, S., Jia, B., Zhu, Y. and Sun, X. (2018) Ectopic expression of GsSRK in *Medicago sativa* reveals its involvement in plant architecture and salt stress responses. *Front Plant Sci*, **9**, 226.

Sun, X.L., Yu, Q.Y., Tang, L.L., Ji, W., Bai, X., Cai, H., Liu, X.F., Ding, X.D. and Zhu, Y.M. (2013a) GsSRK, a G-type lectin S-receptor-like serine/threonine protein kinase, is a positive regulator of plant tolerance to salt stress. *J Plant Physiol*, **170**, 505-515.

Sun, Y., Li, L., Macho, A.P., Han, Z., Hu, Z., Zipfel, C., Zhou, J.M. and Chai, J. (2013b) Structural basis for flg22-induced activation of the Arabidopsis FLS2-BAK1 immune complex. *Science*, **342**, 624-628.

Sun, Y., Qiao, Z., Muchero, W. and Chen, J.G. (2020) Lectin receptor-like kinases: The sensor and mediator at the plant cell surface. *Front Plant Sci*, **11**, 596301.

Takai, R., Isogai, A., Takayama, S. and Che, F.S. (2008) Analysis of flagellin perception mediated by flg22 receptor OsFLS2 in rice. *Mol Plant Microbe Interact*, **21**, 1635-1642.

Takayama, S. and Isogai, A. (2005) Self-incompatibility in plants. *Annu Rev Plant Biol*, **56**, 467-489.

Tamura, K., Stecher, G. and Kumar, S. (2021) MEGA11: Molecular Evolutionary Genetics Analysis Version 11. *Mol Biol Evol*, **38**, 3022-3027.

Tanaka, K., Gilroy, S., Jones, A.M. and Stacey, G. (2010) Extracellular ATP signaling in plants. *Trends Cell Biol*, **20**, 601-608.

Tang, J., Han, Z., Sun, Y., Zhang, H., Gong, X. and Chai, J. (2015) Structural basis for recognition of an endogenous peptide by the plant receptor kinase PEPR1. *Cell Res*, **25**, 110-120.

Teixeira, M.A., Rajewski, A., He, J., Castaneda, O.G., Litt, A. and Kaloshian, I. (2018) Classification and phylogenetic analyses of the Arabidopsis and tomato G-type lectin receptor kinases. *BMC Genomics*, **19**, 239.

Tordai, H., Bányai, L. and Patthy, L. (1999) The PAN module: the N-terminal domains of plasminogen and hepatocyte growth factor are homologous with the apple domains of the prekallikrein family and with a novel domain found in numerous nematode proteins. *FEBS Lett*, **461**, 63-67.

Trdá, L., Fernandez, O., Boutrot, F., Héloir, M.C., Kelloniemi, J., Daire, X., Adrian, M., Clément, C., Zipfel, C., Dorey, S. and Poinssot, B. (2014) The grapevine flagellin receptor VvFLS2 differentially recognizes flagellin-derived epitopes from the endophytic growth-promoting bacterium *Burkholderia phytofirmans* and plant pathogenic bacteria. *New Phytol*, **201**, 1371-1384.

Trempel, F., Kajiura, H., Ranf, S., Grimmer, J., Westphal, L., Zipfel, C., Scheel, D., Fujiyama, K. and Lee, J. (2016) Altered glycosylation of exported proteins, including surface immune receptors, compromises calcium and downstream signaling responses to microbe-associated molecular patterns in *Arabidopsis thaliana*. *BMC Plant Biol*, **16**, 31.

Tsuda, K. and Katagiri, F. (2010) Comparing signaling mechanisms engaged in pattern-triggered and effector-triggered immunity. *Curr Opin Plant Biol*, **13**, 459-465.

Ursache, R., Fujita, S., Denervaud Tendon, V. and Geldner, N. (2021) Combined fluorescent seed selection and multiplex CRISPR/Cas9 assembly for fast generation of multiple Arabidopsis mutants. *Plant Methods*, **17**, 111.

Vaid, N., Pandey, P.K. and Tuteja, N. (2012) Genome-wide analysis of lectin receptor-like kinase family from Arabidopsis and rice. *Plant Mol Biol*, **80**, 365-388.

van Oers, M.M., Pijlman, G.P. and Vlak, J.M. (2015) Thirty years of baculovirus-insect cell protein expression: from dark horse to mainstream technology. *J Gen Virol*, **96**, 6-23.

Varden, F.A., De la Concepcion, J.C., Maidment, J.H. and Banfield, M.J. (2017) Taking the stage: effectors in the spotlight. *Curr Opin Plant Biol*, **38**, 25-33.

Vauquelin, G., Van Liefde, I. and Swinney, D.C. (2015) Radioligand binding to intact cells as a tool for extended drug screening in a representative physiological context. *Drug Discov Today Technol*, **17**, 28-34.

Vlot, A.C., Sales, J.H., Lenk, M., Bauer, K., Brambilla, A., Sommer, A., Chen, Y., Wenig, M. and Nayem, S. (2021) Systemic propagation of immunity in plants. *New Phytol*, **229**, 1234-1250.

Walden, N., German, D.A., Wolf, E.M., Kiefer, M., Rigault, P., Huang, X.C., Kiefer, C., Schmickl, R., Franzke, A., Neuffer, B., Mummenhoff, K. and Koch, M.A. (2020a) Nested whole-genome duplications coincide with diversification and high morphological disparity in Brassicaceae. *Nat Commun*, **11**, 3795.

Walden, N., Nguyen, T.P., Mandáková, T., Lysak, M.A. and Schranz, M.E. (2020b) Genomic blocks in *Aethionema arabicum* support arabideae as next diverging clade in Brassicaceae. *Front Plant Sci*, **11**, 719.

Walker, J.C. and Zhang, R. (1990) Relationship of a putative receptor protein kinase from maize to the S-locus glycoproteins of *Brassica*. *Nature*, **345**, 743-746.

Wan, J., Tanaka, K., Zhang, X.C., Son, G.H., Brechenmacher, L., Nguyen, T.H. and Stacey, G. (2012) LYK4, a lysin motif receptor-like kinase, is important for chitin signaling and plant innate immunity in Arabidopsis. *Plant Physiol*, **160**, 396-406.

Wang, C., Huang, X., Li, Q., Zhang, Y., Li, J.L. and Mou, Z. (2019) Extracellular pyridine nucleotides trigger plant systemic immunity through a lectin receptor kinase/BAK1 complex. *Nat Commun*, **10**, 4810.

Wang, C., Zhou, M., Zhang, X., Yao, J., Zhang, Y. and Mou, Z. (2017) A lectin receptor kinase as a potential sensor for extracellular nicotinamide adenine dinucleotide in *Arabidopsis thaliana*. *Elife*, **6**.

Wang, J., Li, H., Han, Z., Zhang, H., Wang, T., Lin, G., Chang, J., Yang, W. and Chai, J. (2015) Allosteric receptor activation by the plant peptide hormone phytosulfokine. *Nature*, **525**, 265-268.

Wang, J., Xi, L., Wu, X.N., König, S., Rohr, L., Neumann, T., Weber, J., Harter, K. and Schulze, W.X. (2022) PEP7 acts as a peptide ligand for the receptor kinase SIRK1 to regulate aquaporin-mediated water influx and lateral root growth. *Mol Plant*, **15**, 1615-1631.

Wang, Z.Y., Seto, H., Fujioka, S., Yoshida, S. and Chory, J. (2001) BRI1 is a critical component of a plasma-membrane receptor for plant steroids. *Nature*, **410**, 380-383.

Waterhouse, A., Bertoni, M., Bienert, S., Studer, G., Tauriello, G., Gumienny, R., Heer, F.T., de Beer, T.A.P., Rempfer, C., Bordoli, L., Lepore, R. and Schwede, T. (2018) SWISS-MODEL: homology modelling of protein structures and complexes. *Nucleic Acids Res*, **46**, W296-W303.

Wei, Y., Balaceanu, A., Rufian, J.S., Segonzac, C., Zhao, A., Morcillo, R.J.L. and Macho, A.P. (2020) An immune receptor complex evolved in soybean to perceive a polymorphic bacterial flagellin. *Nat Commun*, **11**, 3763.

Willmann, R., Lajunen, H.M., Erbs, G., Newman, M.A., Kolb, D., Tsuda, K., Katagiri, F., Fliegmann, J., Bono, J.J., Cullimore, J.V., Jehle, A.K., Gotz, F., Kulik, A., Molinaro, A., Lipka, V., Gust, A.A. and Nurnberger, T. (2011) Arabidopsis lysin-motif proteins LYM1 LYM3 CERK1 mediate bacterial peptidoglycan sensing and immunity to bacterial infection. *Proc Natl Acad Sci U S A*, **108**, 19824-19829.

Winkelmüller, T.M., Entila, F., Anver, S., Piasecka, A., Song, B., Dahms, E., Sakakibara, H., Gan, X., Kułak, K., Sawikowska, A., Krajewski, P., Tsiantis, M., Garrido-Oter, R., Fukushima, K., Schulze-Lefert, P., Laurent, S., Bednarek, P. and Tsuda, K. (2021) Gene expression evolution in pattern-triggered immunity within *Arabidopsis thaliana* and across Brassicaceae species. *Plant Cell*, **33**, 1863-1887.

Wouters, M.A., Rigoutsos, I., Chu, C.K., Feng, L.L., Sparrow, D.B. and Dunwoodie, S.L. (2005) Evolution of distinct EGF domains with specific functions. *Protein Sci*, **14**, 1091-1103.

Wu, B., Li, P., Hong, X., Xu, C., Wang, R. and Liang, Y. (2022) The receptor-like cytosolic kinase RIPK activates NADP-malic enzyme 2 to generate NADPH for fueling ROS production. *Mol Plant*, **15**, 887-903.

Wu, F., Chi, Y., Jiang, Z., Xu, Y., Xie, L., Huang, F., Wan, D., Ni, J., Yuan, F., Wu, X., Zhang, Y., Wang, L., Ye, R., Byeon, B., Wang, W., Zhang, S., Sima, M., Chen, S., Zhu, M., Pei, J., Johnson, D.M., Zhu, S., Cao, X., Pei, C., Zai, Z., Liu, Y., Liu, T., Swift, G.B., Zhang, W., Yu, M., Hu, Z., Siedow, J.N., Chen, X. and Pei, Z.M. (2020) Hydrogen peroxide sensor HPCA1 is an LRR receptor kinase in Arabidopsis. *Nature*, **578**, 577-581.

Xia, L., de Vries, H., IJzerman, A.P. and Heitman, L.H. (2016) Scintillation proximity assay (SPA) as a new approach to determine a ligand's kinetic profile. A case in point for the adenosine A1 receptor. *Purinergic Signal*, **12**, 115-126.

Xiao, Y., Stegmann, M., Han, Z., DeFalco, T.A., Parys, K., Xu, L., Belkhadir, Y., Zipfel, C. and Chai, J. (2019) Mechanisms of RALF peptide perception by a heterotypic receptor complex. *Nature*, **572**, 270-274.

Xing, S., Li, M. and Liu, P. (2013) Evolution of S-domain receptor-like kinases in land plants and origination of S-locus receptor kinases in Brassicaceae. *BMC Evol Biol*, **13**, 69.

Xu, P., Huang, S., Guo, S., Yun, Y., Cheng, X., He, X., Cai, P., Lan, Y., Zhou, H., Jiang, H., Jiang, Y., Xie, X. and Xu, H.E. (2022) Structural identification of lysophosphatidylcholines as activating ligands for orphan receptor GPR119. *Nat Struct Mol Biol*, **29**, 863-870.

Xue, D.X., Li, C.L., Xie, Z.P. and Staehelin, C. (2019) LYK4 is a component of a tripartite chitin receptor complex in *Arabidopsis thaliana*. *J Exp Bot*, **70**, 5507-5516.

Yamaguchi, Y., Huffaker, A., Bryan, A.C., Tax, F.E. and Ryan, C.A. (2010) PEPR2 is a second receptor for the Pep1 and Pep2 peptides and contributes to defense responses in Arabidopsis. *Plant Cell*, **22**, 508-522.

Yamaguchi, Y., Pearce, G. and Ryan, C.A. (2006) The cell surface leucine-rich repeat receptor for AtPep1, an endogenous peptide elicitor in Arabidopsis, is functional in transgenic tobacco cells. *Proc Natl Acad Sci U S A*, **103**, 10104-10109.

Yang, C., Liu, R., Pang, J., Ren, B., Zhou, H., Wang, G., Wang, E. and Liu, J. (2021) Poaceae-specific cell wall-derived oligosaccharides activate plant immunity via OsCERK1 during *Magnaporthe oryzae* infection in rice. *Nat Commun*, **12**, 2178.

Yang, R., Jarvis, D.E., Chen, H., Beilstein, M.A., Grimwood, J., Jenkins, J., Shu, S., Prochnik, S., Xin, M., Ma, C., Schmutz, J., Wing, R.A., Mitchell-Olds, T., Schumaker, K.S. and Wang, X. (2013) The reference genome of the halophytic plant *Eutrema salsugineum*. *Front Plant Sci*, **4**, 46.

Yuan, M., Jiang, Z., Bi, G., Nomura, K., Liu, M., Wang, Y., Cai, B., Zhou, J.M., He, S.Y. and Xin, X.F. (2021) Pattern-recognition receptors are required for NLR-mediated plant immunity. *Nature*, **592**, 105-109.

Zhang, L., Hua, C., Pruitt, R.N., Qin, S., Wang, L., Albert, I., Albert, M., van Kan, J.A.L. and Nurnberger, T. (2021) Distinct immune sensor systems for fungal endopolygalacturonases in closely related Brassicaceae. *Nat Plants*, **7**, 1254-1263.

Zhang, L., Kars, I., Essenstam, B., Liebrand, T.W., Wagemakers, L., Elberse, J., Tagkalaki, P., Tjoitang, D., van den Ackerveken, G. and van Kan, J.A. (2014) Fungal endopolygalacturonases are recognized as microbe-associated molecular patterns by the arabidopsis receptor-like protein RESPONSIVENESS TO BOTRYTIS POLYGALACTURONASES1. *Plant Physiol*, **164**, 352-364.

Zhang, W., Fraiture, M., Kolb, D., Loffelhardt, B., Desaki, Y., Boutrot, F.F., Tor, M., Zipfel, C., Gust, A.A. and Brunner, F. (2013) Arabidopsis receptor-like protein30 and receptor-like kinase suppressor of BIR1-1/EVERSHED mediate innate immunity to necrotrophic fungi. *Plant Cell*, **25**, 4227-4241.

Zhang, X., Henriques, R., Lin, S.S., Niu, Q.W. and Chua, N.H. (2006) *Agrobacterium*-mediated transformation of *Arabidopsis thaliana* using the floral dip method. *Nat Protoc*, **1**, 641-646.

Zhang, X. and Mou, Z. (2009) Extracellular pyridine nucleotides induce PR gene expression and disease resistance in Arabidopsis. *Plant J*, **57**, 302-312.

Zhao, J., Gao, Y., Zhang, Z., Chen, T., Guo, W. and Zhang, T. (2013) A receptor-like kinase gene (GbRLK) from *Gossypium barbadense* enhances salinity and drought-stress tolerance in Arabidopsis. *BMC Plant Biol*, **13**, 110.

Zhou, F., Emonet, A., Denervaud Tendon, V., Marhavy, P., Wu, D., Lahaye, T. and Geldner, N. (2020) Co-incidence of damage and microbial patterns controls localized immune responses in roots. *Cell*, **180**, 440-453 e418.

Zhou, H., Casas-Finet, J.R., Heath Coats, R., Kaufman, J.D., Stahl, S.J., Wingfield, P.T., Rubin, J.S., Bottaro, D.P. and Byrd, R.A. (1999) Identification and dynamics of a heparin-binding site in hepatocyte growth factor. *Biochemistry*, **38**, 14793-14802.

Zipfel, C. (2014) Plant pattern-recognition receptors. *Trends Immunol*, **35**, 345-351.

Zipfel, C., Kunze, G., Chinchilla, D., Caniard, A., Jones, J.D., Boller, T. and Felix, G. (2006) Perception of the bacterial PAMP EF-Tu by the receptor EFR restricts *Agrobacterium*-mediated transformation. *Cell*, **125**, 749-760.

Zou, X., Qin, Z., Zhang, C., Liu, B., Liu, J., Zhang, C., Lin, C., Li, H. and Zhao, T. (2015) Over-expression of an S-domain receptor-like kinase extracellular domain improves panicle architecture and grain yield in rice. *J Exp Bot*, **66**, 7197-7209.

6 Appendix

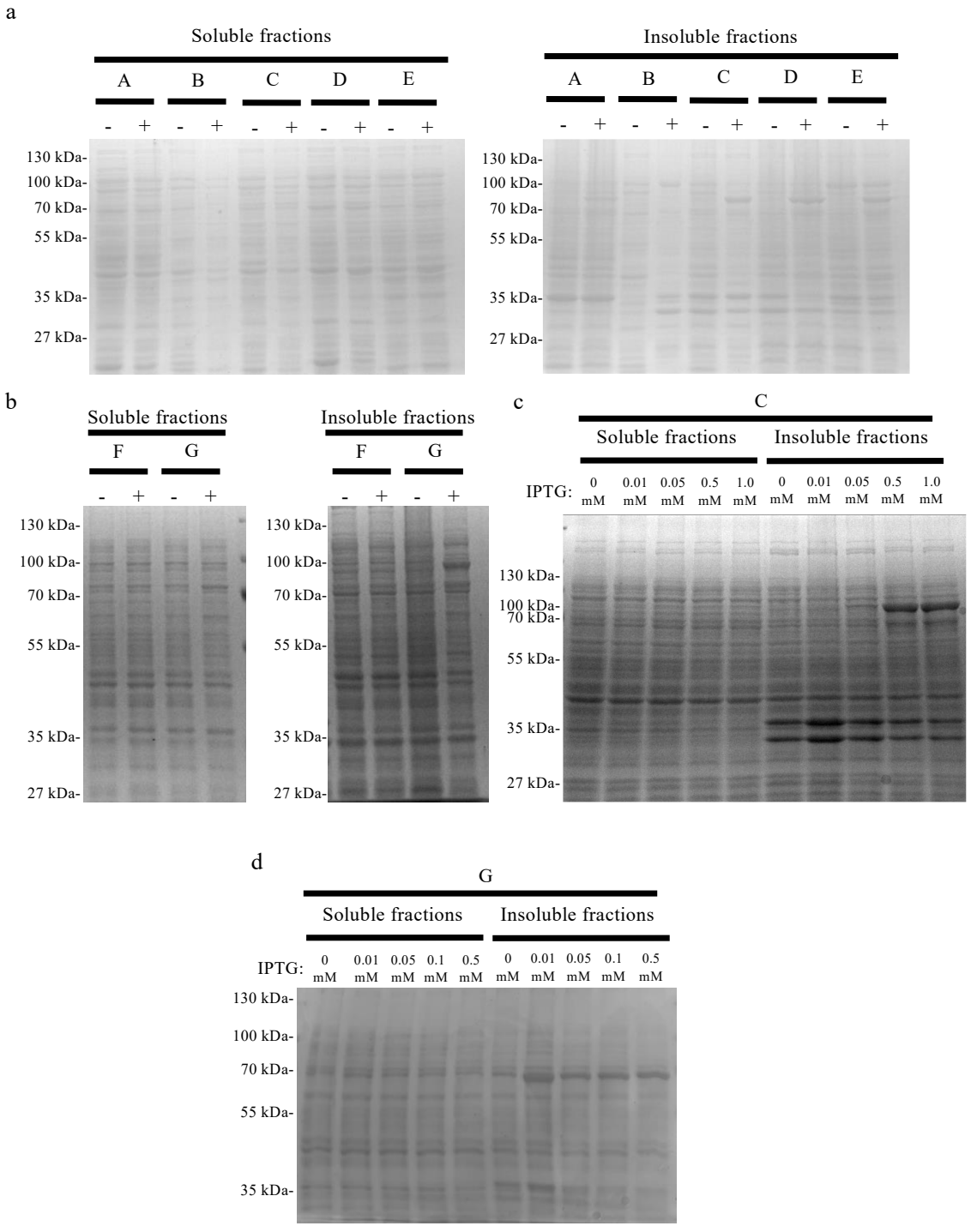

Supplementary Figure 1. Insoluble AtLORE ECD recombinant protein expressed in different *E. coli* strains. **a,b** SDS-PAGE analysis by Coomassie Brilliant Blue staining of AtLORE ECD (eAtLORE)-maltose-binding protein (MBP) fusion protein expression in different E. coli strains, A: Rosetta 2, B: Rosetta-gami 2, C: Rosetta-gami B, D:

Rosetta Blue, E: Origami 2, F: SHuffle T7 Express, G: SHuffle T7 Express LysY. Symbols "+" and "-" indicate whether the *E. coli* strains carried expression vector or not. The soluble and insoluble fractions from IPTG-induced *E. coli* lysates were prepared as labeled and described. The *E. coli* strains were induced by 0.25 mM IPTG at 28°C, for 3 hours. The predicted molecular weight of eAtLORE-MBP is 89.6 kDa. **c**. SDS-PAGE analysis by Coomassie Brilliant Blue staining of AtLORE ectodomain (eAtLORE)-maltose-binding protein (MBP) fusion protein expression in E. coli strain Rosetta-gami B with different inducing conditions. The soluble and insoluble fractions from IPTG with different concentrations induced *E. coli* lysates were prepared as labeled and described. The *E. coli* was induced by IPTG at 16°C, for 18 hours. The predicted molecular weight of eAtLORE-MBP is 89.6 kDa. **d.** SDS-PAGE analysis by Coomassie Brilliant Blue staining of eAtLORE lectin-like domain 1 and lectin-like domain 2-MBP fusion protein expression in SHuffle T7 Express LysY. The soluble and insoluble fractions from IPTG with different concentrations induced *E. coli* lysates were prepared as labeled and described. The *E. coli* strain was induced by IPTG at 16°C, for 18 hours. The predicted molecular weight of eAtLORE lectin-like domain 1 and lectin-like domain 2-MBP is 73 kDa.

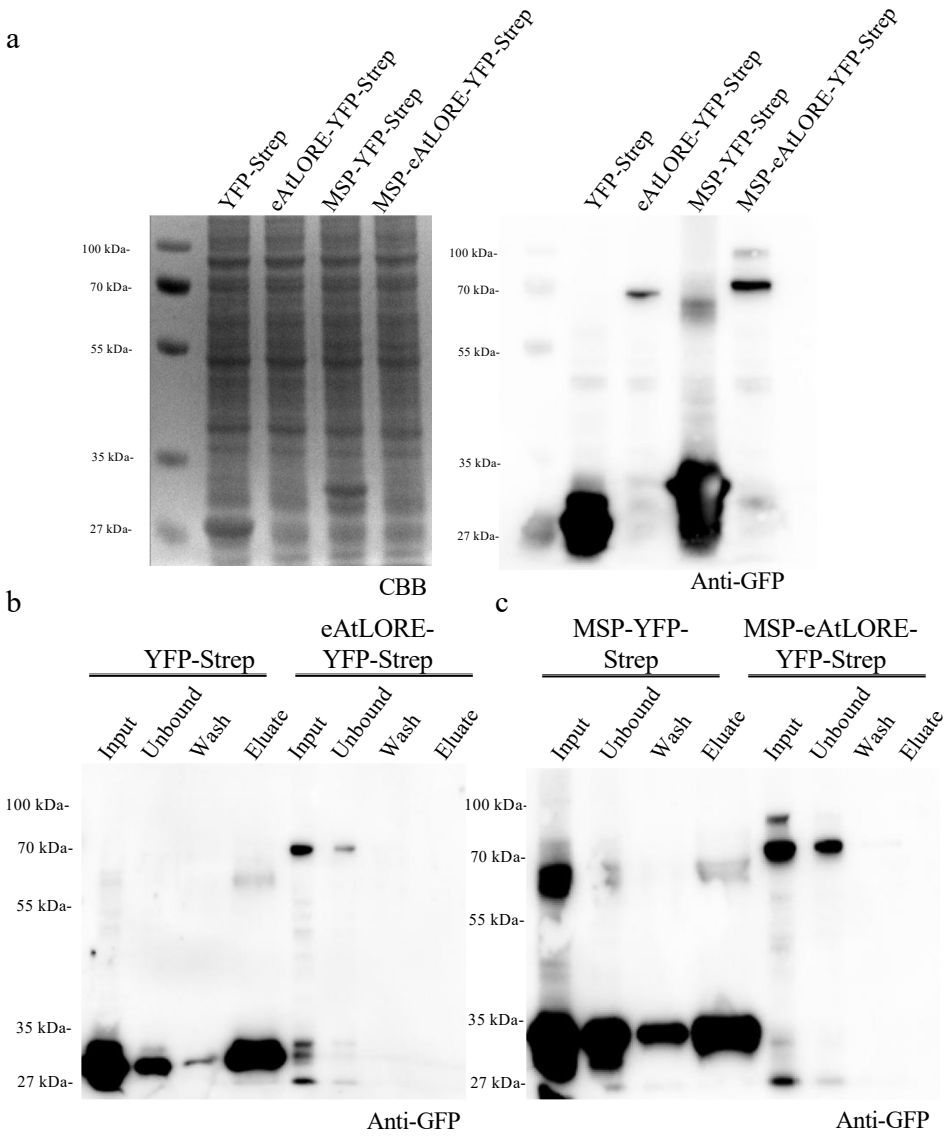

Supplementary Figure 2. Cell-free protein expression system for expressing AtLORE ECD (eAtLORE) and purification. a. Anti-GFP immunoblot of ALiCE cell-free protein expression system expressing eAtLORE-YFP-Strep fusion proteins and YFP-Strep proteins. MSP: melittin signal peptide. 0.5 μL cell lysate from 50 μL was loaded. The calculated molecular weights of eAtLORE-YFP-Strep and -MSP-eAtLORE-YFP-Strep fusions and YFP-Strep are 70-75 kDa and 26.7 kDa, respectively. The loading of the samples was confirmed by Coomassie Brilliant Blue (CBB) staining of the SDS-PA gel before blotting. Triangles in red indicate AtLORE-YFP-Strep. **b, c.** Anti-GFP immunoblot of Strep-Tag purification of ALiCE expressing eAtLORE-YFP-Strep fusion proteins and YFP-Strep proteins. 5 μL cell lysate was diluted to 100 μL and subjected to be purified. Expressed proteins with or without MSP were in two independent blots. Lane Input: cell lysate before subjecting into the column. Lane Unbound: column flow-through (100 μL). Lane Wash: the column was washed with four times of wash buffer, and the first wash fraction was collected (400 μL in total). Lane Eluate: elution fraction having the purified proteins (100 μL). 10 μL of all fractions were loaded.

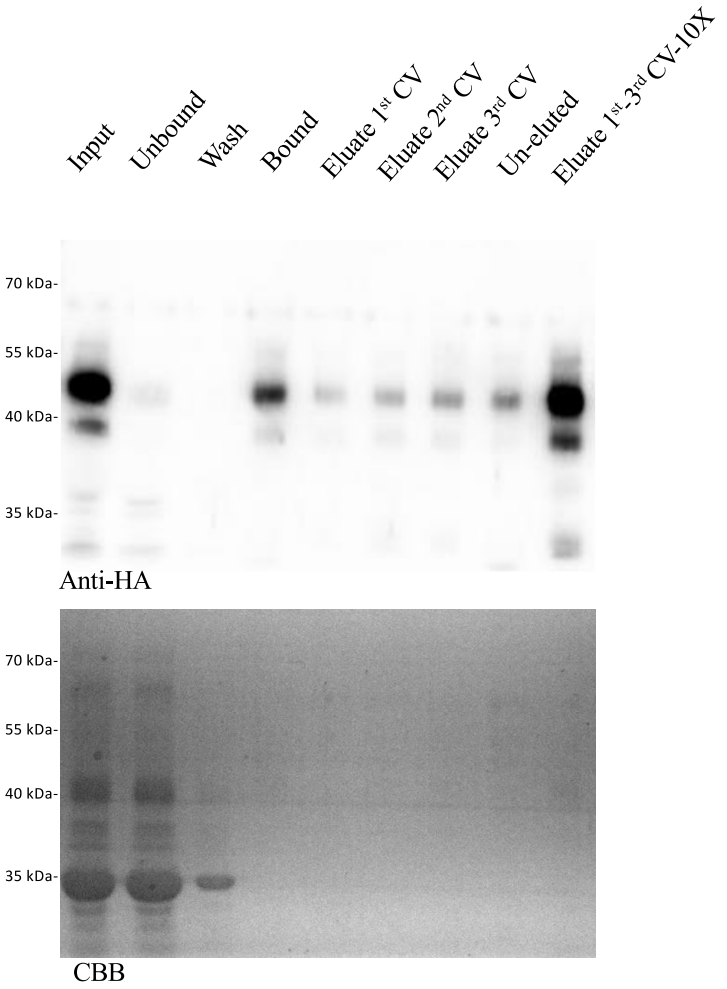

Supplementary Figure 3. **Purification of AtLORE ECD with HA-tag.** The AtLORE ectodomain (eAtLORE) fused at its N terminus with HA tag was expressed by *Nicotiana benthamiana* in the apoplast of leaves by *Agrobacterium*-mediated transient expression. The eAtLORE was purified by using 120µL (1 CV) of Pierce Anti-HA Agarose (Thermo, USA) resin from 400 µL of concentrated AWF with high protein concentration (1.5 mg/mL). Anti-HA immunoblot analysis of the protein purification. The calculated molecular weight of the protein is 55-60 kDa. Lane Input: apoplast washing fluid (10 µL; 400 µL in total) before subjecting into the cartridge. Lane Unbound: column flow-through (10 µl; 400 µL in total). Lane Wash: the agarose was washed with wash buffer (10 µL; 480 µL in total). Lane Eluate 1st CV to 3rd CV: elution fractions having the purified eAtLORE (10 µL each lane; 200 µL each fraction in total). Lane Un-eluted: the remaining proteins on agarose with anti-HA (10 µL; 200 µL each fraction in total). Lane Eluate 1st -3rd CV-10X: concentrated: pooled elution fractions were concentrated from 550 µL to 55 µL by concentrator (30 kDa cut-off) (10 μL, 55µL in total). The loading of the samples was confirmed by Coomassie Brilliant Blue (CBB) staining of the SDS-PA gel before blotting.

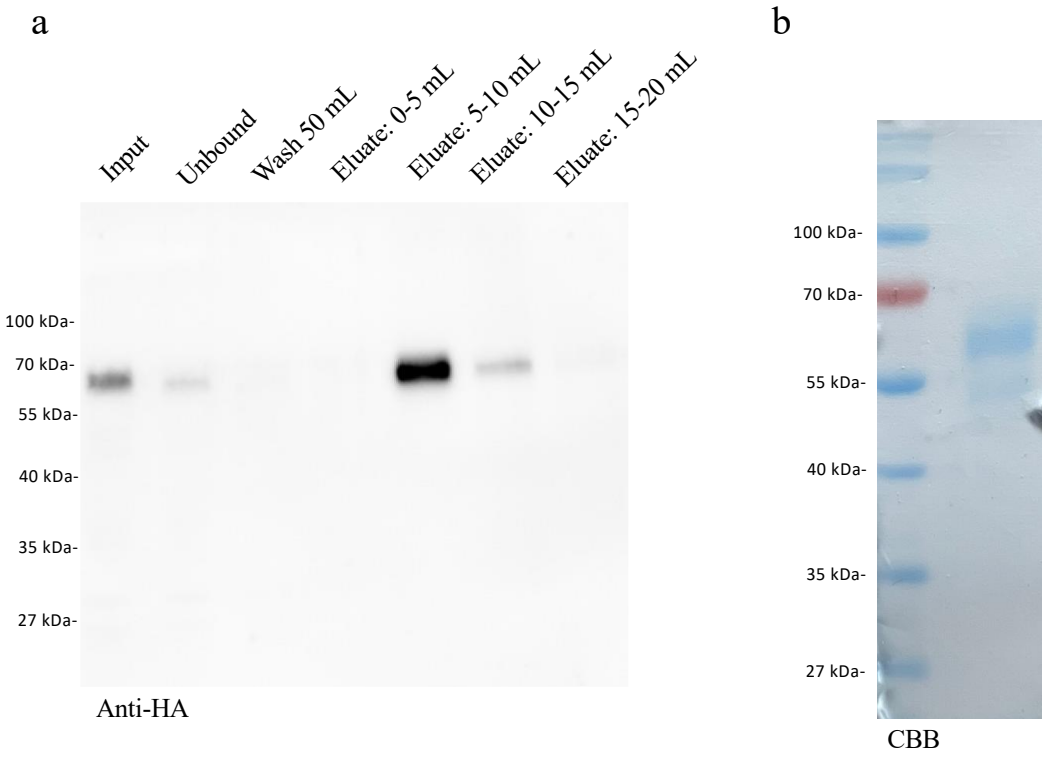

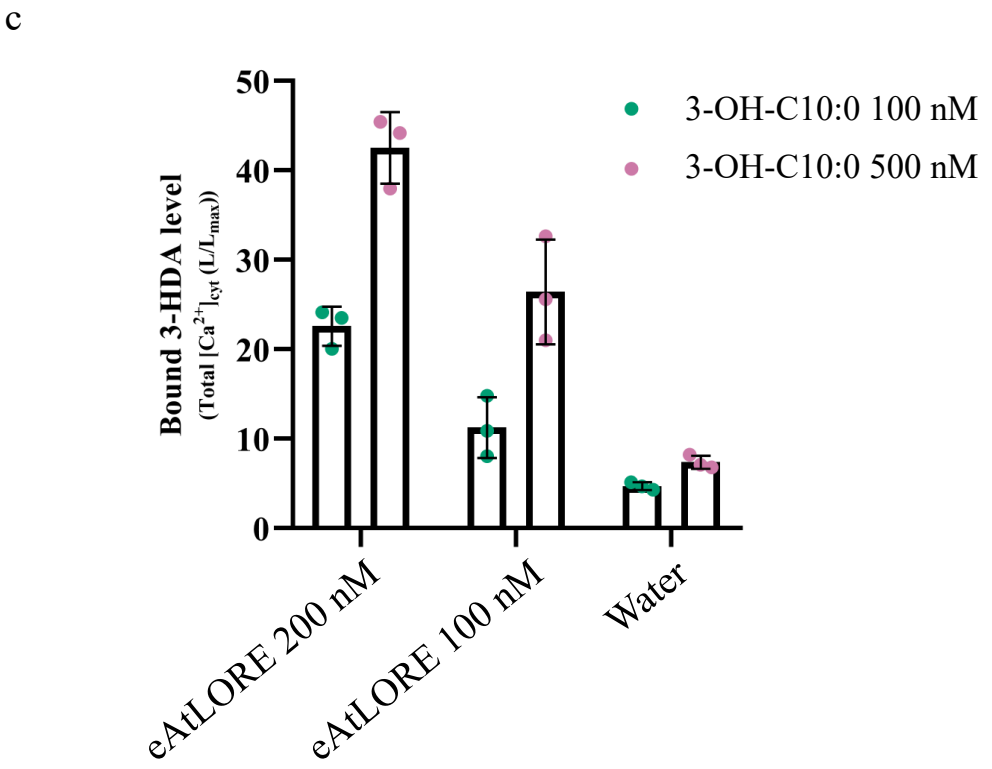

Supplementary Figure 4: **Purification of AtLORE ECD with Strep-tag and functional verification by ligand depletion binding assay.** The AtLORE ECD (eAtLORE) fused at its N terminus with Twin-Strep-tag and at its C terminus with HA tag was expressed by *Nicotiana benthamiana* in the apoplast of leaves by *Agrobacterium*-mediated

transient expression. The eAtLORE was purified using Strep-tag column Strep-Tactin®XT 4Flow cartridge with 5 mL column bed volume (CV) coupled with ÄKTA system. **a**. Anti-HA immunoblot analysis of the protein purification. The calculated molecular weight of the protein is 55-60 kDa. Lane Input: apoplast washing fluid (10 µl; 30 mL in total) before subjecting into the cartridge. Lane Unbound: column flow-through (10 µl; 30 mL in total). Lane Wash: the cartridge was washed with wash buffer (10 µl; 50 mL in total). Lane Eluate 1st CV to 4th CV: elution fractions having the purified eAtLORE (10 µl each lane; 5 ml each fraction in total). **b.** Purified eAtLORE in SDS-PAGE stained with Coomassie brilliant blue. The purified protein pooling from all fractions of the eluates was concentrated to 0.15 μg/μL by concentrator (30 kDa cut-off), and 10 μL of concentrate was loaded. **c.** The ligand binding assay was performed using 100 nM and 500 nM 3-OH-C10:0 with 100 nM and 200 nM purified eAtLORE, and water was used as negative protein control. Increases in $[Ca^{2+}]_{cyt}$ of Arabidopsis LORE-OE or *lore*-1 seedlings treated with the respective filtrates of heat-denatured retentates obtained in the binding assay. (mean ± SD, LORE-OE: n = 3 seedlings). Data from one experiment were shown.

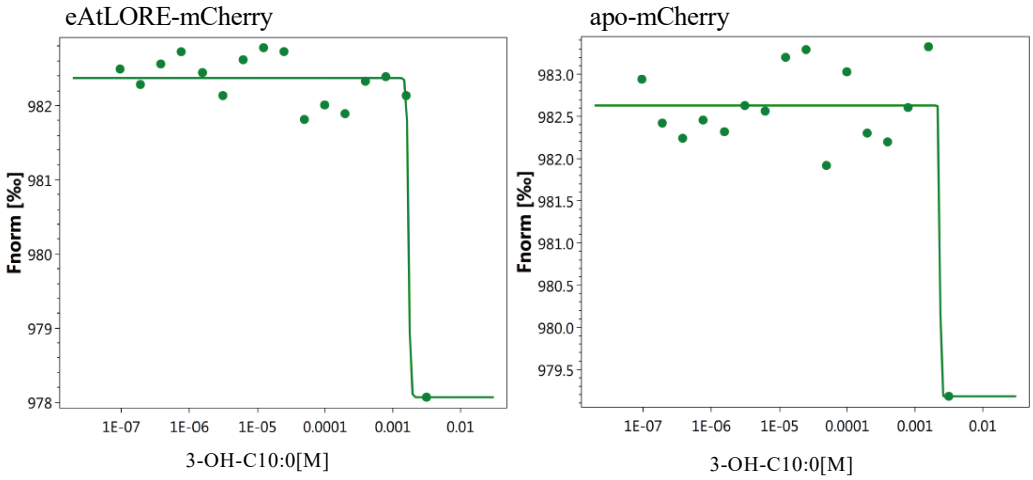

Supplementary Figure 5. Microscale thermophoresis cannot measure 3-OH-C10:0-eAtLORE interaction. Measurement of binding between 3-OH-C10:0 and the eAtLORE-mCherry and apo-mCherry by MST. Data points indicate the red fluorescence intensities of proteins bound to different concentrations of 3-OH-C10:0 (Fnorm, normalized fluorescence). Fluorescent proteins were concentrated and utilized directly. Measurements were performed at 40% LED power and medium MST power at room temperature.

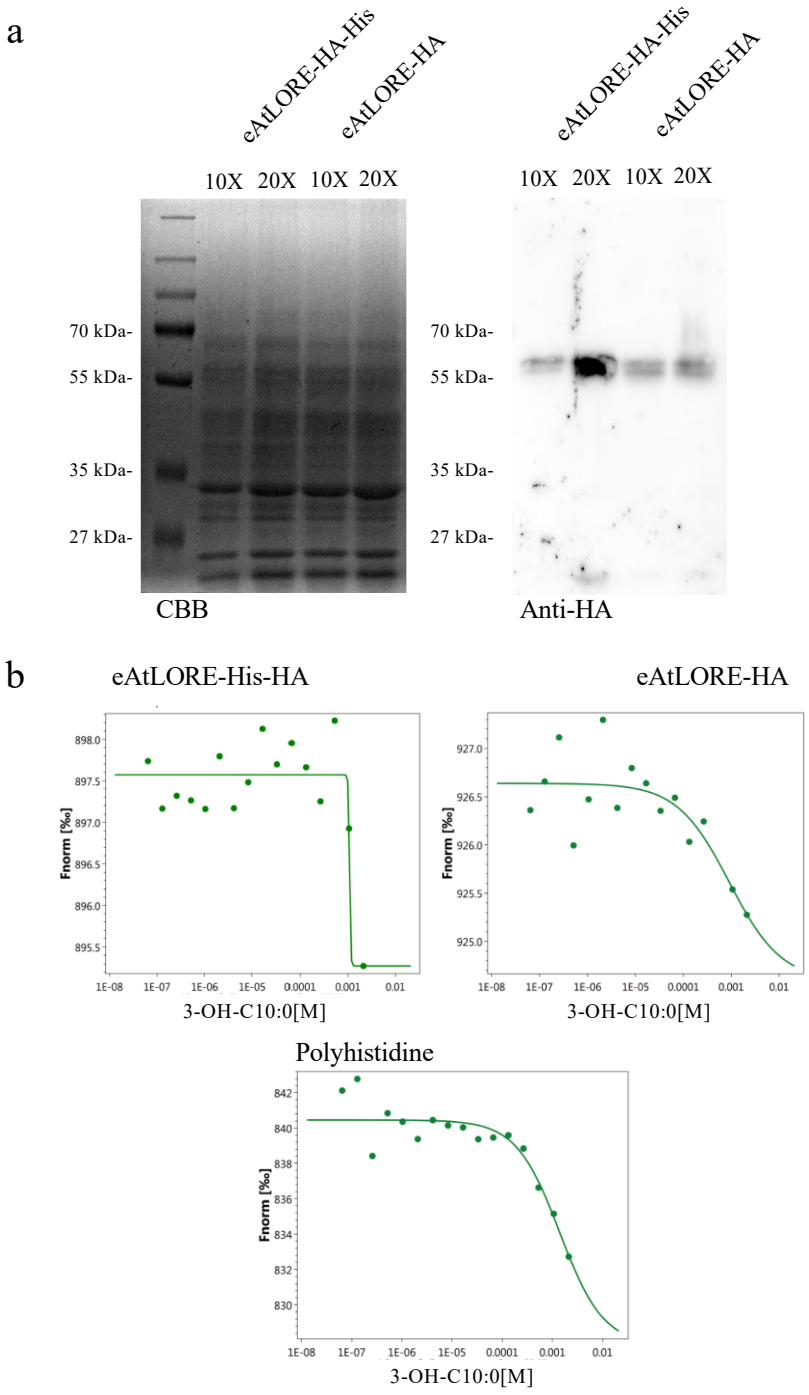

Supplementary Figure 6. 3-OH-C10:0 binds proteins and dyes non-specifically under high concentrations. a. Anti-HA immunoblot of desalted and concentrated AWFs from *N. benthamiana* leaves expressing eAtLORE with different tags fusion proteins. The numbers above each lane indicate the folds of protein concentration, and 10-fold concentrates were used for labeling and MST assays. The calculated molecular weights of eAtLORE-His-HA and eAtLORE-HA fusions are 55-60 kDa. The loading of the samples was confirmed by Coomassie Brilliant Blue (CBB) staining of the SDS-PA gel before blotting. One representative immunoblot of three experiments is shown. **b.**

Appendix

Measurement of binding between 3-OH-C10:0 and the eAtLORE fused with His-tag and HA-tag or only HA-tag and polyhistidine peptide by MST. Data points indicate the red fluorescence intensities of His-tag labeled proteins bound to different concentrations of 3-OH-C10:0 (fraction bound). Proteins were fluorescently labeled using the His-Tag labeling kit. eAtLORE-HA was negative control of labeling, and polyhistidine was positive control of labeling as well as a negative control of binding. Measurements were performed at 40% LED power and medium MST power at room temperature.

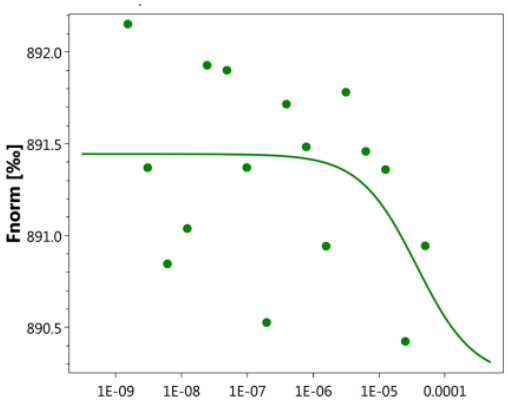

Supplementary Figure 7. Microscale thermophoresis cannot measure 3-OH-C10:0-eAtLORE interaction. Measurement of binding between 3-OH-C10:0 and the Strep-tag purified eAtLORE by microscale thermophoresis (MST). Data points indicate the red fluorescence intensities of labeled proteins bound to different concentrations of 3-OH-C10:0 (Fnorm, normalized fluorescence). The purified eAtLORE were fluorescently labeled by the amine labeling kit. Measurements were performed at 60% LED power and medium MST power at room temperature.

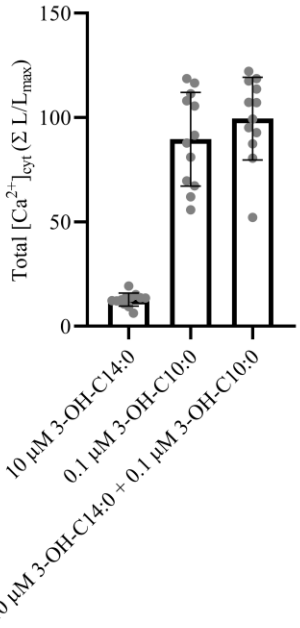

Supplementary Figure 8. LORE-dependent increase of $[Ca^{2+}]_{cyt}$ induced by 3-OH-C10:0 was not inhibited by 3-OH-C14:0 treatment. Total $[Ca^{2+}]_{cyt}$ level measurements of LORE-OE elicited with 0.1 µM 3-OH-C10:0, 10 µM 3-OH-C14:0, or 0.1 µM 3-OH-C10:0 and 10 µM 3-OH-C14:0 together (mean ± SD, n = 12 seedlings, data from two independent experiments were pooled).

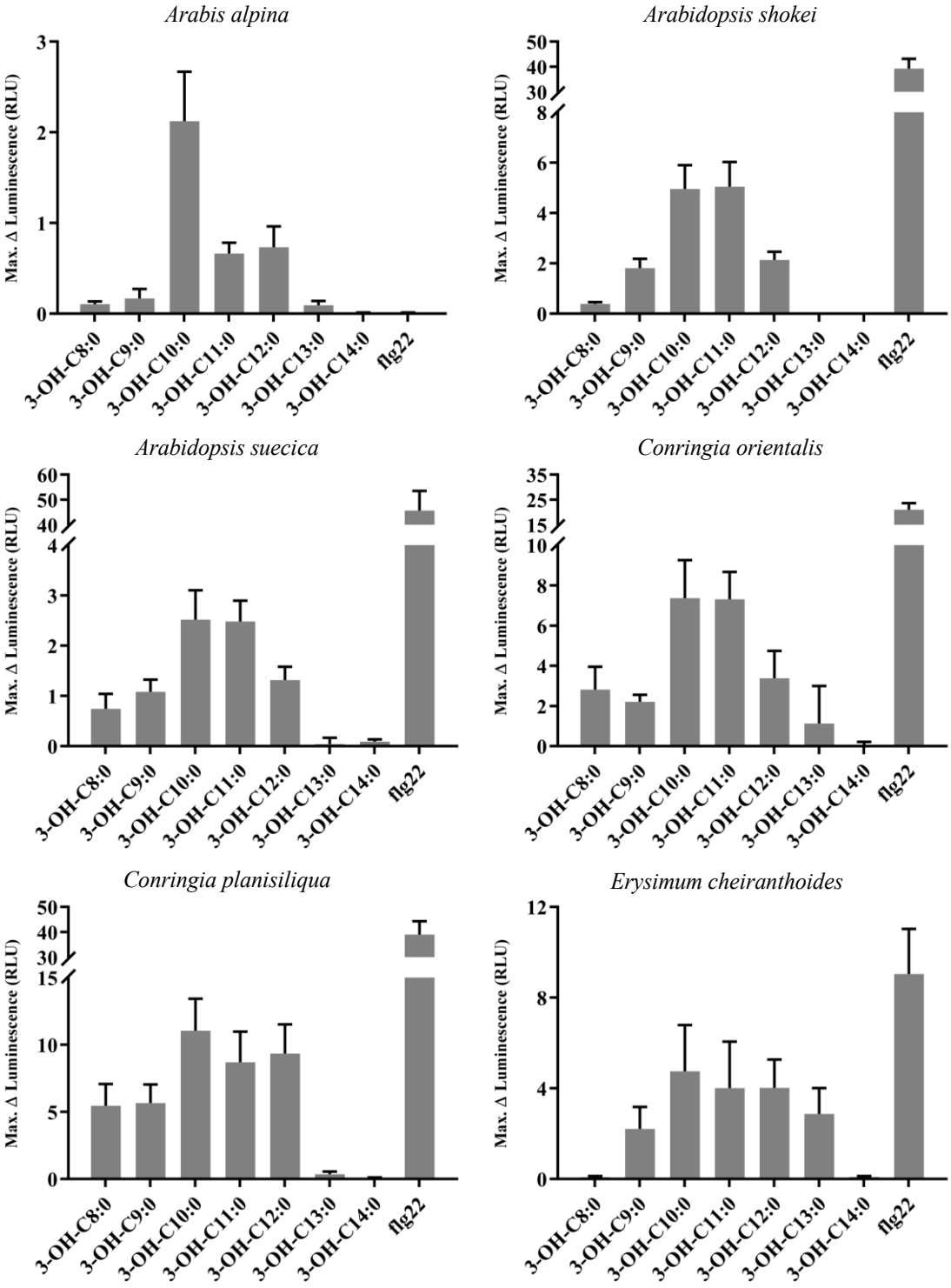

Supplementary Figure 9. (Continued)

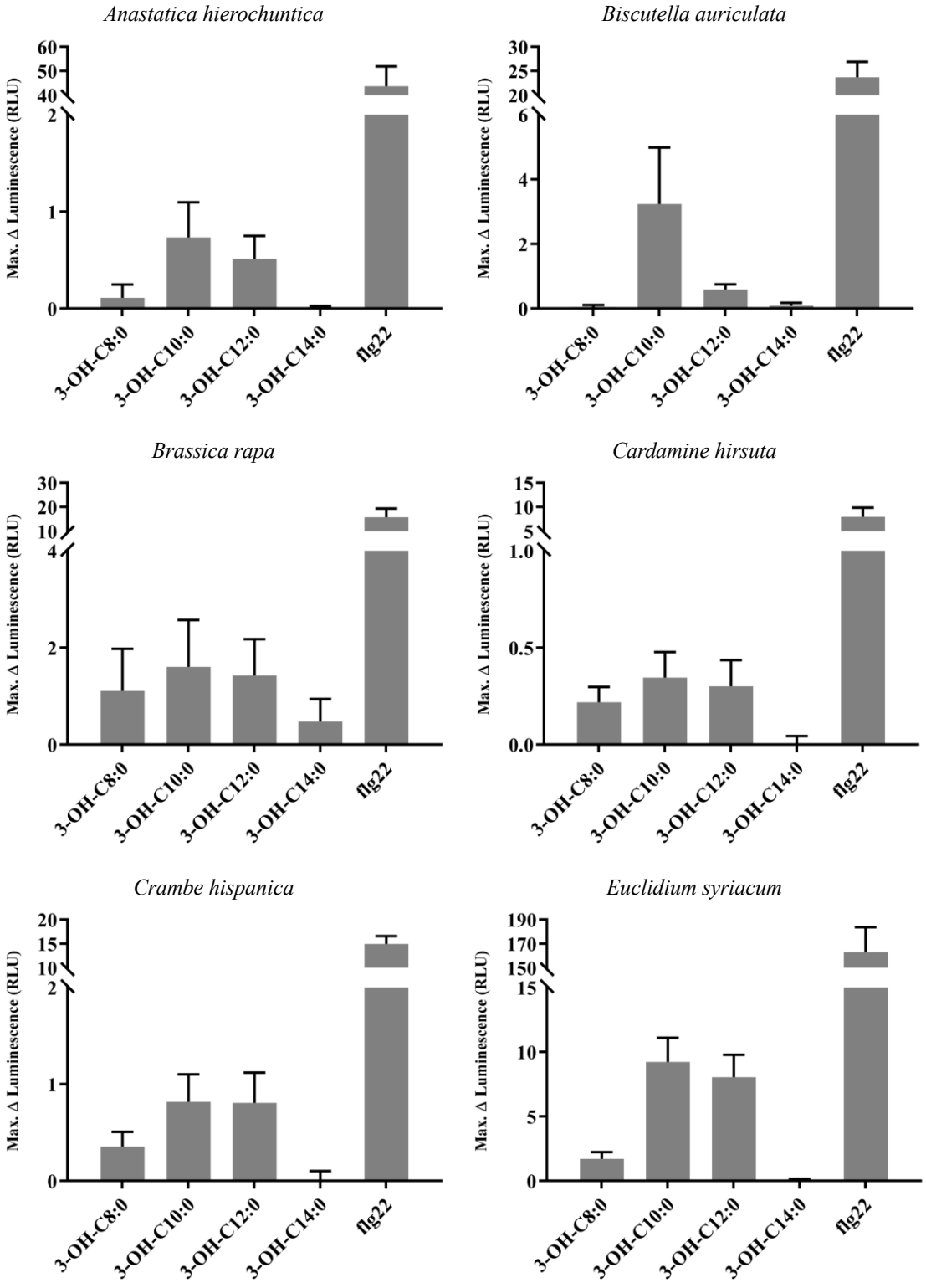

Supplementary Figure 9. (Continued)

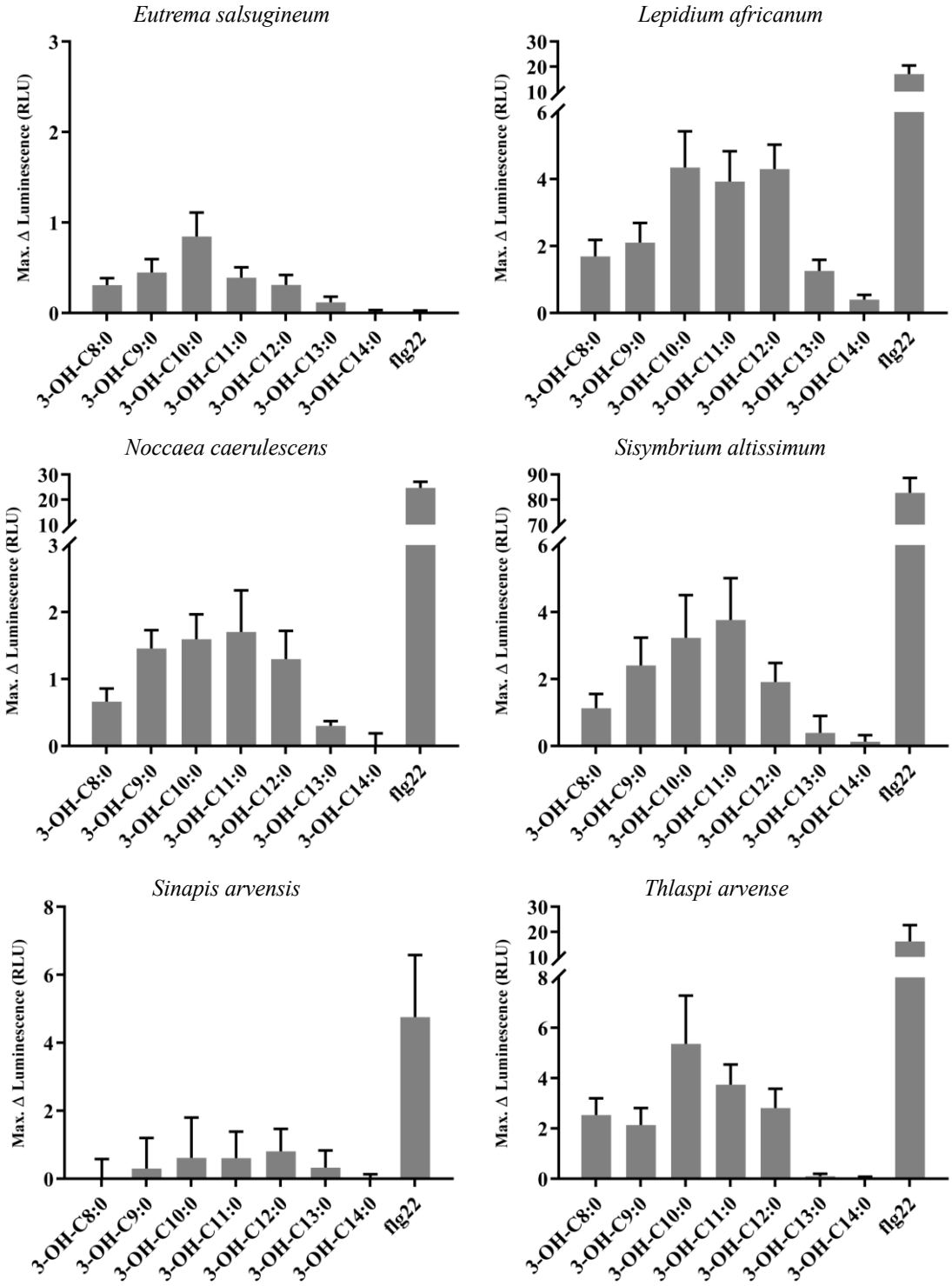

Supplementary Figure 9. (Continued)

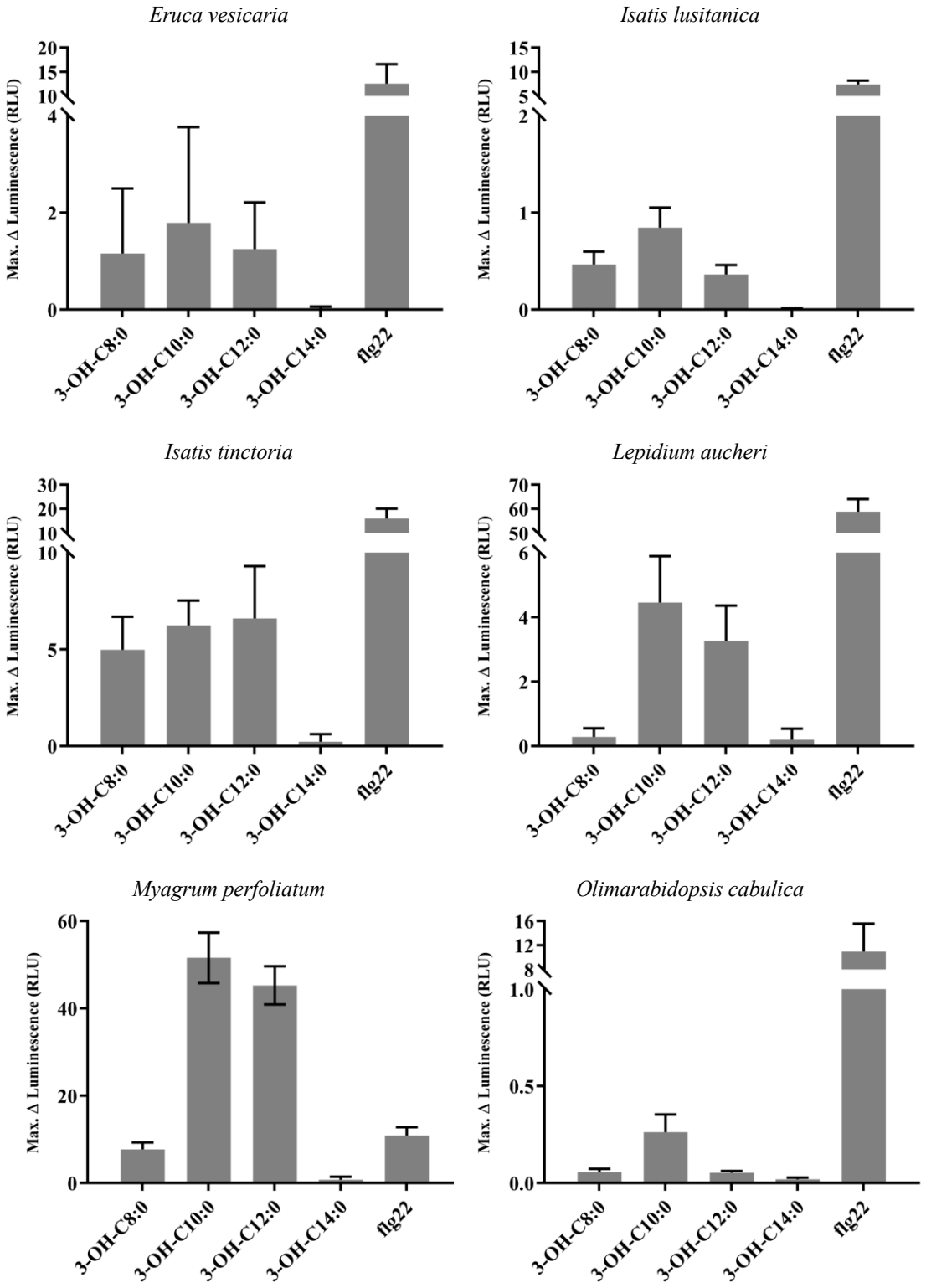

Supplementary Figure 9. (Continued)

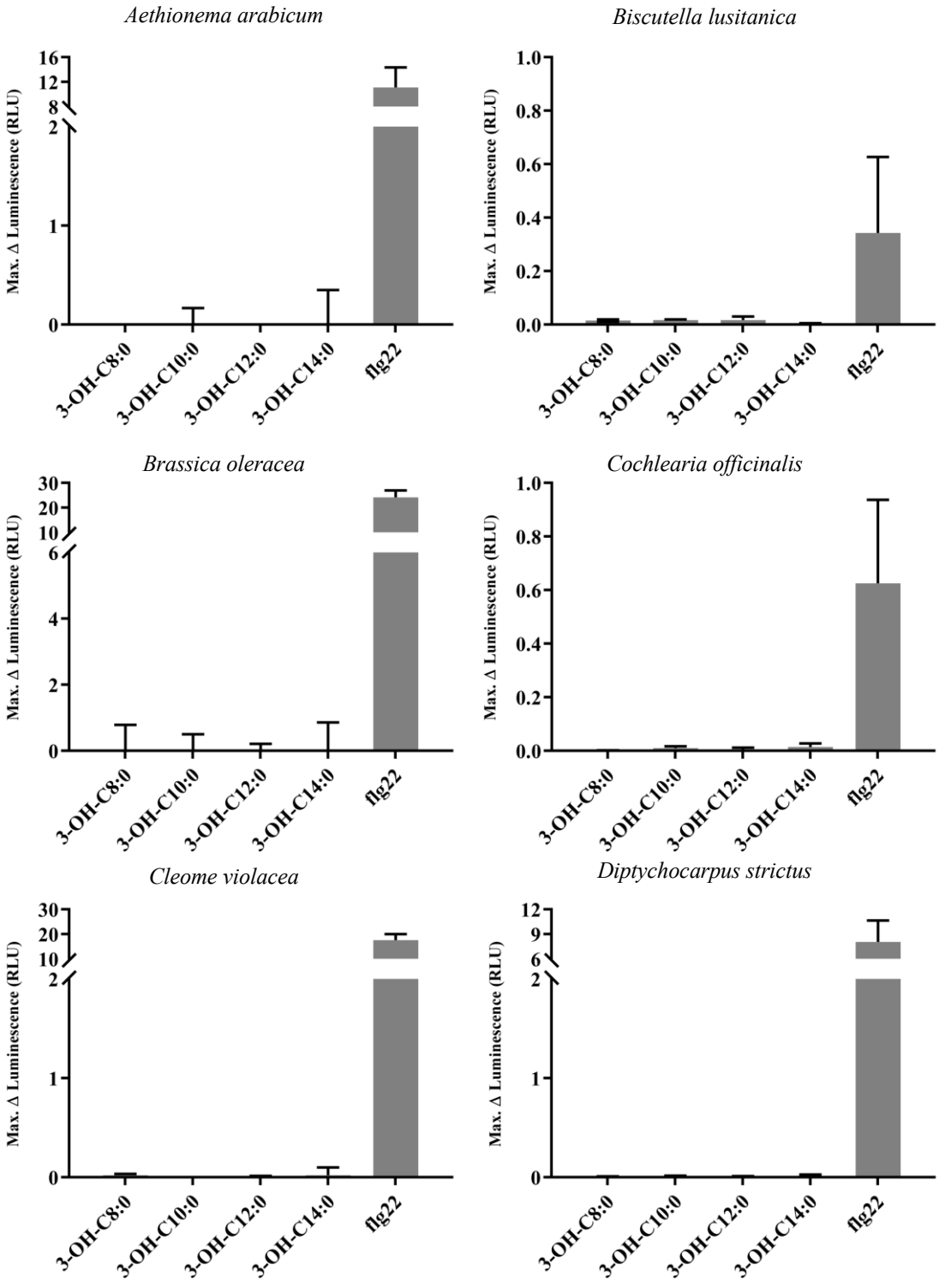

Supplementary Figure 9. (Continued)

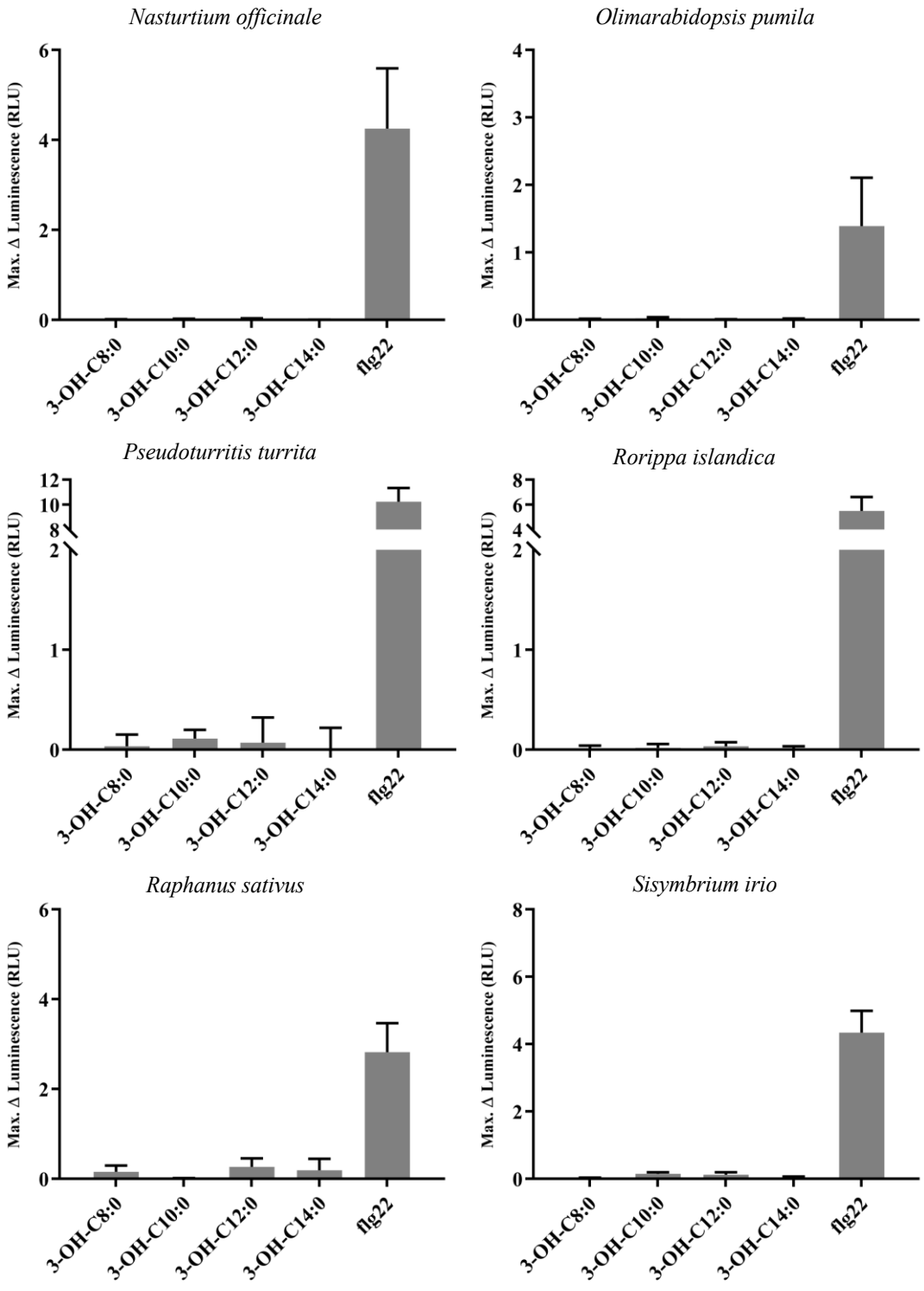

Supplementary Figure 9. 3-OH-FAs trigger ROS accumulations in acyl chain length-specific manners in sensitive Brassicaceae species. Maximum ROS accumulation in leaf discs of 36 Brassicaceae species elicited by 5 μM 3-OH-FAs and 0.5 μM flg22 (mean ± SD, n = 8). Maximal luminescence was normalized by the average

luminescence of 5 minutes before treatment and subtracted by mock controls. Two or three independent experiments were done with similar results.

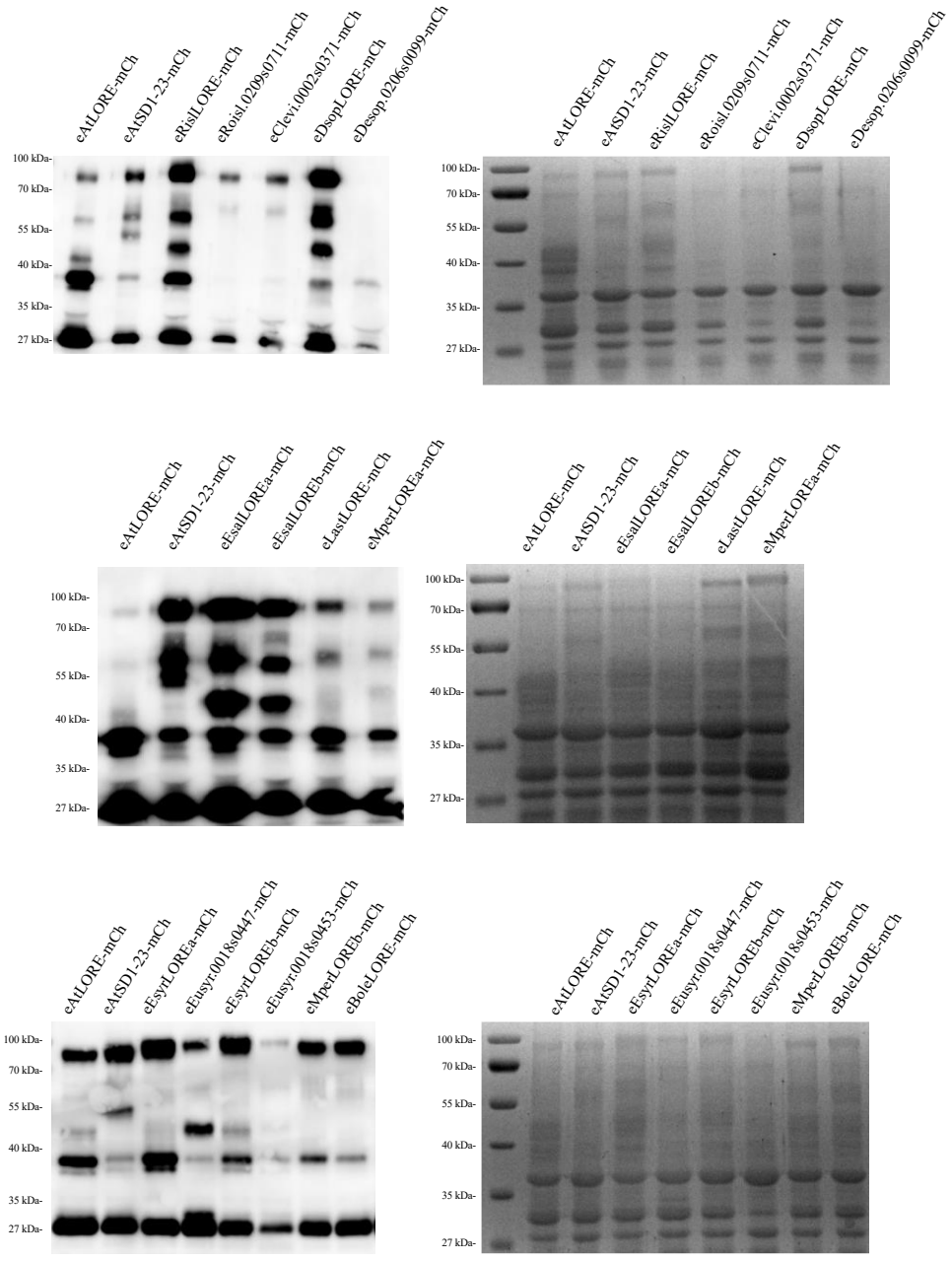

Supplementary Figure 10. (Continued)

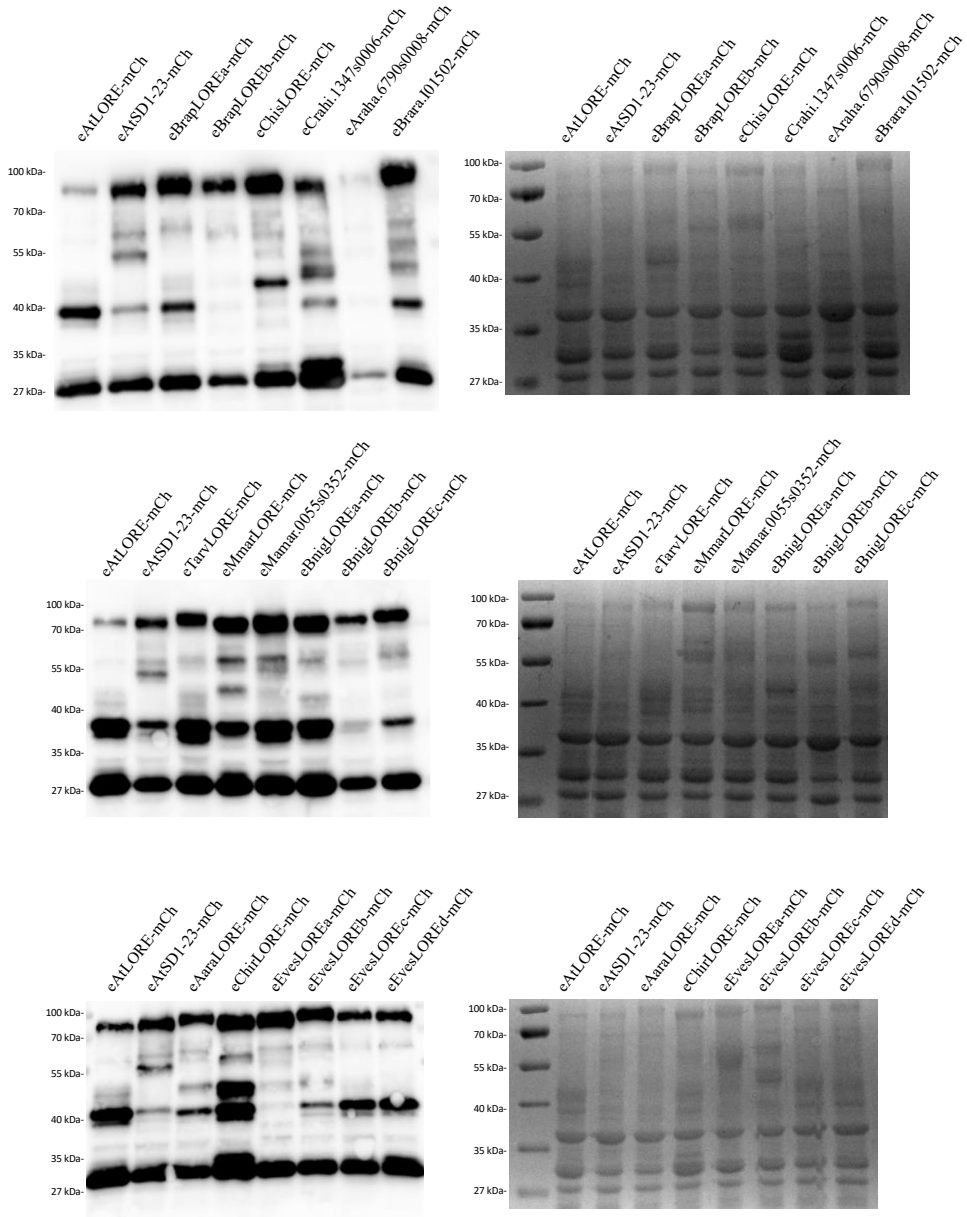

Supplementary Figure 10. Anti-RFP immunoblot of desalted and concentrated AWFs from *N. benthamiana* leaves expressing different SD-RLK ECD-mCherry fusion proteins. AWFs were harvested five days after infiltration of agrobacterium in *N. benthamiana*, and concentrated AWFs corresponding to 7.5 μg total proteins were loaded. The calculated molecular weights of SD-RLK ECD-mCherry fusions are 70-80 kDa. The loading of the samples was confirmed by Coomassie Brilliant Blue (CBB) staining of the SDS-polyacrylamide gel prior to blotting. One representative immunoblot of two experiments is shown.

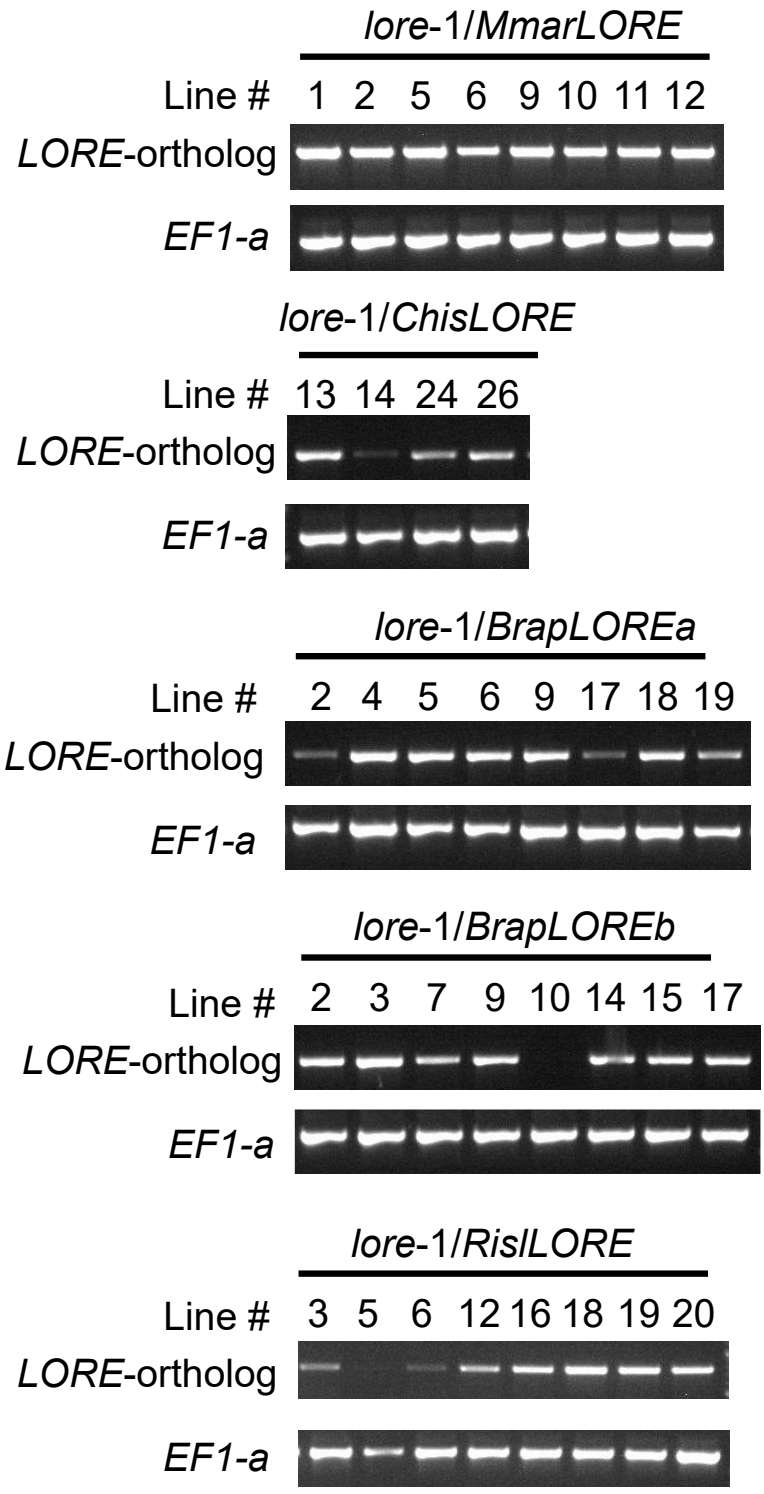

Supplementary Figure 11. (Continued)

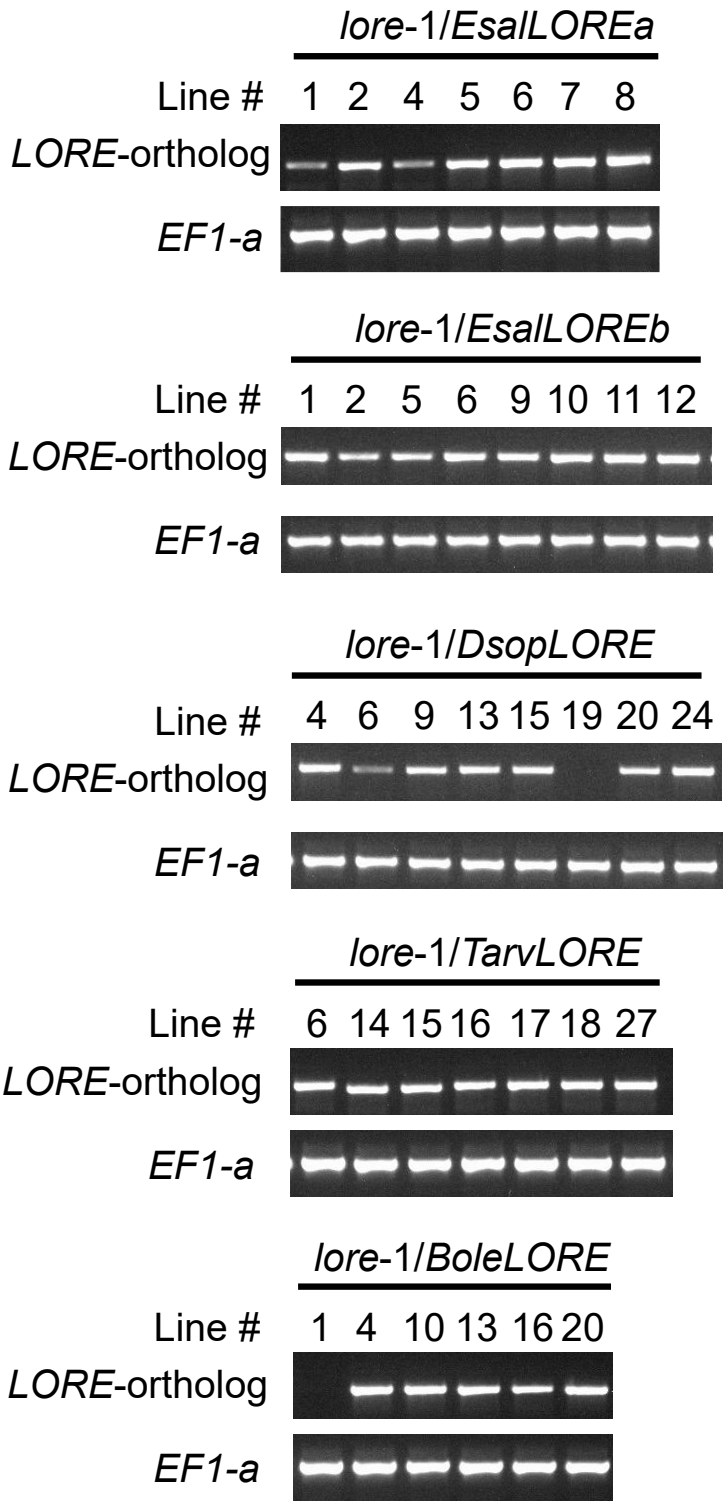

Supplementary Figure 11. (Continued)

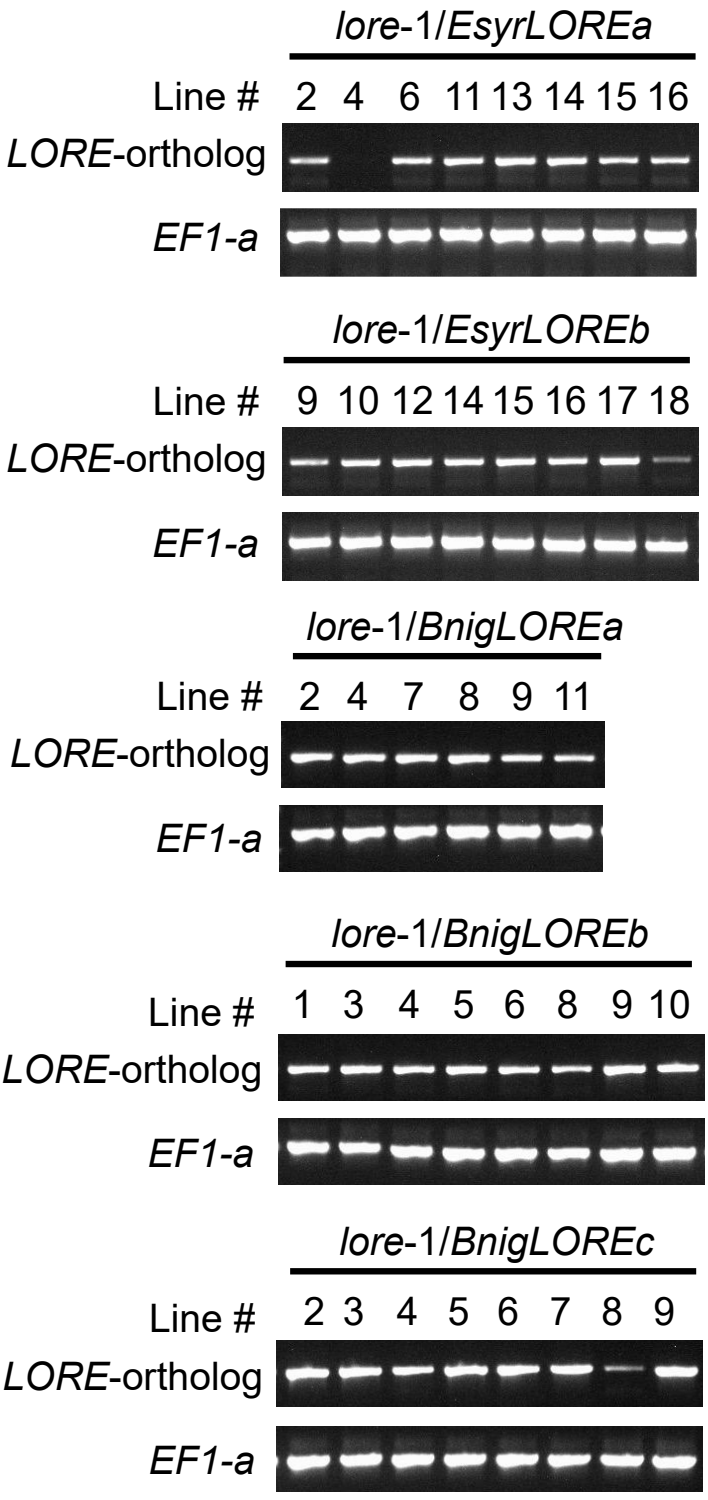

Supplementary Figure 11. (Continued)

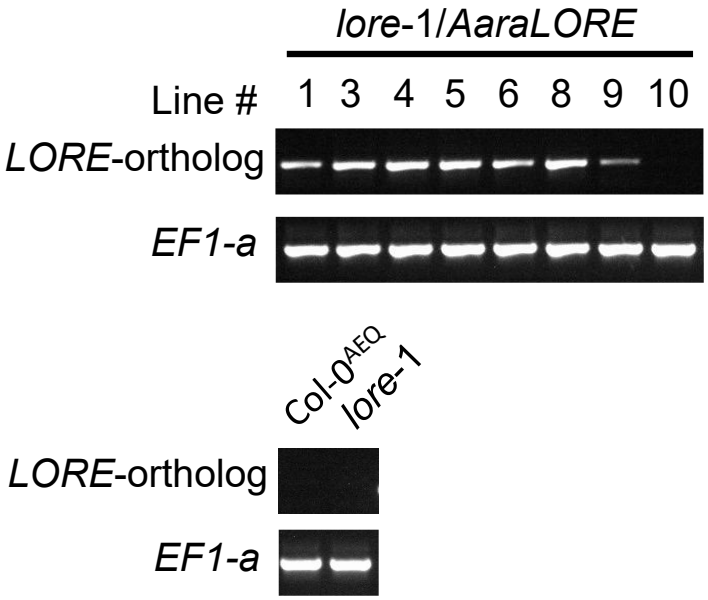

Supplementary Figure 11. Expression of *LORE* orthologs in complementation lines. The expression of transgenes in complementation lines shown in Figure 24 was analyzed by RT-PCR. The names of *LORE* orthologs indicate the genes for restoring *lore*-1, and the numbers above each graph represent independent transgenic lines. Col-0^{AEQ} and *lore*-1 were used as negative controls of transgene expression. Arabidopsis cytosolic apoaequorin-expressing *LORE* orthologs complementation lines were cultured in half-strength MS liquid medium under long day (16-hour daylight) conditions and harvested for RT-PCR analysis after nine days. *EF-1a* was used as an internal control of RT-PCR. Primer sequences are listed in Table 8.

Appendix

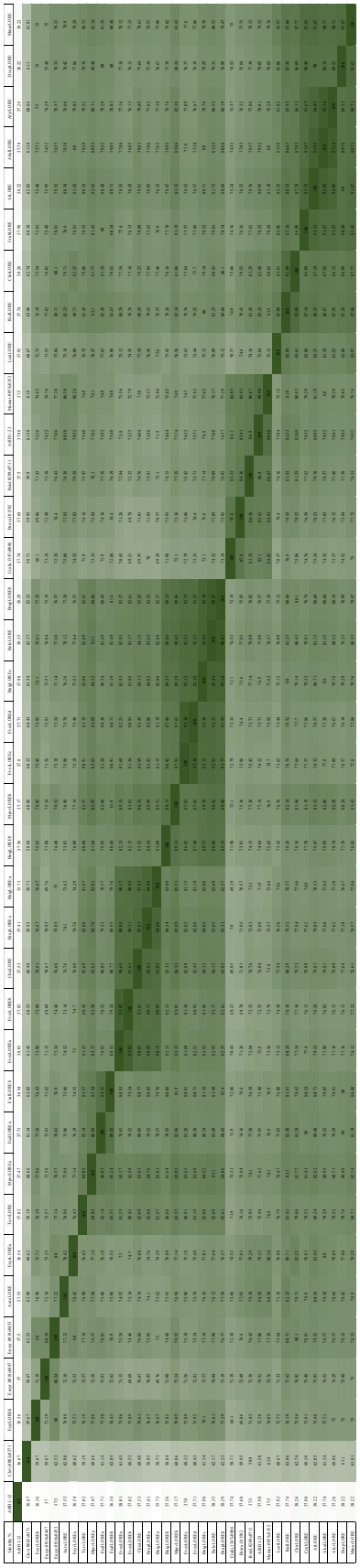

Supplementary Figure 12. The protein sequence identity matrix of LORE orthologs and other SD-RLKs. 37 candidate protein sequences were acquired from several databases, according to Table 3. Multiple sequence alignment was generated by MUSCLE, and the protein sequence identity matrix (%) was illustrated and visualized by ClustalW2 and Window Excel, respectively.

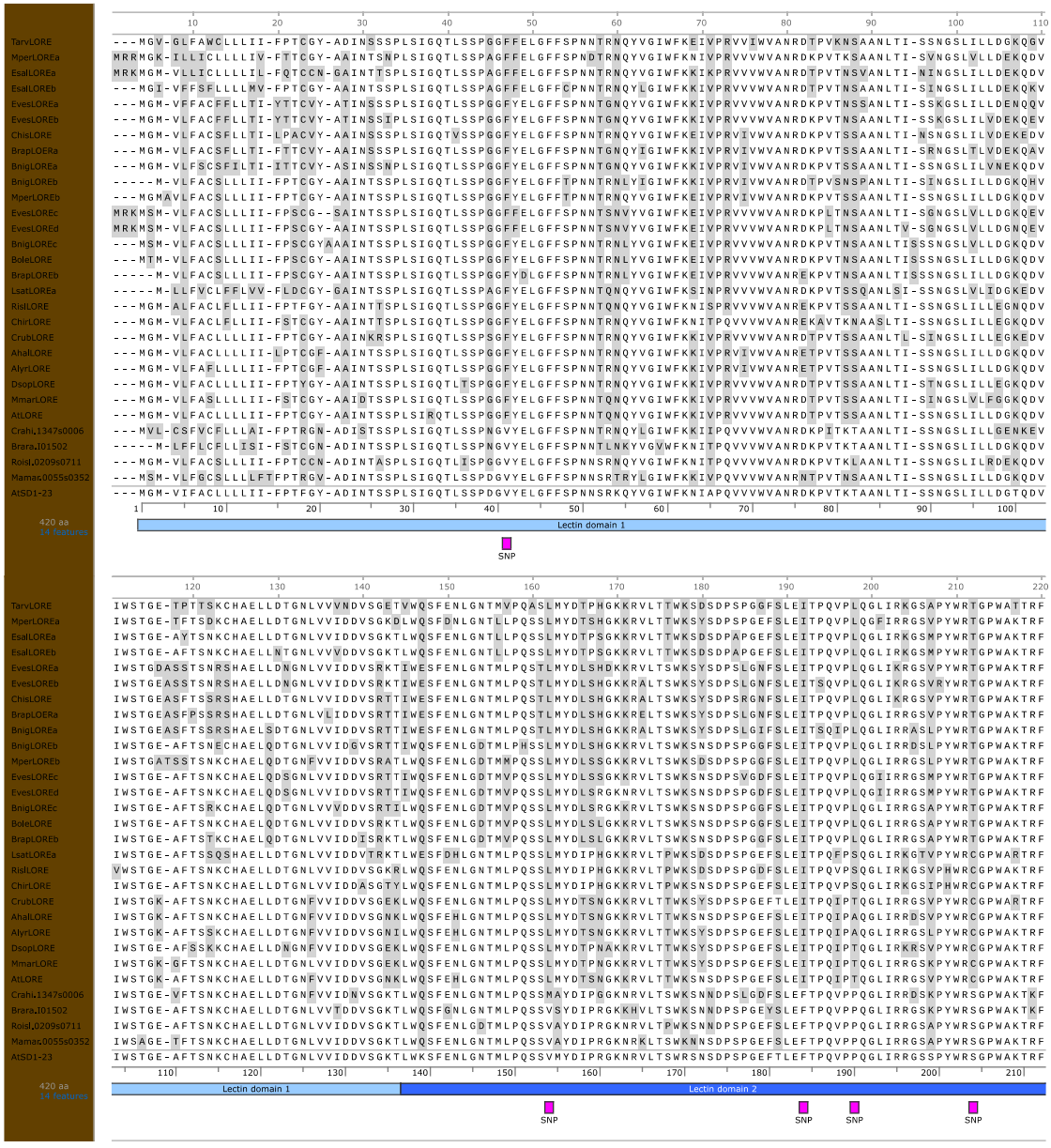

Supplementary Figure 13. (Continued)

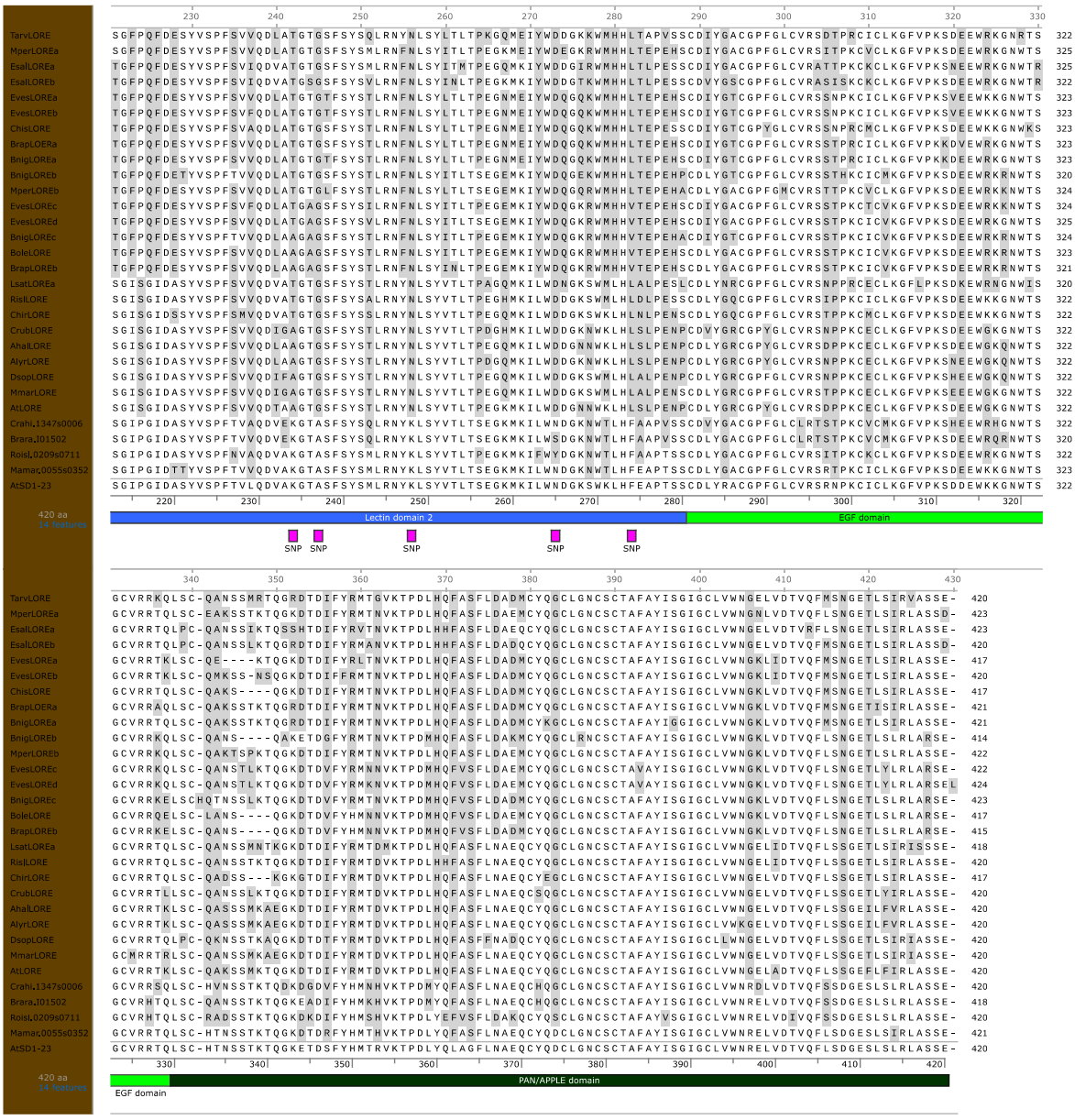

Supplementary Figure 13. Multiple sequence alignment of extracellular domains of LORE and SD1-23 orthologs. The alignment of 30 protein sequences was constructed by MUSCLE. Multiple sequence alignment of amino acid sequences (80% of all) was illustrated by SnapGene, and AtSD1-23 was set as a reference. The conserved residues of all sequences are highlighted. The domains of sequences are annotated according to Naithani *et al.* (2007). The residues marked as SNP indicate the unique but conserved amino acids between LORE and SD1-23 orthologs.

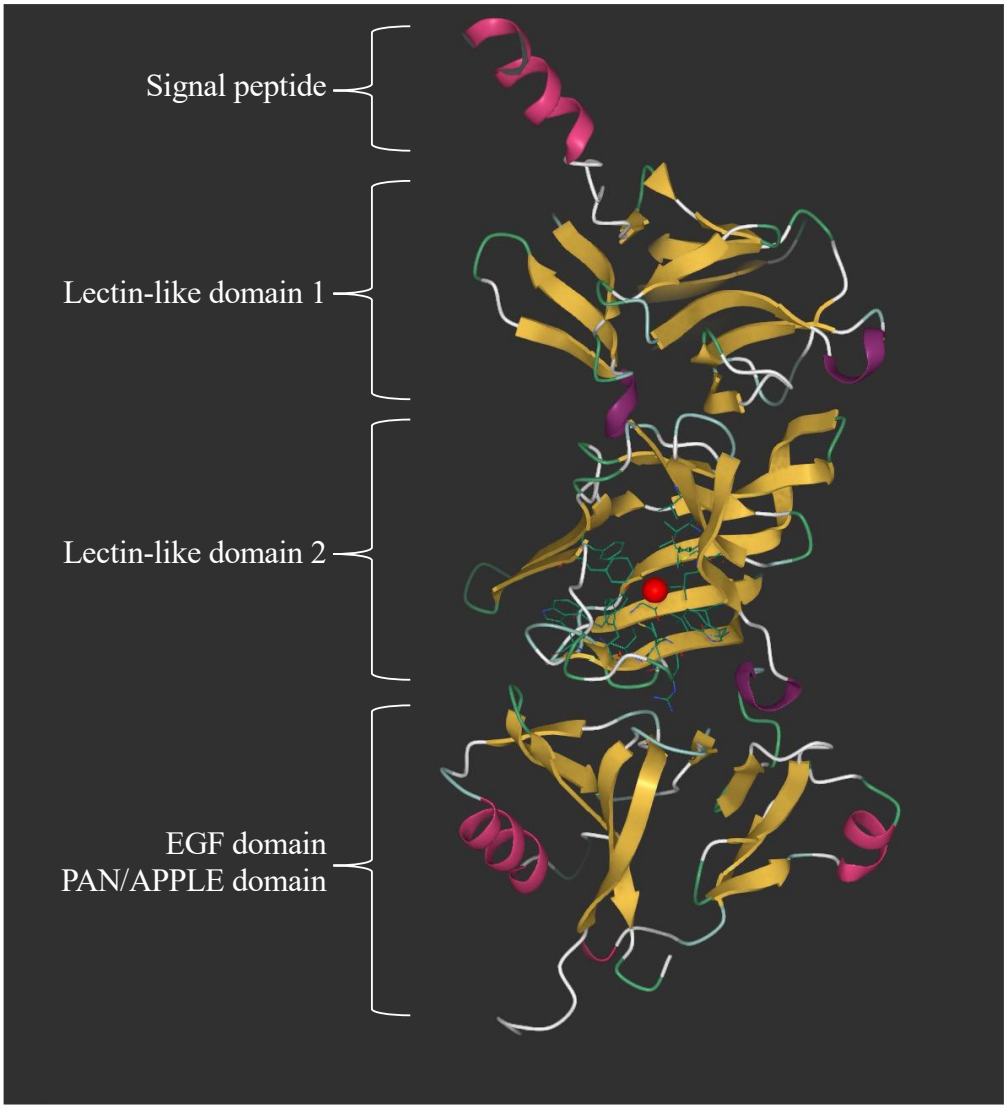

Supplementary Figure 14. Prediction of AtLORE ectodomain model and its ligand binding pocket. The protein model of eAtLORE was predicted by Alphafold, and the potential ligand binding was predicted and visualized by DEEPSITE, PlayMolecule. The red dot in lectin-like domain 2 is the putative ligand binding site. The side chains of amino acids around the red dot, which interact with the ligand, are shown in green.

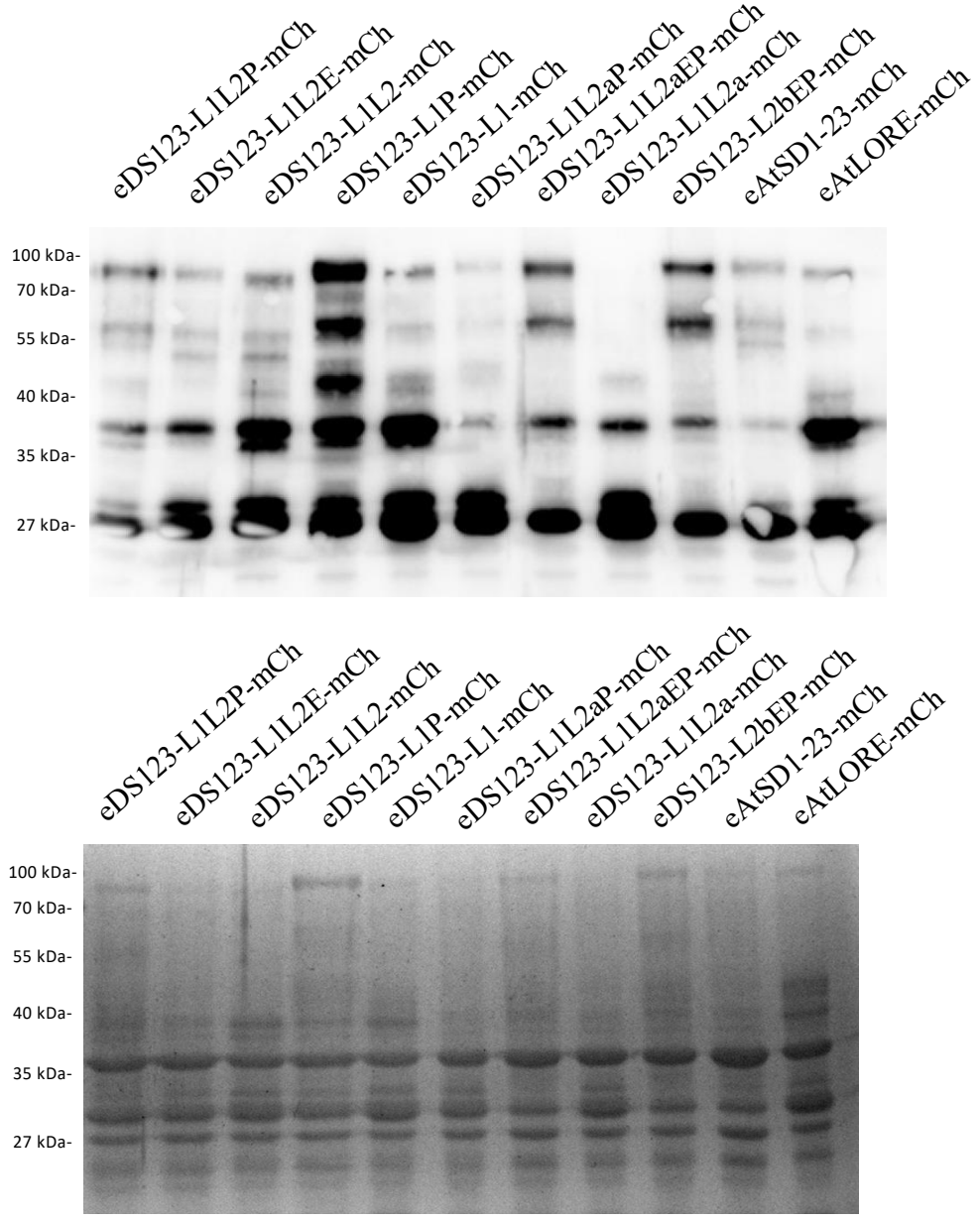

Supplementary Figure 15. The Anti-RFP immunoblots of desalted and concentrated AWFs from *N. benthamiana* leaves expressing different domain-swapped AtLORE-AtSD1-23 ECD-mCherry fusion proteins. AWFs were harvested 5 days after infiltration of agrobacterium in *N. benthamiana*, and concentrated AWFs corresponding to 7.5 μg total proteins were loaded. The calculated molecular weights of SD-RLK ECD-mCherry fusions are 70-80 kDa. The loading of the samples was confirmed by Coomassie Brilliant Blue (CBB) staining of the SDS-polyacrylamide gel before blotting. One representative immunoblot of two experiments is shown.